[This blank, unnumbered page will be the back of your front cover]

Technical Report Document Page

1. Report No.	2. Government Accession No.	3. Recipient's Catalog No.

4. Title and Subtitle	5. Report Date
Recycled Ground-Glass Pozzolan (RGGP) for Use in Cement Concrete -and Comparison with Other Alternative Constituent Materials	July 15, 2025
	6. Performing Organization Code
7. Author(s) Jianqiang Wei, Kara Peterman, Sergio Brena, Reza Zadeh, Arkabrata Sinha, Souvik Das	8. Performing Organization Report No.
9. Performing Organization Name and Address University of Massachusetts Lowell 1 University Avenue, Shah Hall 200, Lowell, MA 01824 University of Massachusetts Amherst 130 Natural Resources Road, 230 Marston Hall, Amherst, MA 01003	10. Work Unit No. (TRAIS)
	11. Contract or Grant No. INTF00X02024A0122821
12. Sponsoring Agency Name and Address Massachusetts Department of Transportation Office of Transportation Planning Ten Park Plaza, Suite 4150, Boston, MA 02116	13. Type of Report and Period Covered Final Report [08/2023 – 06/2025]
	14. Sponsoring Agency Code n/a

15. Supplementary Notes
Richard Mulcahy - Project Champion, MassDOT

16. Abstract
Cement concrete is the most widely used building material in construction for infrastructure. However, hydraulic cement, the key ingredient of cement concrete, produces an immense amount of heat and carbon dioxide during the manufacturing process. According to the International Energy Agency (IEA), manufacturing hydraulic cement accounts for 7% of human-made carbon dioxide emissions. Other hydraulic cement replacement materials used in today's cement concrete, such as fly ash and slag, are the byproducts of coal-fired power stations and steel manufacturing, respectively, which also increases our carbon footprint. These materials are also becoming increasingly scarce, resulting in a problematic supply crunch and increases in cost. Recycled ground-glass pozzolan is a potential hydraulic cement replacement material, manufactured from recycled glass products, with the potential to greatly reduce the amount of hydraulic cement in cement concrete. Other promising alternative constituent materials for use in concrete, including performance-based cement, Class N Natural Pozzolans, and Type S Specific Performing nano silica chemical admixtures, also require investigations. The objective of this research project is to validate the efficacy of recycled ground-glass pozzolan and other low-carbon alternative constituent materials, to decrease our carbon footprint and increase the quality and long-term durability of cement concrete used in MassDOT projects.

17. Key Word	18. Distribution Statement
Recycled ground-glass pozzolan, Alternative Materials, Concrete, Cement Hydration, Mixture Design, Mechanical Performance, Durability	

19. Security Classif. (of this report)	20. Security Classif. (of this page)	21. No. of Pages	22. Price
unclassified	unclassified	218	n/a

Form DOT F 1700.7 (8-72) Reproduction of completed page authorized

This page left blank intentionally.

Recycled Ground-Glass Pozzolan (RGGP) for Use in Cement Concrete

- and Comparison with Other Alternative Constituent Materials

Final Report

Prepared By:

Jianqiang Wei
Principal Investigator
University of Massachusetts Lowell

Kara Peterman and Sergio Breña
Co-Principal Investigators
University of Massachusetts Amherst

Reza Zadeh
Graduate Research Assistant
University of Massachusetts Amherst

Arkabrata Sinha
Graduate Research Assistant
University of Massachusetts Lowell

Souvik Das
Graduate Research Assistant
University of Massachusetts Lowell

Prepared For:

Massachusetts Department of Transportation
Office of Transportation Planning
Ten Park Plaza, Suite 4150
Boston, MA 02116

July 2025

This page left blank intentionally.

Acknowledgements

This study was prepared in cooperation with the Massachusetts Department of Transportation, Office of Transportation Planning, and the United States Department of Transportation, Federal Highway Administration.

The Project Team would like to acknowledge the efforts of Arkabrata Sinha (graduate student), Souvik Das (graduate student), Reza Zadeh (graduate student), Dr. Kara Peterman, (Co-PI), Dr. Sergio Breña (Co-PI), and Dr. Jianqiang Wei (PI), as well as the MassDOT Research and Materials Section. We thank Urban Mining, E5 Incorporated, Dicalite Management Group, and Boston Concrete for providing raw materials for this project. The research team would also like to thank Boston Concrete for their help in casting concrete specimens. The Project Team would like to acknowledge the efforts of Construction Services, HOLCIM, and Master Builder Solution Companies, who supported us during this research.

Disclaimer

This page left blank intentionally.

Executive Summary

This study of Recycled Ground-Glass Pozzolan (RGGP) for Use in Cement Concrete and Comparison with Other Alternative Constituent Materials was undertaken as part of the Massachusetts Department of Transportation (MassDOT) Research Program. This program is funded with Federal Highway Administration (FHWA) State Planning and Research (SPR) funds. Through this program, applied research is conducted on topics of importance to the Commonwealth of Massachusetts transportation agencies.

As the most consumed man-made material with over 4 billion metric tons of annual production, cement plays a crucial role in shaping our world by providing concrete structures with strength, rigidity, and stability. The highly energy-intensive clinkering process, however, renders cement production one of the largest industrial CO_2 emitters, responsible for about 7-8% of global CO_2 emissions. Over 100 Gtons of CO_2 per year will be emitted in the following 40 years to meet the cement demand for the estimated double-sized infrastructure expansion. These challenges highlight the urgency of utilizing cement alternatives so that future infrastructure can be built based on truly sustainable concrete with low carbon footprints.

According to the 2018 data from the Environmental Protection Agency and Glass Packaging Institute, only 31.3% of the 12.3 million tons of waste glass in the United States was recycled, and the remainder is often buried in landfills or stockpiled, resulting in wasting resources and environmental pollution. In light of the high silica content and amorphous structure, recycled ground glass can trigger pozzolanic reactions in the matrix of cement, making it suitable to be used as a pozzolan for high-quality concrete design, while its role in cement modification and concrete performance remains unclear. To fill the knowledge gaps in using other alternative constituent materials in concrete, natural pozzolan (metakaolin), diatomaceous earth, and nano-silica chemical admixtures will also be investigated.

The overall research objective of this project is to evaluate the viability of RGGP and other alternative constituent materials as suitable alternatives to traditional supplementary cementitious materials (SCM) in replacing hydraulic cement, to decrease the carbon footprint and increase the quality and long-term durability of cement concrete used in MassDOT projects. Anticipated outcomes and deliverables include:

- A comprehensive literature review and fundamental understanding of the current state of knowledge and existing knowledge gaps with the utilization of RGGP in concrete.
- A comprehensive understanding of the pozzolanic reactivity of RGGP and the approaches to enhance its reactivity.
- Insights into the hydration behavior of Portland cement containing RGGP in terms of hydration kinetics and phase evolutions.
- Development of cement concrete mix design formulations incorporating RGGP and other alternative constituent materials.
- Evolutions of physical, mechanical, and durability properties of cement concrete incorporating RGGP and other alternative constituent materials.
- Performance evaluation of RGGP-based cement concrete through mock-ups.

This project report consists of 8 sections. Section 1 is a brief introduction to the problem and a description of the scope of the research. Section 2 compiles a fundamental understanding of the current state of knowledge and existing knowledge gaps in using RGGP in concrete as a cement alternative based on a literature review. Section 3 presents the main research methodologies used in this project. Section 4 reports the primary findings and results, including the influence of the incorporation of RGGP, at a variety of substitution levels, on the hydration behavior of cement, cement hydration kinetics, and the evolution of hydration products, the development of concrete mix design formulations based on modified cement using RGGP and other alternative materials, physical and mechanical properties of mortar and concrete with RGGP and alternative materials, as well as the influences of RGGP and alternative materials on the durability-related properties of concrete. Section 5 presents the findings from field tests for the concrete containing RGGP.

Table of Contents

List of Tables

List of Figures

List of Acronyms

Acronym	Expansion
SCM	Supplementary Cementitious Material
RGGP	Recycled Ground Glass Pozzolan
ASR	Alkali-Silica Reaction
ACCT	Accelerated concrete cylinder test
MCPT	Miniature concrete prism test
MassDOT	Massachusetts Department of Transportation
FHWA	Federal Highway Administration
UMASS Amherst	University of Massachusetts Amherst
UMASS Lowell	University of Massachusetts Lowell
IEA	International Energy Agency
LCA	Life-Cycle-Assessment
HP Concrete	High-Performance Concrete
AASHTO	American Association of State Highway and Transportation Officials
ASTM	American Society for Testing and Materials
DE	Diatomaceous earth
FA	Fly Ash
MK	Metakaolin
MIC	Metakaolin-based internal conditioning
FMIC	Fully saturated metakaolin-based internal conditioning
DMK	Dry metakaolin
SF	Silica Fume
RCA	Rice Husk Ash
FRP	Fiber Reinforced Polymer
SAI	Strength Activity Index
CH	Calcium Hydroxide
CSH	Calcium Silicate Hydrate
DOS	Degree of saturation
OPC	Ordinary Portland Cement
PLC	Portland Limestone Cement
Type IL	Portland Limestone Cement
SSD	Saturated Surface Dry
w/cm	Water-to-cementitious ratio
TAT	Truck Turn-Around Time
SCC	Self-Consolidating Concrete
CI	Corrosion Inhibitor
ACI	American Concrete Institute
f'c	Compressive Strength of Concrete at 28 days
ft	Splitting tensile strength
fr	Modulus of rupture
pH	Pondus Hydrogenii

Acronym	Expansion
TGA	Thermogravimetric analysis
XRD	X-ray diffraction (XRD).
ATR-FTIR	Attenuated Total Reflectance-Fourier Transform Infrared
GEMs	geochemical modeling program

1.0 Introduction

1.1 Overview of the project

This study of Recycled Ground-Glass Pozzolan (RGGP) for Use in Cement Concrete was undertaken as part of the Massachusetts Department of Transportation (MassDOT) Research Program. This program is funded with Federal Highway Administration (FHWA) State Planning and Research (SPR) funds. Through this program, applied research is conducted on topics of importance to the Commonwealth of Massachusetts transportation agencies.

Cement concrete is the most widely used building material in construction for infrastructure. However, hydraulic cement, the key ingredient of cement concrete, produces an immense amount of heat and carbon dioxide during the manufacturing process. According to the International Energy Agency (IEA), manufacturing hydraulic cement accounts for 7% of human-made carbon dioxide emissions. Additionally, other hydraulic cement replacement materials used in today's cement concrete, such as fly ash and slag, are the byproducts of coal-fired power stations and steel manufacturing, respectively, which also increases our carbon footprint. These materials are also becoming increasingly scarce, resulting in a problematic supply crunch and increases in cost. It is clear that we must find environmentally conscious alternatives to the way we produce concrete.

Recycled ground-glass pozzolan (ASTM C1866) is a potential hydraulic cement replacement material, manufactured from recycled glass products, with the potential to greatly reduce the amount of hydraulic cement (up to 50% reduction) in cement concrete. Other promising alternative constituent materials for use in concrete, including performance-based cement (ASTM C1157), Class N Natural Pozzolans (AASHTO M 295), and Type S Specific Performing nano silica chemical admixtures (AASHTO M 194), also require investigations. The objective of this research project is to validate the efficacy of recycled ground-glass pozzolan (RGGP) and other low-carbon alternative constituent materials, to decrease our carbon footprint and increase the quality and long-term durability of cement concrete used in MassDOT projects. To accomplish the objectives of the project, the following six tasks were conducted in this project:

1.1.1. Task 1: Literature review on utilizing RGGP in concrete and material source identification

This project starts with a comprehensive literature review to obtain a fundamental understanding of the current state of knowledge and existing knowledge gaps in using RGGP in concrete as a cement alternative based on open sources, reports, literature, and related projects. By collecting and synthesizing available research papers and reports, committee documents, and testing protocols, comprehensive insights into (i) the types of waste glass for RGGP, (ii) the challenges in using waste glass as pozzolan in concrete, (iii) the influence of RGGP, metakaolin, and nano-silica admixtures on concrete performance, and (iv) the

applications of RGGP-modified concrete in civil infrastructure, were obtained. In addition, a fundamental understanding of the processing, treatments, and applications of RGGP was obtained and used to guide the concrete design in this project.

1.1.2. Task 2: Characterization of pozzolanic reactivity of RGGP

In Task 2, the pozzolanic reactivity of two RGGP materials was characterized. The research efforts include (i) quantification of the chemical and mineral compositions and degree of amorphousness of RGGP will be quantified, (ii) determination of the activation energy and reaction kinetics between RGGP and calcium hydroxide (which triggers the formation of C-S-H) will be determined, and (iii) investigation of the lime consumption capacity of RGGP as a direct evaluation of the pozzolanic reactivity. The lime consumption capacity of RGGP was determined via a lime consumption test after 1, 7, 28, and 56 days by quantifying the calcium hydroxide consumption using thermogravimetric analysis (TGA) and X-ray diffraction (XRD).

1.1.3. Task 3: Evaluation of cement hydration kinetics and phase evolutions

In Task 3, the research efforts were placed on understanding the influence of the incorporation of RGGP, at a variety of substitution levels, on the hydration behavior of cement, which is directly related to the properties of concrete. We started with thermodynamic simulation based on a geochemical modeling program (GEMs) to predict the phase assemblages of hydrated cement at different replacement levels and provide initial insights into the mixture design. The experimental activities of this task include uncovering the role of RGGP in modifying cement hydration and analyzing the influence of RGGP on the evolution of hydration products.

1.1.4. Task 4: Cement concrete mix designs incorporating RGGP and other alternative constituent materials

Based on the insights from Tasks 2 and 3, the emphasis of this task was placed on the development of concrete mix design formulations based on the RGGP-modified cement. Additionally, mix design formulations incorporating other alternative constituent materials were designed per the high-performance concrete formulations of MassDOT RMS and the recommendations from manufacturers of alternative constituent materials.

1.1.5. Task 5: Evaluation of cement concrete mix designs incorporating RGGP and other alternative constituent materials via fresh and hardened property investigations

In Task 5, the concrete formulations developed in Task 4 were evaluated based on the fresh and hardened concrete performance by investigating (i) workability (flowability), (ii) autogenous shrinkages of selected mixes, and (iii) mechanical strength. UMass Lowell and UMass Amherst prepared the raw materials for lab tests, including concrete groups with different dosages of RGGP and alternative materials other than the high-performance concrete formulations.

1.1.6. Task 6: Evaluation of concrete durability

The durability of the concrete mixes developed through Tasks 4 and 5 was preliminarily determined after their acceptable short-term performance was established. Concrete durability is an important property to ensure acceptable long-term performance in transportation infrastructure applications under extreme conditions. In Task 6, multiple durability properties, including permeability of concrete will be determined by following AASHTO T 358 (Standard Method of Test for Surface Resistivity Indication of Concrete's Ability to Resist Chloride Ion Penetration) and AASHTO TP 119 (Standard Method of Test for Electrical Resistivity of a Concrete Cylinder Tested in a Uniaxial Resistance Test), mortar bar test according to ASTM C1260 (Standard Test Method for Potential Alkali Reactivity of Aggregates (Mortar-Bar Method)), AASHTO T 380 (Standard Method of Test for Potential Alkali Reactivity of Aggregates and Effectiveness of ASR Mitigation Measures (Miniature Concrete Prism Test, MCPT)), AASHTO TP 142 Provisional Standard Method of Test for Accelerated Determination of Potentially Deleterious Expansion of Concrete Cylinder Due to Alkali–Silica Reaction (Accelerated Concrete Cylinder Test, ACCT), and rapid chloride penetration test per AASHTO T 357-22 (Predicting Chloride Penetration of Hydraulic Cement Concrete by the Rapid Migration Procedure), were tested to understand the influences of RGGP and alternative materials on the performance of concrete.

1.1.7. Task 7: Mock-up reinforced concrete sidewalk panels

In this task, sidewalk panels were fabricated and placed on the campus of UMass Amherst to evaluate the ease of placement, workability, and finishing in real-life settings for the concrete containing RGGP.

1.2 Problem statement

Concrete, the most fundamental construction material in the world, contributes towards 8% of global CO_2 emissions, in which the production of cement serves as the main governing factor contributing to approximately 90% of concrete carbon intensity [1]. Replacing cement with supplementary cementitious materials (SCMs), such as fly ash (FA) [2], silica fume (SF) [3], rice husk ash (RHA) [4], and slag [5], has been proven an effective approach to decrease the embodied carbon and improve sustainable and performance of concrete. Upcycling solid wastes from industry and daily life into SCMs not only diverts waste from landfills but also reduces the reliance on virgin materials, promoting resource efficiency, aligning with circular economy principles, and lowering environmental impacts

Among the current waste resources, recycled glass is considered a practical option with promising prospects owing to its abundant availability, wide distribution, and unique amorphous silica nature, which renders pozzolanic reactions possible in cement systems. Waste glass is a non-biodegradable material derived from waste streams like glass containers, plate glass, and E-glass that occupies significant landfill space. Its extreme underutilization is apparent as the United States reported disposal of 52.9% of the waste glass to landfill, and only 26.6% of the waste glass was recycled in 2017 [6]. As a promising avenue, upcycling waste glass into concrete pozzolans to partially replace cement has the potential to offer dual benefits of reducing landfill waste and enhancing concrete properties.

1.3 Objectives

The primary objective of this research project is to assess the viability of using RGGP in concrete as an alternative to traditional SCMs. The anticipated outcomes and deliverables for the tasks, either in whole or in part, are as follows:

- A comprehensive literature review and fundamental understanding of the current state of knowledge and existing knowledge gaps with the utilization of RGGP in concrete.
- A comprehensive understanding of the pozzolanic reactivity of RGGP and the approaches to enhance its reactivity.
- Insights into the hydration behavior of Portland cement containing RGGP in terms of hydration kinetics and phase evolutions.
- Development of cement concrete mix design formulations incorporating RGGP and other alternative constituent materials.
- Evolutions of physical, mechanical, and durability properties of cement concrete incorporating RGGP and other alternative constituent materials.
- Performance evaluation of RGGP-based cement concrete through mock-ups.

1.4 Concrete strength target and applicable material specifications

The performance targets of the concrete for this research project are defined by the Commonwealth of Massachusetts Department of Transportation Standard Specifications for Highways and Bridges, Division III: Material Specifications (MassDOT Specification) [7] for High Performance (HP) Concrete, specifically Section M4.06.2. HP Concrete should be designed and produced with precise proportions of the constituents to exhibit a homogenous composition. This composition should feature a well-distributed, spaced, and sized air void system and quality concrete properties, and is described further below:

The nominal 28-day compressive strength target of the concrete selected is 5,000 psi based on the Producer's approved 5,000 psi high performance concrete mix design. This approved mix was used as the control (refer to RMS 043 mix design sheed in the Appendices to this report). This mix includes a nominal maximum coarse aggregate size of ¾ in. and total cementitious content of less than 685 lb/yd^3 as required by MassDOT Specification Section M4 Cement Concrete and Related Materials. Relevant information from the Specification is shown in Table 1.1.

Table 1.1: Classification of HP Concrete

Class 28-Day Compressive Strength (psi)	Nominal Maximum Coarse Aggregate Size (in.)	Maximum Total Cementitious Content (lb/yd^3)
5,000	3/4	685
5,000	3/8	710
6,500	3/8, 1/2, 3/4	-
8,000	3/8, 1/2, 3/4	-

Admixtures must meet the standard specification for chemical admixture defined by AASHTO M 194 [2]. Although there is no limit for RGGP content in concrete mixtures, the total amount of SCM content is limited to 50 percent replacement of hydraulic cement. The ratio of water to cementitious material is limited to 0.40. Based on the MassDOT Specification, reinforced concrete or non-reinforced (plain concrete with nominal maximum aggregate size (NMAS) of ¾ in., should meet air content targets of 6% and 7.0%, respectively, as listed in Table 1.2. Any air-entraining admixture used in the concrete mix must meet the AASHTO M 154 [3] standard specification. A tolerance of ±1.5% in percentages is allowed. Moreover, a 1.0% reduction from the air content target is permitted for $f'_c \geq 5000$ psi.

Table 1.2: Air content target

NMAS (in.)	Reinforced Concrete (%)	Non-Reinforced Concrete (%)
3/8	7.5	7.5
1/2	7.0	7.0
3/4	6.0	7.0
1	6.0	6.5
1 1/2	5.5	6.5

Chemical admixture dosages are proportioned according to the admixture manufacturer recommendations and the requirement so AASHTO M 194 to obtain the required properties of HP Concrete. HP Concrete must also be formulated using 3.0 gallons of corrosion inhibiting admixture per cubic yard of concrete to increase the active threshold to 9.9 lb. of chloride per cubic yards of concrete at reinforcing bar level. Corrosion inhibiting admixture must meet the requirements of ASTM C1582 standard specification.

This page left blank intentionally.

2.0 Literature Review

In an effort to improve the sustainability of the concrete industry, innovative approaches are being explored towards enhancing its performance while reducing environmental impact. The traditional approaches of replacing cement in concrete involve the use of supplementary cementitious materials (SCM) such as fly ash (FA) [2], silica fume (SF) [3], rice husk ash (RCA) [4], and slag [5]. Among these approaches, the addition of Recycled Ground Glass Pozzolan (RGGP) is a promising prospect for replacing cement with existing waste materials due to its abundant availability and favorable chemical composition that results in effects like SCMs. Glass is a non-biodegradable material that occupies significant landfill space and thereby warrants alternative recycling options. The underutilization of ground glass as a sustainable material is apparent by the amount of landfilled waste container glass that is almost three times the recycled quantity [8].

The United States reported a disposal of 52.9% of the waste glass to landfills and recycled 26.6% of the waste glass in 2017 [6]. An increased demand for landfill space, along with the enhanced landfill taxes, has triggered an effort to find alternative methods for recycling waste glass and decreasing disposal costs while increasing the prolonged existence and preservation of the landfills. One of the most promising avenues for recycling waste glass is through the construction industry, with the possibility of partial replacement of cement-based materials. The feasibility of using RGGP as a pozzolan was first explored by Pattengil & Shutt (1973) [9], where soda-lime container waste glass was crushed below a 45 μm particle size. Since then, the number of studies on GGP has steadily increased, and beyond 2005, there is an exponential increase and a peak during the last 5 years, as shown in Figure 2.1.

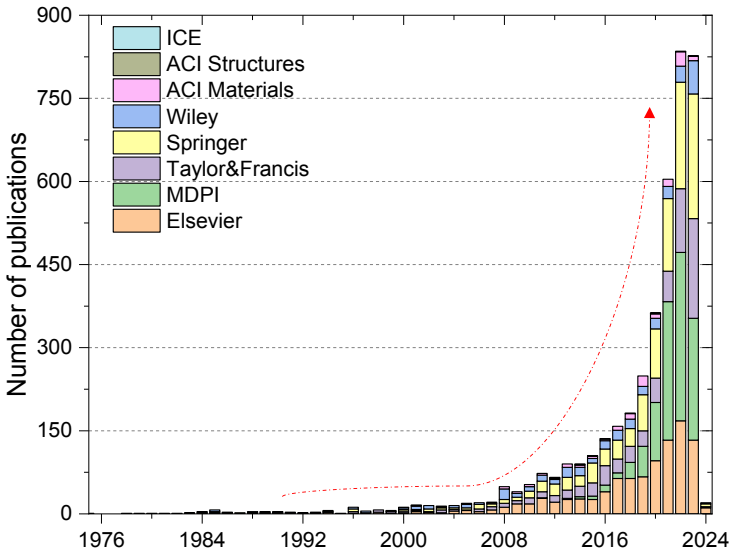

Figure 2.1: Distribution of annual number of publications for studies in RGPP (ACI: American Concrete Institution, MDPI: Multidisciplinary Digital Publishing Institute, and ICE: Institution of Civil Engineers).

2.1 Types of ground glass

Ground glass, sourced from various waste streams such as containers, plates, and E-glass, presents an opportunity to not only divert waste from landfills but also improve concrete properties through its pozzolanic characteristics. Based on the source, waste glass can be classified into container glass that is generally used in packaging, plate glass that is used in glazing buildings or automobiles, and E-glass that is used in fiber reinforced polymer (FRP) rebars.

Based on the distinctive oxide compositions (SiO_2, CaO, Na_2O_{eq}, Fe_2O_3, Al_2O_3, etc.), both container glass and plate glass can be classified into soda lime glass with SiO_2 and CaO contents in the range of 70-73% and ~10% while the E-glass has a lower SiO_2 and higher CaO contents around ~60% and ~21%, respectively [8]. Borosilicate glass, with highly variable SiO_2 content ranging between 60-80% and devoid of CaO and extraordinary chemical resistance and high temperature softening points, is unsuitable for use as a concrete material due to the high Na_2O_{eq} content of ~45%, which has the potential of triggering alkali-silica reaction (ASR) by supplying alkali ions [10]. Conversely, the compositions of soda-lime glass and E-glass, characterized by varying SiO_2 content and lower Na_2O_{eq} of ~13% and <1%, respectively, and with reactive properties, introduce a spectrum of possibilities for enhancing concrete matrices. Notably, the reactivity of E-glass (also known as Type GE) in mitigating ASR and the compatibility of Type GS glass (sourced from Bottle and Plate Glass) in mixes without reactive aggregates merit detailed investigation.

The comparative composition of the two RGGPs and with traditional SCMs such as fly ash, metakaolin, and silica fume is shown in Figure 2.2. Numerous studies have delved into the effects of ground glass on concrete properties, exploring replacement ratios, particle sizes, and their impact on fresh properties as well as early-age and long-term properties. Investigations have revealed intriguing correlations between particle fineness, CaO content, and compressive strength, delineating the nuances of glass pozzolans' influence on concrete formulations. The pozzolanic activity of RGGP was found to be heavily dependent on the particle size, where the particle size above 300 μm did not display pozzolanic activity and the pozzolanic properties were only achieved under a particle size of 45 μm [11]. Similar studies by Meyer et al. [12], Carpenter and Cramer [13] and Bazant et al. [14] showed that RGGP with particle size below 75 μm can be used to enhance the compressive strength of concrete and act towards mitigating ASR via their pozzolanic behavior. Another study found that soda lime RGGP crushed below 38 μm can be used to substitute 30% of cement and achieve 90% of the compressive strength at an early age and achieve 108% of the compressive strength after 90 days, along with reducing the ASR expansion by half [15]. Shayan et al. [16] found that the early-age strength is reduced with increased GGP content, whereas the strength continued to grow in later ages due to the pozzolanic reaction but still fell short of the regular concrete by around ~16.7% at a replacement level of 30% after 270 days.

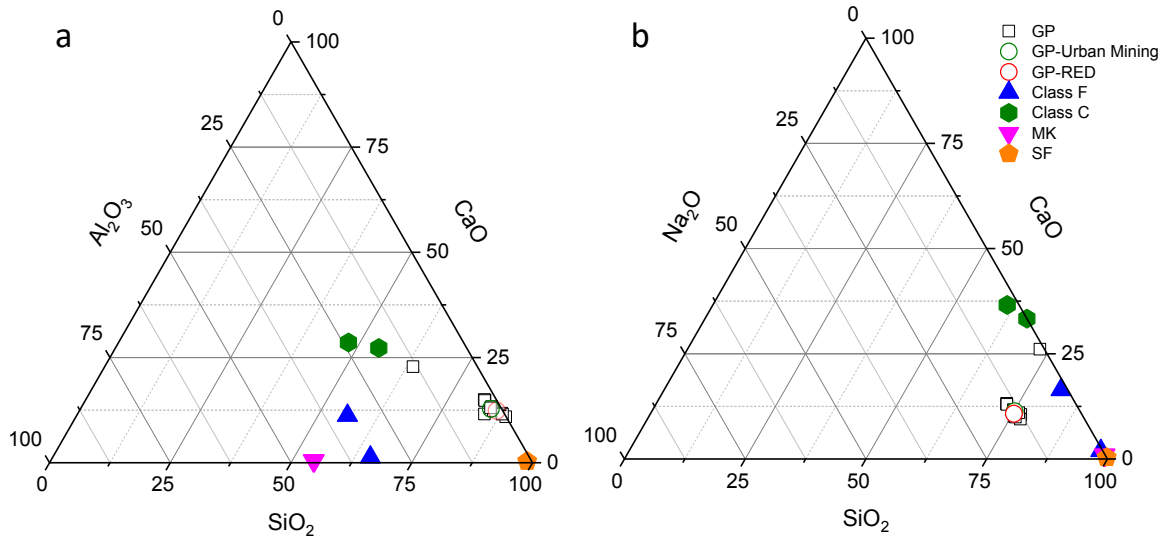

Figure 2.2: Ternary diagram showing the normalized weight percentages in (a) SiO_2-Al_2O_3-CaO and (b) SiO_2-Na_2O-CaO systems in different GP and SCMs (Class F: Class F fly ash, Class C: Class C fly ash, MK- Metakaolin, and SF- Silica fume).

2.2 Applications of glass in concrete

2.2.1. Use of RGGP as an SCM

Omran et al. [17] summarized a suite of research studying the use of RGGP as an SCM and concluded that it can improve workability, durability, structural properties, and lower embodied carbon. Aliabdo et al. [18] justified up to 25% replacement based on cube compressive strength across two grades of concrete, and identified the improvement of compressive properties over time. Zidol [19] ndicated that these properties stabilize after a year in concrete with 20 and 30% replacement levels, and that finer particles correlated with higher strength. Niang et al. [20] performed structural column tests on reinforced concrete columns and found that a 20% replacement performed comparably to the control specimen, with test-to-control ratios between 0.89 and 1.07.

In a study conducted by Liang et al. [21] the feasibility of substituting microsilica with RGGP in the preparation of MgO-SiO_2 formulation was explored with the aim of forming magnesium-silicate-hydrate (M-S-H). The experimental design involved the creation of several mixtures. Apart from the control sample, which consisted entirely of MgO, the other mixtures were composed of 50% MgO by weight, serving as the primary binder, and 50% by weight of microsilica and/or RGGP. The study found that a partial substitution of microsilica with RGGP, specifically a half substitution, was not only feasible but also beneficial. This substitution strategy was able to maintain the mechanical efficiency of the MgO-SiO2 binders. Furthermore, it offered the advantages of reducing the pH value of the concrete and achieving satisfactory hardening properties.

2.2.2. Combined use of RGGP as SCM and aggregate in concrete

Gebremichael et al. [22] studied the combined effects of waste glass utilized as cement replacement and aggregate substitution. The study involved 14 trials, each varying in grain size and replacement ration. The research posits that the substitution of cement, fine aggregate, and coarse aggregate with crushed and ground waste glass is feasible and suggests that the optimal replacement proportions are 10%, 15% and 20%, respectively. The researchers reported that despite these substitutions, the resulting concrete maintained acceptable properties in its fresh and hardened states and showed adequate durability.

2.2.3. Effect of chemical composition in glass

The performance of ground glass when used as pozzolan in portland cement concrete is primarily influenced by three factors: (1) its chemical composition, (2) the particle size distribution, and (3) the level of replacement. The study conducted by Christiansen et al. specifically investigated the effect of the chemical composition of RGGP on its performance in concrete. In this research, eighteen different waste glass streams from across the United States were analyzed for composition. The results obtained over the course of six months indicated that the composition of the glass mixtures tested had a significant effect on the pozzolanicity of the glass. This was evident in the varying compressive strength results, with the difference between the control and the lowest 90-day compressive strength being 33% for the mortars made with 20% glass replacement, and 40% for those made with 30% glass replacement. This suggests that not all glasses behave the same when used as a pozzolan. In particular, mortars made with soda-lime container glasses typically reached lower compressive strength than those made with plate and plate/container glasses. However, the E-glass surpassed even the control at 90 days, reaching the highest compressive strength at both 20 and 30% replacement levels [23].

2.2.4. Coarse Glass Powder

As previously stated, the particle size of pulverized glass is one of the main factors affecting the reactivity of RGGP in concrete. The research conducted by Kalakada et al. focused on the performance of coarse ground glass with a size below 150 micrometers as a supplementary cementitious material, highlighting the critical role of particle size in the reactivity of ground glass. The strength activity index (SAI) of the mixes consistently surpassed the required 75% at all curing ages and substitution levels, demonstrating the pozzolanic attribute of the coarser RGGPs. The replacement of cement with coarse RGGP resulted in higher compressive strength than the plain mix, with the highest strength improvement being 17% for a 30% substitution. A 30% substitution of cement with coarse RGGP significantly enhanced the resistance to chloride ion penetration by 32%, validating its use as a binder replacement for structures susceptible to corrosion induced by chloride ions. Most ground glass mixes exhibited greater shrinkage than the control mix, but all reported values of drying shrinkage were within acceptable limits. As the RGGP replacement level increased, the heat of hydration decreased, with the mix containing 30% glass replacement showing a maximum reduction of 24%. This suggests the potential use of ground glass in areas where mass concreting occurs to mitigate cracking arising from thermal stresses [24].

2.2.5. Reactivity of ground glass compared with other pozzolans

Kasaniya et al. evaluated the reactivity of various pozzolanic supplementary cementitious materials (SCMs). This research employed a range of test methods, encompassing the modified lime-reactivity test, the modified ASTM C311/C618 test, the R^3 heat release test, and the lime consumption test. In the context of supplementary cementitious materials, a spectrum of reactivity was observed. RGGP and coal fly ash were characterized by low to moderate reactivity. Limestone and ground quartz were distinguished by negligible or very low reactivity. Blended pozzolans exhibited moderate reactivity, while ground bottom ash was associated with high reactivity. Silica fume is notable for its very high reactivity. Natural pozzolans present a broad range of reactivity, spanning from non-reactive to highly reactive [25]. Suraneni et al. employed two distinct methodologies, namely the consumption of calcium hydroxide and heat release, to ascertain the reactivity of various SCMs, and both methodologies converged on the same conclusion, categorizing RGGP as a less reactive pozzolan [26].

2.3 Effect of glass powder on concrete properties

2.3.1. Fresh properties

2.3.1.1 Workability

The workability of concrete is considered a critical fresh property that can determine the feasibility of use in specific applications. The addition of SCMs has been known to have mixed effects on the workability. The variation of the slump of fresh concrete with the addition of RGGP is shown in Figure 2.3. While most of the studies showed an increased slump with glass powder replacement [18, 27-29], a few studies also showed the opposite trend [30-32] when measured according to ASTM C143. While some researchers attribute the increased slump to the low water absorption of the glass, which enhances concrete flowability by reducing aggregate friction [29], others believe the slump decrease is due to the non-spherical and rough geometry of milled waste glass particles [32].

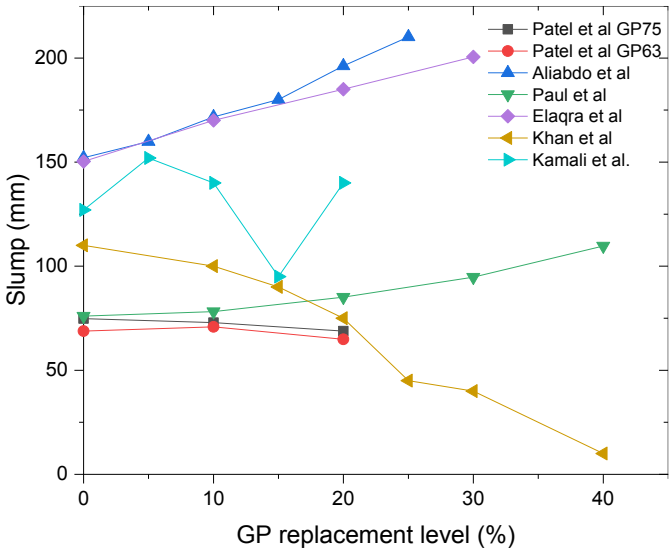

Figure 2.3: Effect of RGGP replacement level on the slump of fresh concrete.

A continuous increase of slump, measured using the same standard, was observed up to RGGP dosage of 40% [28]. Wang et al. [33] studied the effect of grinding method on RGGP-based concrete and found that the flow, at a w/cm ratio of 0.5 and RGGP replacement ratio of 10% and measured according to GB/T 8076-2008, increased by 5.6% and 14.8% when the RGGP was dry ground and ground in deionized water, respectively, but reduced by 15% when the grinding was carried out in ethyl alcohol. The slump flow of RGGP-modified concrete, at a water-to-binder ratio of 0.45 and measured according to EN-1015-3, showed an increasing trend with the RGGP dosage up to 20% replacement [34]. While Jiang et al. [35] believe the reason for the enhanced workability with RGGP dosage was due to the smooth surface of the RGGP particles, the authors suspect that the larger particle size might play a critical role. The flowability of RGGP-modified mortar with a water-to-binder ratio of 0.5, a mean particle size of 17.68 μm, and measured according to EN 1015–3, showed similar flow diameters for 10% and 25% replacement levels, while the flow reduced by 1.7% and 5.6% when the replacement levels were increased to 35% and 60%, respectively. Another study using the Australian standard AS 1012.3.1 found an increase in slump up to a replacement level of 30% followed by a reduction from 30% to 50% dosages for RGGP with mean particle sizes below 75 μm and 150 μm [36].

The reason for the enhanced workability of mixes with RGGP is most likely because of the lower water absorption of the RGGP compared to the cement, thereby causing an increase in effective water-to-cement ratio in RGGP-modified concrete. Workability enhancement from RGGP inclusion, which results in void micro-filling, becomes more effective with finer particles[29]. In another study, RGGP passing through a 75 μm sieve was found to improve the workability up to 83.3% for RGGP replacements up to 20% [37]. The flow of RGGP concrete, performed according to ASTM C1437, increased by 6.5% after replacing 30% of cement with RGGP with a mean particle size of 18.2 μm at a water-to-binder ratio of 0.45 and without the use of any chemical admixtures. SCMs like FA, SF, and RGGP all tend to improve the workability of the concrete, but the RGGP was found to be more efficient in

improving the workability than both FA and SF at a much lower superplasticizer content [38].

It is apparent that the substitution of cement by RGGP has shown both reduced and enhanced workability, and the effects are heavily dependent on the particle size and specific surface area of the RGGP, as well as the mix design of the concrete or mortar and uses of superplasticizer, as well as the method of flow or slump measurement.

2.3.1.2 Setting time

Setting time is a crucial property for cement that refers to the time it takes to convert the freshly mixed cement paste, mortar, or concrete from a fluid state to a solid state. It is widely reported that the setting time of cement can be changed by incorporating RGGPs into the cement matrix. However, some controversial results were obtained from different studies. On the one hand, the insignificant effect on both the initial and final setting times was found by Aliabdo et al [39] when up to 25% of cement was replaced by the RGGPs. Only a 2.5% increase in the final setting time of concrete was observed with a RGGP dosage increased to 30%, but since the additives of RGGPs can slow down the condensation of cement pastes at the initial stage, an 18.9% increase in initial setting time was obtained [35]. This is due to the relatively more water available for cement hydration due to the addition of RGGPs.

Compared with the native cement, the lower water absorption capability of RGGP leads to the increased efficiency of water content in the cement mixtures; thereby, the prolonged setting times were observed with the higher proportions of RGGP [40]. However, the prolonged setting time due to the incorporation of RGGPs was also attributed to the lower rate of hydration, as proposed by [41]. On the other hand, a few researchers [42] have observed the shortened initial and final setting times with the higher dosage of RGGPs used in the cement matrix. Moreover, the grinding process may impact the effect of RGGP on setting time. For example, dry ground RGGP was found to increase the initial and final setting time at 10% dosage and measured according to GB 1346–2011, by 5.2% and 1.8%, while grinding in deionized water reduced both the initial and final setting times by 6.7% and 8.6%, respectively [43]. The lowest initial and final setting time was found for the RGGP ground in ethyl alcohol, and it was 33.3% and 24.5% lower than the Ordinary Portland Cement (OPC) samples.

2.3.2. Hardened Properties

2.3.2.1 Shrinkage

One of the critical hardened properties of the RGGP-modified concrete is the changes in chemical and autogenous shrinkage behavior. The shrinkage behavior is directly related to the hydration of concrete, which is altered after adding RGGP, and excessive shrinkage can cause cracks, causing durability issues in concrete structures. After 48 hours of hydration, the normalized chemical shrinkage of RGGP-modified mortars, measured according to the gravimetric method, showed up to a two times increase when the RGGP dosage was increased to 60% [43]. The reason for the enhanced shrinkage might be due to the greater availability of water for cement hydration by increasing the effective water-to-cement ratio.

Another reason for enhanced hydration and shrinkage might be the rapid reaction between the C_3A and the alkali supplied by the RGGP, as also observed by Yodsudjai and Wang [44].

Chemical shrinkage measurements according to ASTM C1608, in 20% RGGP-modified concrete where the RGGP had a mean particle size of 8.4 μm and the water-to-binder ratio was fixed at 0.4, showed an enhanced chemical shrinkage of up to 14.7%. The chemical shrinkage was higher for the RGGP with a greater CaO and AlO_2 and lower SiO_2 content. Another study measured drying shrinkage of RGGP-modified mortar with 20% replacement of different-sized RGGP using the BS ISO, Part 8: 1920, and found that the shrinkage after 7 days was reduced with increasing fineness. The reduction in shrinkage was attributed to the dilution effect of the cement with the RGGP replacement that increased the effective water-to-cement ratio [45]. The drying shrinkage was reduced by the addition of 10% RGGP. The reduction was most prominent amongst the RGGP-modified concrete when compared to other SCMs such as FA and SF, where the SF showed a greater shrinkage than the control concrete specimens [46].

2.3.2.2 Creep

Apart from the strength and durability, another important property that determines the serviceability of concrete structures is deformation. One of the major contributions to long-term deformations is creep, that is, deformation under constant loading. The effect of replacing cement with various SCMs such as slag, RCA, and metakaolin is known to have a significant impact on the creep behavior of concrete. While ground granulated blast furnace slag (GGBFS) can increase the creep strain due to slower hydration [47], RCA and MK were found to reduce the creep strains [48, 49]. The evolution of creep strain and creep coefficient for different studies and in different exposure conditions is summarized in Figure 2.4. A study by He et al. showed that the creep strain and creep coefficient decreased with the addition of RGGP, and the lowest creep strain was found to be 20% replacement [50]. Another study showed that after 60 days, the creep deformation was reduced with the addition of RGGP in the dry condition, where desiccation in the air was allowed. At similar RGGP replacement, samples where the water loss was prevented showed a higher creep. Again, in line with the other studies, the 20% RGGP replacement showed the lowest creep rate than the 40% RGGP replacement [51]. RGGP performed better in terms of lowering creep deformation in comparison to FA that increased the creep and SF, which did not affect the creep significantly.

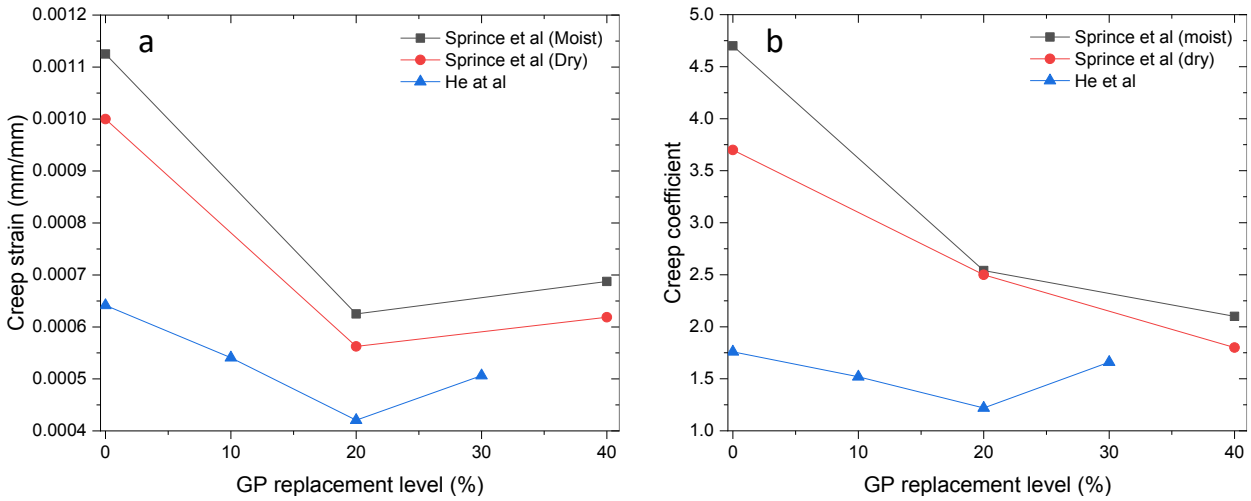

Figure 2.4: Effect of GP replacement level on the (a) creep strain and (b) creep coefficient of concrete [50, 51].

2.3.2.3 Compressive strength

According to ASTM C618 [52], the 7-day and 28-day strength activity index (SAI), computed by dividing the compressive strength of the sample containing pozzolans by the compressive strength of the pure cement group, can be used to evaluate the pozzolanic reactivity of pozzolans, which determines the impact of pozzolans on cementitious systems [53]. For materials to pass the requirements of ASTM C618, either the 7-day or 28-day SAI must be at least 75%.

Figure 2.5a summarizes the SAI of samples containing various dosages of RGGP. It can be seen that most of the groups have an SAI higher than 75%, which meets the requirements of ASTM C618. Moreover, the average SAI increased from 95.9% to 104.7% when the replacement level of RGGP increased from 2.5% to 5%. When the replacement level further increased, however, the SAI decreased, except for the dosage of 45%, showing an SAI value of 104.2%, which might be due to the limited data available. When the replacement level increased to 60%, the lowest averaged SAI value of 69.8% was obtained, which is lower than 75% as proposed by ASTM C618. Therefore, the higher dosage of RGGP can negatively impact the compressive strength of concrete, and it was widely reported that the optimized compressive strength of concrete can be reached when the RGGP replacement level is within the range of 10%-25% [18, 54]. The higher dosage of RGGP in concrete can negatively affect the physical properties of concrete, as the RGGP can dilute the cement and also the pozzolanic reaction is restricted due to the limited resource of calcium hydroxide from cement hydration when the filler effect dominates the role of RGGP in concrete [55, 56].

Figure 2.5b exhibits the evolution of SAI over time. It can be seen that the initial averaged SAI after 1 day was only 66.1%, and then increased over time, eventually reaching 112.7% after 365 days. It is also widely reported that the pozzolanic reaction of RGGP in concrete mainly occurs in the long term, i.e., after 28 days [57]. Idir et al. [58] systematically investigated the relationship between the relative strength of mortars and the fineness of

RGGP. Firstly, the results from this study demonstrated that increasing RGGP dosage from 10% to 40% generally reduced the compressive strength. Then, the pozzolanic reaction of RGGP can be observed after 28 days, which compensates for the strength loss caused by the dilution effect. This compensation is due to the pozzolanic reaction of SiO2 in glass with CH, forming an extra binding gel of CSH. This additional binder, resulting from the interaction of RGGP with available lime, contributes to the development of strength over time [29]. Moreover, with the decrease in particle size, the pozzolanic reaction of RGGP can be dramatically enhanced. In addition, based on the research conducted by Kasaniya et al., neither the low-alkali nor high-alkali RGGP mixes achieved 7-day strength parity with the 100% Portland cement control mix. These mixes, which utilized low-alkali and high-alkali RGGP as their supplementary cementitious material (SCM) and were considered to have low to moderate reactivity, demonstrated a significant increase in strength between the 28 and 91-day marks. However, while the mix incorporating low-alkali RGGP exceeded the strength of the control mortar at 91 days, the high-alkali mixes, despite showing a substantial strength increase, still fell short of the 91-day strength of the control mix [59, 60].

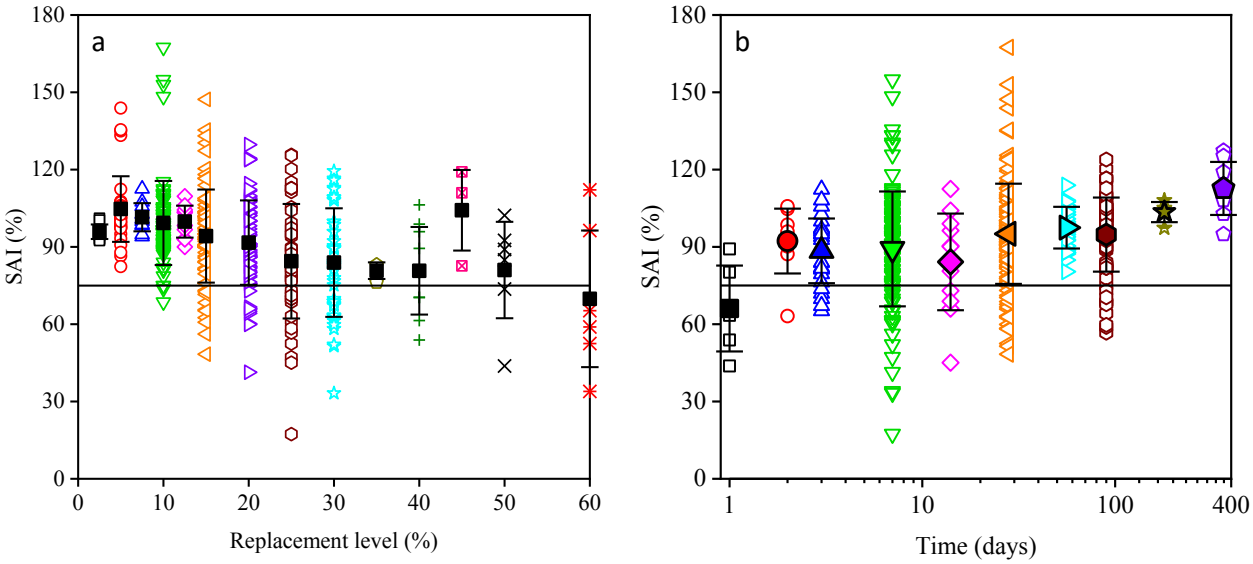

Figure 2.5: Evolution of Strength activity index (SAI) with (a) RGGP replacement level and time (data collected from [18, 24, 27, 35, 43, 50, 54, 55, 57, 61-73]).

2.3.2.4 Tensile strength

Although concrete splitting tensile strength (f_{sp}) is not considered in the design calculations for structural elements, measuring it helps to determine the occurrence of concrete cracking. Given that the cracks open when the internal strains in concrete overcome its tensile strength value. Figure 2.6 summarizes the relative tensile strength (=tensile strength of the sample containing RGGP/tensile strength of the control group ×100%) collected from publications. It can be seen that the relative tensile strength was generally decreased with the higher dosage of RGGP incorporated into the samples. 5% of RGGP replacement showed the highest averaged relative tensile strength of 110.0%, while it decreased to 98.8% and 83.4% with higher RGGP dosages of 15% and 30%, respectively. The improved tensile strength at the low replacement level (i.e., <10%) might be due to the pozzolanic reaction, filler effect,

and the improved bonding between the cementitious matrix and aggregate [74]. However, the dilute effect of RGGP with a higher replacement level dominates the tensile strength gain of the concrete, which leads to decreased tensile strength [75]. However, it has also been observed that the formation of hydration products and a decrease in the porosity of the concrete containing glass, result in an optimal bond between the adjacent cement paste and glass, leading to the attainment of the maximum split tensile strength for mixes containing a 20% glass mixture [29].

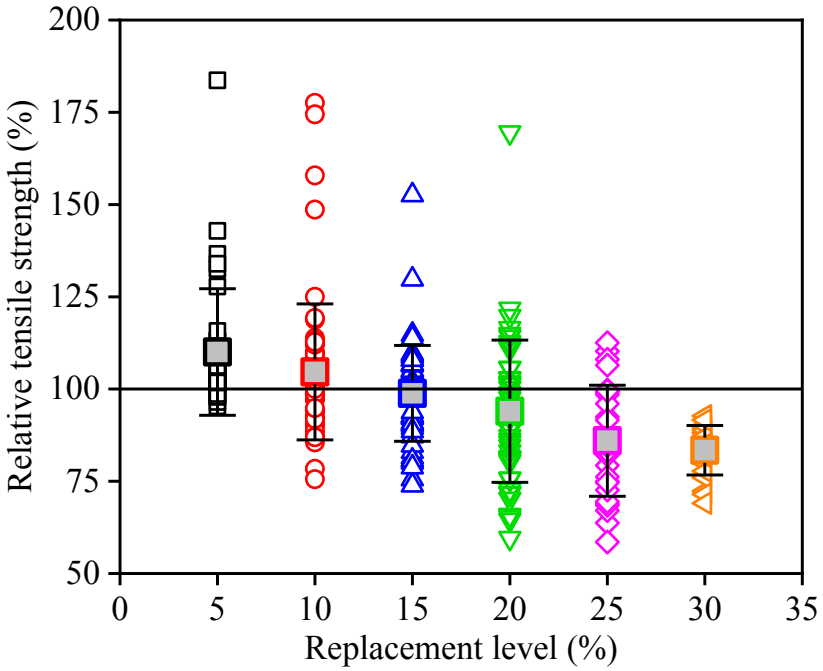

Figure 2.6: Relative tensile strength of mortars/concrete containing various dosages of RGGP (data collected from [55, 69, 70, 76-89]).

2.3.2.5 Flexural strength

The relative flexural strength of mortars/concrete containing different dosages of RGGP is summarized in Figure 2.7. It can be seen that the flexural strengths of mortars/concrete follow a similar trend to the compressive strengths, which is consistent with the observations as reported in various publications [90-92]. With the addition of RGGP up to 25% of replacement, the relative flexural strength of the samples is higher than 100%, indicating better performance in flexural strength of the modified samples than the control one. Especially, the highest average relative flexural strength, with the value of 125.5%, was reached when 15% of RGGP was incorporated into the concrete. Therefore, the optimized dosage of RGGP in terms of flexural strength is about 15%. However, when the RGGP replacement level increased to 30%, the average relative flexural strength was lower than 100%, showing a value of 86%.

Another study indicates that the flexural strength of the concrete, like compressive strength, initially decreases with RGGP addition. However, in the long term (28 and 56 days), it improves with up to 20% glass substitution, then declines [29]. Therefore, it can be

concluded that the flexural strength of concrete can be satisfied by the higher dosage of RGGP. The increase of flexural strength in the low replacement level might be due to the densification of microstructure by pozzolanic reaction and the filler effect of RGGP. On the contrary, the dilution effect and limited pozzolanic reaction with the consumption of calcium hydroxide in the system might contribute to the decreased flexural strength when a higher dosage of RGGP was used. Again, the negative impact on the flexural strength of modified concrete with a high dosage of RGGP is still a challenge to using RGGP in concrete applications.

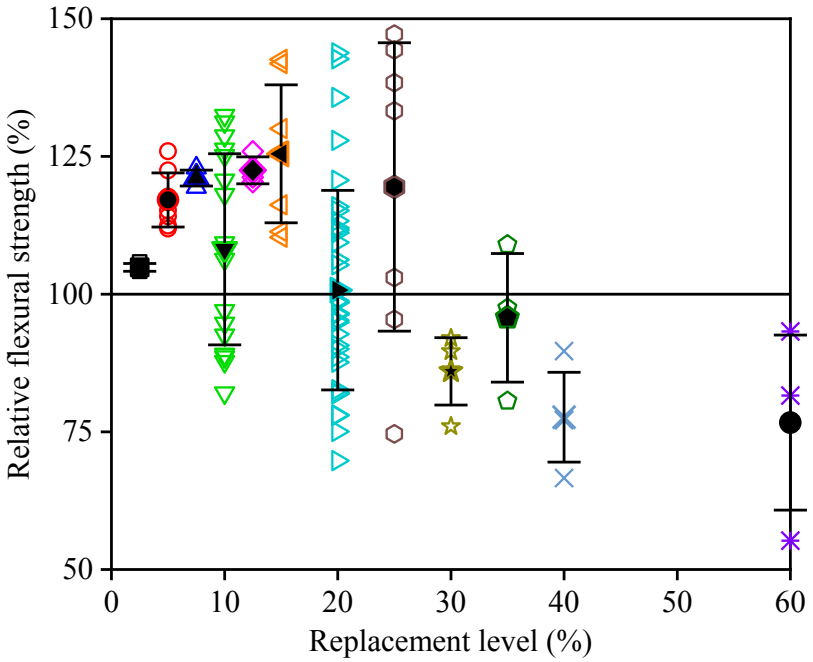

Figure 2.7: Relative flexural strength of mortars/concrete containing various dosages of RGGP (data collected from [43, 69, 75, 90, 91, 93-95]).

2.3.2.6 Young's modulus of elasticity

The addition of RGGP also affected the value of Young's modulus of elasticity (E) of concrete. After 28 days of curing, Young's modulus of elasticity increased with up to 20% addition of RGGP and declined when more than 20% of RGGP was incorporated into the concrete, as indicated by Ahmad et al [29].

2.3.3. Transportation properties

2.3.3.1 Water absorption

Water absorption is an important property that determines the durability of concrete and can lead to major deterioration via freeze-thaw damage, chloride penetration, carbonation, and sulfate attacks. Lowering the water absorption by adding SCMs can have a positive impact on the long-term concrete performance in aggressive conditions. The variation of water absorption in RGGP-modified concrete with replacement levels and mean particle size is

shown in Figure 2.8. The water absorption test, according to ASTM C642, showed that 10% replacement of RGGP can reduce the water absorption by 16.7% [38]. Using the same methodology, continuous reduction in water absorption was observed up to 15% at a 40% RGGP replacement level that is considered mainly due to the densification of the pore structure via pozzolanic reactions [28] and is in line with observations from other studies that show 34% and 15% reduction at a 20% RGGP replacement [18, 30]. The grade of mix had a positive effect on reducing the water absorption at similar RGGP replacement levels. Synergistic effects of RGGP with other SCMs such as FA and SF were also found to reduce the water absorption than the control specimen, and the replacement level had a positive impact. However, the GP alone could reduce the water absorption more efficiently than in conjunction with FA and SF [38].

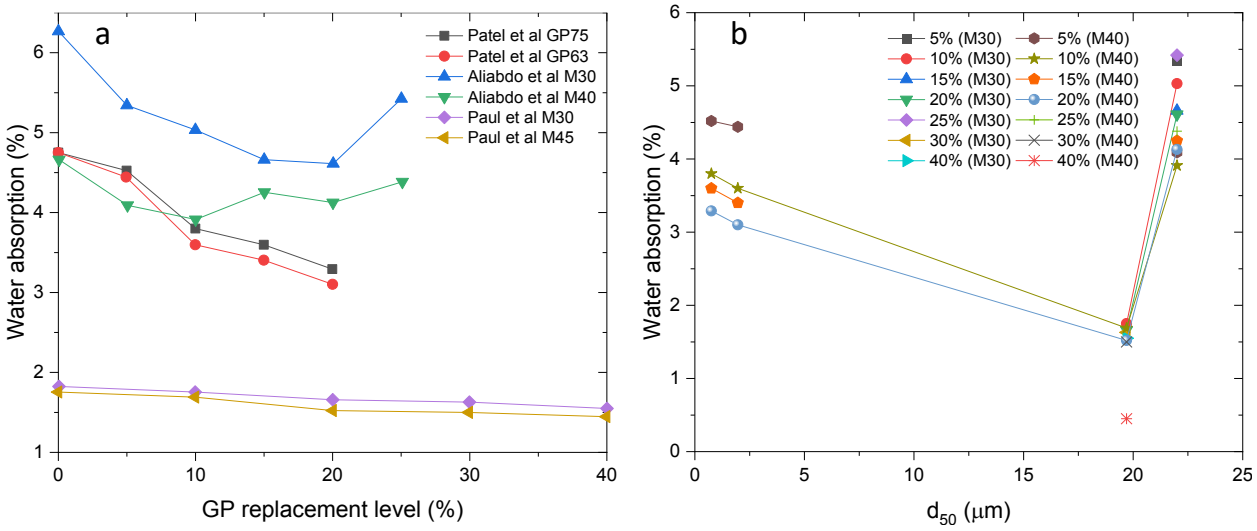

Figure 2.8: Variation of water absorption of concrete with (a) RGGP replacement level and (b) mean particle size d_{50} [18, 28, 30].

Although most studies showed that RGGP can decrease water absorption, one of the studies showed an increase in water absorption with an increase in RGGP replacement from 20% to 25% [18]. Also, similar dosages of FA and SF were found to outperform the RGGP by reducing water absorption by 55.6% and 43.5%, respectively [38]. Water absorption, measured according to the RILEM recommendations, showed that at an early age (14 days) the mortars made with 10% RGGP replacement show a higher and lower absorption than the control samples and the sample with 10% FA. At a later age, the FA-modified concrete outperforms the RGGP-modified concrete, indicating that initially the FA acts as a filler but shows a better pozzolanic performance in the long term [54].

2.3.3.2 Permeability and pore size

Another measure of the permeability of concrete is usually measured according to ASTM C642, which is an indirect method that measures the bulk density of concrete. The RGGP-modified concrete showed a decreasing bulk resistivity with the increase in RGGP content and reached the minimum values at 45% and 30% RGGP after 28 and 91 days, respectively.

The increase in water absorption and permeable voids at later ages beyond a 30% replacement level may be due to the dissolution of unstable hydrates at higher RGGP replacement levels [96]. Similarly, another study showed a reduction in bulk density with RGGP replacement level, while the water absorption was decreased. The RGGP with a greater particle size (d_{50}=1.96 μm) showed a greater bulk density and lower moisture absorption at comparative replacement levels than the smaller-sized RGGP (d_{50}=0.75 μm) [75]. Comparison with FA and SF showed that RGGP can improve the electrical resistivity, an indirect measure of permeability, more significantly [97].

In a study by Du et al. [96], the pore-size distribution evaluated via mercury intrusion porosimetry (MIP) becomes more refined with the increase in RGGP content, but the pore volume stays the same, along with a reduction of median pore diameter. Similar findings were reported by Lu et al. [45], where the pore structure was refined as the fineness of the RGGP increased. The addition of RGGP reduced the overall porosity at 10% and 20% replacements, whereas increasing the RGGP replacement to 30% increased the total porosity, which may be due to the degradation of the microstructure [50].

2.3.3.3 Chloride penetration

An important transport property of concrete is the chloride diffusion that may cause degradation via corrosion of reinforcements. It is desirable to have a low chloride penetration rate in concrete that can enhance the long-term durability of concrete structures. The resistance to chloride penetration, measured as the charge passed in the rapid chloride penetration test (RCPT), is shown in Figure 2.9. RCPT, according to ASTM C1012, showed that a replacement level of 20% was capable of reducing the chloride permeability of field concrete by 62.2% and 64.9% after 56 days and 90 days, respectively, and the chloride permeability decreased with increased dosage of RGGP up to 30% [98]. At an early age (14 days), the pore refinement by the addition of RGGP can lower the chloride penetration than the control concrete, but FA shows a greater reduction. However, at a later age (91 days), the RGGP outperformed the fly ash due to the enhanced pozzolanic reaction. The RCP value also depends on the conductivity of the pore solution and may have influenced the results to show a higher RCP value due to the greater supply of alkali ions by the RGGP as compared to cement and fly ash [54]. Another comparative study between RGGP and FA showed that both the SCMs are capable of reducing the RCP values compared to plain concrete, but the RGGP showed a more efficient reduction in RCP values than FA, despite having a more conductive pore solution due to the release of a greater amount of alkalis [99]. A high replacement ratio of 40% RGGP was found to reduce the RCP by up to 37.5% due to the synergistic effect of pozzolanic reaction that produces C-S-H to plug the pores and reduce connectivity, as well as the ability to perform as a micro filler and provide optimum particle packing [28]. These results are in agreement with field tests that showed resistance to chloride ion penetration increases with RGGP replacement level by 65% after 90 days [100] and laboratory tests that show that high-volume RGRGP replacement (60%) can reduce the RCP by a remarkable 90% [72].

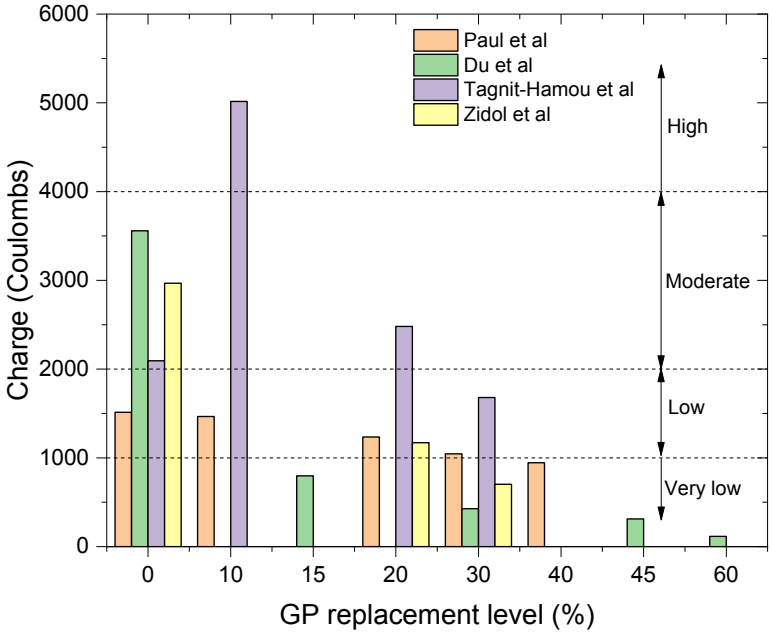

Figure 2.9: Effect of RGGP replacement level on the resistance to chloride penetration of concrete [28, 72, 98, 101].

The chloride migration coefficient according to NT BUILD 492 test was found to decrease by up to 88.9% with the 45% replacement of soda-lime RGGP with a mean particle size of 3.4 μm, along with a monotonous decrease of chloride diffusion up to a RGGP replacement level of 60% [96]. Another study following the same method showed that RGGP was capable of reducing the chloride migration coefficient more significantly than slag and FA after 28 days. RGGP performed similarly to SF after 180 days at both low and high replacement ratios 25% and 50% [102]. Resistance to chloride penetration after 91 days, evaluated using the Resipod method, which is in compliance with AASHTO TP 95, showed a reduction in resistivity with the addition of RGGP (d_{50}<150 μm) up to a dosage of 30% followed by an increase from 30% to 50% [36]. The reason for the enhanced resistivity at 50% RGGP replacement may be due to the synergistic effect of pozzolanic activity and filler effect that causes a refinement of the concrete microstructure. The RGGP levels up to 30% replacement showed chloride penetration resistance values that were classified as high risk, warranting further research into concrete durability after adding RGGP. Curing under an elevated temperature (40°C) had a positive impact on the chloride resistivity of RGGP-modified concrete up to a replacement level of 30%, which is most likely due to the enhanced hydration and pozzolanic activity at a higher temperature [36]. The study by Kasaniya et al. corroborates the observation of resistivity increasing with age. Even though both low and high-alkali RGGP demonstrated lower resistivity at the 7-day mark compared to the 100% Portland cement control mix, they both exhibited an increase in resistivity at 28 days, surpassing that of the control mix. Furthermore, at 91 days, a significant rise in resistivity was observed for both types of RGGP used [60]. Chloride penetration was reduced by adding the RGGP after 28 days and was comparatively higher and lower than the SF and FA, respectively, indicating that SF has a better resistance to chloride penetration compared to RGGP which may be due to the increased conductivity caused by the high amount alkali ions

supplied by the RGGP as compared to FA, SF, and cement [46]. Another study showed that the chloride diffusion coefficient, measured according to NT Build 443, can be reduced by the addition of RGGP, but the reduction was lower than FA and SF, where SF can be the most effective [97]. Similar findings also indicated that RGGP could lower the chloride migration coefficient more efficiently than slag and FA at a later age, but not SF [102]. The reason for this may be that the early-age pozzolanic activity of RGGP is slow, and the high Na_2O content in RGGP might increase the conductivity of the pore solution in concrete.

2.3.4. Durability

2.3.4.1 Acid attack

For concrete structures to last for their entire service life, durability parameters play a crucial role, while resistance to deterioration of concrete when exposed to an acidic atmosphere (i.e., hydrochloric acid, HCl or sulfuric acid, H_2SO_4) is also an alarming concern. When exposed to such a medium, concrete longevity reduces, which starts with acid damage [103]. This damage normally indicates the growth of reaction products that strip out the concrete surfaces, leading to changes in the mass, size, and shape of the concrete [104]. In the case of HCl attack, the general process of corrosion for C-S-H and $Ca(OH)_2$ is as follows [105]:

$$3CaO{\cdot}2SiO_2{\cdot}3h_2O(s)+6HCl(aq) \rightarrow 3CaCl_2(aq)+2SiO_2(s)+6H_2O$$

$$Ca(OH)_2+HCl \rightarrow CaCl_2+2H_2O$$

Migration of sulfate ions into concrete has been reported to cause chemical reactions in that acids can react aggressively with calcium hydroxide from cement hydration products and lead to the production of highly soluble calcium sulfate and gypsum, as follows [106]:

$$Ca(OH)_2+ H_2SO_4 \rightarrow CaSO_4+2H_2O$$

$$CaSiO_2{\cdot}2H_2O+ H_2SO_4 \rightarrow CaSO_4+Si(OH)_4+H_2O$$

$$3CaO{\cdot}Al_2O_3{\cdot}12H_2O+3(CaSO_4{\cdot}2H_2O)+14H_2O \rightarrow 3CaO{\cdot}Al_2O_3{\cdot}3CaSO_4{\cdot}32H_2O$$

The primary reaction product manifested on the concrete surface is gypsum, which is associated with volume expansion (factor of 2.2 compared to the volume of reactants), which can induce tensile stresses in concrete, resulting in cracking and spalling [107]. If not washed out, the accumulation of gypsum on the surface of concrete may slow down the corrosion rate due to surface sealing [108]. Further reaction of gypsum with calcium aluminate phases in the cementitious matrix can form ettringite, which has a greater volume increase (up to a factor of 7) than that of gypsum, thus leading to more micro- and macro-cracking. In addition, sulfuric acid decomposes the cementitious matrix by decalcifying C–S–H, thus contributing to strength loss [109].

ASTM C 267 [110] is normally used for evaluating the resistance of concrete to acid attack, which immerses the samples in an acid solution (either HCl or H_2SO_4) with a pH value

between 1 and 1.5. It was reported [103] that the mass of samples increased during the early-age curing in an acid solution due to the absorption of the acid solution and leading to the formation of products. In this stage, a lower mass increase was observed in the groups containing RGGP. Then, in the long term (i.e., after 90 days), mass loss was found in the concrete, while RGGP contributed to the lower mass loss, indicating that less mortar paste was being lost on continued exposure [111]. The lower mass loss due to the incorporation of RGGP indicates the reduced damage to concrete. As reviewed by Mansour et al. [112], the optimum replacement level of RGGP in concrete for acid attack resistance is 10-20%, which is consistent with the mechanical properties as summarized above. This explains that RGGP incorporation reduces the calcium oxide content of the binder and leads to low production of calcium hydroxide compared to the control mix. The pozzolanic reaction of RGGP consumes part of the calcium hydroxide and clings to the aggregate surface, forming secondary C-S-H, which enhances the density of cement paste around the aggregate [113]. However, values for loss in compressive strength are observed at higher RGGP replacement levels (i.e., >20%) in concrete [64], This may be because of the increased proportion of blends, due to which enough bond strength is not achieved, resulting in lower compressive strength [103, 114].

2.3.4.2 Sulfate attack

Sulfate attack is a significant durability concern for cement-based materials that threaten many concrete structures. External sulfate attack in concrete primarily includes the formation of ettringite ($3CaO \cdot Al_2O_3 \cdot CaSO_4 \cdot 32H_2O$) and gypsum ($CaSO_4 \cdot 2H_2O$). Ettringite is a primary hydration product associated with expansion, cracking, and spalling [115]. Sulfate comprises different types, namely, calcium, sodium, magnesium, and potassium. The performance of pozzolans in terms of controlling expansion due to sulfate exposure was not only influenced by the pozzolanic reactivity of materials but also by the chemical composition and substitution level. As reported, the utilization of ground glass fibers as a pozzolan to partially replace 30% of cement reduced the expansion of mortar bars under sulfate attack by 88.9% [116]. It is concluded that RGGP depleted the amount of calcium hydroxide, which is vulnerable to sulfate attack, by reacting pozzolanically [97]. A refined and tortuous pore network due to the formation of additional C-S-H in the incorporation of RGGP was observed, which increased the resistance to sulfate ion penetration.

Another study performed by Durgun and Sevinc [117] also found that the optimal replacement level for RGGP in compressive strength after sulfate attack was 5% for 28 days, while it increased to 10% in 360 days. The increased optimal dosage in the long term again revealed that the pozzolanic reaction of RGGP normally occurred in the long term. In addition, based on the results of the research conducted by Kasaniya et al., RGGP was found to be very efficient in improving sulfate resistance, with both low-alkali and high-alkali glasses resulting in blended cements with a very high level of sulfate resistance (less than 0.10% expansion at 18 months) [59]. According to the findings of Esselami et al., when 20% of High Sulfate Resistance Cement (HS) is substituted with RGGP, it results in a delay in deterioration, a contrast to the effects observed with plain HS cement. On the other hand, the replacement of 10% of the cement with limestone leads to an accelerated rate of damage [118].

2.4 Challenges of using glass powder in concrete

2.4.1. Size and amorphous silica supply (alkali-silica reaction)

RGGP can be used to substitute natural sand as a fine aggregate [119, 120]. Additionally, widespread use of glass powder as a binder substitute has been studied, where the glass powder has been crushed to a fine powder and used to induce pozzolanic reactions and form a dense matrix that can enhance strength [18, 121]. However, the most common concerning factors regarding using RGGP as a construction material are its potential to initiate expansion and cracking due to alkali-silica reaction (ASR), a deleterious reaction that is triggered by the combination of amorphous silica from aggregates and alkali from the concrete pore solution, resulting in the formation of a hygroscopic and expansive gel that causes internal stresses and cracking in concrete [122].

Due to the high content of amorphous silica (~70% by wt.), the RGGP used as aggregate might react with the alkali in cement. Mortar bars made with RGGP with a particle size less than 300 μm were found to have less than 0.1% expansion, which is considered below the threshold of harmful ASR expansion according to ASTM C1260. However, the pessimum size for innocuous behavior was found to be heavily dependent on the glass type and color, which governs their reactivity.

The clear soda lime glass showed the maximum reactivity, followed by the amber glass, while the green glass caused the maximum expansion [123]. The ASR was triggered when coarse glass aggregates were above the pessimum quantity of 20%, but the ASR was mitigated by substituting part of the cement with 25% of fly ash [124]. The evolution of ASR expansion with the RGGP replacement level and the particle size at different ages is shown in Figure 2.10 [125]. The RGGP with a particle size between 38 μm and 300 μm showed a decreasing ASR expansion with enhanced replacement levels (Figure 2.10a to 2.10d). For the RGGP with particle size between 300 μm and 900 μm, the trend reversed, and the ASR expansion increased with replacement level (Figure 2.10d and 2.10e). Another study found that glass aggregates smaller than 600 μm were found to participate in pozzolanic reaction in the presence of portlandite and thus does not participate in ASR [126]. Moreover, the ASR was found to occur only within the cracks of the glass aggregates, while the interparticle zone between the cement paste and glass aggregates is dominated by the pozzolanic reaction to form C-S-H.

The critical size of the glass aggregates was further elucidated by Corinaldesi et al. [127], who found that glass aggregates with a size between 36 μm and 50 μm can be used to replace 70% or regular aggregates without incurring ASR-related damage. Hence, glass aggregates with surface cracks, microcracks, and pores were found to be more prone to ASR. In support of the above evidence, RGGP with a mean size of 10 μm was found to reduce the ASR expansion with replacement level, where the maximum dosage of 30% was found to perform better than slag and SF and reduce expansion below the criterion of ASTM C1260 [128]. Similarly, Afshinnia and Rangaraju [129] uncovered the pozzolanic behavior of the RGGP with a mean size of 17 μm and 70 μm that was capable of replacing glass and argillite

reactive aggregates and reducing the expansion by 95% and 85%, respectively, at a dosage of 30%. Other studies using RGGP for ASR mitigation found 87.5% [130] and 95.8% [131] reductions in expansion via 30% substitution of RGGP with particle size below 100 µm. Another study showed that glass aggregates with a nominal size of 2.5 mm can be used to replace up to 40% of natural aggregates without triggering ASR [132]. Therefore, the major factors governing the ASR potential of the glass aggregates include the chemical properties such as silica and alkali content, replacement level, the particle size, concrete mix design and the water to binder ratio.

Based on the research conducted by Kasaniya et al., the low-alkali RGGP was efficient in controlling ASR, reducing expansion by almost 75% compared to the control. On the other hand, high-alkali RGGP was not effective in controlling expansion at a 25% level of replacement. The mortar containing 25% high-alkali glass expanded slightly more than the control at 56 days. However, increasing the level of replacement of high-alkali RGGP to 40% resulted in a significant reduction in expansion, but neither of these combinations reduced expansion by more than 75% compared with the control. The proportion of a pozzolan required to prevent deleterious ASR expansion was highly dependent on the reactivity of that pozzolan, and the extent to which ASR was suppressed was reliant on the equivalent alkali content of the RGGP. Therefore, while RGGP can help mitigate ASR, their effectiveness varies depending on their alkali content and the proportion used in the concrete mix [59].

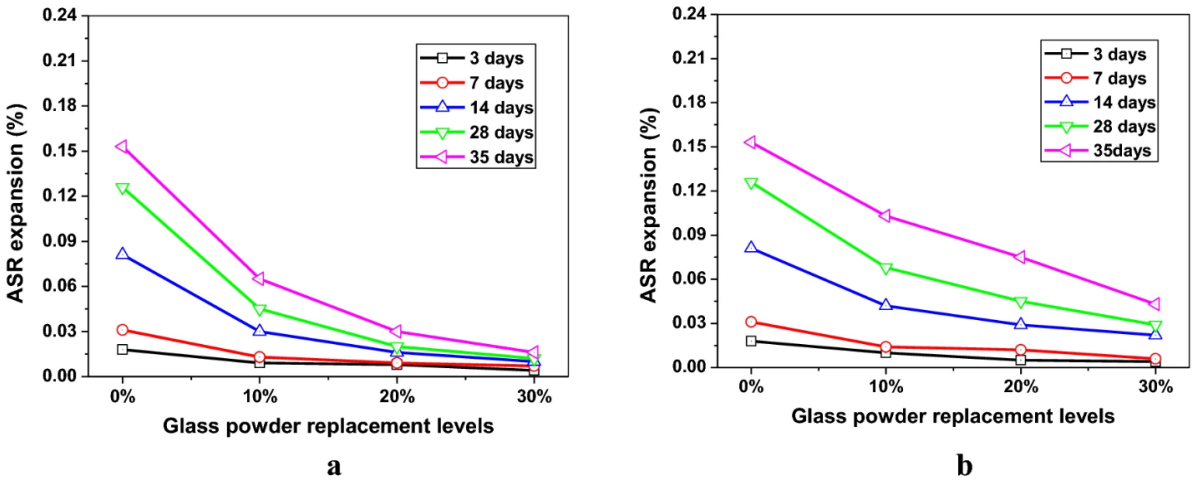

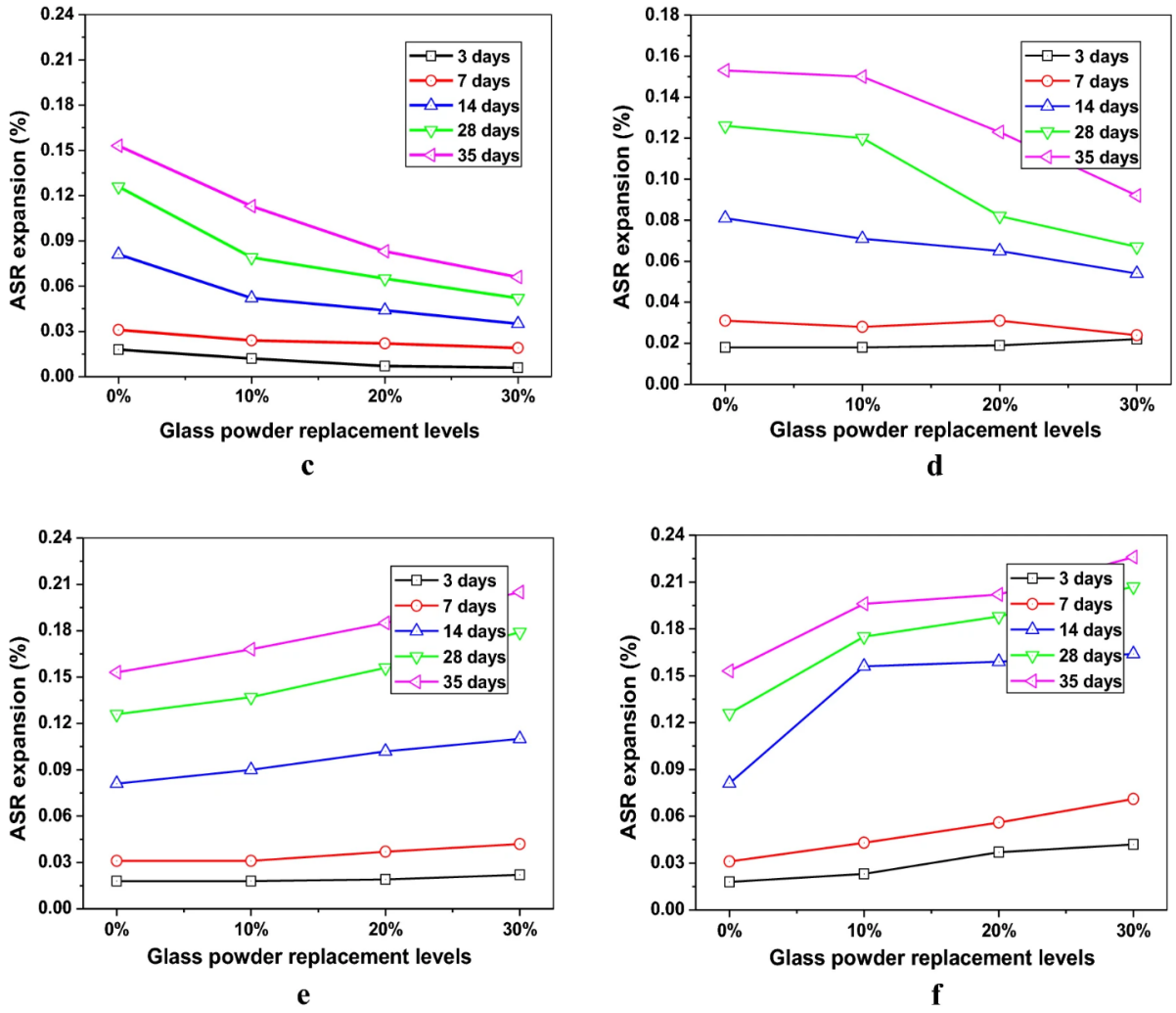

Figure 2.10. Effect of replacement level on ASR expansion of mortar containing RGGP with particle size in the ranges of (a) 38-53 µm, (b) 53-75 µm, (c) 75-150 µm, (d) 150-300 µm, (e) 300-600µm and (f) 600-900 µm [125].

2.4.2. Alkali supply

Soda lime glass, often referred to as container glass, is the most common type of glass and contributes to almost 90% of the entire manufactured glass [133]. The main components of the soda-lime glass, one of the most widely used types of RGRGP, are silica and soda lime that supply a relatively high content of alkalis in terms of sodium and potassium oxide. Recycled glass usually has Na_2O_{eq} of ~14% which can supply a significant amount of alkali ions and aggravate the ASR. Dhir et al [134] found that the alkalis can leach out from glass to trigger ASR in the high pH environment of concrete. Compared with high-alkali fly ashes with an Na_2O_{eq} between 5% and 10%, RGGP was not able to control ASR when used to replace 25% cement [135].

Glass with an alkali content lower than 3% and originating from low-emission glass, fiberglass, and vitrified calcium aluminosilicate is known as low-alkali glass [136]. This type

of glass can reduce the risk of ASR in concrete. However, one of the major limitations of this type of glass is the low availability when compared to soda-lime glass. Moreover, the separation of low-alkali glass and soda-lime glass from the waste stream results in a higher cost, thus rendering the use of low-alkali RGGP impractical. In the research conducted by Mejdi et al., the authors believe that in the process where silica is released from the dissolution of glass, it interacts with calcium hydroxide, resulting in the formation of C-(N)-S-H. The composition of this compound varies based on the system. In the specific binder system of CH-GP that was examined, the fine quality of RGGP provides an extensive surface area for the silica to react. This allows sufficient time for the pozzolanic reaction to occur. However, even after all the calcium hydroxide has been consumed, the glass continues its reaction. Over an extended period, this ongoing reaction could potentially result in the formation of alkali-silica gels surrounding the particles [137]. In a different study that investigates the role of alkalis in supplementary cementing materials and their impact on controlling pore solution chemistry and alkali-silica reaction, it was found that, with the exception of high-alkali RGGP and class C fly ash, the employment of all other reactive SCMs notably reduces the concentration of alkali ions in the pore solution after 91 days. This is presumably due to the encapsulation of available alkalis in hydration products. Consequently, this leads to a mitigation of Alkali-Silica Reaction (ASR) and a decrease in the associated expansion [138].

2.4.3. Workability and setting time

Although a significant number of studies found enhanced workability after RGGP, Patel et al. [75] observed a reduction in slump with RGRGP replacement ratios of 10% and 20% which may be due to the fineness of the glass powders with mean particle sizes of 0.75 μm and 1.96 μm, resulting in a larger specific surface area and greater moisture demand. In this study, contrary to expectations, a larger RGGP particle size caused a greater reduction in workability. Field trials showed that the slump before using high-range water reducing admixtures (HRWRA) was reduced by 7.1% and 30% at a replacement level of 20% at water to binder ratios of 0.48 and 0.38, respectively. The slump was reduced with the RGGP replacement level [98]. In another study, concrete modified with 10% RGGP can reduce the initial slump (according to ASTM C143) by ~4.7% while in comparison to similar replacement levels of SF and FA, the slump was higher and lower by 21.5% and 5.9% respectively. The FA showed slightly higher workability than the control concrete, while the irregular-shaped RGGP particles were considered the primary reason for the reduced workability [46].

Setting time may vary depending on the specific application of RGGP, in terms of the particle size, dosage, grinding process, etc. Therefore, it might be a practical challenge to control the setting time of concrete incorporating RGGP to a preferred target.

2.4.4. Bleeding

Bleeding in concrete is a phenomenon that occurs during the early stages of the concrete mix curing process. It involves the upward movement of water within the freshly placed and compacted concrete mix. This water, often along with some fine particles of cement, rises to the surface of the concrete and forms a thin layer of water on top. Excessive bleeding can

lead to an increase in the w/cm ratio at the surface of the concrete, which can potentially reduce the strength and durability of the concrete. The excess water at the surface can also result in poor finishing and may lead to surface defects, such as scaling, dusting, or an uneven appearance. Moreover, bleeding increases the risk of segregation, where the heavier aggregates settle at the bottom of the concrete mix while the lighter cement particles and water rise to the top, which results in a non-homogeneous distribution of materials. Yin et al. [139] have tested the bleeding water of cement-based grouts with RGGP following the procedure of ASTM C 940 [140] and recording the volume of excess water every 30 min until 2 h. It was observed that the amount of bleeding water of grouts gradually decreased with time, and this phenomenon was closely related to the particle size and the dosage of RGGP, superplasticizer (SP), and viscosity-modifying admixtures (VMA). When keeping the SP and VMA constant, the amount of bleeding water slowly decreased as the replacement percentage of cement by WGP increased from 15 to 40%. Bleeding capacity was 6.8%, 4.9%, and 4.2% for reference grout, grouts with 15% RGGP, and grouts with 40% RGGP, respectively. This phenomenon was ascribed to settlement capacity due to gravity, internal friction, and the Van Der Waals force between particles. The results obtained by Yin et al. [139] were registered after 2 h and benefited from the use of VMA, which increases the stability of grouts and contributes to water retention, preventing bleeding. Mohammadi et. al [141] also found that an increase of RGGP replacement percentage from 0% to 75% by the weight of the total filler decreased the sand adhesion and bleeding potential of the micro surfacing mixture. However, severe bleeding and segregation were observed in another study [142] when the natural sand was replaced by recycled glass sand in concrete, which is due to the smooth surface and non-absorbent nature of glass.

A decrease in strength because of the non-absorbent nature of the glass resulted in localized bleeding of water around the glass cullet was also observed in [143]. In addition, Ahmad et. al concluded that at a higher substitution level of 30% RGGP, bleeding is notable [29]. Glass powder can affect the surface tension of the concrete mix, influencing the ability of water to rise to the surface. This altered surface tension may lead to changes in bleeding characteristics, making it challenging to predict and manage the bleeding behavior.

2.4.5. Shrinkage

Some studies have found that RGGP increases the shrinkage in concrete, which might cause issues with cracking. In one study, the effective shrinkage measured according to IS 2185 was found to decrease by up to 35.78% at a replacement level of 40%, but it was found to be within the acceptable limit of 0.06% as prescribed by the BIS [28]. One of the reasons is considered to be the increased effective water to cement ratio that can increase the available water for hydration and hence enhance drying shrinkage. Similar findings were also reported by Patel et al. [30], where the drying shrinkage increased twice at an RGGP replacement of 20% but still stayed within the prescribed limit. Another reason may be due to the enhanced accumulation of the fine RGGP particles on the cement-RGGP interface via the adherence of the RGGP with cement, thereby reducing the water demand and increasing shrinkage. Field applications also showed similar results of enhanced drying shrinkage due to the zero moisture absorption of RGGP powder that enhances the effective water to cement ratio [100].

2.4.6. Mechanical properties

The early strength of concrete containing RGGP is low due to the low pozzolanic reaction of RGGP and the dilution effect. The optimum replacement level of RGGP is low due to the low pozzolanic reactivity of RGGP and limited calcium resources from cement only. The dilution effect and low reactivity of the RGGP limit its application in concrete, which may induce decreased tensile strength. Depending on the RGGP content and reactivity, there may be a reduction in the early-age strength of the concrete. RGGP often acts as an SCM, and if not properly optimized in the mix design, it can affect the development of early strength, including flexural strength. Proper curing is essential for the development of concrete strength, including flexural strength. The use of RGGP may require adjustments to curing practices to optimize the performance of the concrete over time.

2.4.7. Low resistance against acid attack

RGGP contains amorphous silica, and some glasses may react with acids, leading to the formation of soluble silicate compounds. This reaction can weaken the concrete matrix and compromise its structural integrity. Acid attack can result in the deterioration of the cement matrix, causing the loss of strength and mass of the concrete. The durability of concrete with RGGP is influenced by the reactivity of the glass and its susceptibility to acid-induced degradation. The chemical resistance of the glass used in the powder can vary based on its composition. Some glasses may be more resistant to acid attack than others. Understanding the specific properties of the RGGP being used is crucial for predicting its performance in acid exposure conditions. Achieving an optimal mix design is essential to minimize the impact of acid attack. This involves carefully balancing the proportions of cement, RGGP, and other additives to enhance the overall resistance of the concrete to acid aggression.

2.4.8. Risk of sulfate attack

Glass is susceptible to sulfate attack, especially if it contains alkalis or alkali-earth elements. Sulfate ions can react with these elements in the glass, leading to the formation of sulfate salts that may contribute to the deterioration of the concrete. The sulfate resistance of RGGP may vary depending on its composition and source. Some types of glass may be more prone to sulfate attack, which can affect the long-term durability of the concrete. Achieving an appropriate mix design that accounts for the potential reactivity of RGGP with sulfates is crucial. This involves balancing the proportions of cement, RGGP, and other supplementary cementitious materials to mitigate the risk of sulfate attack. Conducting thorough testing of the RGGP and the concrete mix, including assessments of sulfate resistance, can help in identifying potential issues and implementing necessary adjustments to the mix design. Quality control measures during production and construction are essential to ensure the long-term performance of the concrete.

From the extensive study of the effect of RGGP on concrete, it is evident that although RGGP has been found to improve concrete properties at dosages below 50%, careful consideration must be given to the property of the RGGP used and the quality of cement, aggregate, SCMs and admixtures that it is mixed with. Very few studies are available on the high-volume replacement of cement with RGGP and the effect on the concrete properties. Furthermore, the synergy between ground glass and cementitious materials like fly ash and

slag has been explored to decipher optimal blends that maximize strength while reducing cement content, thereby curbing carbon emissions. Insights gleaned from these studies underscore the complex interplay between particle characteristics, replacement ratios, and the resulting mechanical properties, offering a comprehensive understanding crucial for informed concrete design and sustainable construction practices. Through a systematic review of studies investigating the influence of waste glass composition, particle size distribution, replacement levels, and their consequent effects on strength, durability, and other mechanical properties, a cohesive understanding essential for leveraging ground glass as a viable and eco-friendly constituent in concrete production can be achieved.

3.0 Research Methodology

3.1 Materials

3.1.1. Cementitious materials

In this project, Type I/II ordinary Portland cement produced by Quikrete, complying with ASTM C150 [144], was used to investigate the influence of RGGP and other alternative materials, such as metakaolin (MK), on the hydration behavior of cement and mechanical development of mortars. Type I/II ordinary Portland cement produced by Coastal Cement, complying with ASTM C150 [144], was used to investigate the influence of RGGP and other alternative materials on the mechanical development and durability of concrete at UMass Lowell. Type IL cement produced by Holcim, which contributes to the sustainability of the concrete mix design, was used in the fresh property and strength tests at UMass Amherst. The chemical compositions of the are detailed in Table 3.1.

Table 3.1: Chemical and mineral compositions of the cements used in this project.

		Type I/II cement 1	Type I/II cement 2	Type IL cement
Oxides	CaO	62.7	63.1	63.6
	SiO_2	20.1	20.1	19.3
	Al_2O_3	4.8	3.6	5.3
	SO_3	3.5	2.6	3.0
	Fe_2O_3	3.2	2.9	3.3
	MgO	3.4	1.4	2.2
	LS	1.2	0.9	9.4
	Total alkalis Na_2O_{eq}	0.6	0.6	0.5
Minerals	C_3S	54	68.6	49.8
	C_2S	17	5.9	16.4
	C_3A	7	4.6	8.5
	C_4AF	10	8.8	9.7

Two types of recycled ground glass pozzolans provided by Urban Mining and R.E.D. Industrial Products (RGGP1 and RGGP2) were investigated in this project. The particle size distribution of the Type I/II cement 1 and RGGPs determined by laser diffraction is shown in Figure 3.1a. RGGP1 has a median particle size of 13.48 μm (coarser than cement) while RGGP2 shows a median particle size of 6.15 μm, which is coarser and finer than the cement, respectively. The chemical compositions of RGGP materials are detailed in Table 3.2.

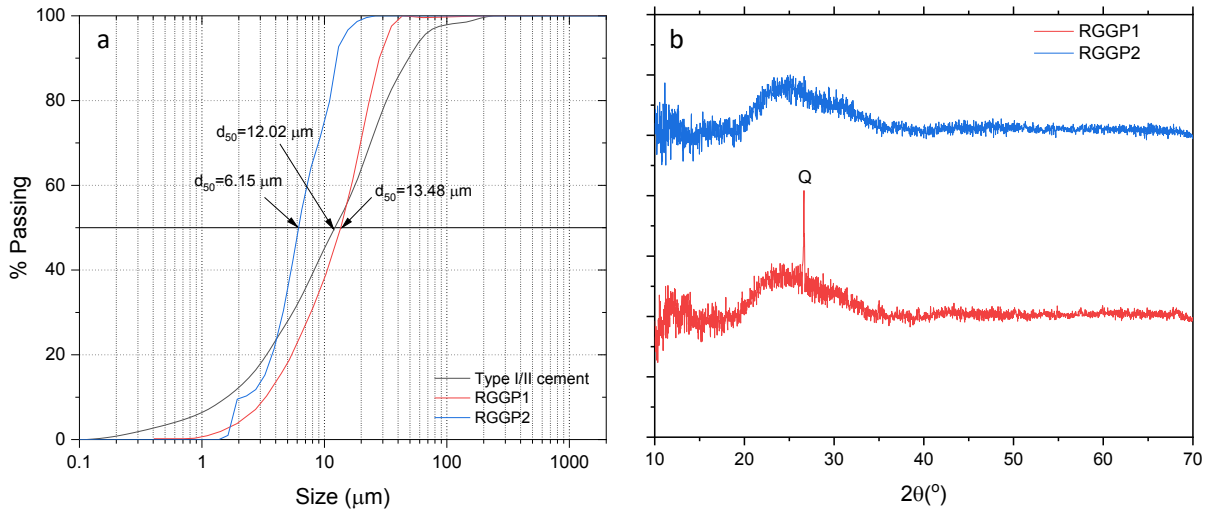

Figure 3.1: (a) Particle size distribution and (b) XRD patterns of Type I/II cement and RGGPs used in this project.

As shown in Table 3.2, the two RGGPs were found to have comparable composition, while RGGP1 possesses slightly higher contents of CaO, SiO_2, and Al_2O_3 and lower Fe_2O_3 content than RGGP2. Compared with cement, both RGGPs showed significantly higher contents of SiO_2 ($\geq$ 70%) and equivalent alkalis (Na_2O_{eq} = ~13%). The XRD data shown in Fig. 3.1b indicated that both RGGP1 and RGGP2 showed a high amorphous content of over 95%, and low contents of crystal phases, such as calcite (0.7% and 0.9%), quartz (1.5% and 0.9%), and wollastonite (2.6% and 2.9%), were also detected from the RGGPs. The compositions of these two RGGPs conform to the specification for ground glass pozzolan detailed in ASTM C1866 [145], indicating their high potential to trigger pozzolanic reactions in the matrix of cement.

Table 3.2: Chemical and mineral compositions of the RGGP used in this project.

		ASTM C1866 limits	RGGP1	RGGP2
Oxides	CaO	2.0-15.0	10.88	10.0
	SiO_2	68.0-80.0	72.29	70.0
	Al_2O_3	0.3-5.0	1.89	1.0
	SO_3	-	0.12	-
	Fe_2O_3	0.1-1.0	0.33	0.5
	LS	0-0.5	0.42	0.2
	Total alkalis Na_2O_{eq}	7.0-15.0	13.03	13.0
Minerals	Amorphous	-	95.2	95.3
	Calcite	-	0.7	0.9
	Quartz	-	1.5	0.9
	Wollastonite	-	2.6	2.9

In addition to RGGP, other alternative materials, including slag, MK, and diatomaceous earth (DE), were also investigated in this project. The slag provided by Boston Concrete and produced by Dragon Products Company showed a specific surface of 493 m^2/kg, an air content of 0.2%, sulfide/sulfur content of 1.0%, and a specific gravity of 2.8 g/ml. The PowerPozz MK was sourced from South Carolina with a specific density of 2.6 g/cm^3. The chemical compositions of cement and MK analyzed by X-ray fluorescence (XRF) are summarized in Table 3.3. The content of silicate and aluminate phases (SiO_2 + Al_2O_3) in MK is higher than 94 wt.%. The particle size distributions (PSD) of Type I/II cement and MK measured by laser diffraction are shown in Figure 3.2. Compared to PC, MK had a smaller particle size of 3.79 μm for MK and a higher specific surface area, which is almost 1.8 times that of cement. The DE was obtained from Dicalite Management Group. It has a moisture content of less than 10%, a median particle diameter of 15-19 μm, a water absorption of 180-220lbs/100lbs, and an ignition loss of 4.0-7.0%, respectively. The chemical compositions of the alternative materials used in this project are summarized in Table 3.3.

Table 3.3. Chemical compositions of the alternative materials (wt.%).

	MK	DE
CaO	0.071	1.88
SiO_2	51.8	81.28
Al_2O_3	42.2	4.39
SO_3	0.11	-
Fe_2O_3	4.15	1.52
MgO	-	0.47
K_2O	0.218	0.73
TiO_2	1.1	0.20
ZrO_2	0.088	-
SrO	0.04	0.01
Cl	0.046	-

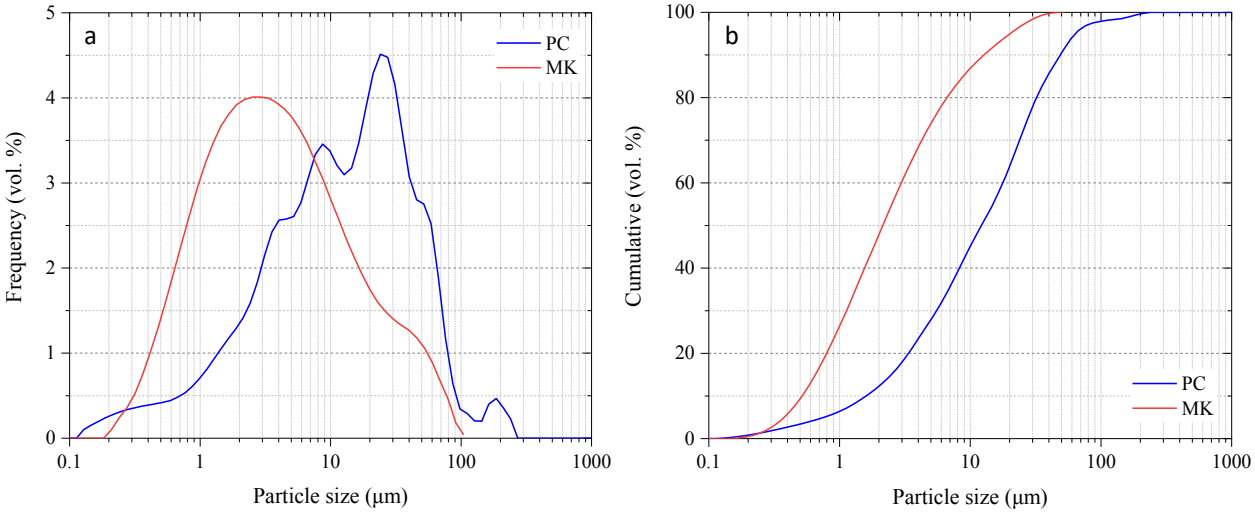

Figure 3.2: Particle size distributions of PC and MK by means of laser diffraction: (a) relative frequency of particles; (b) volume of the particles smaller than a certain diameter.

3.1.2. Aggregates

All-purpose sand and 3/8-inch gravel were used for mortar and concrete specimens at UMass Lowell. The specific gravity of the fine and coarse aggregates is 2.7, and 2.6, respectively. The 3/4" and 3/8" coarse aggregates used at Boston Concrete were obtained from Dracut, MA, and Hudson, NH, respectively. The aggregates used in the concrete at UMass Amherst were obtained from two of the major sources of aggregate in western Massachusetts. J S Lane Amherst quarry as the source of coarse aggregate and Delta Sand and Gravel located at Sunderland as the source of fine aggregate. For ASR-related tests, highly reactive sand from El Paso, Texas, United States, with a relative density of 2.39 and a fineness modulus of 2.96, was used.

3.1.2.1 Particle size distribution and gradation

To determine the particle size distribution of fine and coarse aggregates, sieve analysis was performed per ASTM C136/C136. The process involves passing the aggregate sample through a series of standard sieves (1 in., 3/4 in., 3/8 in., #4, #8, #16, #30, #50, and #100). The material retained on each sieve is then weighed and compared with the acceptable range proposed by a method of aggregate gradation.

#4 #8 Pan

Figure 3.3: Sieve analysis of coarse aggregate (J S Lane)

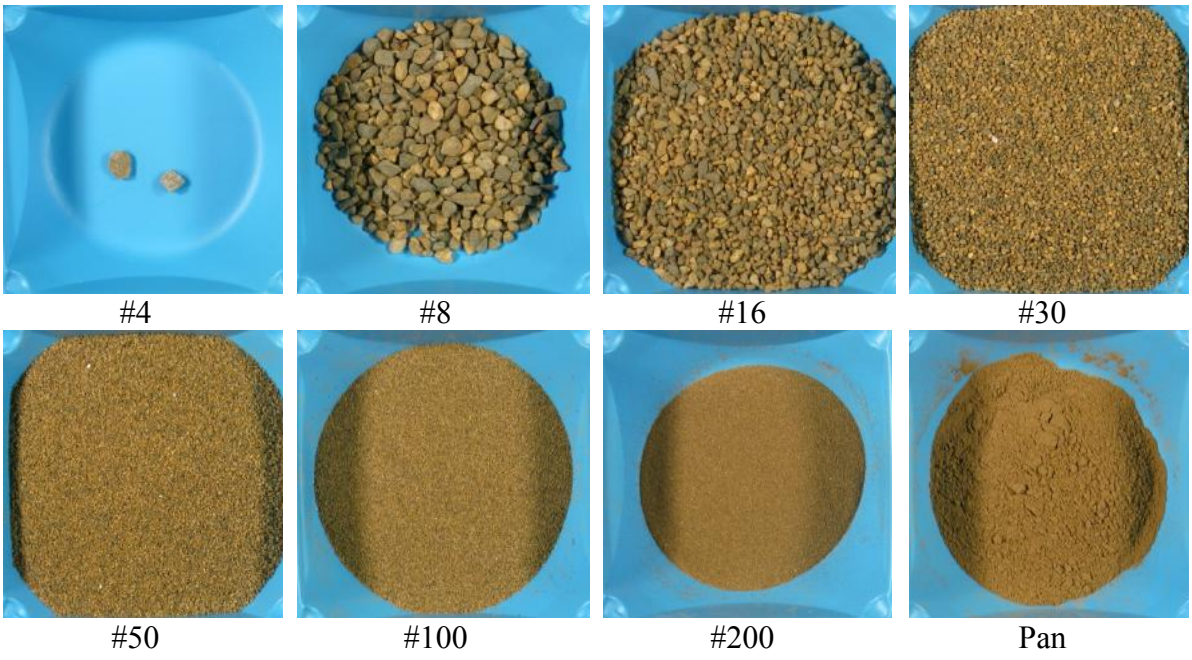

Figure 3.4: Sieve analysis of fine aggregate (Delta Sand and Gravel)

The Tarantula Curve Method is an established method for evaluating the proper gradation of aggregate in concrete. This method compares the percentage of retained aggregate on each sieve against the sieve size and establishes upper and lower bounds for acceptably gradated aggregate. The coarse aggregates retained on sieves No. 8 to No. 30 should exceed 15% to ensure cohesiveness of the concrete and its ability to resist segregation and edge slump. For fine aggregates, the amount retained on Sieves No. 30 to No. 200 should be between 25% and 40% for flowable concrete. This ensures the finishability of the concrete. Based on the results presented in Table 3.4, the aggregates selected for this project are expected to yield concrete with desirable workability, finishability, and cohesion. Figure 3.5 shows the Tarantula Curves for the aggregates used by UMASS Amherst for lab tests and by Construction Service Company for field test concrete.

Table 3.4: Particle size distribution per tarantula curve recommended limits

Sieve Opening	Passing % by mass	Retained % by mass	Retained range % by mass
1 ½ in.	100.0	0.0	0
1 in.	100.0	0.0	0-16
3/4 in.	97.4	2.5	0-20
1/2 in.	77.3	20.1	4-20
3/8 in.	64.9	12.4	4-20
No. 4	45.2	19.6	4-20
No. 8	37.4	7.8	0-12

No. 16	32.8	4.6	0-12
No. 30	17.6	15.1	4-20
No. 50	5.4	12.1	4-20
No. 100	1.9	3.4	0-10
No. 200	0.8	1.1	0-1
Pan	0.1	0.7	-

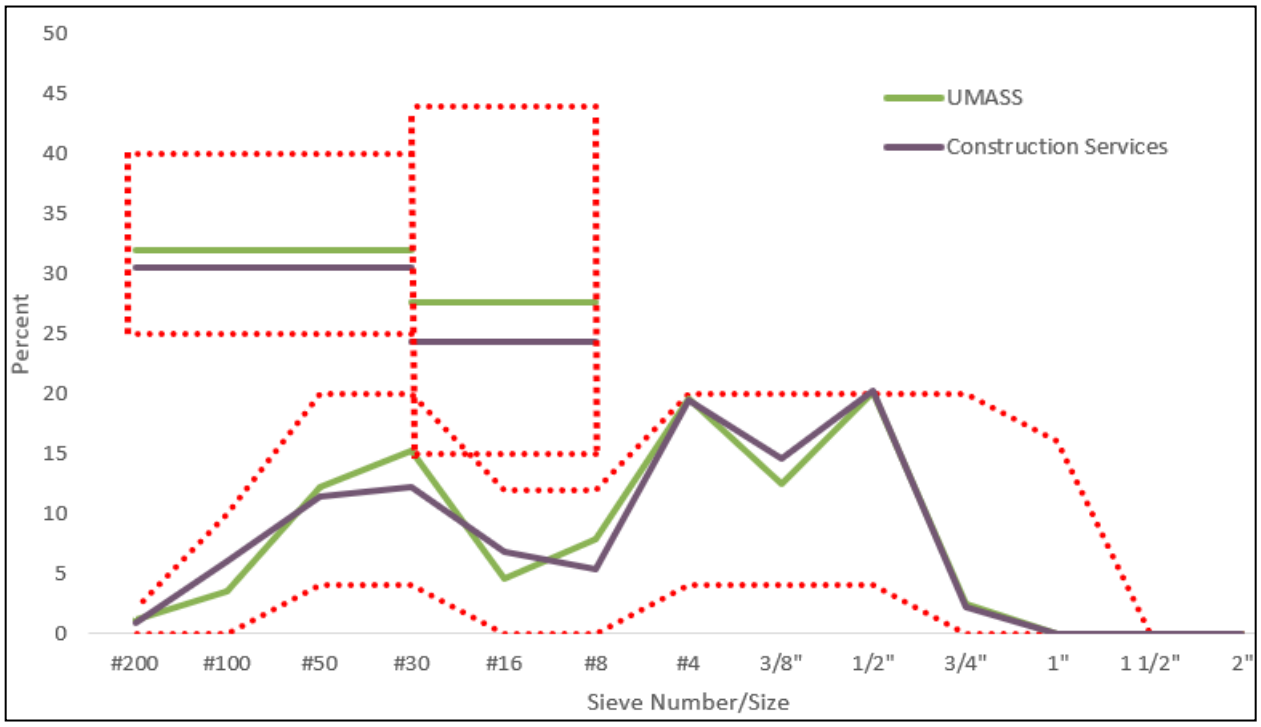

Figure 3.5: Particle size distribution per tarantula curve recommended limits

3.1.2.2 Absorption capacity, specific gravity, unit weight, fineness modulus

To determine the physical properties of both fine and coarse aggregates, a series of tests was conducted in accordance with ASTM standards. The reference standards for each test, along with the corresponding results, are presented in Table 3.5. The absorption capacity of aggregates, particularly in their saturated surface-dry (SSD) condition, is crucial because it determines the amount of water the aggregate can absorb. This directly affects the water-cement ratio and, consequently, the workability of the concrete mix. Specific gravity is essential for calculating the volume occupied by the aggregate, ensuring proper proportioning and achieving the desired strength and durability of the concrete. Additionally, unit weight (bulk density) measures the mass of aggregate per unit volume, including voids, and is vital for determining the concrete's density and weight, which influences mix design calculations. The void content of aggregates, which measures the empty spaces between particles, is important for achieving the desired concrete density and strength. Lastly, the fineness modulus represents the average particle size of the aggregate, impacting the grading, workability, strength, and durability of the concrete.

Table 3.5: Physical properties of aggregates.

Type	Reference Standard	Description	Quantity
Fine Aggregate	ASTM C12	Absorption Capacity (%)	1.2
	ASTM C29	Unit Weight (pcf)	108.7
	ASTM C29	Void Content (%)	33.9
	ASTM C128	Specific Gravity	2.64
	ASTM C136	Percent by Mass Passing (%) – 1 in.	100
	ASTM C136	Percent by Mass Passing (%) – 3/4 in.	100
	ASTM C136	Percent by Mass Passing (%) – 3/8 in.	100
	ASTM C136	Percent by Mass Passing (%) – #4	99.2
	ASTM C136	Percent by Mass Passing (%) – #8	90.96
	ASTM C136	Percent by Mass Passing (%) – #16	80.29
	ASTM C136	Percent by Mass Passing (%) – #30	42.59
	ASTM C136	Percent by Mass Passing (%) – #50	12.31
	ASTM C136	Percent by Mass Passing (%) – #100	3.7
	ASTM C136	Percent by Mass Passing (%) – #200	1.07
	ASTM C136	Percent by Mass Passing (%) – Pan	0.13
	ASTM C136	Fineness Modulus	2.7
Coarse Aggregate	ASTM C127	Absorption Capacity (%)	88
	ASTM C29	Unit Weight (pcf)	111
	ASTM C29	Void Content (%)	39
	ASTM C127	Specific Gravity	2.92
	ASTM C136	Percent by Mass Passing (%) – 1 in.	100
	ASTM C136	Percent by Mass Passing (%) – 3/4 in.	95.81
	ASTM C136	Percent by Mass Passing (%) – 3/8 in.	41.5
	ASTM C136	Percent by Mass Passing (%) – #4	9.36
	ASTM C136	Percent by Mass Passing (%) – #8	1.76
	ASTM C136	Percent by Mass Passing (%) – #16	1.18
	ASTM C136	Percent by Mass Passing (%) – #30	1.02
	ASTM C136	Percent by Mass Passing (%) – #50	0.92
	ASTM C136	Percent by Mass Passing (%) – #100	0.85
	ASTM C136	Percent by Mass Passing (%) – #200	0.66
	ASTM C136	Percent by Mass Passing (%) – Pan	0
	ASTM C136	Fineness Modulus	6.47

3.1.2.3 Chemical properties

Following a series of tests conducted by CTL Group to evaluate the chemical properties of aggregates for Construction Services Company, the key parameters have been summarized in Tables 3.6 and 3.7.

Table 3.6: Chemical properties of deleterious materials in coarse aggregate sample (finer than #8 Sieve).

Reference Standard	Description	Deleterious Materials (% by mass)
ASTM C117	Materials Finer than #200 Sieve	1.0
ASTM C142	Clay Lumps and Friable Particles	0.1
ASTM C123	Lightweight particles in aggregate, ZnCl (2.0 Sp. Gr.)	None Found
ASTM C123 and C295	Chert and Cherty Stone (less than 2.4 Sp. Gr.)	None Found
ASTM C295	Shale	None Found
ASTM C295	Clay Ironstone	None Found
ASTM C295	Claystone, Mudstone, and Siltstone	None Found
ASTM C295	Shaly and Argillaceous Limestone	None Found
COE CRD-C13	Other Soft Particles	0.3

Table 3.7: Weighed percentage of constituents in fine aggregate

Mineral Type	Weighed (%)
Quartz grains with little to no strain strained	24 (20) (4)
Meta-igneous rocks (excluding schist and quartzite) with little to no strained quartz with strained quartz	23 (13) (10)
Schist	19
Quartzite	15
Feldspar	6
Clay-rich particles	4
Sandstone with little to no strained quartz with strained quartz	3 (1) (2)
Mica	2
Other constituents	3
Passing #200 sieve	2

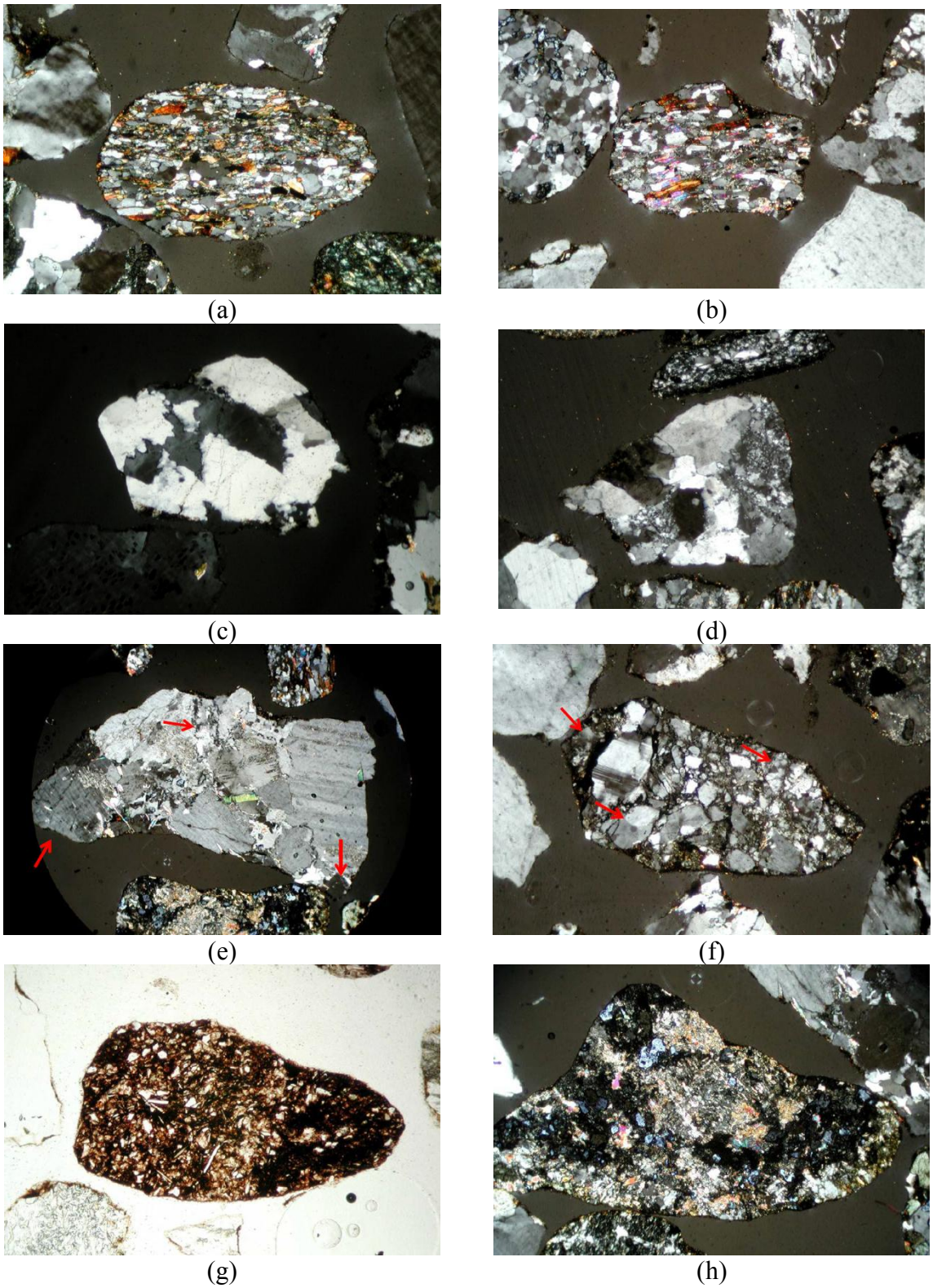

Figure 3.6: Microstructure of fine aggregate (Delta Sand): (a),(b) schist particles from #30 sieve, (c),(d) quartz particles from #30 sieve, (e) meta-granite particle from #16

sieve, (f) sandstone particles from #30 sieve, (g) clay-cemented siltstone particle from #16 sieve, (h) meta-igneous particle from #16 sieve

Figure 3.6 illustrates the microstructure of fine aggregates from Delta Sand Corporation. Parts 3.6a and 3.6b depict subrounded and subangular schist particles from the #30 sieve. Parts 3.6c and 3.6d show subangular and subrounded quartz particles from the #30 sieve. Part 3.6e presents an angular meta-granite particle from the #16 sieve. Part 3.6f displays a subangular sandstone particle from the #30 sieve with strained quartz grains. Part 3.6g features a subrounded clay-cemented siltstone particle from the #16 sieve, and part 3.6h shows a subangular meta-igneous particle from the #16 sieve.

Figure 3.7 displays thin-section photomicrographs of the minus #200 materials from J S Lane's coarse aggregate. The material is predominantly composed of angular to subangular mineral fragments, including feldspar, green to brown silicate minerals such as pyroxene and chlorite, and opaque minerals.

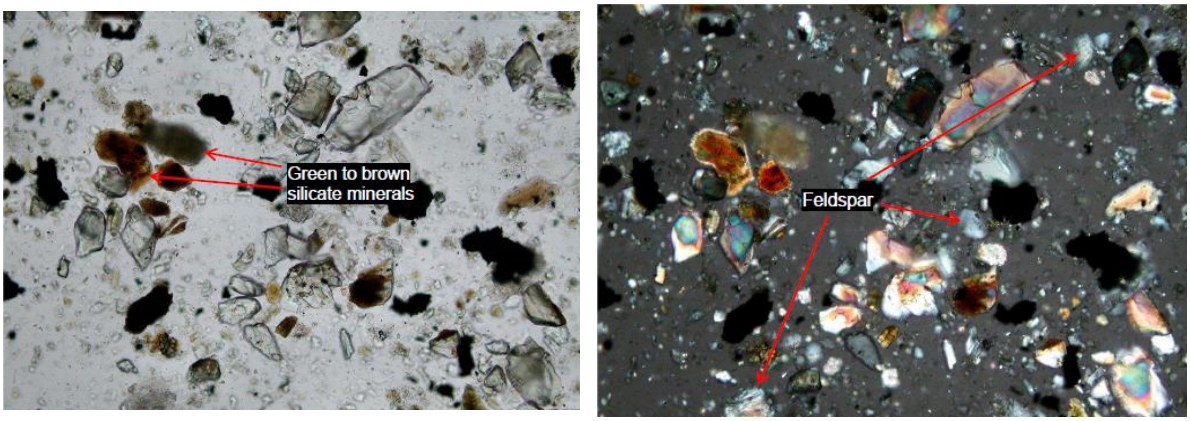

(a) (b)

Figure 3.7: Microstructure of minus #200 particles of coarse aggregate (J S Lane)

3.1.3. Chemical admixtures

To improve the workability of RGGP-cement composites, a high-performance water-reducing admixture (Optimum 380) was used. Calcium hydroxide (CH), calcium carbonate (CC), potassium sulfate (K_2SO_4) and potassium hydroxide (KOH) with purity of 98%, 99%, 99% and 86%, respectively, were used in the rapid, relevant, and reliable (R^3) test per ASTM C 1897 [146] to provide a paste where the dissolved ions from the chemicals can simulate the pore solution in Portland cement systems. According to the MassDOT "Standard Specification for Highways and Bridges (27)" for high-performance concrete and adhering to the specified water-to-cementitious material ratio and the manufacturer's instructions for admixtures, five types of admixtures were incorporated into the concrete mix to enhance the performance of concrete. These admixtures are detailed in Table 3.8.

Table 3.8: Admixtures used in concrete mixes

Item	*Source*	*Commercial Name*	*Description*	*Specific Gravity*
1	Master Builders Solution	MasterAir AE 200	Air Entraining	1.01
2	Master Builders Solution	MasterSure Z 60	Workability Retaining	1.04
3	Master Builders Solution	MasterGlenium 7500	High Range Water Reducing	1.05
4	Master Builders Solution	MasterSet R 100	Water Reducing and Retarding	1.22
5	Master Builders Solution	MasterLife CI 30	Corrosion Inhibiting	1.30
6	Master Builders Solution	MasterROC MS 675	Viscosity Modifying	1.16

In addition, two E5 Nano Silica admixtures, internal cure and liquid fly ash, were used in this project as alternative materials. Detailed information on the concrete formulations incorporating these admixtures is provided below.

3.2 Cement and mortar specimen preparation

The paste samples for the R^3 test were prepared according to ASTM C1897 [146] by first mixing the dry RGGPs with CH and CC powders in a ratio of 1:3 and 2:1, respectively. The solid mixture was then mixed with a solution prepared by dissolving 4 g of KOH and 20 g of K_2SO_4 in 1 liter of DI water under 23°C at a solution-to-solid ratio of 1.2. The mixing was performed in a high-shear blender at a speed of 1600 rpm for 3 minutes or until a homogeneous mixture was obtained. The samples were cast in sealed plastic cylindrical containers and cured at both 23°C and 40°C for 7, 28, and 90 days. At each age, samples collected from the core of the cylinders were ground into fine powders, followed by vacuum drying performed at 23°C for 30 minutes before the XRD and TGA characterizations.

The cement paste samples for hydration characterization tests were prepared by replacing 5%, 10%, 30% and 50% of the cement with each RGGP at a water-to-binder (w/b) ratio of 0.485. As per the recommendations in ASTM C109 [147], the superplasticizer amount was adjusted for each RGGP dosage so that the flow was 110 ± 5% after 25 drops of the flow table. After obtaining homogenous mixtures via the same mixing process presented above,

the paste samples were cured in a sealed condition at 23°C for 7, 28, and 90 days until the TGA, XRD, and FTIR tests.

Cubic mortar specimens of size 50×50×50 mm were cast by using a binder-to-sand ratio of 1:2.75 and a water-to-binder ratio of 0.485, according to the ASTM C109/C109M-20 [147]. As per the recommendations in ASTM C109/C109M-20 [147], the superplasticizer amount was adjusted for each RGGP dosage so that the flow was 110 ± 5% after 25 drops of the flow table. The water absorption of the aggregates was considered to adjust the mixing water volume. The mortar specimens were demolded after 24 hours, and half of the specimens were cured in saturated lime solution, and the other half was cured in a steam chamber at 75°C for 48 hours and subsequently transferred to the saturated lime solution. Care was taken to raise the temperature of the samples gradually at both the start and end of the steam curing process to minimize the cracking from sudden temperature changes.

Prismatic mortar bars (25 mm × 25 mm × 250 mm) were prepared with the aggregate grading defined in ASTM C1260 [148], where the water-to-cement and cement-to-sand ratios were fixed at 0.47 and 2.03, respectively. Sodium hydroxide was added to the mixing water to reach an equivalent alkali content of 1.5% in the mortar to accelerate ASR. The mortars were cast by mixing cement, water containing sodium hydroxide, and sand using a mechanical mortar mixer at 60 rpm for 2 minutes, followed by 1 minute of rest, and then another 3 minutes of mixing at 120 rpm. The well-mixed mortars were cast in 25 mm×25 mm×286 mm stainless steel molds with pre-embedded studs to reach a 250 mm effective testing length. Two repetitions for each group, with a total of 14 samples, were prepared. The mortar bar samples were demolded after 24 hours, followed by a 24-hour pre-conditioning at 50ºC, 95% RH, and 0% CO_2 for moisture equilibrium.

To understand the ASR mitigation mechanisms at the ASR gel level, an ASR gel with Ca/Si, K/Si, and Na/Si ratios of 0.3, 0.2, and 0.8, respectively, was synthesized and carbonated. The composition was determined based on the ranges of Ca/Si (0.05–0.5), K/Si (0.0–0.3), and Na/Si (0.1–1.0) ratios as reported in [149] based on 100 ASR gels collected from field concretes. To avoid the generation of extreme heat and agglomeration during mixing, the solid raw materials, including CH, NaOH, and KOH, were cooled at -20 °C for 3 hours, and the colloidal nano-silica solution was cooled at 1 °C. Sodium hydroxide and potassium hydroxide were first dissolved in deionized water, followed by the addition of CH and colloidal silica solution during mixing. The overall water-to-solid ratio was kept at 1.0. After being homogeneously mixed, the ASR gel was cast in a 25 mm × 25 mm × 25 mm cube and cured at 23 ± 2 °C in a sealed condition for 420 days to ensure the completion of reactions.

3.3 Pozzolanic activity and hydration tests

3.3.1 Isothermal calorimetry

Isothermal calorimetry was conducted using an I-Cal 2000 HPC High Precision Isothermal Calorimeter at a constant temperature of 23°C to monitor the heat flow and cumulative heat release during the first 50 hours of cement hydration and uncover the influences of different

dosages of RGGP on the hydration kinetics. Prior to mixing, the cement, RGGP, and DI water at the desired amounts were conditioned inside the calorimetry chamber for 24 hours to reach the target testing temperature. Approximately 50 grams of paste samples were homogenously mixed at the testing temperature (23°C) within 1 minute, followed by immediate sealing of samples into plastic containers and starting of hydration heat measurements.

3.3.2 XRD and Rietveld refinement

The evolution of mineral phases formed in RGGP-modified cement paste samples after 7, 28, and 90 days was studied using a benchtop XRD device manufactured by Proto Manufacturing Inc. The powdered specimens were scanned from 10-70° 2θ with a step size of 0.02° 2θ and a step time of 2 seconds using a CuKα X-ray tube (30 keV, 20 mA) with a 1.0 mm divergence slit and Ni filter. Highscore Plus software was employed for background removal, peak identification, crystallinity calculation, and phase quantification via Rietveld refinement. Reference powder diffraction files (ICDD database), encompassing the phases like calcium silicate hydrate (PDF-01-081-9793), clintobermorite (PDF-04-012-1762), kenotobermorite (PDF-04-017-1028), calcium hydroxide (PDF-01-089-2779), and calcite (PDF-04-002-9082) were used for the quantification of the R^3 specimens. The RGGP-modified cement paste samples were quantified using reference files of calcium hydroxide (PDF-00-002-0969), hydrotalcite (PDF-00-014-0191), tobermorite (01-073-8502), jennite (PDF-04-016-1684), hillebrandite (04-012-1668), okenite (PDF-04-011-6871), calcite (PDF-00-01-0837), hydrogarnet (PDF-01-076-0557), gehlenite (PDF-00-009-0216), ettringite (PDF-00-041-1451), gypsum (PDF-00-006-0046), alite (PDF-01-070-8632) and belite (PDF-01-077-0388). A 100% crystalline LaB_6 crystal was used as an external standard for Rietveld refinement in quantifying the amorphous content.

3.3.3 TGA

TGA tests were performed after 7, 28, and 90 days of reaction using a Perkin Elmer TGA 4000 thermogravimetric analyzer. To ensure accurate quantifications, powdered R^3 and cement paste samples weighing approximately 20 mg were heated from 30°C to 900°C at a heating rate of 5°C/min and 10°C/min, respectively, under an inert atmosphere controlled by N_2 gas at a flow rate of 20 mL/min. The weight losses in specific temperature ranges were used to quantify the contents of chemically bound water and CH. The ignition and burnout temperatures corresponding to the degradation of CH were considered in a range of 400-510°C based on the modified tangent method [150]. However, it should be noted that the degradation temperatures can vary slightly rather than a fixed temperature range, and the exact temperatures were determined by the tangent to the minimum of derivative thermogravimetric (DTG) curves. The contents of *CH* were determined using the following equation [151]:

$$CH_1 = \left[\frac{W_{400} - W_{510}}{W_{510}}\right] \times \frac{M_{CH}}{M_{H_2O}} \times 100\% = \left[\frac{W_{400} - W_{510}}{W_{510}}\right] \times 4.1 \times 100\% \quad (1)$$

Where W_n is the mass at temperature n°C, and M_{CH} and M_{H2O} are the molar mass of CH and H_2O, respectively.

The chemically bound water content (W_b) of the R^3 blends and cement pastes was calculated based on the weight loss between around 115°C and around 510°C on TGA curves by using Eq. (2). Again, the temperature boundaries here are not fixed, which may slightly vary for each sample based on the tangent method. It should be noted that the primary component of the R3 blends, CH, contains chemically bound water even before the pozzolanic reactions. Therefore, the CH consumption was taken into account for the determination of chemically bound water content to elucidate the newly formed bond water due to the pozzolanic reactions only.

$$W_{ne} = [(W_{115} - W_{510})/W_{510} - (W_{400} - W_{510})/W_{510}] \times 100\% = (W_{115} - W_{400})/W_{510} \times 100\% \quad (2)$$

The degree of hydration (DOH) of cement and the degree of reaction (DOR) of the RGGPs were calculated from Eqs. 3 and 4, where CH and W_{ne} are the calcium hydroxide and the non-evaporable water from in the RGGP-modified cement pastes at different ages, f_c and f_{GP} are the parts of cement and RGGP in the binder, and CH_{PC} (0.32 [152]) and W_{PC} (0.25 [153, 154]) are the calcium hydroxide and non-evaporable water produced by the hydration of 1 unit of fully reacted cement. Since RGGP has a pozzolanic reactivity and can consume CH to form additional products like C-S-H, ettringite, and hydrogarnet, the CH content of RGGP-modified cement is determined by subtracting the CH consumed by RGGP from the CH produced via cement hydration. Similarly, the non-evaporable or chemically bound water content in the RGGP-modified cement constitutes the non-evaporable water from the cement hydration and the one formed from the pozzolanic reaction of RGGP. The CH consumption (CH_{GP}) and the non-evaporable water (W_{GP}) produced by 1 unit mass fully reacted RGGP were determined from the analysis of the TGA results of the R^3 blends after 56 days of reaction.

$$CH = CH_{PC} * f_c * DOH - CH_{GP} * f_{GP} * DOR \quad (3)$$

$$W_{ne} = W_{PC} * f_c * DOH + W_{GP} * f_{GP} * DOR \quad (4)$$

3.3.4 FTIR spectroscopy

The chemical bonds and molecular structure of the hydration products in RGGP-modified cement pastes after 7, 28, and 90 days were characterized based on FTIR spectra between 500-4000 cm^{-1} collected using a Thermo Fisher Scientific Nicolet IS10 FTIR spectrometer. The spectra with a resolution of 4 cm^{-1} were collected in the ATR mode by capturing 128 scans with a scanning time of 270 seconds. Background removal was done using the OMNIC software by Fischer Scientific.

3.3.5 Thermodynamic modeling

Thermodynamic modeling of the hydration of cement containing high-volume RGGP was performed by using Gibbs Free Energy Minimization Software (GEMS3) Selektor [155, 156]

employing the PSI/Nagra [157] and Cemdata18 databases [158] for cementitious phases to calculate the equilibrium phase assemblages and speciation precipitation in the systems. The Gibbs free energy of the input system was minimized by using an aqueous electrolyte model utilizing the Debye-Huckel equation, utilizing a common ion size parameter of 3.67 Å and a common third parameter (b_γ) of 0.123 for KOH solution at 25ºC, and the activity coefficient according to Helgeson's extended equation (Eq. 4), where z_i is the charge of the species i, I is the effective molal ionic strength, b_γ is the common third parameter, and A_y and B_y are constants dependent on temperature and pressure [158]. For simplicity, the main oxide components of cement, including CaO, SiO_2, Al_2O_3, Fe_2O_3, MgO, $Na_2O_{eq,}$ and SO_3, and the main oxides of RGGP, i.e., CaO, SiO_2, Al_2O_3, Fe_2O_3, SO_3, and Na_2O_{eq} were selected as inputs. A water content of 50% and RGGP dosages varied from 0 to 50% were considered. To obtain a comprehensive understanding of the role of RGGP in cement hydration, two simulations, one predicting phase assemblages over time, based on the calculated DOH of cement and DOR of RGGP, and one predicting phase assemblages as a function of RGGP reaction degree at an assumed cement DOH of 80%, were conducted.

$$\log \gamma_i = \frac{-A_y z_i^2 \sqrt{I}}{1+B_y a_i \sqrt{I}} + b_\gamma I \quad (5)$$

3.4 Physical property tests

3.4.1 Flowability test

The flowability of the RGGP modified mixtures was determined using a flow table by following the guidelines of ASTM C1437 [159]. A flow mold with a bottom diameter of 100 mm, a top diameter of 70 mm, and a height of 50 mm was positioned at the center of the table. Figure 3.8 shows a typical flow table used during the flowability test. Initially, a layer of freshly mixed mortar, approximately 25 mm thick, was placed into the mold and tamped 20 times using a standard tamper to ensure uniform filling. The mold was then filled to the top with a second layer of mortar and tamped again in the same manner. Afterwards, the excess mortar was struck off to make the surface flat with the top of the mold using a straightedge with a sawing motion. After waiting for 1 minute from the completion of filling, the mold was carefully lifted vertically. Immediately after that, the flow table was dropped 25 times within 15 seconds. The resulting spread of the mortar was measured along four lines scribed on the table surface using a slide caliper, and the average of these four measurements was recorded as the flow diameter for the mixture. The flow value was then calculated as a percentage increase over the original mold base diameter using the following equation:

$$Flow\ (\%) = \frac{(Avg.of\ four\ readings\ in\ mm - Inside\ base\ dia.of\ mold)}{100} * 100\% \quad (6)$$

Where the inside base diameter of the mold is 100 mm. As per the recommendations from ASTM C109/C109M [160], the superplasticizer amount was adjusted for each RGGP dosage so that the flow was 110 ± 5% after 25 drops of the flow table.

Figure 3.8: Flowability test of RGGP-modified mortar

3.4.2 Early-age autogenous shrinkage

The early-age (initial) autogenous shrinkage during the first 3 days was measured by a Schleibinger shrinkage cone [161]. As shown in Figure 3.9, Schleibinger shrinkage cone is a precision laser-based apparatus capable of touchless measuring the height change of cement samples. This system enables the immediate measurement of the initial autogenous shrinkage right after the fresh cement paste is poured into the inverted circular cone-shaped container, the unique geometry of which ensures that the recorded distance change between the laser sensor and the sample surface corresponds to the isotropic volume change of the specimens. In total, nine different mixtures were tested, which included one control group (Portland cement) and eight mixtures that incorporated supplementary cementitious materials in combination with Portland cement. Immediately after mixing, 300 g of fresh cement paste was carefully poured into the inverted cone-shaped container. A thin, cone-shaped plastic bag fitting the cone container was used to minimize the friction between the cement pastes and the cone surface and ensure that smooth downward movements of the samples can occur when they shrink. To minimize water evaporation, paraffin oil was used to form a thin sealing layer on the top of the cement pastes after installing the laser reflector in the center of the top surface. The laser sensor continuously recorded the vertical displacement, and the measurement data with a resolution of <2 μm were automatically stored through a data logger.

Figure 3.9: Laser-based shrinkage cone for early-age shrinkage measurement.

3.4.3 Chemical shrinkage

The chemical shrinkage of cement pastes was measured through the dilatometry method according to [162] at a temperature of 23 ± 2°C with two repetitions. For each group, about 10g of the mixed fresh cement paste was put in a 50-ml rigid plastic vial, yielding a sample thickness of approximately 10mm. Rubber stoppers equipped with graduated capillary pipettes with graduations of 0.01mL in their center were used to seal the vials without air bubbles and the reading of volume change. DI water was used to fill the vial and capillary pipets to a certain level and paraffin oil was used on top of the water in the graduated capillary pipets to minimize water evaporation. Reading of water level was carried out every 30 minutes during the first 4 hours, then every 1 hour up to 8 hours, followed by once a day until 28 days.

3.4.4 Drying shrinkage

According to [163], mortar bars measuring 25mm × 25mm × 250mm were cast for the drying shrinkage test. After a 24 h ± 30 min period of moisture curing in molds covered with plastic sheets, length comparator readings were promptly recorded upon demolding and served as the initial measurement. The mortar bars were then placed in a curing box with an RH of 50

± 3% at 23 ± 2˚C, maintained by a saturated magnesium nitrate solution. Length comparator readings were recorded daily throughout the initial week and subsequently on 9, 11, 14, 18, 25, and 32 days. Since water loss is the primary trigger of drying shrinkage, the mass change of the mortar bars was closely monitored. The average values from two repetitions were calculated and presented as representative results for each group.

3.5 Concrete mixture design and laboratory tests

The main objective of this project was to develop a concrete mixture containing RGGP that could be compared with the performance of pre-approved concrete mixtures used by MassDOT. To accomplish this, the first step in the research project was to develop a mixture design in the laboratory using locally sourced aggregates and RGGP in addition to MassDOT-approved cement and admixtures. The mixture would have to be pre-approved so that the only difference would consist of a percentage replacement of cement for RGGP. This chapter describes the mix design and presents the nomenclature used for laboratory tests. Finally, a description of field tests and alkali-silica reactivity (ASR) tests is presented.

For this part of the research, various strength tests were conducted using multiple samples. A nomenclature was developed to identify each test by assigning a unique identifier (sample ID) to each test as indicated below:

[Mix Design]-[Cement Type]-[SCM]-[Replacement %]-[Test Date]-[Test Type]-[Sample No.]

where: **Mix Design:** High Performance Concrete (**HP**)
Cement Type: Cement Type IL (**1L**)
SCMs: Ground Glass (**GG**)
Replacement Percentage: 5% (**05**), 10% (**10**), 15% (**15**), 20% (**20**), 25% (**25**), 30% (**30**)
Test Date: 7 Days (**07**), 28 Days (**28**), 91 Days (**91**)
Test Type: Compression Test (**CT**), Splitting Tensile Test (**ST**), Four-Point Bending Test (**BT**)
Sample Number: 1, **2,** and **3** for CT and ST, and **1**, **2** for BT

This identification scheme will be used in the results section of the report.

3.5.1. Mix design

The concrete mix design is provided by Construction Service based on MassDOT-approved mix design No.24-04-09-08-39-48-02, with varying replacement levels of ground glass to determine an effective replacement level that would satisfy the specified strength. Properties of wet concrete were also measured to determine if the mixtures were suitable for workability. -The design is in full compliance with ACI 318 [19] and ACI 201 [20] requirements and meets the target specifications outlined above.

Table 3.9: Mix design formulation

Constituent Material	Description	Source	Quantity	Unit
Fine Aggregate	Normal Weight/M6	Delta Sand and Gravel	1,230.00	(lbs./yd^3)
Coarse Aggregate	Normal Weight67/M80	J S Lane	1,830.00	(lbs./yd^3)
Total Cementitious Material	Type IL Cement	HOLCIM	660.00	(lbs./yd^3)
	POZZOTIVE Ground Glass	Urban Mining Industries		
Water	Potable Water	Amherst, MA Municipal Supply	264.00	(lbs./yd^3)
Air Entraining Admixture	MasterAir AE 200	Master Builders Solution	2.00	(oz./yd^3)
Workability Retaining Admixture	MasterSure Z 60	Master Builders Solution	13.20	(oz./yd^3)
High Range Water Reducing Admixture	MasterGlenium 7500	Master Builders Solution	46.20	(oz./yd^3)
Water Reducing and Retarding Admixture	MasterSet R 100	Master Builders Solution	29.70	(oz./yd^3)
Corrosion Inhibiting Admixture	MasterLife CI 30	Master Builders Solution	384.00	(oz./yd^3)

3.5.2. Laboratory testing

The laboratory testing for this study was conducted at the Boyle Lab at the University of Massachusetts Amherst, where concrete specimens with varying replacement levels of ground glass were prepared to evaluate their properties. Standard concrete cylinders measuring 4 × 8 in. were cast for compressive strength testing (ASTM C39) [24] and split tensile strength tests (ASTM C496) [25], while 6 × 6 × 21in. Beams were fabricated to conduct a four-point bending test (modulus of rupture tests, ASTM C78) [26]. Fresh concrete properties, including slump, air content, and unit weight, were also measured for each batch of concrete to ensure all mixes satisfied the target wet concrete properties.

Before batches were developed to cast specimens for testing, several trial batches were conducted to refine the dosage of air-entraining admixture. Through these trials, it became evident that the relationship between batch volume and air-entraining admixture dosage was non-linear, necessitating adjustments to ensure an appropriate amount of air-entraining admixture.

Each batch made in the laboratory consisted of 2.7 cu ft of concrete to fabricate the necessary samples for testing. Before each batch, all required materials were brought into the lab and

stored in sealed buckets to preserve their existing moisture content. For each batch, a small sample from each aggregate was oven-dried to determine its moisture content, to adjust the water in the batch.

3.5.2.1 Slump, air content, and density tests (wet concrete properties)

Immediately after mixing, prior to casting the concrete into cylinder molds and beam forms, slump tests were performed in the laboratory in accordance with ASTM C143/C143M standard [21]. The results are presented in Section 3.2.3.1. Air content was measured in accordance with ASTM C231 [22], and the results are presented in Section 7.2. The ASTM C138 [23] test method is used to determine the unit weight (density) of freshly mixed concrete and the results are presented in Section 7.2.

3.5.2.2 Curing method

Prior to mechanical testing, all cylindrical and beam specimens, including those for compression, splitting tensile, and four-point bending tests were cured using lime water from the date of casting through to their respective testing ages (7, 28, and 91 days). This method ensured consistent moisture conditions to support proper hydration and strength development. The curing solution was prepared by dissolving 5 grams of hydrated lime per liter of water, forming a saturated lime water bath. This high-pH environment prevented the leaching of calcium hydroxide and helped maintain stable curing conditions throughout the testing period.

3.5.2.3 Compression tests

Compressive strength tests were carried out using standard 4 by 8-in. concrete cylinders. A 500-kip Forney testing machine was used to conduct the tests in accordance with ASTM C39 standard [24]. Each specimen was carefully aligned in the machine and then tested under compression at a controlled rate of 35 psi per second. Testing was conducted at 7, 28, and 91 days after casting, and three specimens were examined at each interval.

Figure 3.10: Forney testing machine used for compression, splitting tensile tests, and four-point bending tests

3.5.2.4 Splitting tensile tests

The splitting tensile strength test using standard 4 by 8 in. concrete cylinders was conducted using a Forney testing machine, in accordance with ASTM C496 [25]. Each specimen was positioned horizontally, with a compressive load applied to the top through a stiff loading strip. This induces indirect tensile stresses perpendicular to the applied force, eventually causing the cylinder to split along its diameter. The peak load at failure was recorded to determine the splitting tensile strength of the concrete. Tests were conducted at 7, 28, and 91 days after casting (three specimens evaluated at each age). The loading rate was maintained at 8.0 psi per second, as recommended by ASTM C496. The splitting tensile strength (f_t) was calculated using the following formula:

$$f_t = \frac{2P}{\pi DL} \tag{7}$$

Where:
f_t = Splitting tensile strength (psi)
P = Maximum applied load at failure (lb)
D = Diameter of the cylinder (in.)
L = Length of the cylinder (in.)

3.5.2.5 Four-point bending tests

Four-point bending tests using beams with a 6 by 6 in. cross section and 21 in. length were conducted in accordance with ASTM C78 [26] for determining the flexural strength

(modulus of rupture) of concrete using a simple beam with third-point loading. Each beam was placed on two support points, with two additional loading points positioned symmetrically along an 18-inch span. A gradual load with a loading rate of 2.5 psi/sec was applied to the top of the beam at these two points until failure occurred. As the fracture initiated within the middle third of the span in all cases, the modulus of rupture (R) was calculated using the following formula:

$$fr = \frac{PL}{bd^2} \tag{8}$$

where:
f_r = Modulus of rupture (psi)
P = Maximum applied load at failure (lb)
L = Span length between supports (in.)
b = Width of the beam (in.)
d = Depth of the beam (in.)

Tests were conducted at 7, 28, and 91 days after casting (two beams at each age) for each mix design.

3.5.3 Field placement and tests

Laboratory mixing and testing were compared with realistic field conditions by placing and sampling two concrete sidewalk slab panels at a UMass Amherst site. The same mix design as used in the laboratory (Mix No. 24-04-09-08-39-48-02) was purchased from an approved MassDOT concrete ready mix plant located in western Massachusetts. Because the objective for this part of the project was to assess practicality and ease of batching under realistic conditions, only one level of RGGP replacement was used. One sidewalk panel incorporated 25% RGGP cement replacement, which was the optimum replacement level based on laboratory testing. The second sidewalk panel was placed using the same concrete mix without RGGP replacement (control mix).

The quantities of concrete ordered for each mix design were 1.75 cubic yards for the mix with 25% RGGP replacement and 7.5 cubic yards for the control mix containing 0% RGGP. Each order volume was calculated based on its respective placement location, with approximately 30% additional concrete included to compensate for potential losses during transportation or pouring.

Before placing concrete for each sidewalk panel, the ground was excavated to the necessary depth, and formwork was installed to shape the sidewalk properly following MassDOT Construction Specifications. A reinforcing wire mesh was placed near the bottom of the sidewalks approximately 2.0 in. from the ground level. A lower concrete cover than required for concrete placed against the ground (3.0 in.) was not satisfied, but was not considered critical for the intent of the field tests.

During the pouring of the concrete with 25% RGGP replacement, the temperature was 72°F and the relative humidity was 38%. Sidewalks were cured using wet burlap under a plastic

sheet for seven days. Burlap and plastic sheets were weighed down using heavy blocks that were inspected periodically so that the sidewalks would not get uncovered.

To analyze the compressive performance of concrete, six cylindrical specimens (4×8 in.) were cast for each mix design and time interval (7, 28, and 91 days). Half were cured in saturated lime water, while the other half followed the same burlap curing method as the sidewalk slabs to compare conditions. In addition, three specimens per time interval and mix design were created for split tensile testing, along with two beams (6×6×21 in.) per time interval and mix design for bending tests, and both were cured in saturated lime water until testing. Additionally, based on instructions of MassDOT, nine concrete cylinders containing 25% RGGP replacement were cast and cured in saturated lime water for delivery to MassDOT for further evaluation.

The sidewalk dimensions using the two different mixes (without and with RGGP replacement) were not equal. The control mix sidewalk was 26 ft by 12 ft in plan and 6 in. in thickness. The sidewalk containing 25% RGGP replacement was 14 ft by 4 ft in plan, by 6 in. in thickness. The differences in dimensions were due to the availability of space at the location.

Figure 3.11: Pre-placement setup for sidewalk construction with 25% RGGP concrete

Figure 3.12: Pre-placement setup for sidewalk construction with 100% hydraulic cement concrete

Finishing activities after placement of the 25% RGGP sidewalk were conducted as follows. To ensure a uniform horizontal surface, excess concrete was screeded immediately after filling the form. Thirty minutes after placement, bull floating was initiated to smooth the surface and remove surface imperfections. Control joints were formed in and around the sidewalk slab using an edger and groover 90 minutes after the concrete was first delivered from the truck. A magnesium trowel was used 2.5 hrs after concrete delivery to finish the surface. Wet burlap was placed over the sidewalk panel 3 hrs after placement initiation, followed by plastic sheeting to retain moisture and facilitate proper curing.

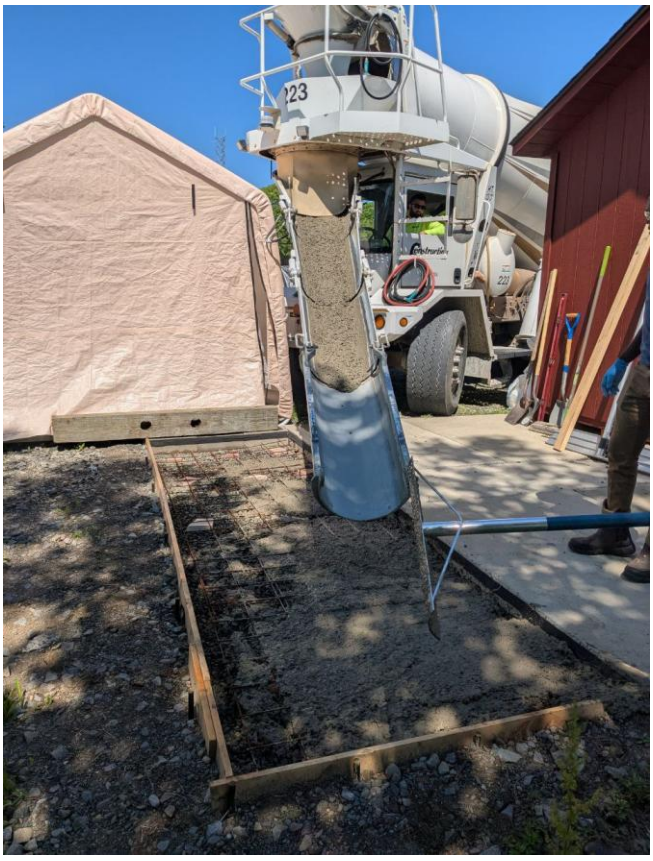

Figure 3.13: Truck mixer discharge into formwork

Figure 3.14: Concrete beam and cylinders cast alongside slab placement

Figure 3.15: 4 by 8-inch cylinder mold filling process

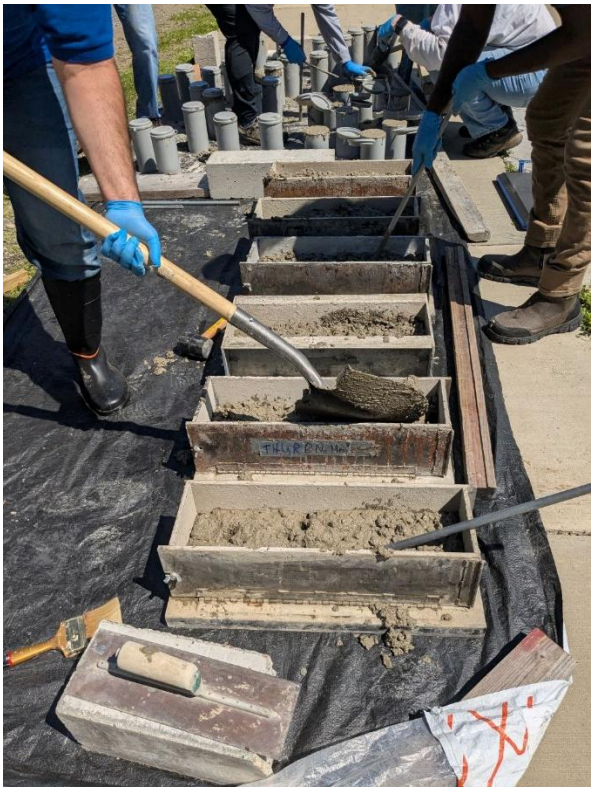

Figure 3.16: Casting of concrete beams

Figure 3.17: Initial finishing of concrete sidewalk with magnesium bullfloat

Figure 3.18: Edging process for sidewalk slabs

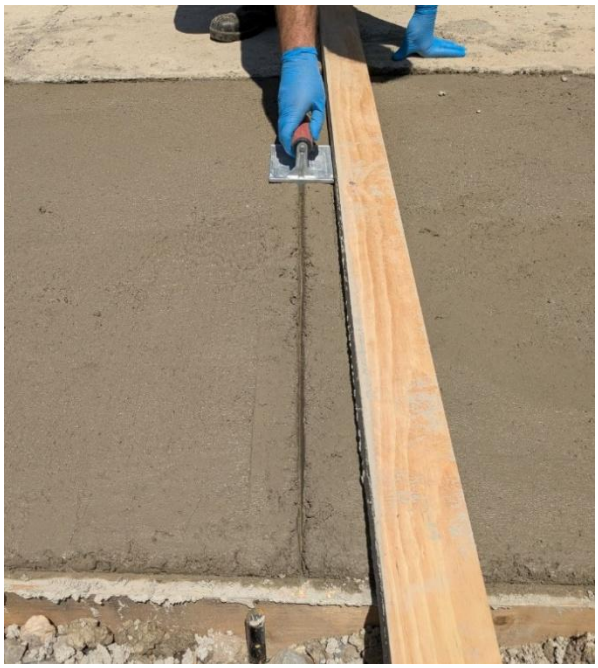

Figure 3.19: Grooving operation for concrete joints

Figure 3.20: Magnesium troweling for surface finishing

Figure 3.21: Broom finish application for sidewalk texture

Figure 3.22: Wet burlap and plastic covering for moisture retention

3.2.3.1 Slump, air content, and density tests

For the delivered concrete, the slump, air content, and density tests were conducted in accordance with ASTM C143/C143M, ASTM C231, and ASTM C138. The results of these tests are presented in Section 4.

Figure 3.23: Slump test

Figure 3.24: Air content measurement

3.6 Durability tests

3.6.1. Bulk electrical resistivity

Using an RCON bulk resistivity meter from Giatec Scientific, the bulk electrical resistivity measurements of concrete were conducted on 3-by-6-inch cylindrical specimens according to AASHTO T402 and ASTM C1876 [164] to evaluate the influences of RGGP, alternative materials, and their combinations on the permeability of the concrete. The specimens were cured in saturated lime water for different ages, including 7 days, 14 days, 28 days, and 56 days. Before each test, the cured specimens were dried in the lab for three hours, followed by a dry vacuum in a vacuum chamber at a vacuum pressure of 900-950 Pa for 2 hours, and then saturated in a simulated concrete pore solution under the same vacuum condition for 1 hour. The specimens were kept immersed in the pore solution after releasing the vacuum for 24 hours. The specimens were wiped using a paper towel to remove the excess water from their surface. Figure 3.25 shows the testing setup used for the bulk resistivity measurement. By placing the saturated surface-dry concrete cylinders between two end caps lined with the conducting sponge pads, the bulk resistivity was measured by recording the resistance at a frequency of 1 kHz.

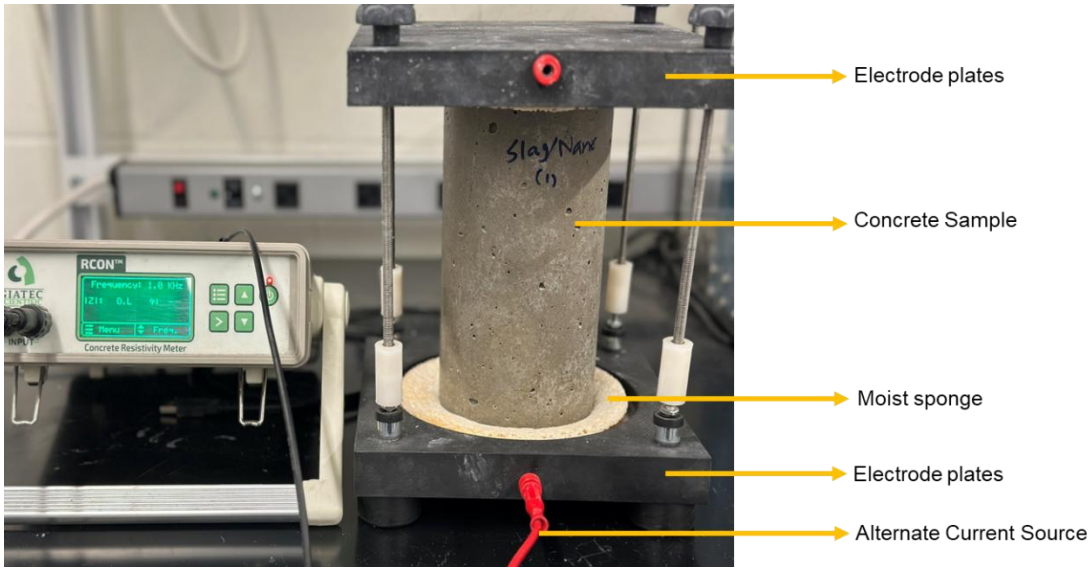

Figure 3.25: Test setup for bulk electrical resistivity measurement

The resistance (R) recorded from the device was used to calculate bulk resistivity using the following equation:

$$\rho = \frac{RA}{L} \tag{8}$$

Where, ρ is bulk electrical resistivity (Ω-m), R is measured resistance, A is the cross-sectional area of the cylinder (m^2), and L is the length of the cylinder in (m).

3.6.2. Mortar bar test for ASR

According to ASTM C1260 [148], mortars with a water-to-binder ratio (w_e/b) of 0.47 and a binder-to-sand ratio of 2.03 were used for the mortar bar test. For the mortar bar test, the reactive sand was sieved and remixed to the particle size distribution suggested by ASTM C1260 [148]. For each group, the cement binders were mixed with water and fine reactive aggregate using a mechanical mortar mixer and then cast in 25 mm × 25 mm × 280 mm stainless steel molds with pre-embedded studs, making a 10-in effective testing length. Two repetitions for each group, with a total of 18 samples, were prepared. After casting, all the specimens were covered with plastic sheets to keep moisture at 23.0 ± 2 ˚C for 24 hours until demolding, further conditioning, or testing.
After being demolded, the specimens were immersed in tap water at 23.0 ± 2 ˚C, then conditioned at 80℃ in a mechanical oven for 24 h, and the initial mortar bar length was measured as zero reading. Then, the mortar bar samples were immersed in a 1 N NaOH solution in sealed boxes at 80.0 ± 2℃. The subsequent comparator readings were conducted after 12 and 24 hours for the first day, once a day for the first week, and then at least two readings per week up to 90 days.

3.6.3. Accelerated concrete cylinder test (ACCT)

As shown in Figure 3.26, an accelerated concrete cylinder test (ACCT) apparatus was developed in this project per AASHTO TP 142 [165]. The containers and lids were developed using stainless steel, and a rubber washer was used in each setup for sealing. Spring-loaded linear variable differential transformers (LVDT) purchased from Harold G Schaevitz Industries LLC and a universal data acquisition system with 16 input channels were used to monitor the volume expansion of concrete cylinders. As shown in Figure 3.27, before each test, the data acquisition system and LVDT were assembled and calibrated to ensure the measurement accuracy.

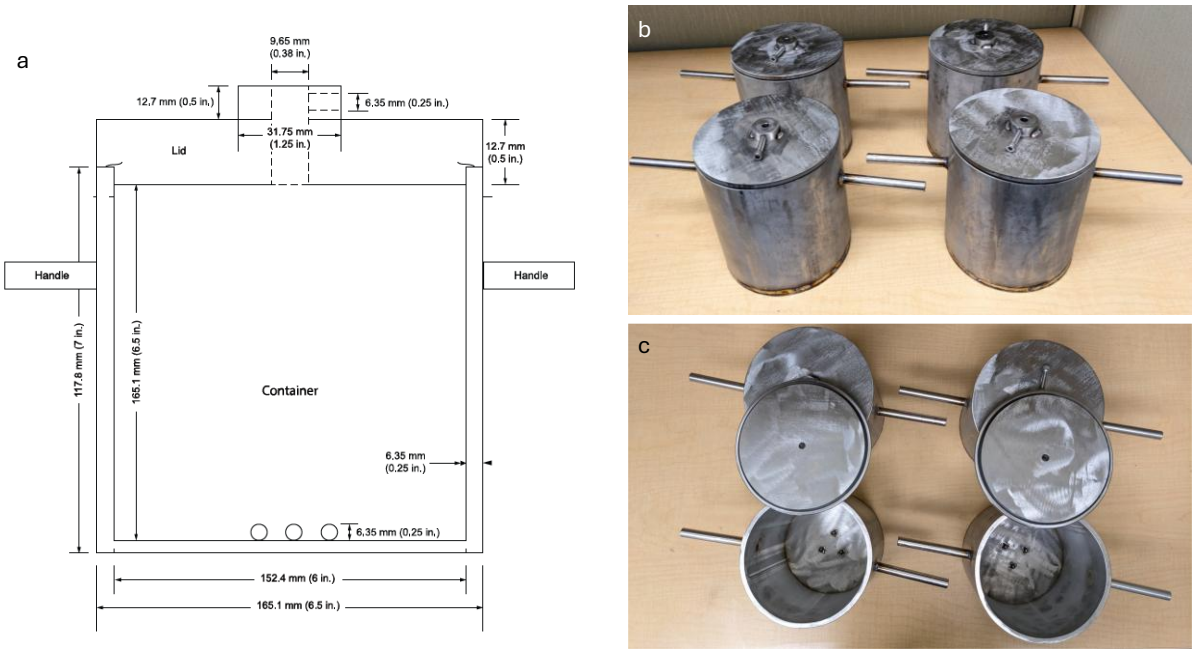

Figure 3.26: (a) Structure of stainless steel container and lid [165], (b) and (c) ACCT testing apparatus developed in this project.

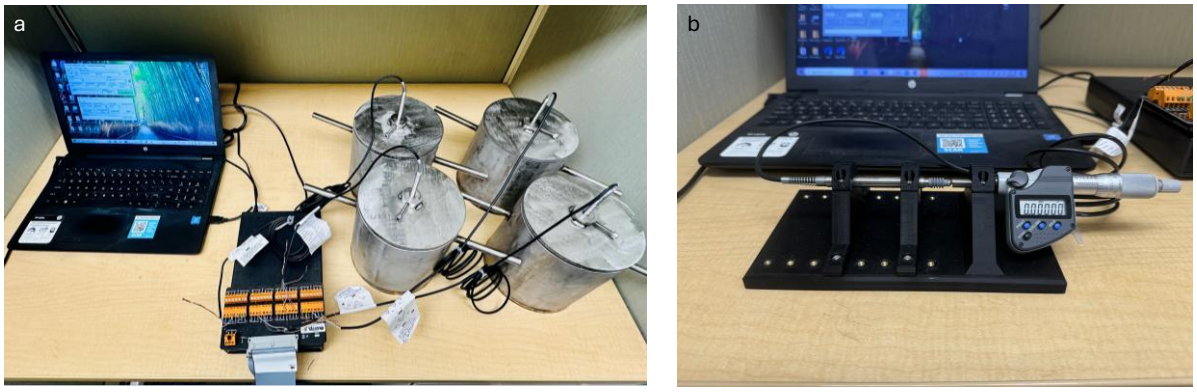

Figure 3.27: Test setup for bulk electrical resistivity measurement (ASTM C1876)

Cylindrical specimens with a diameter of 3-by-6-inch concrete cylinders were cast and cured for 7 days at a temperature of 23 ± 2°C with a relative humidity greater than 95%. After curing, the specimens were placed inside the steel containers (one specimen per container), and the container was filled with the soak solution that matched the pore solution alkalinity of the specimens. The pore solution alkalinity of the concrete mixtures was estimated from the NIST pore solution calculator available at (https://www.nist.gov/el/estimation-pore-solution-conductivity), where total equivalent alkali content from both cement and the respective SCM was considered for the calculations. It is worth mentioning that, given the age of concrete when starting the test (7 days), a 70% estimated degree of hydration and

sealed curing conditions were chosen for the estimation. Following this, the LVDT was inserted through the center hole of the base plate on the lid, and the steel container was placed inside an oven at a temperature of 60°C for a period of 45 days (Figure 3.28). The displacement due to ASR expansion was recorded automatically by the attached computer.

Figure 3.28: Fully assembled ACCT test setup inside an oven

3.6.4. Rapid chloride penetration test

As shown in Figure 3.29, a non-steady-state migration testing setup was developed in this project according to AASHTO T357 [166] to evaluate the penetration resistance of the concrete against chloride ions. 4-by-8-inch cylindrical concrete specimens were prepared and cured in saturated lime water for 28 days, then they were cut into 50 ± 2 mm thick discs using a slow-speed diamond saw. Afterwards, the side surfaces of the samples were sealed with epoxy to prevent side leakage or chloride migration. The specimens were then placed in a vacuum chamber with both ends exposed and vacuumed under a pressure of 1 kPa for 3 hours. Subsequently, the vacuum chamber was filled with de-aired water, and the vacuum was maintained for an additional hour. After releasing the vacuum, the specimens were kept submerged in this condition for 18 ± 2 hours until testing.

Before testing, each disc was mounted in a split-cell apparatus, with one side exposed to a 0.3N NaOH solution (anolyte) and the other end to a 10% NaCl solution (catholyte). The negative and positive poles of the power supply were connected to the cathode and anode separately and based on the initial current value, the voltage was adjusted between 10V, 30V, or 60V according to AASHTO T357 [166] recommendations. The details of the experimental setup are illustrated in Figures 3.29a-3.29c. After 18 hours, the test was stopped, and the specimens were split axially. A 0.1M $AgNO_2$ solution was evenly sprayed on the freshly

exposed split surfaces of the specimens. After 15 minutes, the chloride penetration depth was measured from the extent of visible white silver chloride precipitate on the split surfaces. The measurements were taken at every 10mm interval from the edge. The rate of penetration (mm/V-h) was calculated by dividing the depth of average penetration (mm) by the product of applied voltage (V) and the duration of the test (h). Two repetitions were conducted for each mixture, and the average chloride penetration depth from both specimens was reported as the penetration rate.

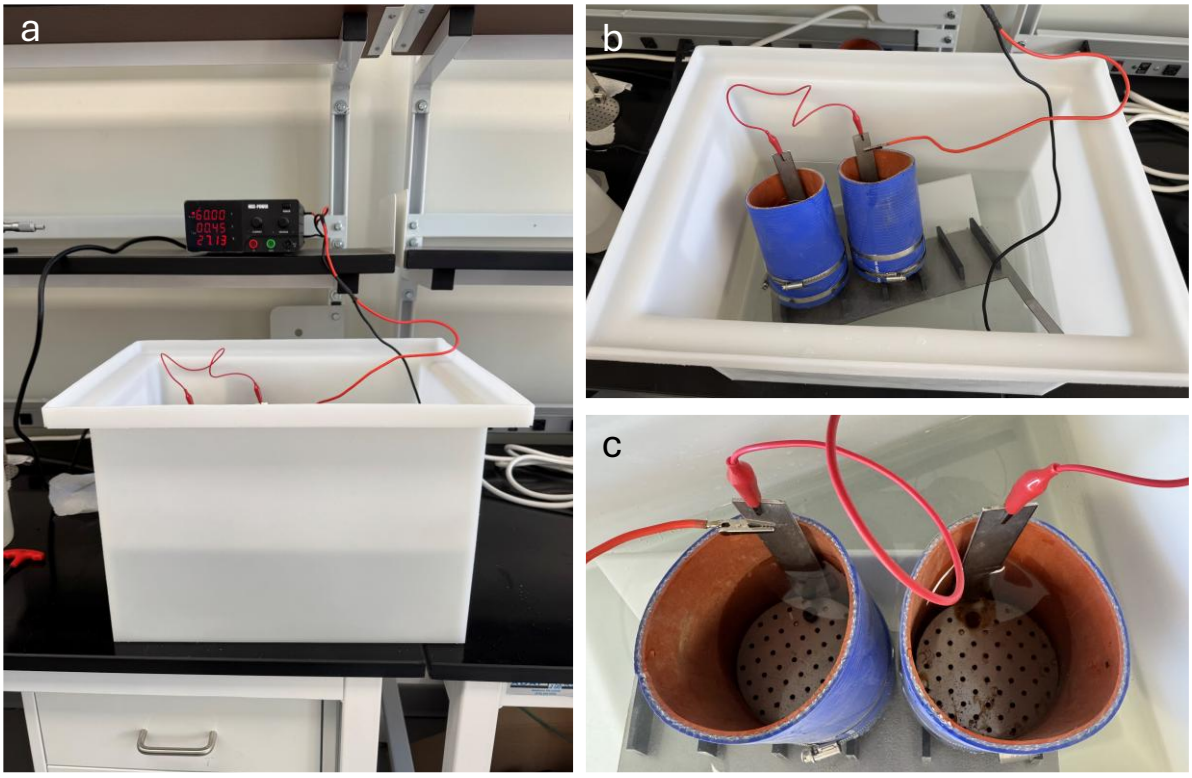

Figure 3.29: Laboratory test setup for the rapid chloride penetration test

3.7 Enforced carbonation for ASR

3.7.1. Enforced carbonation protocols

After the pre-conditioning, the mortar samples were cured under different CO_2 concentrations to investigate the role of enforced carbonation in ASR. In addition to the carbonation condition itself, the time that carbonation is applied to ASR-impacted concrete is also crucial, as the extent of ASR can change the components, microstructure, and permeability of concrete, thereby modifying the interaction with CO_2. As shown in Figure 3.30, to investigate the efficacy of carbonation in ASR mitigation at different stages and ASR extents, two enforced carbonation protocols (ECPs) were employed in this study. In ECP-1,

carbonation starts after 24 hours of pre-conditioning (48 hours after casting). In ECP-2, carbonation starts after 8 days of pre-conditioning (9 days after casting), when an ASR-induced volume expansion of 0.2% was reached. The sample cured at 50ºC, 95% RH, and 0% CO_2 throughout the whole testing period was studied as the control group (C_0). In both ECP-1 and ECP-2, 50ºC, 95% RH, and three CO_2 concentrations at 3%, 10%, and 20% were investigated. The carbonation was stopped at 30 days and 23 days after the pre-conditioning in ECP-1 and ECP-2, respectively.

The carbonation of ASR gels was conducted in a CO_2 incubator set at 50ºC, 75%RH with two CO_2 concentrations of 3% (G3) and 10% (G10) to elucidate the role and mechanisms of enforced carbonation in modifying the composition, structure, and hygroscopicity of ASR products. Phase and structural characterizations were carried out after carbonating for 3, 24, and 168 hours, while the moisture uptake behavior was evaluated after 168 hours of carbonation.

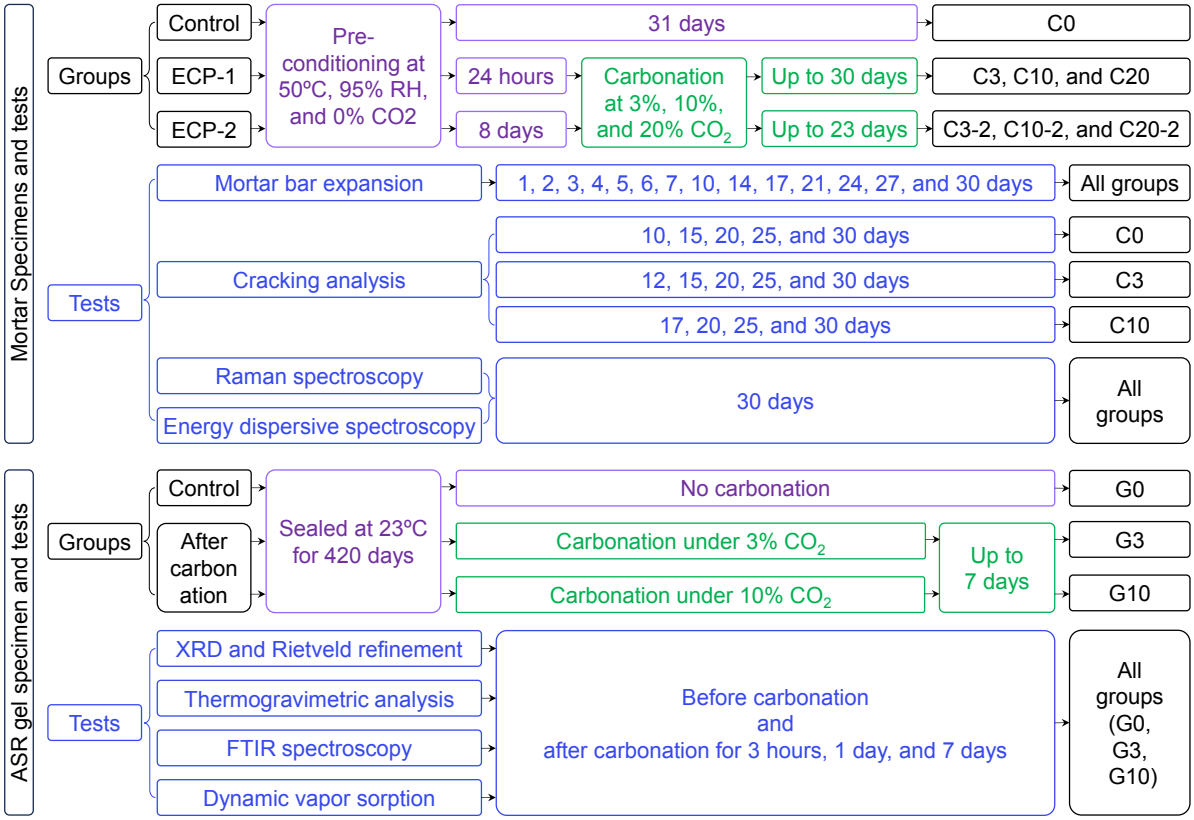

Figure 3.30: Overview of the specimen groups and testing methods of this study.

3.7.2. Expansion and cracking behavior of mortars with reactive aggregates

3.7.2.1 Mortar bar tests

The ASR expansion was evaluated by monitoring the length change of mortar bars using a digital comparator with a resolution of 0.0025 mm. For both ECP-1 and ECP-2, the initial

mortar length after 24 hours of pre-conditioning was measured as zero reading. Subsequent comparator readings were conducted after 12 and 24 hours for the first day, once a day for the first week, and then two readings each week up to 30 days.

3.7.2.2 Cracking analysis

The surface cracking behavior of the mortar cubes of C0, C3, C10, and C20 was evaluated by a digital microscope once the detectable crack was initiated (i.e., 10, 12, and 17 days for C0, C3, and C10, respectively) and then at 15 (for C0 and C3), 20, 25, and 30 days of curing. A grayscale method with an image processing program in ImageJ and MATLAB [167, 168] was applied to quantify the cracks formed on the sample surfaces. The original images were transformed into binary ones to distinguish the cracks and background. After pixel denoising and surface defects removal with a filter function built in ImageJ, the crack area and the maximum and average crack widths were quantified based on the identified pixels and structures. A transparent scale was used for benchmarking. It also should be noted that the physical size of the pixel is 0.009 mm. Therefore, cracks with a size smaller than that could not be measured, which may underestimate the cracks formed in the mortar bars. The average cracking density (ρ) was determined by dividing the crack area (A_c) by the surface area of the mortar cube (A_s) from three samples in each group, as shown in Eq. 9.

$$\rho = (A_c/A_s) \times 100\% \quad (9)$$

3.7.3 In-situ characterizations of ASR products formed in mortars

3.7.3.1 Raman spectroscopy

After 30 days of curing, the mortar bars of C0, C3, C10, and C20 were cut into thin disks with a precise low-speed saw, which were then dried in a vacuum desiccator for 2 days. The desiccator was equipped with soda lime to minimize carbonation. Raman spectroscopy was conducted on the cutting surface of the disk samples using a Horiba LabRam HR Evolution Raman Spectrometer-confocal Raman microscope over the range of 100 cm^{-1} to 1800 cm^{-1} at a resolution of 0.5 cm^{-1} by focusing on two different areas of interest: ASR products inside the cracks of aggregate and the hydrated cement pastes. A 633 nm excitation laser with a maximum power of 3.25 mW was used under a 50× objective lens with an acquisition time of 10 s. Two accumulations were collected for each testing point to eliminate irregularities in the spectra. The as-received data was processed with LabSpec 6 Spectroscopy Suite to remove the background and fit the peaks with the Gaussian function.

3.7.3.2 Energy dispersive spectroscopy

The elemental compositions of ASR products formed in selected mortars after 30 days of curing at 50ºC, 95%RH, and various CO_2 concentrations (C0, C3, C10, and C20) were quantified on polished surfaces cut from mortar bars using a JEOL JSM 7401F FE-SEM equipped with an EDS Genesis XM2 imaging system composed of a 10 mm^2 Si (Li) detector with a SUTW window under an accelerating voltage of 10.0 kV. The mortar samples were dried for 2 days in a vacuum desiccator with soda-lime to avoid carbonation. A gold coating was applied to the samples with a vacuum sputter coater (Denton Vacuum Desk IV). At least

30 points were collected from the ASR products formed in cracks of each group to capture the key elemental ratios.

3.7.4 Characterizations of synthetic ASR gels in carbonation

3.7.4.1 X-ray diffraction and Rietveld refinement

The XRD test was conducted using an AXRD powder X-ray diffractometer at 30 kV and 20 mA and the ASR gels were scanned on a rotary support between 5º and 65º 2θ in a stepwise mode at a step size of 0.1° (2θ) with a scanning time of 4 s per step before and after carbonation for 3 hours, 3 days, and 7 days. Commercially available software Highscore Plus, along with the International Centre for the Rietveld Diffraction Data (ICDD) database for reference powder diffraction files (PDF) was used for background correction, peak identification, and phase quantification via Rietveld refinement. The PDF cards used for the Rietveld refinement include clintobermorite (PDF-04-009-2235), sodium (Na)-kanemite (PDF-04-013-6127), and sodium (Na)-makatite (PDF-00-023-0703), constituting the ASR phases, and calcite (PDF-00-002-0629), vaterite (PDF-00-002-0261), and nahcolite (PDF-00-015-0700) as the carbonates. Lanthanum hexaboride (LaB_6) with 100% crystallinity was used as an external standard for the Rietveld refinement.

3.7.4.2 Thermogravimetric analysis

TGA was carried out on ASR gel samples after 0 hours, 3 hours, 3 days, and 7 days of carbonation using a Perkin Elmer TGA 4000 thermogravimetric analyzer. For each sample, approximately 30 mg ASR gels were used for the TGA test with an initial stage maintained at 30ºC for 5 minutes, followed by a stage of temperature increase from 30ºC to 900ºC at a heating rate of 10ºC/minute under N_2 purge gas at a flow rate of 20 mL/minute.

3.7.4.3 ATR-FTIR spectroscopy

ATR-FTIR spectra were acquired for ASR gels before and after carbonation under 3% CO_2 and 10% CO_2 for 3 hours, 3 days, and 7 days with a Thermo Fisher Scientific Nicolet iS10 FTIR spectrometer. A co-addition of 128 scans with a canning time of 190 seconds was employed to acquire the spectra between 4000 to 400 cm^{-1} with a resolution of 4 cm^{-1}. The background of the spectra was removed by the OMINIC software.

3.7.4.4 Dynamic vapor sorption

The dynamic absorption behavior under varying RH and water uptake capacity at a constant condition of the control group and the carbonated ASR gels after 7 days of CO_2 curing at 3% CO_2 and 10% CO_2 were investigated using a DVS Intrinsic II system (Surface Measurement System LTD, PA). Around 15 mg of ASR gels were tested under stepped RH between 0 % and 95 % at 25 °C. In the drying (desorption) stage, the RH started from 95%, then decreased to 90%, followed by a 10 % decrement until 0% RH. Upon mass equilibrium at 0% RH, the wetting (absorption) stage was started via an inverse RH increase to 95 % with the same step size intervals. Equilibrium was considered to be reached when the mass change rate became

lower than 0.0015 %/min over 10 min. The temperature, humidity, and equilibrium mass at each RH step were recorded with a 1-minute interval.

c

A modified drying rate method adapted from [169, 170] was applied to determine the water uptake capacity (WUC) of the ASR gels to reach the saturated surface-dry (SSD) condition. The mass change of around 15 mg of pre-saturated ASR gels was monitored at constant 40% RH and 40ºC using DVS. The data was recorded based on a 1-minute interval and the equilibrium was assumed when the mass change was less than 0.001%/min for 10 minutes. The dry weights of the samples were obtained based on the equilibrium mass at 0% RH. The drying rate and drying acceleration were calculated based on the first and second derivatives of the mass development over time, respectively. At the beginning of the drying process, the extra free water on the surface of the gels evaporates at a high rate, which decreases gradually. Then, the complete removal of the surface water can be indicated by an inflection point from the drying acceleration curve, which suggests the SSD condition. After the inflection point, internal water started to evaporate with a lower drying rate until an equilibrium mass was reached, from where the WUC of the control and carbonated ASR gels to reach their SSD conditions were determined.

4.0 Results

4.1 Pozzolanic reactivity of RGGP

Previous studies have demonstrated the potential of RGGP as a sustainable supplementary cementitious material (SCM) for partial cement replacement in concrete. However, achieving high levels of cement substitution remains challenging due to reductions in the physical and mechanical performance of concrete. Moreover, there are still significant knowledge gaps regarding the pozzolanic reactivity of RGGP and its influence on hydration kinetics and the development of hydration products. To address these gaps, this study investigates two types of RGGP with varying particle size distributions and chemical compositions, focusing on their pozzolanic characteristics and their effects on cement hydration processes.

Thermogravimetric (TGA) and derivative thermogravimetric (DTG) analyses of RGGP–CH–CC blends, shown in Figures 4.1a to 4.1d, were conducted at 23°C and 40°C after 1, 7, 28, and 56 days of curing. The results reveal that higher curing temperatures promote pozzolanic reactions, as indicated by the reduced mass loss in the 350–500°C range associated with calcium hydroxide (CH) decomposition. In contrast, the mass loss between 550–800°C corresponds to the breakdown of calcium carbonate (CC), which may result from both the added CC and carbonation of CH during testing, despite stringent efforts to limit carbonation. RGGP2 consistently exhibited greater CH consumption and higher levels of chemically bound water than RGGP1 at both temperatures, suggesting enhanced pozzolanic reactivity. This improved performance is likely linked to RGGP2’s finer particle size and greater amorphous content."

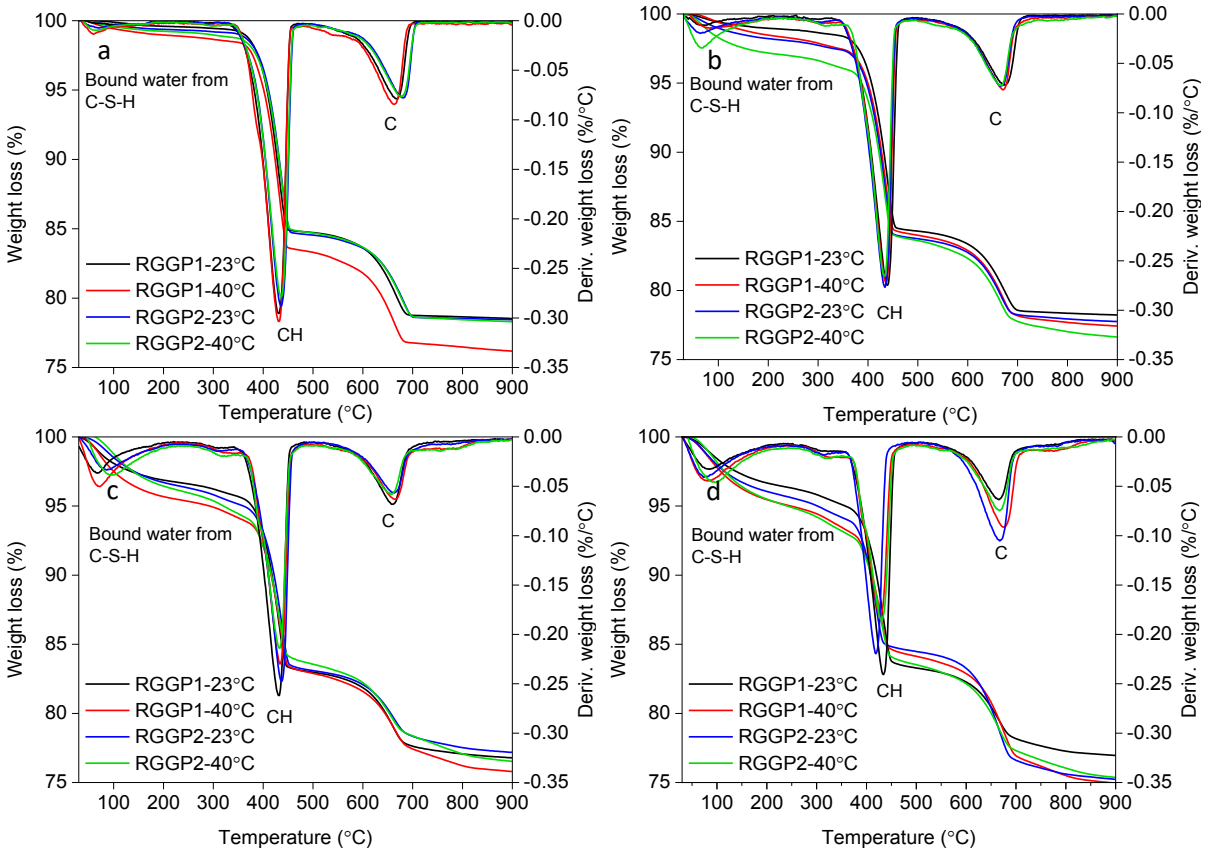

Figure 4.1: TGA and DTG curves of RGGP-CH-CC blends for the R3 test after (a) 1, (b) 7, (c) 28, and (d) 56 days.

The pozzolanic performance of RGGP was assessed through CH consumption and chemically bound water evolution, as shown in Figures 4.2a and 4.2b. Initially, both RGGP1 and RGGP2 consumed similar amounts of CH (~29 g/100 g) after 1 day at 23°C, and CH consumption increased with time. From day 7 onward, RGGP2 exhibited higher CH reactivity at both 23°C and 40°C. However, after 56 days at 40°C, RGGP1 slightly surpassed RGGP2, consuming 150.5 g CH per 100 g, suggesting that temperature plays a key role in enhancing late-stage reactivity. Bound water analysis indicated the ongoing formation of hydration products, such as C-S-H. After 1 day, RGGP1 produced notably more bound water at 40°C than RGGP2, likely due to rapid initial hydration. Yet between 1 and 7 days, RGGP2's bound water increased sharply by 93.6% eventually surpassing RGGP1. Overall, RGGP2 showed stronger performance under both temperatures, while the observed gap between CH consumption and bound water in RGGP1 at 40°C may reflect CH carbonation rather than continued pozzolanic reaction.

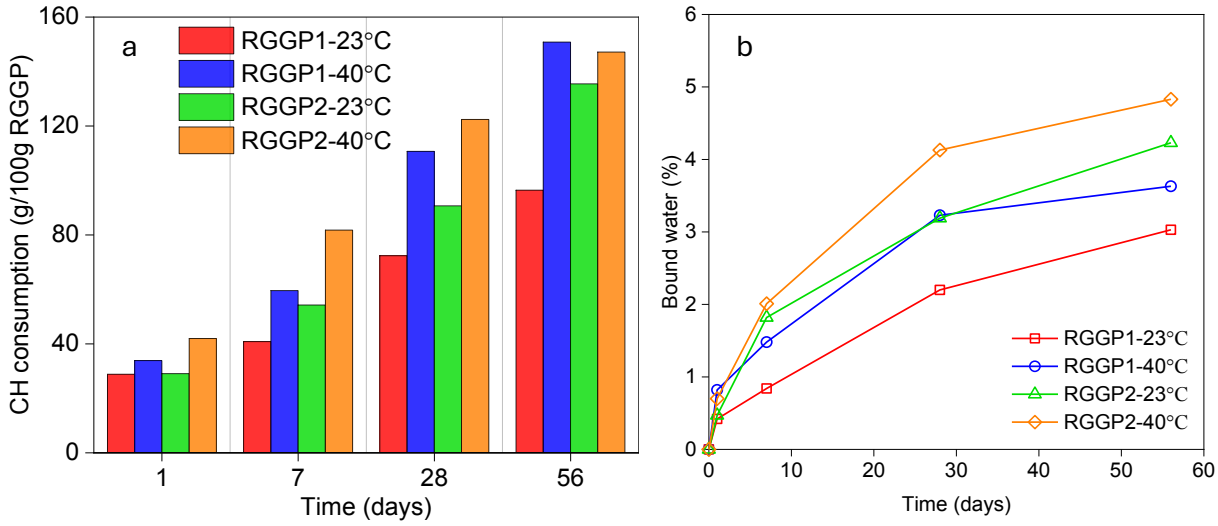

Figure 4.2: Quantification of (a) CH consumption and (b) evolution of chemically bound water of the RGGP blends according to ASTM C1897 for determining the pozzolanic activity.

4.2 Modifications in cement hydration in the presence of RGGP

4.2.1. Influence of RGGP on cement hydration kinetics

Figure 4.3 shows the heat flow and the cumulative heat release from the neat cement and binary RGGP-modified cement blends normalized by the weight of cement for the first 72 hours of hydration. All the samples showed the classic five-stage heat flow behavior that is observed in the hydration of cement: (i) the initial extreme exothermicity due to the rapid hydration of C_3A in cement in contact with water resulting in a high initial peak, (ii) the induction period where the reaction slows down, (iii) the acceleration period which was due to the hydration of the C_3S and resulted in the prominent peak, (iv) the deceleration period which also includes a broad secondary peak most likely due to the transformation of ettringite to monosulfate between 22 and 30 hours and (v) the steady state or the diffusion controlled step which is very slow and depends on the opportunity for further hydration of the cement. Both the control group with plain Portland cement (PC) and the RGGP-modified groups show a secondary peak beside the main C_3S peak on the deceleration side around 10 hours, which may be due to the secondary reaction of C_3A.

Figure 4.3 illustrates the impact of RGGP1 and RGGP2 on cement hydration. For RGGP1, increasing the replacement level delayed the main C_3S hydration peak, likely due to a prolonged induction period. Peak heat flow was highest at 5% replacement but declined at higher levels, suggesting a balance between enhanced reactivity and dilution effects. The secondary peak from C_3A hydration increased with RGGP1 content, likely due to added silica. In contrast, RGGP2 generally boosted the C_3S peak across most dosages, aided by its finer particles and larger surface area, which promote nucleation. Cumulative heat release

was greater with RGGP2, especially in the early stages, and exceeded RGGP1 by up to 7% after 72 hours, indicating stronger pozzolanic and hydration synergy.

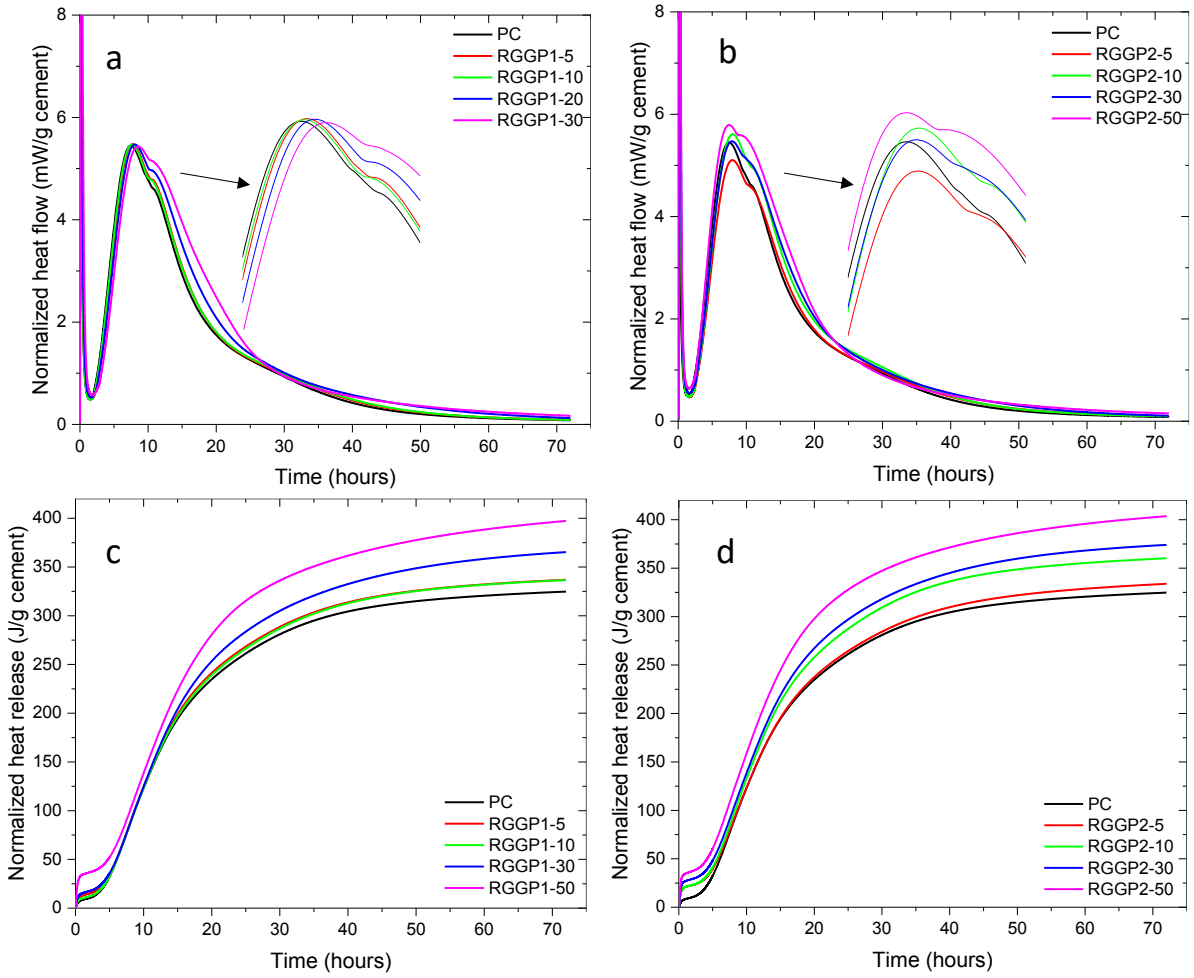

Figure 4.3: (a, b) Normalized specific heat flow and (c, d) cumulative heat release of the RGGP-modified cement pastes.

4.2.2. Evolution of hydration products

Figure 4.4 displays TGA and DTG results of RGGP-modified and control cement pastes after 7, 28, and 90 days of sealed hydration. Hydration products were identified by weight loss in defined temperature ranges using a modified tangent method [150]. The degree of hydration can be determined by the reduction of bound water between 30°C and 105°C [171] and between 105°C and 200°C [152]. The pozzolanic reaction can be determined by the change in CH weight drop between 400°C and 500°C [170]. At 7 days, both materials showed reduced free and loosely bound water, suggesting enhanced hydration, while the lower chemically bound water—especially in RGGP1—implied a dilution effect due to partial cement replacement. This also led to a reduction in CH formation, which became more evident as RGGP content increased. From 7 to 28 days, a rise in chemically bound water and

a drop in CH weight loss pointed to the activation of the pozzolanic reaction, particularly in mixes with higher RGGP dosages. For RGGP1, the pozzolanic contribution became more pronounced at 50% replacement by 90 days, while lower dosages showed minimal additional reactivity. RGGP2 followed similar trends but showed stronger performance overall. At 7 days, higher chemically bound water and lower CH content in RGGP2-30 and RGGP2-50 indicated earlier and more effective pozzolanic activity than RGGP1. From 28 to 90 days, RGGP2-50 exhibited near-complete CH consumption, with a corresponding increase in bound water from C-S-H, suggesting highly efficient pozzolanic conversion. Overall, RGGP2 demonstrated greater pozzolanic reactivity than RGGP1 across all ages and replacement levels.

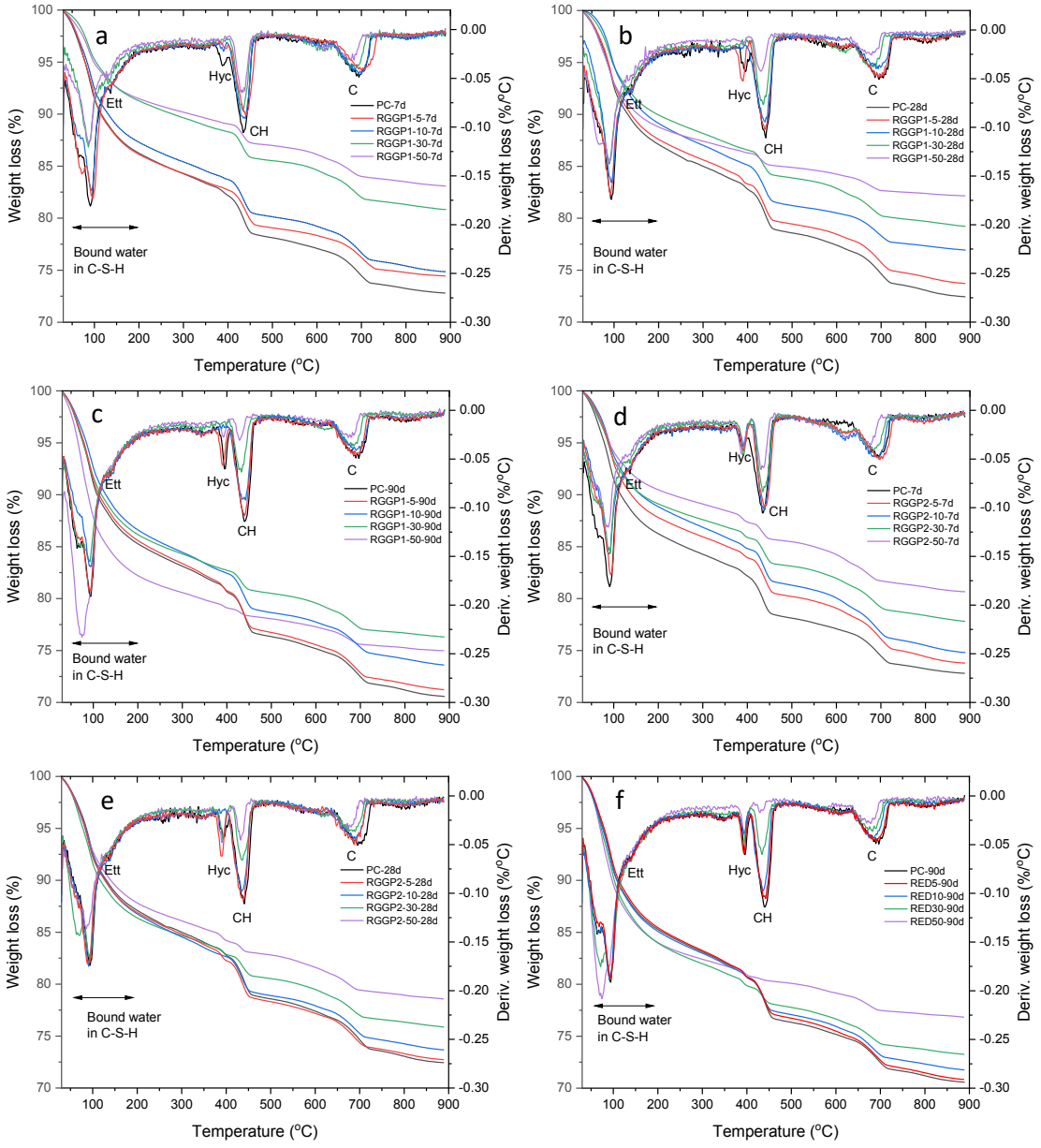

Figure 4.4: TGA and DTG curves of (a, b, c) RGGP1 and (d, e, f) RGGP2 modified pastes after (a, d) 7, (b, e) 28, and (c, f) 90 days.

Figure 4.5 illustrates the CH content in RGGP-modified cement pastes over time. After 7 days, 5% RGGP1 slightly reduced CH by 1.6%, while 10% replacement unexpectedly increased CH by 2.1%, likely due to insufficient pozzolanic activity to offset CH generation from cement hydration. At higher dosages (30% and 50%), CH dropped significantly by 13.7% and 35.8%, suggesting active pozzolanic reaction and dilution effects. From 7 to 28 days, CH levels rose in low-dosage pastes due to continued cement hydration, while RGGP1-30 and RGGP1-50 showed minimal or significant CH reductions. Between 28 and 90 days, CH continued to decrease in RGGP1-30 and RGGP1-50, confirming sustained pozzolanic activity. RGGP2 showed a slightly different trend. At 5% dosage, CH content increased by 10.3%, possibly due to enhanced hydration from its higher fineness. However, at 30% and 50% replacement, CH dropped by 18.6% and 37.8% at 7 days. Continued reductions from 28 to 90 days, 20.2% and 41% for 30% and 50% dosages, highlighted the superior long-term pozzolanic reactivity of RGGP2 compared to RGGP1. Even at lower dosages, RGGP2 still outperformed RGGP1 in CH consumption over time.

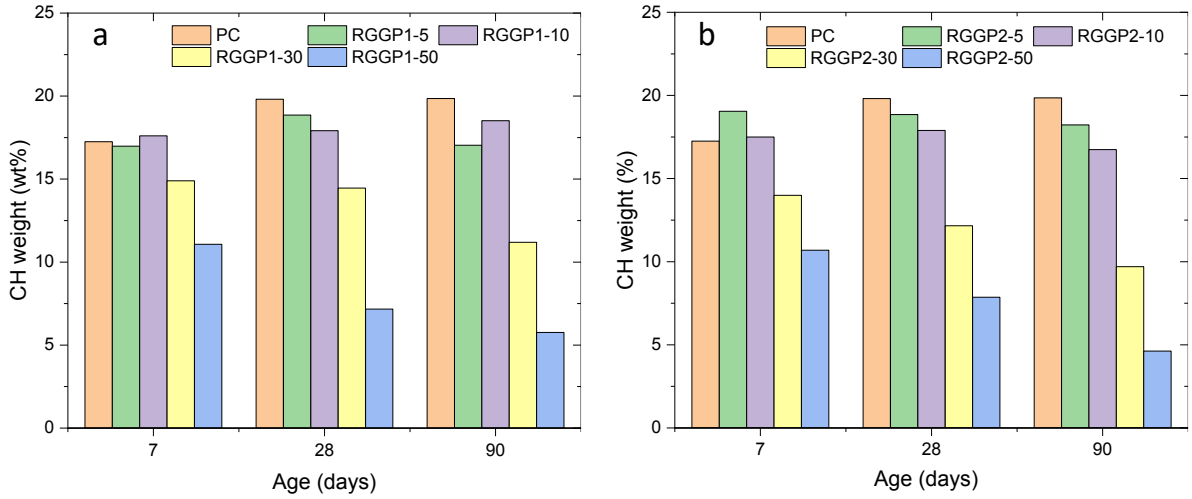

Figure 4.5: Evolution of CH contents of cement pastes modified with (a) RGGP1 and (b) RGGP2.

Figure 4.6 illustrates the degree of hydration (DOH) of cement and the degree of reaction (DOR) of RGGPs over time, based on the CH consumption and chemically bound water over time. For RGGP1, DOH increased with dosage, reaching up to 95.1% by 90 days, indicating continued hydration. In contrast, DOR decreased as RGGP1 dosage increased. As a result, RGGP1-50 had a 50.6% lower DOR than RGGP1-30 at 7 days, and even at 90 days, RGGP1-30 maintained a 47.1% higher DOR. Similarly, RGGP2 showed higher cement DOH at 50% replacement after 7 days, but by 90 days, both 30% and 50% samples converged. Like RGGP1, RGGP2's DOR was inversely related to dosage. RGGP2-30 had 44.7% and 86.6% higher DOR than RGGP2-50 at 7 and 90 days, respectively, which indicates that increased RGGP content doesn't necessarily lead to higher pozzolanic reactivity.

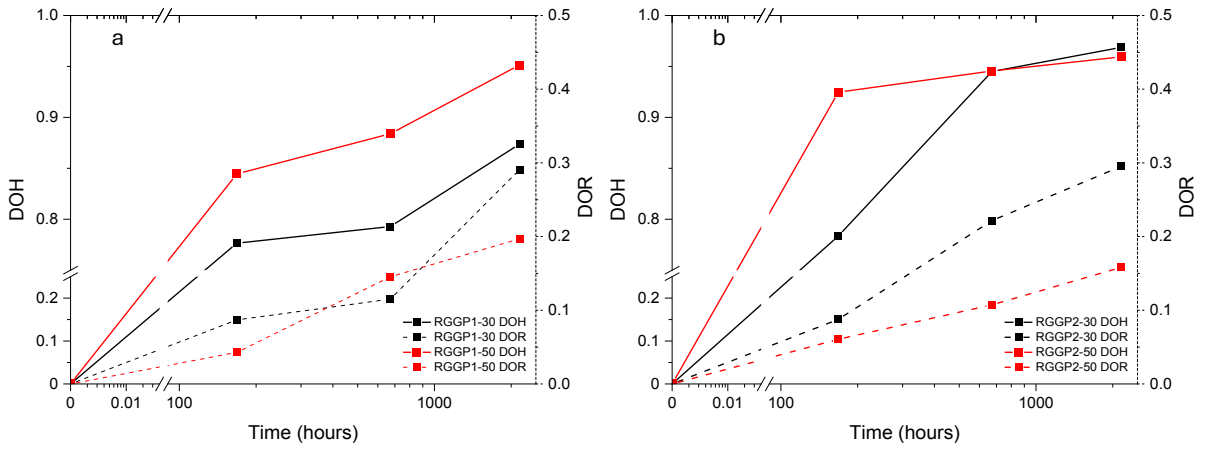

Figure 4.6: The degree of hydration (DOH) of cement and degree of reaction (DOR) of (a) RGGP1 and (b) RGGP2 in cement pastes at replacement levels of 30% and 50%.

4.2.3. Thermodynamic simulation

Figure 4.7 shows how RGGP and its degree of reaction (DOR_{GP}) influence cement hydration product formation, assuming 80% cement hydration. At 0% DORGP, typical hydration phases like C-S-H, CH, ettringite, hydrogarnet, and hydrotalcite were present. CH initially made up 18.6 g/100 g binder for RGGP1 but was fully consumed by ~51.6% DORGP, while C-S-H nearly doubled. Beyond this point, C-S-H growth slowed, and phases like hydrogarnet and natrolite (due to RGGP1's high Na_2Oeq) became more prominent. At 50% RGGP1, dilution reduced early CH and C-S-H, but CH was consumed faster (~22% DORGP), and phases like natrolite and M-S-H formed at higher DOR. Even after full RGGP1 reaction, C-S-H gain was only 4.8% higher than at 30% replacement, suggesting CH availability limits further C-S-H formation. For RGGP2, phase changes followed a similar trend, with CH depletion occurring at similar DORGP ranges (52.9% at 30%, 22.1% at 50%). Differences in SiO_2 content may explain the slightly delayed CH consumption compared to RGGP1. Although RGGP2's finer particles likely enhance reactivity, thermodynamic models don't capture this. Predicted CH contents at 90 days were 19.4% and 25.9% lower than experimental results at 30% and 50% RGGP2, indicating model limitations in accounting for particle size effects.

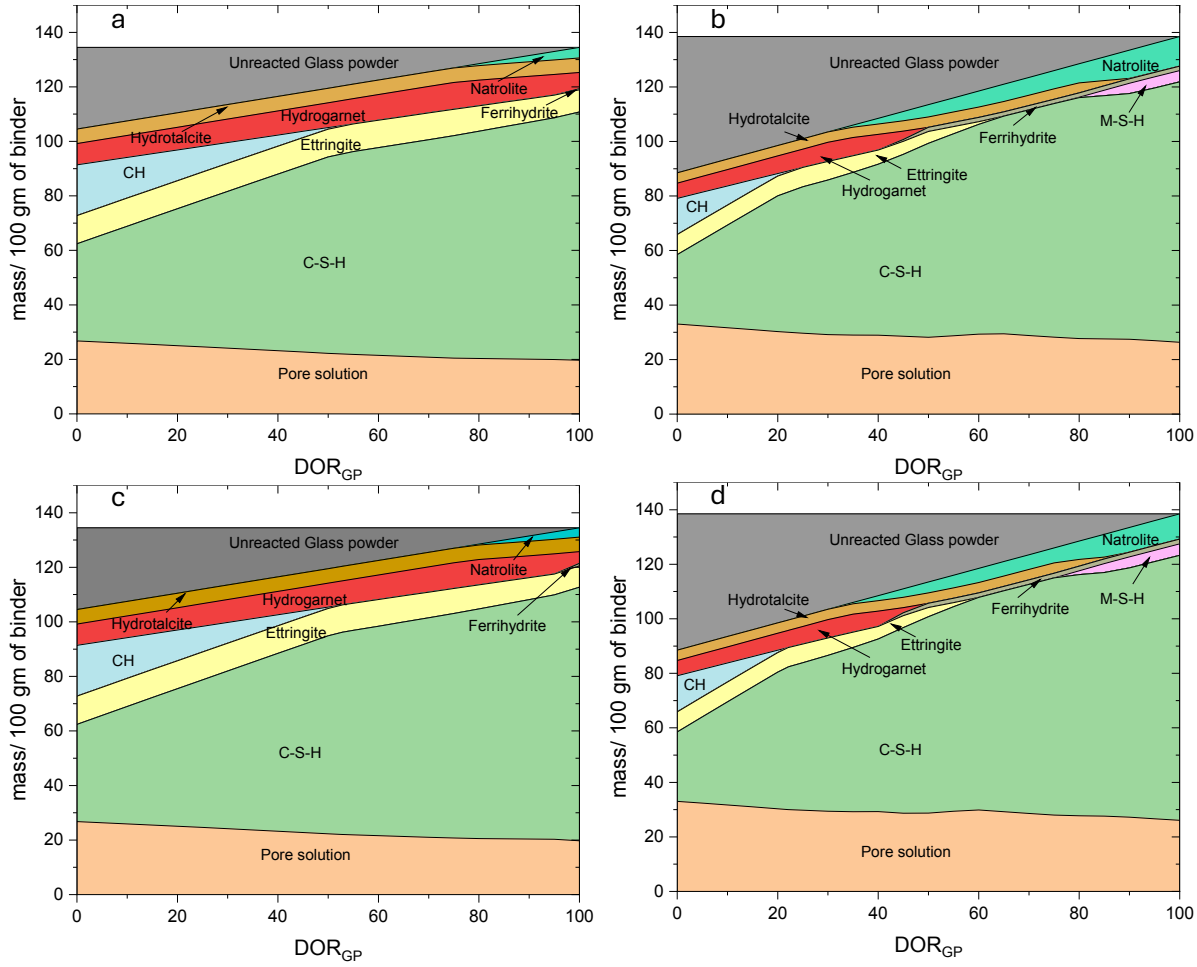

Figure 4.7: Thermodynamic modeling of (a, b) RGGP1 and (c, d) RGGP2 at replacement levels of (a,c) 30% and (b, d) 50% with varying DOR of RGGP and a constant DOH of cement at 80%.

4.3 Changes in the workability of cement mortar and the adjustment of superplasticizer

Figure 4.8 illustrates the impact of RGGP1 and RGGP2 on mortar workability across different replacement levels. As RGGP1 content increased, flowability steadily declined dropping by 22% at 10% replacement and reaching a 36.1% reduction at 50%. RGGP2 caused even sharper decreases, with flow reductions of 41.2% and 52.2% at the same replacement levels. This greater loss in workability is attributed to RGGP2's finer particles and larger surface area, which increase water demand. Additionally, the angular shape and high surface area of both glass powders contribute to reduced flow, consistent with prior studies [172, 173]. To maintain adequate workability, flow values were controlled within

±5% of the control mix by adjusting the high-range water reducer dosage. Table 4.1 lists the required superplasticizer amounts for each RGGP1 and RGGP2 replacement level.

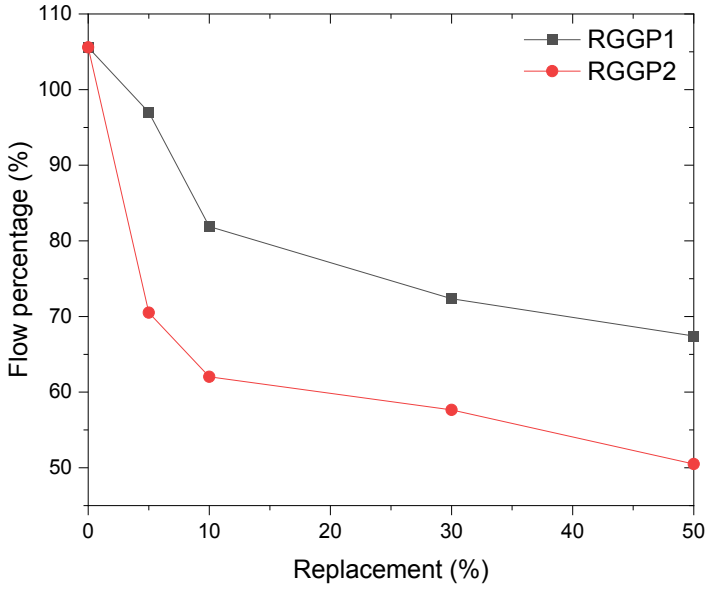

Figure 4.8: Evolution in workability of RGGP modified mortar at different replacement levels

Table 4.1: Adjusted superplasticizer dosage for flow consistency

Replacement percentage	RGGP1		RGGP2	
	Dosage of SP	Flow (%)	Dosage of SP	Flow (%)
0	0%	105.58	0%	105.58
5	0.03%	105.62	0.06%	105.62
10	0.04%	105.33	0.08%	106.19
30	0.08%	105.97	0.10%	105.82
50	0.10%	108.14	0.15%	106.53

4.4 Effect of RGGP on the development of compressive strength

Figure 4.9 illustrates the compressive strength development of RGGP-modified mortars under lime water curing. The control mix (PC) reached 34.45 MPa at 7 days, with strength increases tapering off after 56 days. With 5% RGGP1, strength dropped 28% at 7 days but improved over time, remaining 13.5% below PC at 90 days. Strength increased with RGGP1 dosage up to 30%, likely due to pozzolanic activity, then declined at 50% due to dilution. RGGP1-30 achieved near-PC strength (only 2.8% lower), while RGGP1-50 showed a 166% strength gain from 7 to 90 days, highlighting delayed but substantial pozzolanic contribution.

Per ASTM C618 [174], the pozzolanic strength activity index (SAI), defined as the strength ratio to the PC mix, requires a minimum of 75% at 20–25% replacement after 7 or 28 days. RGGP1 meets this threshold up to 30% replacement at early ages, and all mixes exceed it by 90 days, confirming its potential for high-volume cement replacement.

As shown in Figure 4.9b, RGGP2 achieved higher early strength than RGGP1 across all dosages. At 5% replacement, strength exceeded the PC mix by 3.8%, then declined with higher dosages, reaching a 41.5% drop at 50%. Over time, strength improved significantly, with RGGP2-10 and RGGP2-30 surpassing PC by over 13% at 90 days. The 75% SAI threshold was met for all mixes by 90 days, and even the 50% group slightly exceeded PC strength. These gains are attributed to RGGP2's finer particles and greater surface area, which enhanced pozzolanic reactivity, consistent with CH consumption and XRD analysis. This is also in line with the enhanced long-term strength evolution under the influence of pozzolanic fly ash [175].

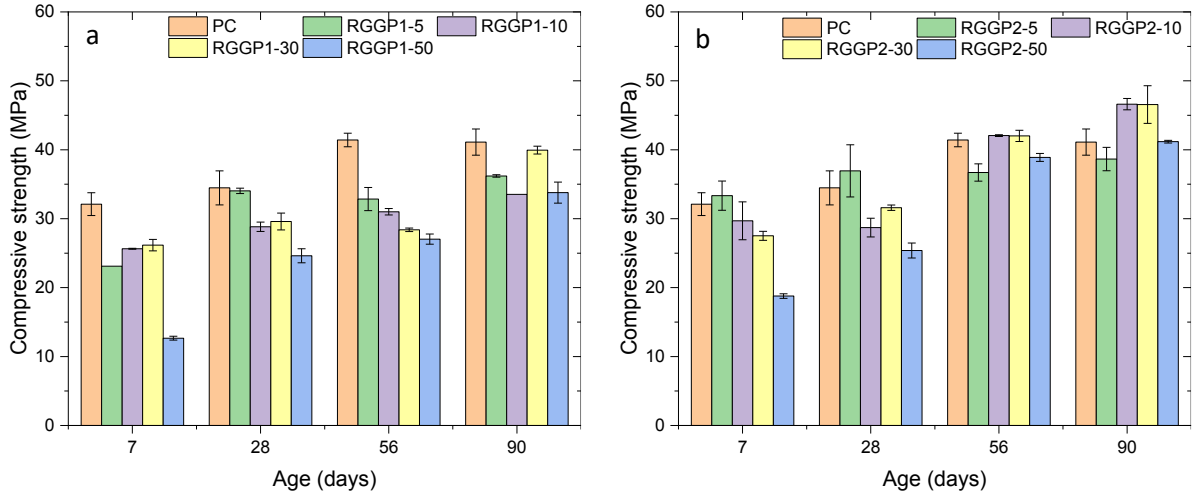

Figure 4.9: Evolution of compressive strength of mortars modified with different dosages of (a) RGGP1 and (b) RGGP2 under lime curing.

Steam curing was used to improve the early-age compressive strength of mortars with high-volume RGGP replacement. For RGGP1, samples with 30% and 50% replacement showed 14.4% and 28.4% lower strength, respectively, than the PC group under lime water curing after 7 days (Figure 4.10a). Although RGGP1-30 gained 23% strength from 7 to 90 days, it still remained 23.6% lower than the PC. RGGP1-50 showed little to no strength gain beyond 7 days, and even a slight drop at 56 days, aligning with prior studies noting that steam curing above 80°C can negatively affect concrete microstructure [176]. However, when cured at 70°C, RGGP1-30 and RGGP1-50 showed 5.1% and 81.4% higher strength at 7 days compared to their lime-cured counterparts, highlighting the benefit of steam curing in accelerating early hydration and pozzolanic reaction in high-RGGP mixes. RGGP2 exhibited a similar trend. After 7 days, RGGP2-30 showed 8% higher strength than the PC mix under lime water, while RGGP2-50 was 8.9% lower. Under steam curing, both improved significantly—RGGP2-30 and RGGP2-50 gained 26% and 55.7% more strength, respectively, than those cured in lime water (Figure 4.10b). Despite minimal strength

increase from 7 to 90 days under steam, both RGGP1 and RGGP2 mixes maintained stable strength over time, unlike the steam-cured PC group, which showed strength reduction after 7 days. This suggests that RGGP incorporation may reduce the negative impact of steam curing on long-term strength while effectively enhancing early-age performance.

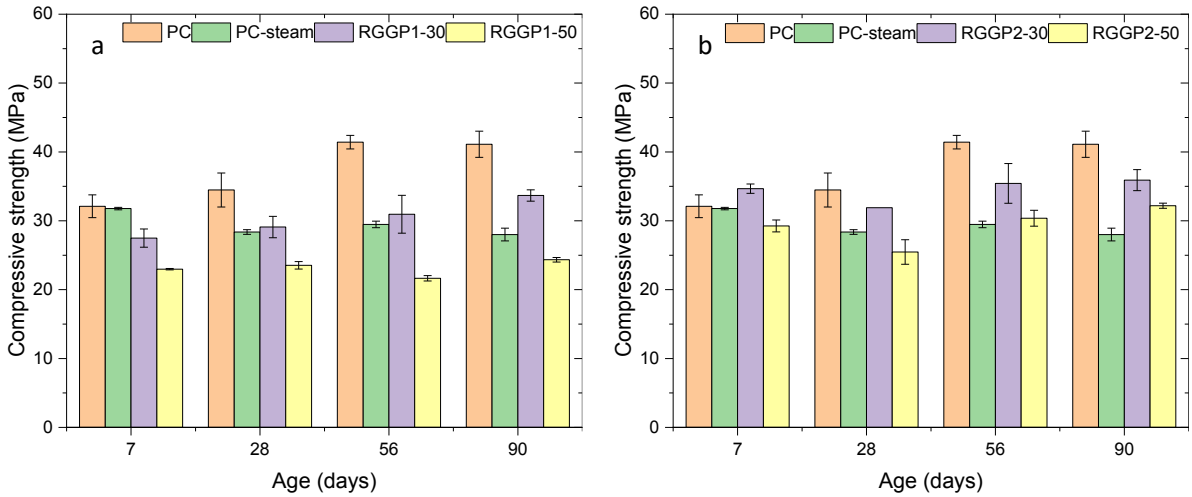

Figure 4.10: Evolution of compressive strength of mortars modified with 30% and 50% replacement of (a) RGGP1 and (b) RGGP2 under steam curing.

4.5 The role of metakaolin as a pozzolan

4.5.1. Characterization of metakaolin

With the same purpose of incorporating RGGP in cement concrete, other alternative materials, such as MK, also show promising pozzolanic roles, which can be leveraged to reduce the amount of cement and improve the performance of concrete. In this study, MK was investigated in an innovative way by utilizing its unique moiture absorption and desorption behavior. Ordinary Portland cement (Type I/II) produced by Quikrete in accordance with [177] and MK obtained from Fishstone Studio were used as cementitious materials in this study. The particle size distributions of the cement and MK were measured by laser diffraction. As shown in Figure 4.11a, the cement has a median particle size and specific surface area of 13.8μm and 1.66m^2/g, respectively. Measured by means of laser diffraction, the MK shows a finer particle size than cement with a median size of 3.79μm and a specific surface area of 2.93m^2/g. Figure 4.11b shows the X-ray diffraction (XRD) patterns of cement and MK. Cement shows peaks for gypsum and main clinker minerals, including alite (tricalcium silicate), belite (dicalcium silicate), tricalcium aluminate, and tetracalcium aluminoferrite. The broad hump indicates the amorphous feature of MK, while crystalline peaks of kaolinite and quartz are also detected.

The chemical and mineralogical compositions of cement and MK were analyzed by X-ray fluorescence and Bogue calculations. As summarized in Table 4.2, MK is an Al-rich material with a combined aluminate and silicate content of over 94%. The water absorption of MK

was measured according to [178], where a water-uptake capacity of 61.3% was obtained. This value was used as a basis for the different degree of saturation (DOS) of MK in MIC. Reagent-grade lithium nitrate powder with a density and purity of 2.38g/cm^3 and >99%, respectively, was used as a lithium source after dissolving in deionized (DI) water before mixing with the cement matrix. Extra pure magnesium nitrate hexahydrate ($Mg(NO_3)_2 \cdot 6H_2O$) with a purity of 99% (Thermo Fisher Scientific) and DI water were used for synthesizing saturated solutions to control the RH in the drying shrinkage test.

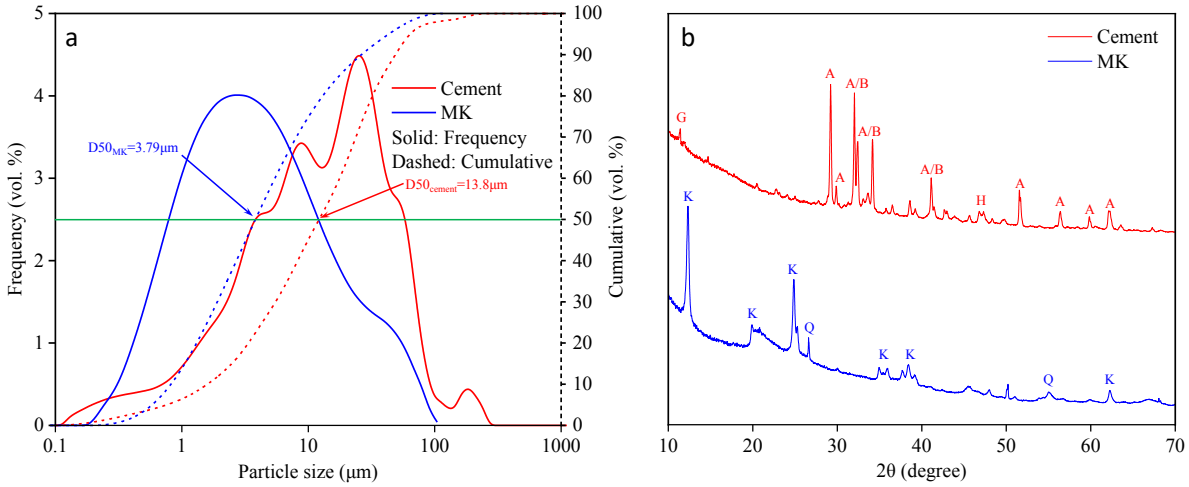

Figure 4.11: (a) Particle size distributions and (b) XRD patterns of cement and MK (G: gypsum, A: alite (tricalcium silicate), B: belite (dicalcium silicate), H: alite, tricalcium aluminate or tetracalcium aluminoferrite, K: kaolinite, and Q: quartz).

Table 4.2: Chemical and mineralogical compositions of cement and MK (wt.%).

	CaO	SiO_2	Al_2O_3	SO_3	Fe_2O_3	MgO	K_2O	Na_2O	TiO_2	ZrO_2	SrO	Cl
MK	0.07	51.80	42.40	0.11	4.15	-	0.22	-	1.1	0.09	0.04	0.05
Cement	62.70	20.10	4.80	3.50	3.20	3.40	Na_2O_{eq}	LS	Mineralogical compositions			
									C_3S	C_2S	C_3A	C_4AF
							0.60	1.20	54.00	17.00	7.00	10.00

Note: C_3S: tricalcium silicate; C_2S: dicalcium silicate; C_3A: tricalcium aluminate; C_4AF: tetra-calcium aluminoferrite; LS: limestone.

4.5.2. Pozzolanic reactivity of MK in metakaolin-based internal conditioning (MIC)

Figure 4.12a shows the TGA and DTG curves of PC and fully saturated metakaolin-based internal conditioning (FMIC) after 28 days of hydration. The main hydration products of cement can be identified from the weight losses from the TGA curves or the corresponding peaks from the DTG curves in their specific thermal decomposition temperature ranges. The first weight loss between 30˚C and 200˚C is due to the evaporation of free water and dehydration of ettringite, calcium silicate hydrates (C-S-H), and strätlingite, which possess loosely bound water. AFm, CH, and CC are decomposed in the range of 250-300˚C, 400-510˚C, and 590-710˚C, respectively. CH is formed from cement hydration, while it can be

consumed by pozzolanic reactions in the presence of MK to form additional C-S-H or C-A-S-H.

The development of CH contents that remained in the cement pastes is shown in Figure 4.12b. It can be seen that approximately 16.6% of CH was precipitated in PC at 7 days, which increased to 17.8% after 90 days, indicating the progress of cement over time. Due to the pozzolanic reaction, a dramatic decrease in CH content was observed from the dry MK group (DMK), which was 40.4% lower than that of PC after 90 days. The MIC groups, however, yielded higher CH contents than DMK during the investigated ages, while they are still lower than that of PC. This might be due to the extra water introduced by MIC can preferentially fuel the hydration of cement as the residual CH content is a result of a dynamic balance between cement hydration (producing CH) and pozzolanic reactions (consuming CH). It is seen that the CH contents in the MIC groups increased during the first 28 days.

It is interesting to find that the CH contents are positively correlated with the DOS of MK, where FMIC showed the highest 28-day CH content of 13.7%, which is 21.7% lower than that of PC but 6.2% and 4.6% higher than that of 0.5MIC and 0.75MIC, respectively. From 28 days to 90 days of hydration, decreasing trends are observed from the CH contents of MIC groups, which are opposite to the increasing trends of PC and DMK. 0.5MIC, 0.75MIC, and FMIC showed 4.2%, 6.9%, and 11.7% lower CH contents at 90 days than those at 28 days, respectively. These changes indicate the increasingly dominant role of pozzolanic reaction over cement hydration at later ages and demonstrate the benefit of MIC in sustaining the reactivity of MK particles in the matrix of cement.

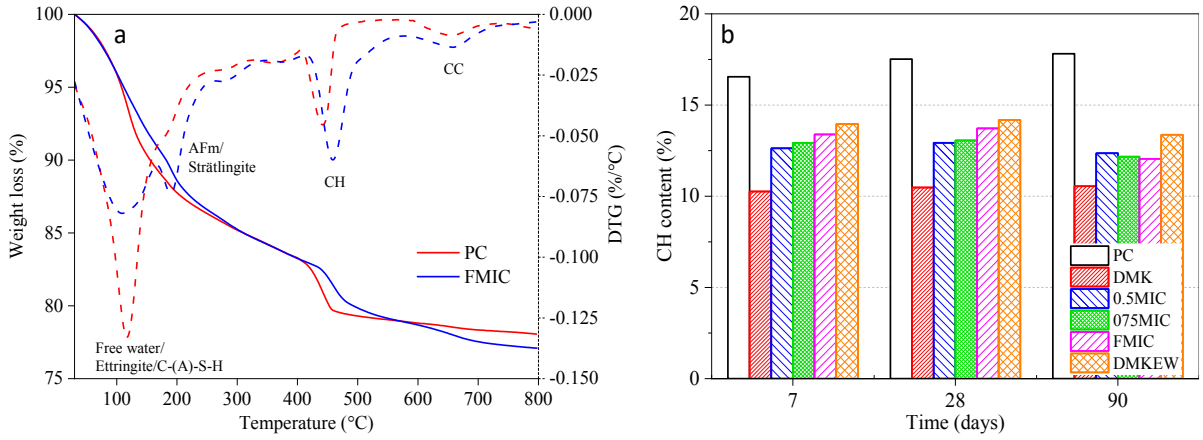

Figure 4.12: (a) TGA and DTG curves of PC and FMIC, and (b) development of CH contents.

4.5.3. Moisture desorption and microstructural modification

Figure 4.13a shows the DVS results of 0.5MK, FMK, and FMKLi. It can be seen that 0.5MK reached its equilibrium from 95% to 0% RH with an overall length of around 800 minutes, while a longer time was taken for FMK. This is expected as more moisture was carried by MK at a higher degree of saturation. In the presence of lithium nitrate, FMKLi took an even

longer time to reach mass equilibrium at high RH steps, which might be due to the hygroscopic nature of nitrate.

The moisture desorption isotherms for 0.5MK FMK, and FMKLi are shown in Figure 4.13b. Approximately 40.9% and 53.7 of % water of 0.5MK was released at 95% RH and 90% RH, respectively. Due to the higher amount of water, these two values of FMK were increased to 54.0% and 74.4%, respectively. As discussed above, the addition of lithium nitrate resulted in less moisture loss from FMKLi at the high RH steps, showing only 26.5% and 59.8% of water release at 95% RH and 90% RH, respectively. Again, this can be explained by the water-retaining effect of nitrate. As defined in [179], an efficient LWA for internal curing shall release more than 85% of its absorbed water when RH drops to 94%. However, it should be noted that different from LWA with an inert nature, MK can play multiple roles in the cement system by releasing moisture to fuel cement hydration and participating in pozzolanic reactions. The gradual release of moisture from the saturated MK will favor both the hydration and pozzolanic reactions, which have been investigated in the authors' previous study [180].

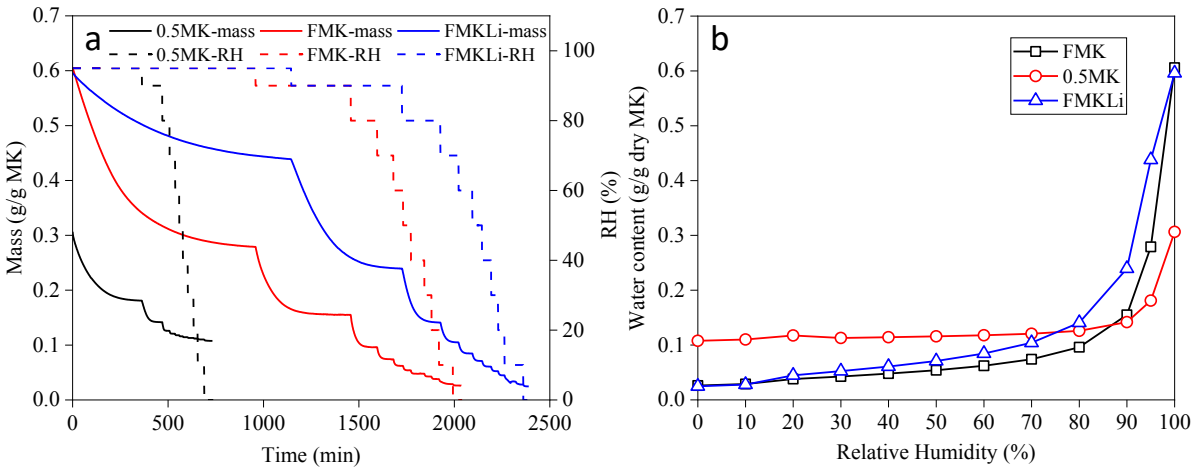

Figure 4.13: (a) Moisture release behavior in the dynamic vapor sorption tests and (b) desorption isotherms of 0.5MK, FMK, and FMKLi.

MK is produced from the dehydroxylation of kaolinite, which was considered irreversible [181], while previous studies [182, 183] revealed that the dehydroxylation of kaolinite to MK is reversible, probably due to (i) the dissolution of MK followed by crystallization, (ii) the crystallization of small kaolinitic nuclei after local dissolution of MK micro-regions, and (iii) rearrangement of chemical bonds in a purely solid-state process [184]. To investigate the influence of the pre-saturation process on the structure of MK, ATR-TFIR, and XRD analyses were conducted on dry MK and saturated MK under various degrees of saturation (0.5MK, 0.75MK, and FMK). As shown from the FTIR spectra in Figure 4.14a, characteristic OH-stretching vibrations at 3690, 3650, and 3620 cm^{-1} are associated with νAl_2OH in Al-kaolinite [185], which became sharper with higher intensity with increasing degree of saturation. The γSi-O stretching vibrations at 1032 and 1007 cm^{-1} [186], Al-Al-OH at 911 $cm^{-1,}$ and γSi-O-Al (octahedral) stretching at 534 cm^{-1} [187] were found to increase from MK to FMIC.

In line with the findings from FTIR, kaolinite-related peaks at 12.26˚ and 24.84˚ 2θ [188] along with peaks of quartz were observed from the XRD patterns of the dry and saturated MK (Figure 4.14b). Therefore, Kaolinite (PDF-00-058-2006) and quartz (PDF-00-001-0649) were used in the Rietveld refinement analysis. The results indicate that the dry MK contains 44.8% kaolinite, which might be due to insufficient calcination. After being saturated to 50%, 75%, and 100% DOS, the kaolinite content was found to decrease to 43.0%, 40.7%, and 36.7%, respectively. The dry MK possesses an amorphous percentage of 54.3%, revealing its highly amorphous nature, which explains the high pozzolanic reactivity. It is interesting to see that 0.5MK, 0.75MK, and FMK exhibited 4.1%, 8.1%, and 15.3% higher amorphousness than dry MK, which supports the finding in Section 3.1.

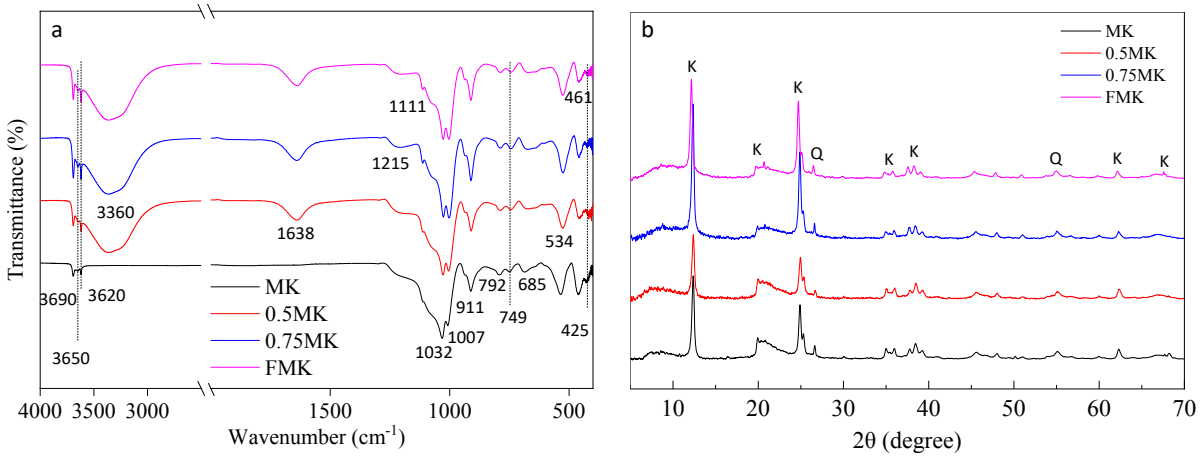

Figure 4.14: (a) FTR and (b) XRD spectra of MK with different degrees of saturation levels (K: kaolinite; Q: quartz).

4.5.4. Sample preparation

To investigate the effects of MIC, lithium nitrate, and their synergistic effect on the early-age shrinkage behavior of the cement mixtures, in terms of chemical, autogenous, and drying shrinkages, 9 groups summarized in Table 4.3 were prepared in this study. PC with a w/cm ratio of 0.35 was prepared as the control group. Two mixtures containing lithium nitrate at lithium-to-alkali (Li/[K+Na]) ratios of 0.28 and 0.74 were prepared as the low-lithium (LLi) and high-lithium (HLi) groups to understand the effect of lithium on the shrinkage behavior of cement. Two cement mixtures with 30% substitution with dry MK, one with a w/b ratio of 0.35 and a high-performance water reducer admixture (ADVA Cast 555) at a dosage of 0.67% of the binder by weight to adjust the workability (DMK) and one with extra mixing water (DMKEW) equal to the total water in the fully saturated MK group (the FMIC discussed below) were prepared to gain insights into the role of dry MK in modifying cement's shrinkages.

In addition, three MIC groups with 30% replacement of cement by MK with DOS of 50% (0.5MIC), 75% (0.75MIC), and 100% (FMIC) were prepared. The MK was first pre-saturated with deionized (DI) water for 24 hours, followed by a drying process in an oven at 70˚C until reaching the weight for the specific DOSs based on the measured water-uptake

capacity of MK. The MK samples at their desired DOSs were sealed for 12 hours for moisture homogenization. The synergistic effect of MIC and lithium nitrate was studied by adding lithium into FMIC at a lithium-to-alkali (Li/[K+Na]) ratio of 0.74 (FMIC-Li). Chemical shrinkage and autogenous shrinkage were studied based on cement paste specimens, while drying shrinkage was investigated based on mortar bar specimens at a binder-to-sand ratio of 1. The cement pastes for chemical shrinkage were mixed in a vacuum mixer at 500 rpm for 3 minutes to ensure homogenous mixtures with no air bubbles, while the fresh admixtures for both autogenous and drying shrinkage were mixed in a mechanical mortar mixer at 60 rpm for 2 minutes, followed by a 1-minute rest, and then 3 minutes of mixing at 120 rpm.

Table 4.3: Mix proportions of cement mixtures.

Group	Cement (g)	Mixing water (g)	Lithium nitrate (g)	MK (g)	MIC water (g)
PC	100.00	35.00	-	-	-
LLi	100.00	35.00	0.38	-	-
HLi	100.00	35.00	0.99	-	-
DMK	70.00	35.00	-	30.00	-
0.5MIC	70.00	35.00	-	30.00	9.14
0.75MIC	70.00	35.00	-	30.00	13.73
FMIC	70.00	35.00	-	30.00	18.24
DMKEW	70.00	53.00	-	30.00	-
FMIC-Li	70.00	35.00	0.69	30.00	18.24

For compressive strength investigations, mortars prepared based on the paste mixtures as summarized in Table 4.3 with a water-to-binder ratio of 0.35 and binder-to-sand ratio of 1:1 for selected groups (PC, FMIC, FMIC-Li) were mixed with gradually added sand in a mechanical mortar mixer at 60 rpm for 2 minutes, followed by a 1-minute rest and 3 minutes of further mixing at 120 rpm. Then, three 50 mm by 50 mm by 50 mm cubic samples were cast for each testing age. Right after casting, the specimens were covered with a plastic sheet to avoid water loss for 24 hours and then demolded and cured in saturated CH solution at 23 ± 2 ˚C until testing.

4.5.5. Influence of MIC on cement hydration

Figure 4.15 shows the evolution of normalized heat flow and cumulated hydration heat of PC and FMIC during the first 50 hours of hydration. Five reaction stages can be identified from the heat flow curves: (i) the pre-induction stage due to rapid hydration of C_3A upon contacting water, (ii) the induction stage with extremely low reaction heat flow, (iii) the acceleration stage due to the reaction of C_3S, (iv) the deceleration stage that covers the secondary hydration of C_3A and the conversion of ettringite to AFm, and (v) the diffusion controlled stage. The high aluminate content and enhanced reactions triggered by FMIC resulted in a substantial increase in the main peak of the heat flow curve, which combines the heat from silicate and aluminate. The enhanced cement hydration in the presence of FMIC

was also evidenced by the higher cumulative heat release. As shown in Table 4.4, the main heat flow peak of PC appeared after 8.68 hours with a peak value of 4.9mW/g. It appeared 0.44 hours earlier in the presence of dry MK with a higher peak value of 6.47mW/g, indicating accelerated and enhanced cement hydration.

Compared with DMK, the MIC groups exhibited comparable time to reach the main heat flow peak, but the peak values were raised. After 50 hours of hydration, 0.5MIC, 0.75MIC, and FMIC yielded normalized cumulative heat of 323.60J/g, 332.30J/g, and 325.50J/g, which are 26.7%, 29.0%, 26.4% higher than that of PC, respectively. The higher heat flow peak and cumulative heat released indicate the further enhancement of cement hydration triggered by MIC. By directly introducing extra water into the system, DMKEW showed its main heat flow peak 0.63 hours earlier and 29.3% higher, as well as a 7.4% higher 50-hour cumulative heat release than FMIC. The more pronounced cement hydration enhancement and acceleration were mainly due to the direct addition of extra mixing water in the system, which was more readily accessible for the early-age hydration reactions than the gradually released water from MIC.

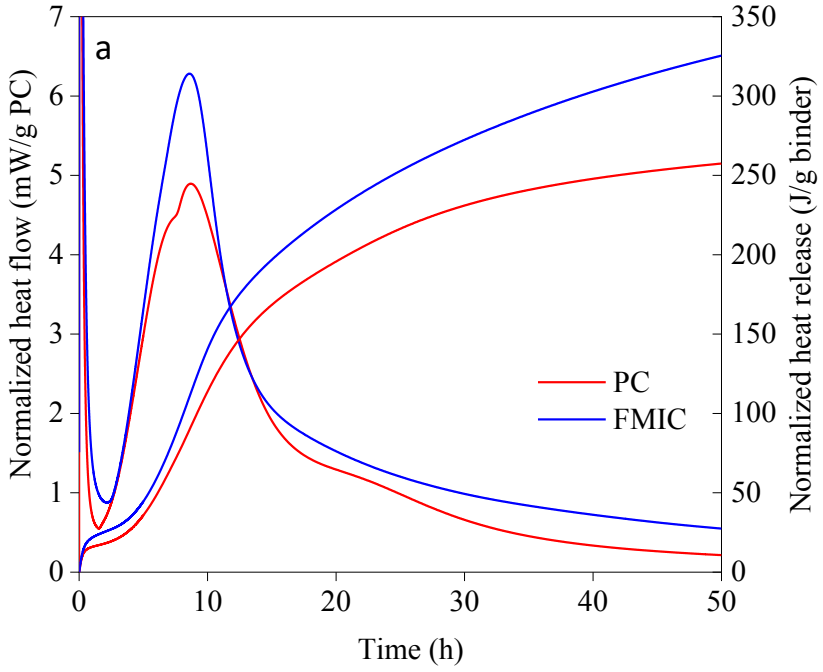

Figure 4.15: Normalized hydration heat of PC and FMIC.

Table 4.4: Time and values of the main heat flow peak and cumulative heat at 50 hours.

Group	Time to reach the main peak (h)	Peak values of normalized heat flow (mW/g binder)	Normalized cumulative heat at 50 h (J/g binder)
PC	8.68	4.90	257.50
DMK	8.24	6.47	293.20
0.5MIC	8.28	6.52	323.60

0.75MIC	8.51	6.94	332.30
FMIC	8.56	6.28	325.50
DMKEW	7.93	8.12	349.50

4.5.6. Influence of MIC on the mechanical strength of cement mortar

Figure 4.16 shows the development of compressive strength of selected cement mortars. It can be seen that the PC group yielded a compressive strength of 44.8MPa at 1 day, which increased to 53.75MPa and 61.55MPa after 7 and 28 days, respectively. Due to the addition of extra water, the 1-, 7-, and 28-day compressive strength of DMKEW was 69.4%, 64.9%, and 41.3% lower than that of PC. Compared with DMKEW, FMIC yielded 2.3%, 24.5%, and 0.6% higher compressive strength after 1, 7, and 28 days, respectively. The higher compressive strength of FMIC than DMKEW indicates the desired effect of MIC in enhancing cement hydration, superior to the direct addition of extra mixing water. Nevertheless, the compressive strength of FMIC is still lower than that of the PC group, which might be due to multiple reasons, including the high volume of MK (30%) and potentially uneven dispersion of MK particles in the cement matrix.

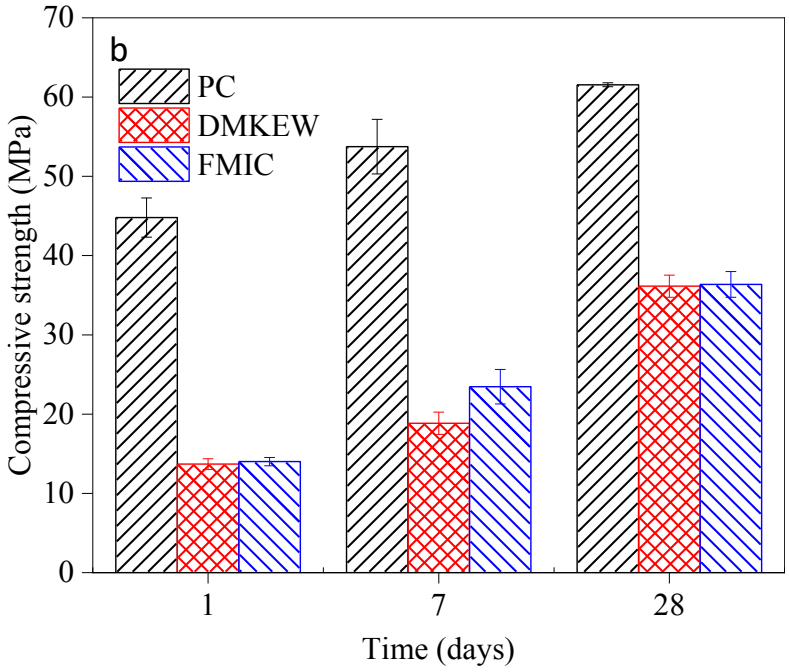

Figure 4.16: Development of compressive strength of PC, DMKEW, and FMIC.

4.5.7. Chemical shrinkage

Figure 4.17 shows the influences of dry MK, lithium, and MIC on the chemical shrinkage of cement. As shown in Figure 4.17a, PC yielded a chemical shrinkage of 0.029mL/g after 1 day of hydration and then increased to 0.059mL/g after 28 days. The presence of lithium led to an elevated chemical shrinkage, which is positively correlated with the lithium dosage during the first 12 hours. LLi and HLi yielded 8.8% and 9.3% higher 12-hour chemical

shrinkage than PC. Thereafter, the LLi group showed a higher increasing rate than HLi. This agrees well with the authors' recent work [180] that lithium can accelerate early-age hydration but retard the hydration of cement after 1 day. Due to its higher activity compared to calcium ions, lithium can preferentially react with cement hydration products, resulting in the formation of lithium aluminate hydrate ($LiAl_2(OH)_7 \cdot 2H_2O$) [189], which can serve as a nucleation site for aluminum hydroxide precipitation [190, 191] and accelerate the hydration of C_3A during the first 24 hours. The 24-hour chemical shrinkages of LLi and HLi are 4.6% and 2.3% higher than that of PC, respectively. After 24 hours, however, the cement setting and hydration process slowed down due to the replacement of calcium with lithium in C-S-H gels, reducing the overall reactivity of these gels [192] or the ion replacement induces a change in the particle surface in the cement pastes, resulting in reductions in electrostatic interactions [193]. This, in turn, hinders the growth and crystallization of hydrates, retards the setting, delays the hardening process of cement, and results in a relatively lower shrinkage in HLi than LLi. It should be noted that, since the cement pastes remain in contact with water throughout the testing period, there is a potential leaching of lithium from the cement pastes during the chemical shrinkage test, which may diminish its later-age retarding effects on cement hydration. After 5 days, the chemical shrinkage of PC slowed down to a nearly consistent and low rate, which yielded an ultimate shrinkage of 0.056mL/g at 28 days. Compared with PC, LLi and HLi yielded 33.9% and 25.4% higher chemical shrinkage, respectively. The incorporation of dry MK resulted in a decrease in chemical shrinkage during the first 24 hours, which then exceeded that of PC at 2 days and yielded a 25.4% higher 28-day shrinkage. This is not only due to the acceleration of the cement hydration with extra nucleation sites provided by the fine MK particles, but also triggered by pozzolanic reactions by forming a denser microstructure with tightly packed hydration products [194]. As reported in previous studies [195, 196], even though a higher w/b ratio could result in higher chemical shrinkage, such an effect on the ultimate cement chemical shrinkage is insignificant. In this study, compared with DMK, DMKEW exhibited a lower chemical shrinkage during the testing period, and similar final shrinkages (0.074mL/g vs. 0.073mL/g) were obtained at 28 days.

As exhibited in Figure 4.17b, in line with the hydration enhancement, more significant increases in chemical shrinkage than the lithium groups were obtained from the specimens with MIC. Similar to DMK, decreased chemical shrinkages were obtained from 0.5MIC and 0.75MIC during the first 7 and 3 days, respectively, and increased shrinkages thereafter. Interestingly, the development of chemical shrinkage is positively correlated to the DOS of the incorporated MK. Among the investigated groups, FMIC exhibited the highest shrinkage, which reveals the significant role of MIC in enhancing the hydration of cement. Compared with the calorimetry test, the development of chemical shrinkage provided an indication of the benefits of gradually released water from the saturated MK. When comparing FMIC and DMKEW, although the two groups shared the same total water amount, FMIC yielded a 21.9% higher 28-day chemical shrinkage than DMKEW. This indicates that the directly added extra free water in DMKEW presented higher accessibility for the initial cement hydration reactions, while the water introduced by MIC sustained its function more persistently. Although the chemical shrinkage of FMIC-Li is lower than that of PC during the first 1.5 hours, it exhibited a rapid increase and yielded a 28-day value of 0.083mL/g, which is between FMIC and HLi.

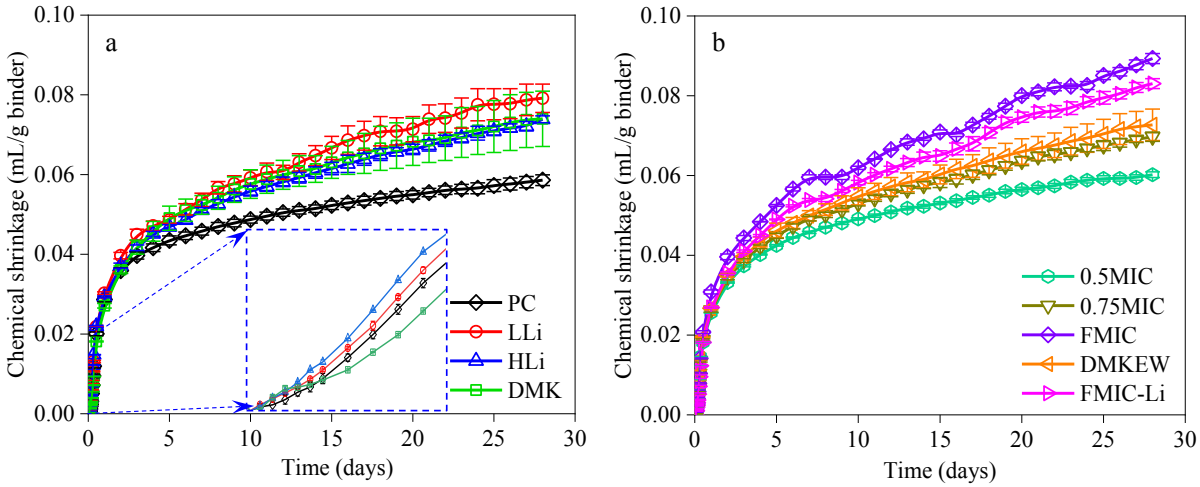

Figure 4.17: Chemical shrinkage of cement pastes containing (a) lithium nitrate and dry MK, and (b) MIC and coupled MIC-Li.

As shown in Figure 4.18, the chemical shrinkage exhibits a linear relationship and the normalized cumulative heat of cement hydration. A higher accumulated heat is typically induced by an enhanced degree of cement hydration, which results in increased chemical shrinkage [197]. At the same cumulative heat, LLi and HLi yielded higher chemical shrinkages than PC (see Figure 4.18a), which indicates the formation of more contracted products or a more densified microstructure under the regulation of lithium nitrate. Due to the enhanced cement hydration degree, decreased content of CH, and the formation of aluminum-containing phases (strätlingite, hydrogarnet, zeolite, and C-A-S-H) in the presence of fine MK particles as found in the authors' previous study [180], DMK showed a much higher chemical shrinkage than PC and lithium groups, when the same normalized cumulative heat was measured.

Compared with DMK, by adding extra mixing water into the system directly, DMKEW showed lower chemical shrinkage when the same normalized cumulative heat was measured (Figure 4.18b). This might be due to the expansion of MK after absorbing moisture with extra water added, leading to a decrease in chemical shrinkage. Since the samples for the chemical shrinkage test were fully immersed in water, the role of the extra water in enhancing the hydration of cement in DMKEW might be compromised. However, the extra water might result in a less densified structure in the hydrated paste with additional capillary pores. In the MIC groups, the gradually released water from the pre-saturated MK behaved more effectively than the directly added extra mixing water in enhancing cement hydration and pozzolanic reactions and triggering structural densification of the hydration products, thereby leading to higher chemical shrinkages than DMKEW at the same heat release. Interestingly, increased chemical shrinkage with the DOS of MK (from 0.5MIC to FMIC) was observed at the same hydration heat, which indicates the formation of further densified reaction products in the presence of MIC. As shown in Figure 4.18b, due to the addition of lithium nitrate into FMIC, FMIC-Li exhibited lower chemical shrinkage than FMIC when the same normalized cumulative heat was released.

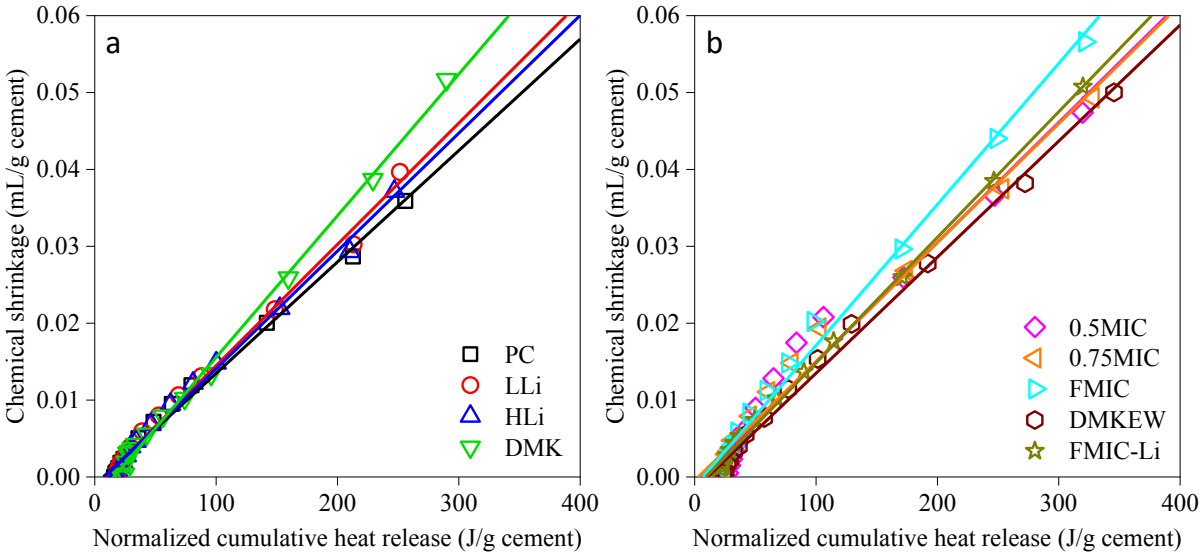

Figure 4.18: Correlation between normalized cumulative heat and chemical shrinkage of cement pastes.

4.5.8. Autogenous shrinkage

Different from chemical shrinkage, autogenous shrinkage is a result of self-desiccation in the pore system of the cement pastes during hardening, when water is consumed as the cement hydration proceeds [198]. The measured initial autogenous shrinkages of the cement pastes during the first 3 days are shown in Figure 4.19a, from which a four-stage development process [170] as a function of time was observed: (i) an initial steep rising stage during the first 1 hour, (ii) a fall-back stage between 1 and 4 hours, (iii) a secondary increase stage after 4 hours, and (iv) the stable stage after 12 hours. Correlating the shrinkage and the hydration heat flow results, the initial increasing stage might be a result of the immediate dissolution of C_3A and its fast hydration reaction upon contacting with water with a high ratio of shrinkage [199], while the volume expansion in the fall-back stage might arise from the crystallization pressure caused by the formation of CH [200] and elevated internal temperature induced by the heat released from the exothermic cement hydration reactions [201]. As shown in Figure 4.19b, concurrent evolutions of internal temperature in the cement pastes and the secondary increase stage were observed. It is believed that there exists a dynamic equilibrium process between the self-desiccation-induced volume shrinkage and thermal/crystallization-induced expansion. When the former exceeds the latter, the shrinkage increases again (i.e., the secondary increase stage).

It can be seen that, in the presence of lithium, the autogenous shrinkage of cement was enhanced with a higher increasing rate. After 3 days, LLi yielded an autogenous shrinkage of 341.3μm, which is 12.5% higher than that of PC. This modification became more significant when increasing the dosage of lithium from 0.28 to 0.74, in which a 3-day autogenous shrinkage of 441.8 μm was observed. The less densified microstructure with a higher volume of large pores formed in the accelerated cement hydration is a possible reason [202]. The

incorporation of dry MK, however, resulted in a 26.9% decrease in autogenous shrinkage after 3 days. This might be due to the filler effect of MK particles that can result in a denser internal structure that prevents water loss [203]. With a higher w/b ratio, DMKEW exhibited a lower autogenous shrinkage, indicating that the extra mixing water helps to maintain the inner humidity with reduced self-desiccation.

The positive role of the saturated MK in progressively and homogenously releasing moisture, thereby enhancing the cement hydration and forming a well-densified microstructure [204], was again indicated by the reduced autogenous shrinkage in the MIC groups. The previous works revealed that the autogenous shrinkage of concrete decreases with the water content in an internal curing agent, especially in low saturation levels, such as up to a 25% DOS of SAP [205] or a 30% DOS of LWA [206]. In this study, the high DOS of MK in MIC resulted in an interesting shrinkage behavior of cement: although it was lower than that of PC, the autogenous shrinkage increased with the DOS of MK. FMIC, 0.75MIC, and 0.5MIC yielded 32.3%, 39.7%, and 54.8% lower 3-day autogenous shrinkage than PC, respectively. Moreover, the coupled FMIC-Li resulted in the lowest autogenous shrinkage among the studied mixtures, which again indicates the synergistic effect between lithium and saturated MK on the property evolution of portland cement that could effectively suppress the adverse effects of singly incorporated MK or lithium on autogenous shrinkage. The reduction in autogenous shrinkage fortifies long-term concrete durability by minimizing the formation of microcracks and improving resistance against chemical attacks.

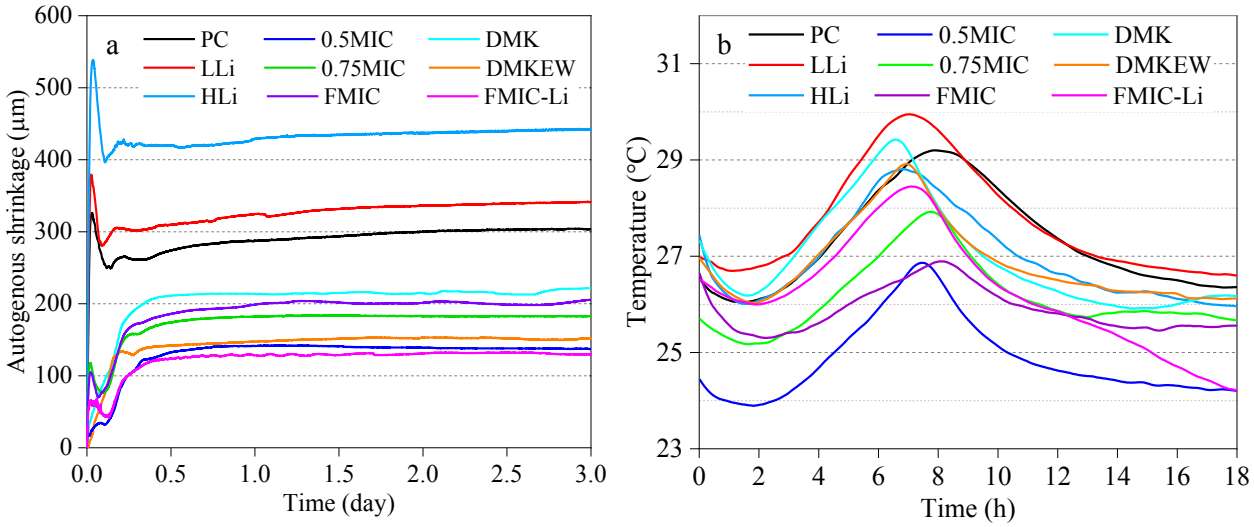

Figure 4.19: Evolutions of (a) autogenous shrinkage and (b) temperature inside the cement pastes.

4.5.9. Drying shrinkage

Different from chemical and autogenous shrinkage tests, the drying shrinkage test was performed by triggering water loss from the mortar specimens under an RH of 50 ± 3% at 23˚C. As presented in Figure 4.20a, PC showed a drying shrinkage of 0.062% and 0.133% after 1 and 7 days, respectively, which then reached an equilibrium level of 0.159% after 32

days. In contrast to the increased chemical and autogenous shrinkages, reduced drying shrinkage was obtained in the presence of lithium. LLi exhibited a 13.5% and 10.1% lower drying shrinkage than PC after 7 and 32 days, respectively, which is in line with the findings by Shen et al. [207]. Another interesting finding is that no significant change in drying shrinkage was induced by increasing the dosage of lithium to 0.74. It is believed that the water retention capacity of NO_3^- present in lithium nitrate plays a potential role in mitigating water loss as it can interact with water molecules hygroscopically and restrain their movement [208, 209]. The incorporation of dry MK, however, resulted in a significant increase in drying shrinkage, which is consistent with the observation from Qin et al. [210]. The adverse effect of MK might be due to the redistribution of water within the cement-MK system, especially at the 30% cement replacement level in this study, or the use of superplasticizer in this group. As reported in the studies by Fu et al. [211] and Lai et al. [212], superplasticizers can induce air entrainment in the matrix and increase the system's porosity. However, it is widely reported that the incorporation of MK is favorable to reducing drying shrinkage of concrete to a certain extent by decreasing the capillary in concrete with a more densified microstructure, thereby inhibiting the migration of water[213, 214]. It should be noted that different from the previous studies, the drying process was initiated after only 24 hours. Although this is close to the real case with a short curing process, the drying at such an early age, when cement was not fully hardened and hydrated, not only removed the capillary water but also negatively impacted the hydration process of cement, as well as the desired pozzolan interactions between cement and MK. This is evidenced by a further increased drying shrinkage observed from DMKEW, in which more readily evaporable mixing water was introduced (see Figure 4.20b). The drying shrinkage of DMKEW at 7 days and 32 days is 48.9% and 52.8% higher than that of PC, and 51.5% and 44.9% higher than those of DMK, respectively.

Compared with DMKEW, although extra water was also introduced into the system, lower drying shrinkage was observed from the MIC groups. The 7-day and 32-day drying shrinkages of 0.5MIC are 30.3% and 31.3% lower than those of DMKEW, while it is still higher than those of PC. This indicates the unique advantage of the gradually released water from the saturated MK, superior to extra mixing water in the system. It is interesting to see that, although with a higher water amount in the system, 0.5MIC yielded 11.0% lower 32-day drying shrinkage than the DMK group. The increase in DOS of MK, however, resulted in increases in drying shrinkage due to the loss of a higher amount of water. FMIC-Li, with the coexistence of MIC and lithium, presented comparable 32-day drying shrinkage with FMIC, while the incorporation of lithium resulted in a lower shrinkage rate during the first 10 days.

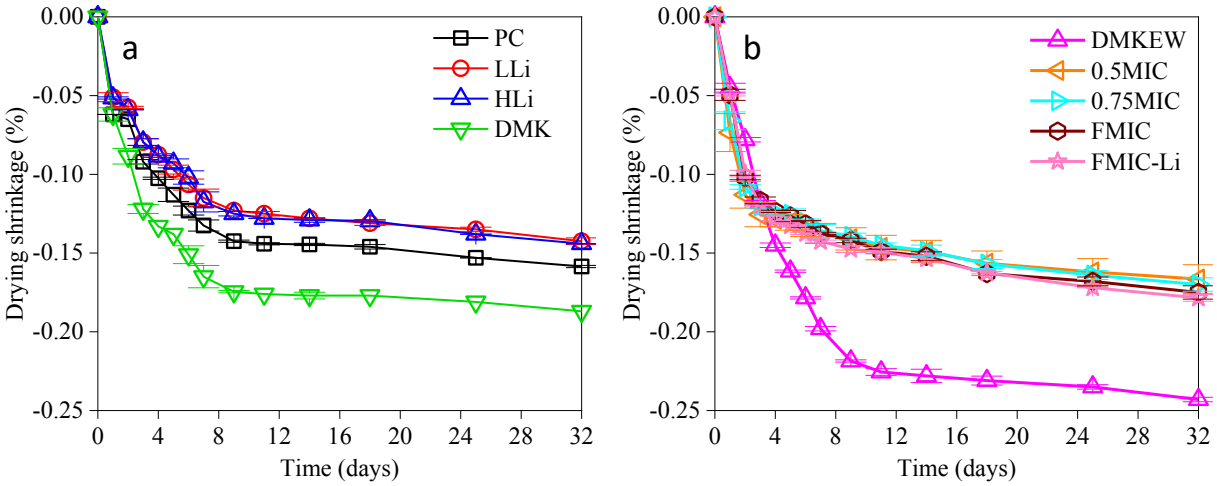

Figure 4.20: Drying shrinkage evolution under 50%RH and 23˚C.

To explain the modified drying shrinkage behavior of cement in the presence of lithium, dry MK, and MIC, the mass changes of the specimen due to the evaporation of water during the drying shrinkage test were monitored. As shown in Figure 4.21a, PC yielded a mass loss of approximately 1.09% and 2.06% after 1 and 6 days, respectively, which then reached almost equilibrium at around 3.10% after 32 days. The incorporation of lithium nitrate, as seen from both LLi and HLi, resulted in a 0.15% less mass loss. Again, this might be attributed to the enhanced cement hydration during the first 24 hours, in which more water was chemically bound, or the water retention capacity of NO_3^-. In line with the enhanced drying shrinkage discussed above, a higher mass loss (1.15% after 32 days) than that of PC was triggered in the presence of 30% dry MK.

As anticipated, by adding extra mixing water directly to the system, DMKEW showed a mass loss of 9.61% after 32 days, which is 200.3% and 120.9% higher than that of PC and DMK, respectively. In the presence of MIC, however, lower mass losses than those of DMKEW were observed. It should also be noted that, compared with DMK, 0.5MIC exhibited a lower water loss, although it contained more water in the matrix, which explains its lower drying shrinkage. The mass loss was found to positively correlate with the DOS of MK. More interestingly, the coexistence of lithium and MIC showed a synergistic effect on moisture evaporation: FMIC-Li showed a 23.3% and 21.0% lower mass loss than FMIC after 7 days and 32 days, respectively, which is in line with the observation in drying shrinkage. What also aligned with the drying shrinkage data is that FMIC-Li exhibited a comparable 32-day mass loss with 0.75MIC but a lower rate during the first 10 days. These results further confirm the water retention benefit triggered by the co-existence of MIC and lithium. The promising results obtained from the previous and current studies covering the hydration of cement, long-term durability, and early-age properties pave a path for the application of MIC in developing sustainable and durable concrete.

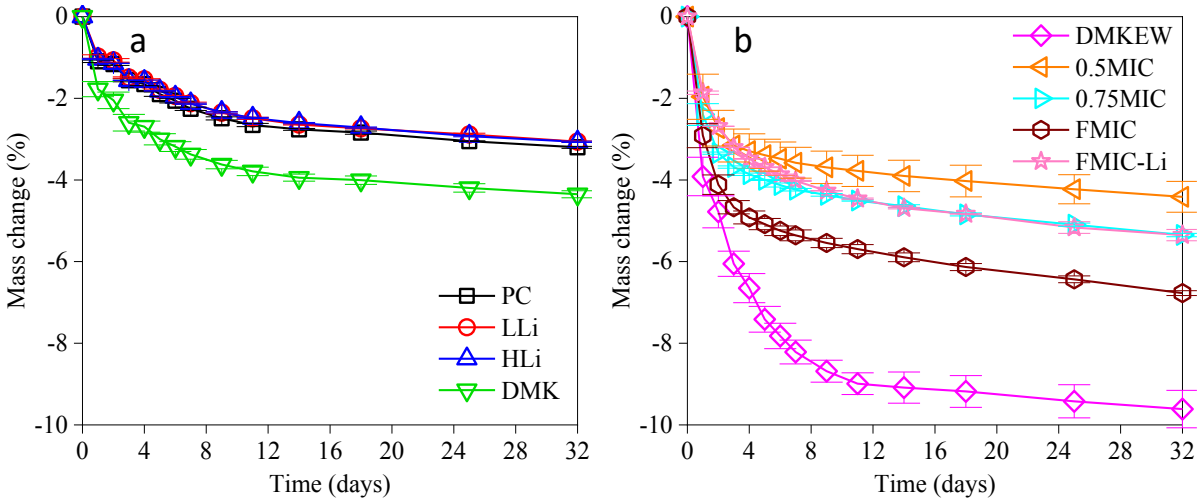

Figure 4.21: Mass change evolution of specimens under 50% RH and 23˚C.

The linear correlation between the mass change and drying shrinkage shown in Figure 4.22 reveals that this volume contraction is mainly driven by capillary tension due to water evaporation, which aligns with the previous findings [215, 216]. The modifications of cement due to the addition of lithium nitrate, MK, or MIC resulted in changed slopes of the fitting line, indicating the variation in the shrinkage kinetics. LLi and HLi, which showed comparable slopes regardless of lithium dosage, experienced higher drying shrinkage than PC at the same mass loss. The less drying shrinkage sensitivity of the lithium groups might be due to the accelerated early-age cement hydration and the restrained movement of water [202]. Compared with the lithium groups, a slight decrease in shrinkage sensitivity was obtained in the presence of dry MK, i.e., a lower drying shrinkage at the same mass loss. It is interesting to see that the drying shrinkage sensitivity of mortar was further decreased in the groups with MIC. By increasing the DOS of MK, higher mass loss was obtained with the same drying shrinkage, which is anticipated as more free water during the drying shrinkage test was available for evaporation. Comparing with FMIC, FMIC-Li showed lower mass change at the same drying shrinkage, which again indicates the synergistic effect between lithium and MIC in enhancing the beneficial role of the gradually released water in the cement matrix.

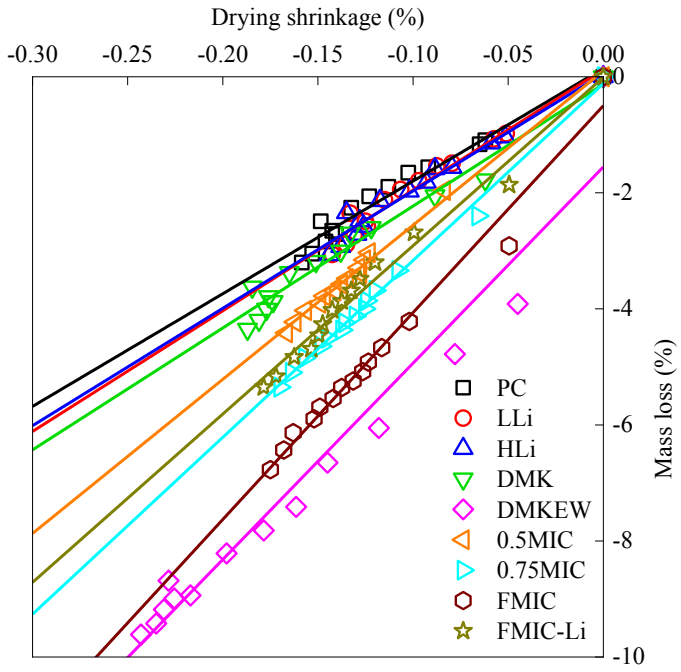

Figure 4.22: Relationship between drying shrinkage and mass change.

4.6 Concrete mix design and property evaluations

4.6.1. Concrete mix design

In this project, concrete mix design was developed with Boston Concrete to investigate the influences of RGGP and other alternative materials on concrete performance based on the MassDOT high-performance concrete formulations. The SCMs considered in this project include slag, RGGP, DE, MK, and nano silica, as well as the combinations of slag with DE, MK, and nano silica. Including the control group, which has no cement substitution, 9 groups in total were developed and investigated. The concrete formulations adopted a consistent water-to-cementitious material (w/cm) ratio of 0.40, except for the two groups with nano silica. The group incorporated with nano silica has a w/cm ratio of 0.43, while the groups containing slag and nano silica have a w/cm ratio of 0.44. All nine concrete groups were designed with an anticipated strength of 5,000 psi, a slump of 4.5 inches, and an air content of 6.0%. Detailed concrete mix design sheets can be found in appendix.

As summarized in Table 4.5, no cement substitution was considered in the control group. To understand the influences of RGGP and other alternative materials on concrete performance, the cement was partially replaced with single SCMs, such as 40% slag, 30% RGGP, 30% DE, and 15% MK. In addition, three ternary groups containing the combinations of slag and nano silica, slag and MK, as well as slag and DE, were also investigated to understand the incorporation of two SCMs on concrete properties. These nice concrete groups were used for investigating a variety of concrete properties, such as mechanical strength, including

compressive strength and split tension strength, physical properties, including early-age shrinkage behavior, and durability-related properties, including permeability, chloride penetration, and resistance against ASR.

Table 4.5: Concrete formulations for the investigations of RGGP and other alternative materials on concrete performance.

Groups	Materials (lb/yd^3)								
	Cement	Slag	RGGP	DE	MK	Nano silica	FA	CA-1	CA-2
Control	685	0	0	0	0	0	1266	953	702.2
Slag-40	411	274	0	0	0	0	1204	967	719
GGP-GS 30	480	0	205	0	0	0	1246	938	691.1
NP-MET 15	582	0	0	0	103	0	1252	942	694.5
NP-DE 30	480	0	0	205	0	0	1236	931	686
Nano silica	620	0	0	0	0	74.4	1293	973.3	717.2
Slag/Nano	369	246	0	0	0	73.8	1239	955.1	739.9
Slag/NP-MET	498	137	0	0	50	0	1204	967	719
Slag/NP-DE	445	137	0	103	0	0	1193	958.1	712.5

4.6.2. Influence of RGGP on slump, air content, and density of concrete

The average slump test results are shown in Figure 4.23. There is a clear positive increment in slump as a function of RGGP replacement level. The mixture with no RGGP replacement (control) had a 7-in. slump, while the mixture with the highest level of replacement (30% RGGP replacement) reached a 9 in. slump for the mix with. This trend appears to indicate that higher RGGP contents enhance workability, making placement and compaction easier. This increase in slump could be attributed to a lower water absorption of ground glass, which helps the concrete flow more easily by reducing friction between aggregates.

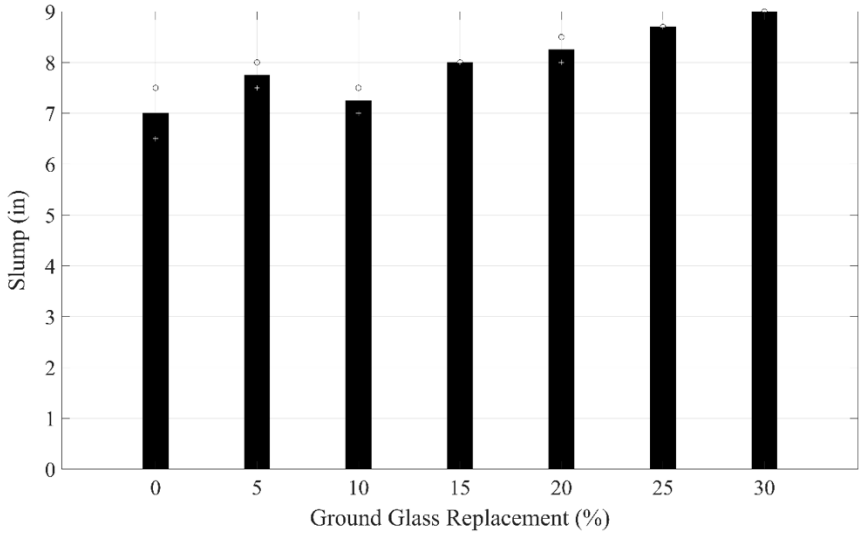

Figure 4.23: Variation in slump values of concrete with different RGGP replacement levels

Table 4.6 summarizes the slump value, entrained air content, and density for each concrete batch with different percentage levels of RGGP.

Table 4.6: Fresh concrete properties

RGGP Replacement, %	Batch No.	Slump (in.)	Air Content, %	Density (lb/ft^3)
0	01	7.5	8.0	146.8
	02	6.5	5.0	155.2
5	03	8.0	6.2	147.2
	04	7.5	7.5	150.4
10	05	7.0	7.0	152.8
	06	7.5	8.0	145.6
15	07	8	8.0	148.8
	08	8	8.0	147.2
20	09	8	6.2	148.0
	10	8.5	8.5	147.2
25	11	8.7	7.0	147.2
	12	8.7	7.0	147.2
30	13	9	7.5	145.6
	14	9	8	144.0

4.6.3. Compression test results

To evaluate the compressive strength of mixes with varying RGGP replacement levels, three samples were tested at 7, 28, and 91-day ages for each replacement level. The average strength test results for each age are summarized in Figure 4.24. In this figure, bars represent the average strength of the three samples tested at each age, and the symbols in each bar represent the results of separate samples. The type of hatching corresponds to the three ages at testing. Pictures of all the cylinders after compression testing are included in Appendix A. The 28-day surface resistance and compressive strength tests were conducted by the MassDOT Research and Materials Section (RMS), and the results can be found in Appendix F.

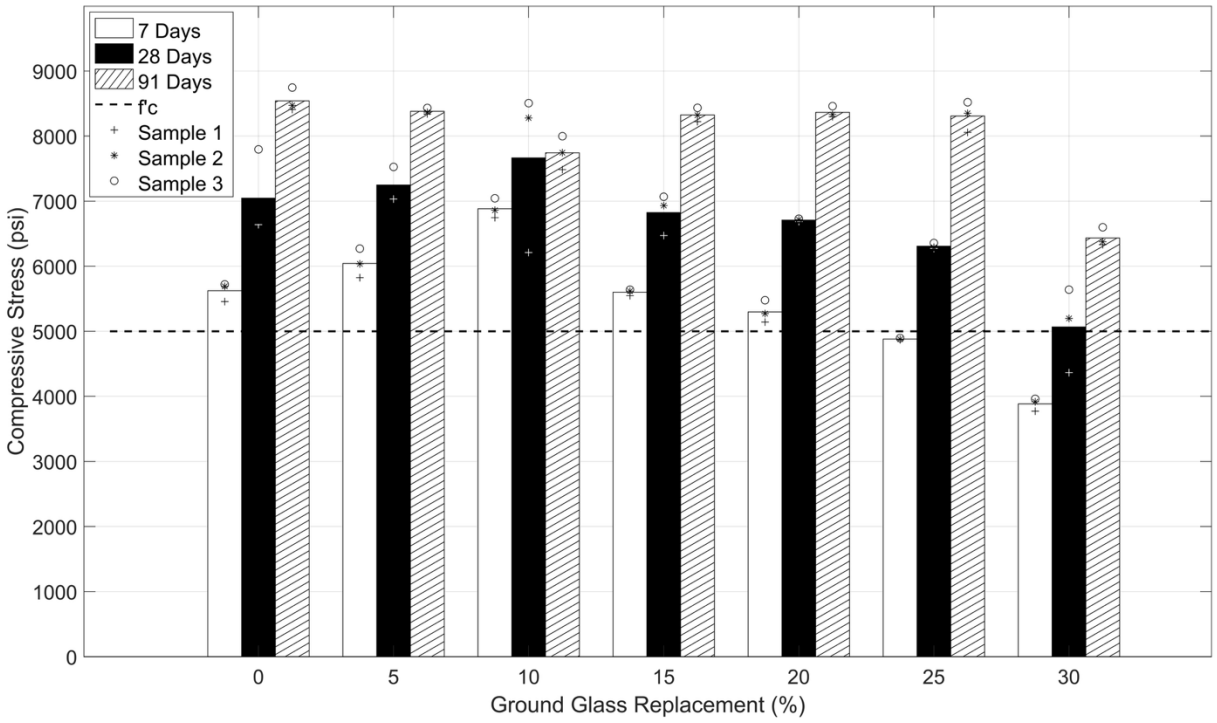

Figure 4.24: Compressive strength of concrete with different RGGP replacement levels

At 7-day and 28-day test dates, an increase in strength was observed in mixes containing up to 10% RGGP replacement compared to the control mix. This improvement is likely due to the high fineness of RGGP used in this research (with just 0.7% retained on No.325 sieve), which has been shown to enhance the filler effect in concrete. This effect is primarily physical rather than chemical, as ultrafine RGGP particles fill voids in the cement matrix, improving packing density and early-age strength. However, at higher RGGP replacement levels, chemical interactions become more dominant, and the reduction in cement content leads to lower early strength. RGGP is not a highly reactive pozzolan and thereby exhibits lower short-term compressive strength at 7 and 27 days compared with the control mix.

Results for the 91-day strength tests were similar for all the RGGP replacement levels tested. The pozzolanic reactions that take place over time allow RGGP to interact with calcium hydroxide in the presence of water, forming additional calcium silicate hydrate (C-S-H), which further strengthens the concrete. This effect is evident across all replacement levels, leading to sustained strength gains over time. Given this trend, higher RGGP replacement levels are, in general, expected to provide higher long-term strength gain. The strength of the 91-day samples remains on par with the control mix up to 25% replacement, with all cases averaging around 8000 psi or higher. Considering the goal of maximizing RGGP incorporation in concrete for sustainability, a 25% replacement level appears to be adequate.

4.6.4. Splitting tensile test results

Three splitting cylinder samples were prepared for each mix design and tested at 7, 28, and 91-day ages. These average results of three samples for each age are presented as bars in

Figure 4.25. The symbols in the figure indicate each sample tested at each age. At 7 and 28 days, the average tensile strength remained relatively consistent for mixes with RGGP replacement levels up to 15%. Beyond a 20% RGGP replacement level, however, a decline in splitting tensile strength was observed. There was no apparent difference between low and high RGGP replacement levels for the 91-day splitting tensile tests, as seen in the figure. The effects of pozzolanic reactions led to a significant increase in tensile strength for mixes with higher RGGP content (25% and 30%).

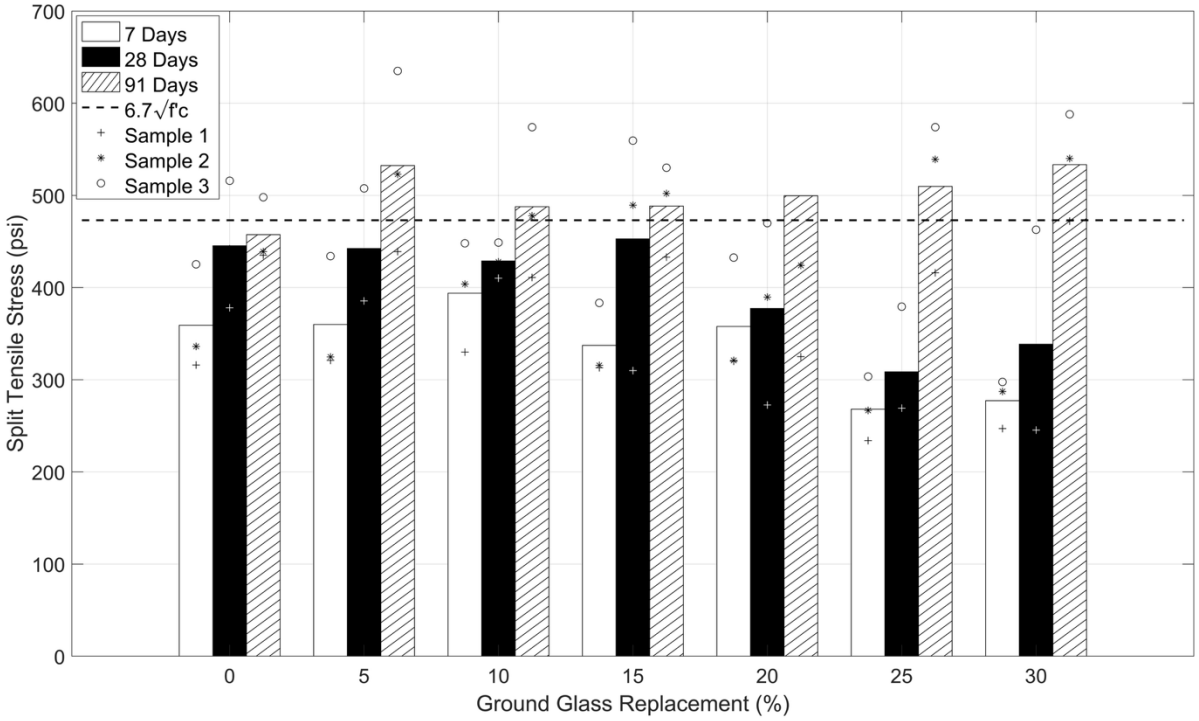

Figure 4.25: Variation in splitting tensile strength of concrete with different RGGP replacement levels

4.6.5. Rupture strength test results

To examine the rupture strength of concrete mixes with varying RGGP replacement levels, four-point bending tests were conducted on two beam samples at each curing age of 7, 28, and 91 days for every RGGP replacement level. Rupture strength initially increased from 0% to 10% RGGP replacement at the 7-day interval, followed by a gradual decline as replacement levels extended to 30%. These results are shown in Figure 4.26. At 28 days, all mixes, except the one with 30% RGGP replacement, exhibit higher rupture strength than the control. At the 91-day interval, the pozzolanic reaction further enhances strength, and all replacement levels from 5% to 30% achieve rupture strength comparable to or greater than the control concrete.

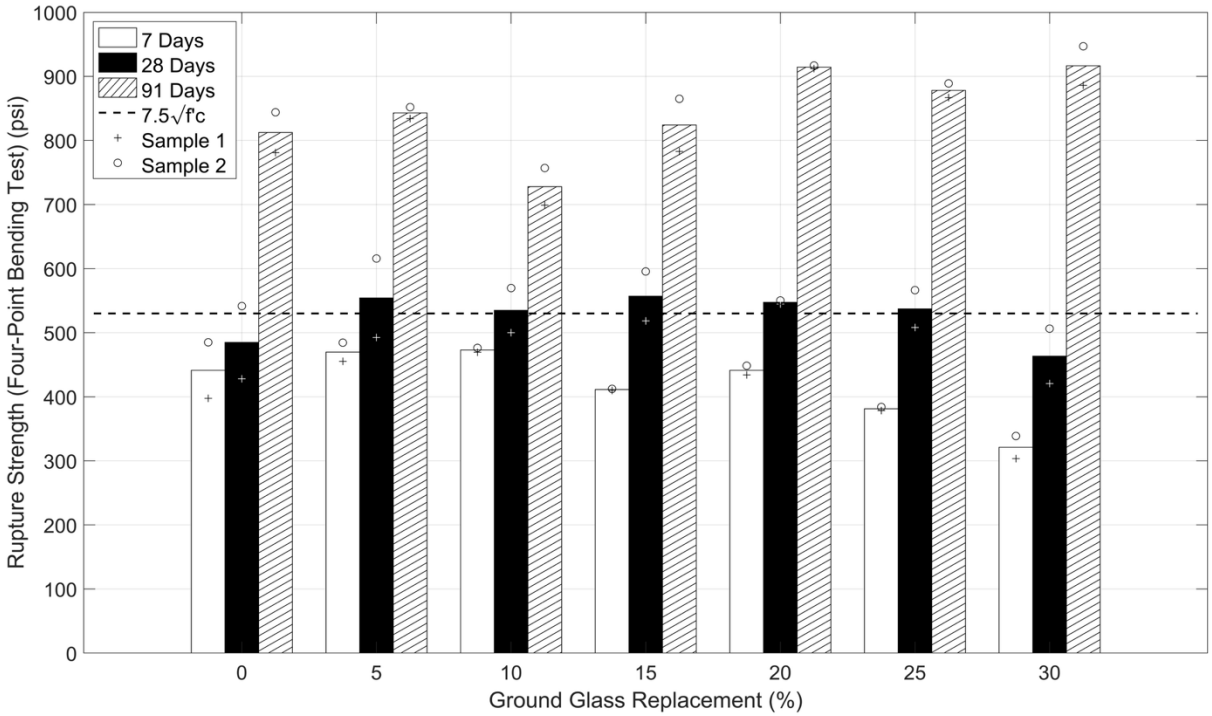

Figure 4.26: Variation in rupture strength of concrete with different RGGP replacement levels

4.6.6. Influence of RGGP and alternative materials on the early-age autogenous shrinkage

Figure 4.27 represents the early-age autogenous shrinkage behavior of concrete mixtures measured over 48 hours using a high-resolution laser-based Schleibinger shrinkage cone apparatus. Autogenous shrinkage is primarily driven by self-desiccation as water is consumed during cement hydration, leading to internal capillary tension and volume reduction [217]. From Figure 4.27, four distinct stages as a function of time were observed: (i) a sharp initial increase within the first hour, (ii) a brief declining phase between 1-4 hours, (iii) a secondary increasing stage after 4 hours, when the self-desiccation exceeds the thermal/crystallization induced expansion [218], and (iv) a stabilization phase that commenced after approximately 10 hours.

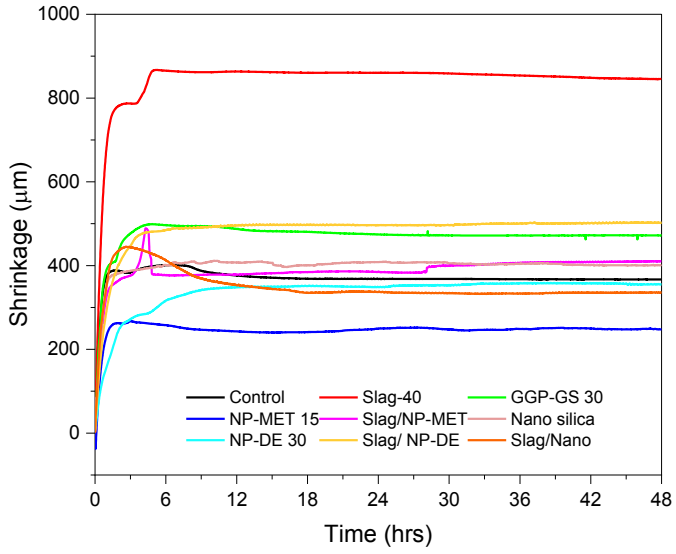

Figure 4.27: Early-age autogenous shrinkage of SCM-modified concrete mixes

From Figure 4.27, it can be seen that the presence of slag yielded the highest autogenous shrinkage of ~865μm, which is 53.7% higher than that of the control group. This is consistent with previous works where slag-rich mixes exhibited more early age shrinkage up to 5 times that of the control, primarily due to the capillary pressure generated during the self-desiccation process [219, 220]. Additionally, studies conducted by Li et al. (2023) [221] suggested that some commonly used admixtures lose their function when used in conjunction with slag and internal curing is an effective approach in mitigating the autogenous shrinkage of slag-based systems.

It is interesting to note that the combination of slag and MK resulted in a 44% decrease in shrinkage compared to the slag group, likely the presence of metakaolin in the slag-based system, which reduces the pore solution pH, delays the C-A-S-H gel formation, and relieves pore pressure without notably affecting the stiffness [222]. In contrast, the NP-MET 15 and NP-DE 30 mixes showed 32% and 14% lower shrinkage than the control group. This might be due to the finer particle size and high pozzolanic reactivity of MK particles, which result in a denser internal structure and prevent water loss [223], while DE contributes to shrinkage mitigation through chemical reactivity, cement dilution and internal humidity regulation via its porous microstructure [224]. However, when DE is used in combination with slag, a 30% enhancement in shrinkage is observed compared to the DE-30 group, possibly because the presence of slag contributes to the increased shrinkage as discussed above.

Furthermore, nano-silica and GGP-GS 30 showed a 1% and 19% increase in shrinkage compared to the control group. Although RGGP is expected to reduce autogenous shrinkage, this study observed the opposite phenomenon. The most probable reason behind this anomaly could be that the incorporation of RGGP at high replacement levels raises chemical shrinkage due to enhanced hydration driven by elevated alkalis from glass and C_3A in the cement, and this rise in chemical shrinkage [43] might contribute as a key factor to increase the early-age autogenous shrinkage through intensified self-desiccation [225].

4.7 Durability

4.7.1. Influence of RGGP and alternative materials on concrete permeability

Figure 4.28 and Table 4.7 show the evolution of the bulk electrical resistivity of the concrete cylinders per AASHTO T402. The cylinder specimens were immersed in the pore solutions at room temperature for up to 56 days. The control group exhibits a relatively low bulk resistivity of 28.8 Ω-m after 7 days, which indicates a "high" chloride penetration level according to AASHTO T 402 and ASTM C1202. The bulk resistivity gradually increased to 60.22 Ω-m at 56 days. This aligns well with the accelerated mortar bar expansion results, where the control group exhibited the most significant expansion, which subsequently leads to their low resistivity or higher permeability in the concrete matrix. However, among all mixes, the nano silica group showed the lowest improvement over the control, which reached a value of only 34.60 Ω-m after 56 days. The reason behind this phenomenon could be the highly conductive nature of the liquid fly ash and the absence of any other pozzolans in this group, which reduced their resistivity. In contrast, the remaining SCM-based blends demonstrated notably enhanced bulk resistivity due to their pozzolanic and micro-filler effects, which helped to densify the matrix and reduce capillary porosity [226]. For instance, the NP-MET 15 group demonstrated an increase of approximately 193%, while the GGP-GS 30 group exhibited a significant increase of 442% in resistivity compared to the control group. This improvement is primarily attributed to the highly pozzolanic reactivity of the metakaolin, which reacts with calcium hydroxide to produce additional C-S-H and leads to significant pore structure refinement [227-230]. Similarly, the reduced permeability with the incorporation of recycled glass powder could be due to the synergistic effects of long-term pozzolanic activity and filler effects of glass pozzolan, which contributed to a tortuous microstructure and restricted the flow of electricity or ions in the concrete [50, 90, 97, 231, 232]. Compared to the control group, the most notable improvement was observed in the NP-DE 30 group, which showed a 10 times higher bulk resistivity than that of the control group after 56 days.

From Figure 4.28, it is also evident that while all SCMs offered varying degrees of enhancement over the control group, the type and combination of SCMs significantly influenced their effectiveness in improving the durability of the concrete. Among all mixtures, the diatomaceous earth-modified concrete showed the highest resistivity, with a value reaching up to 630 Ω-m at 56 days. According to a coulomb range to equivalent range of bulk electrical resistivity level adapted from CSA A23.2-26C [233, 234], this resistivity falls under a very low chloride penetrability/ permeability region, which suggests a highly dense microstructure with the addition of diatomaceous earth. The reason behind this is the electrovalent instability of the Si–O tetrahedra in diatomaceous earth which allows it to readily bind with Ca^{2+} and facilitates the formation of additional C–S–H phases linked with calcium hydroxide. This pozzolanic reaction reduces $Ca(OH)_2$ content while increasing the C-S-H production and leads to lower porosity and improved durability properties [235, 236]. Similarly, the combination of slag and diatomaceous earth also displayed a ~3.2 times higher resistivity than slag alone. This suggests that the combination of slag and diatomaceous earth likely benefited from a synergistic effect, where the delayed reaction of slag combined with the rapid pozzolanic reactivity of diatomaceous earth led to a progressive densification. This

latent behavior of slag is also evident from the slag 40 group, where the resistivity improved by only 24% at 56 days compared to 28 days counterparts, due to the latent hydraulic behavior of slag and the absence of any secondary pozzolans in the system. It is interesting to note that the nano silica group alone resulted in very high permeability; however, the blend of slag and nano silica exhibited a 72% and 70% improvement compared to nano silica at 28 and 56 days, respectively. This is likely due to the presence of slag, which offsets the highly conductive nature of the liquid fly ash and results in a better resistivity or improved permeability than the nano silica mixture. In comparison to slag, the addition of recycled glass powder showed a 34% higher permeability at early ages, likely due to its slower reaction kinetics. However, as time progresses, it shows a ~174% increase in resistivity at 56 days compared to slag, which provides an insight that glass powder initially delays the reaction while significantly enhancing it in later periods [34, 237, 238]. These observations indicate that while all SCMs improved the resistivity to an extent, the improvement largely depends on their pozzolanic reactivity, particle size, and synergistic effects.

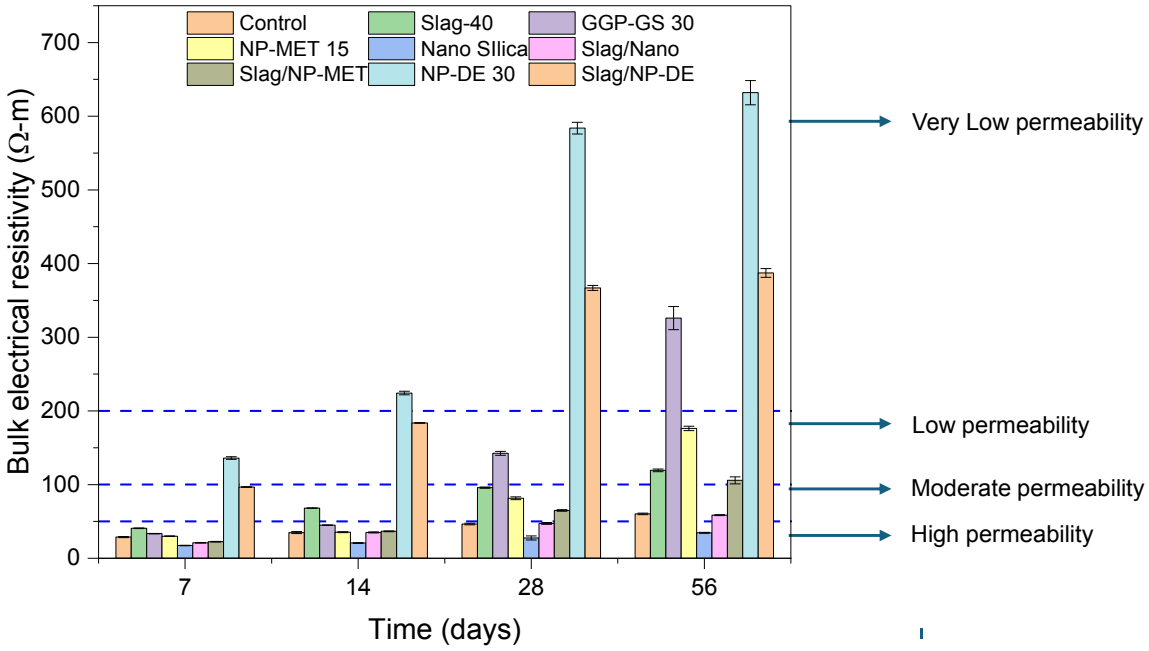

Figure 4.28: Developments of bulk electrical resistivity of concrete with chloride ion penetrability classification defined in AASHTO T 402 and ASTM C1202.

Table 4.7: Developments of bulk electrical resistivity of concrete with chloride ion penetrability classification defined in AASHTO T 402 and ASTM C1202

	Control	Slag-40	GGP-GS30	NP-MET 15	Nano Silica	Slag/Nano	Slag/NP-MET	NP-DE 30	Slag/NP-DE
7 days	28.8	40.7	33.4	30.0	17.3	21.0	22.4	136.0	96.7
14 days	34.9	68.0	44.9	35.5	20.7	35.1	36.6	224.3	183.7
28 days	46.4	95.9	142.4	81.5	27.6	47.3	64.9	583.8	367.0
56 days	60.2	119.4	326.0	176.2	34.6	58.6	105.7	632.0	387.3

4.7.2. Influence of RGGP and alternative materials on chloride penetration in concrete

Chloride penetration is a critical transport property of concrete, as it can lead to reinforcement corrosion and subsequent structural degradation. It is desirable to have a low chloride penetration in concrete that can enhance the long-term durability of concrete structures. Although the investigation of bulk electrical resistivity of concrete cylinders in Section 4.7.1 can provide an indication of concrete permeability and the ability to resist a chloride passage, it should be noted that the bulk resistivity of a concrete cylinder has a high dependence on the flow of electrical current moving through the pores of the non-conductive material. If conductive materials are incorporated into concrete, the values of bulk resistivity cannot accurately reflect the porous network and interconnections in it, and therefore, cannot be used as a sole measurement of concrete permeability. In this work, the rapid migration test was conducted per AASHTO T 357, in which the extent of the chloride ingress was measured by assessing the penetration rate and depth, as shown in Figure 4.29.

Figures 4.29a-4.29i show the observed penetration depth and measurement locations for each mixture, along with their respective repetitions. From Figure 4.29a, the visual observation confirms a relatively high level of chloride permeability in the control mix, consistent with its classification as Grade 1 according to FHWA performance criteria. In contrast, Figure 4.29h shows a very negligible amount of silver chloride precipitation on the split surface for the diatomaceous earth modified concrete. The lowest penetration observed for the DE could be attributed to that the calcium hydroxide formed in cement hydration can react with the alumina and amorphous silica present DE to promote the formation of additional C-S-H gel. The increased C-S-H content helped to fill capillary pores within the concrete matrix and also contributed to refining and densifying the interfacial transition zone (ITZ) between the aggregate particles and the surrounding cement paste [239-241]. However, the combined use of slag and DE resulted in a 67% higher penetration rate than that of the DE 30 group. This increase is likely due to the simultaneous interaction between DE and slag, which led to competing pozzolanic reactions and limited the efficient consumption of calcium hydroxide

and reduced the formation of C-S-H. As a result, the pore-refining effects typically achieved with DE alone were weakened in this group.

Except for DE, RGGP and metakaolin outperformed other alternative materials in inhibiting the chloride ingress. Compared to slag, both RGGP and metakaolin showed 15% improvement in mitigating chloride penetration. This might be attributed to the presence of metakaolin, which increased the formation of chloride-binding phases, particularly Friedel's salt, due to its high alumina content and thereby reduced the concentration of free chlorides available to penetrate deeper into the concrete [242-244]. Likewise, the enhancement in resistivity with the replacement of glass powder might be due to the synergistic effect of pozzolanic activity and filler effect. This observation agrees well with previous studies where an improvement in chloride resistivity was observed with the incorporation of glass powder [17, 28, 72, 245, 246]. Although all SCMs individually improved chloride resistance, their combined use sometimes led to diminished performance, likely due to non-synergistic or competing reactions between the materials.

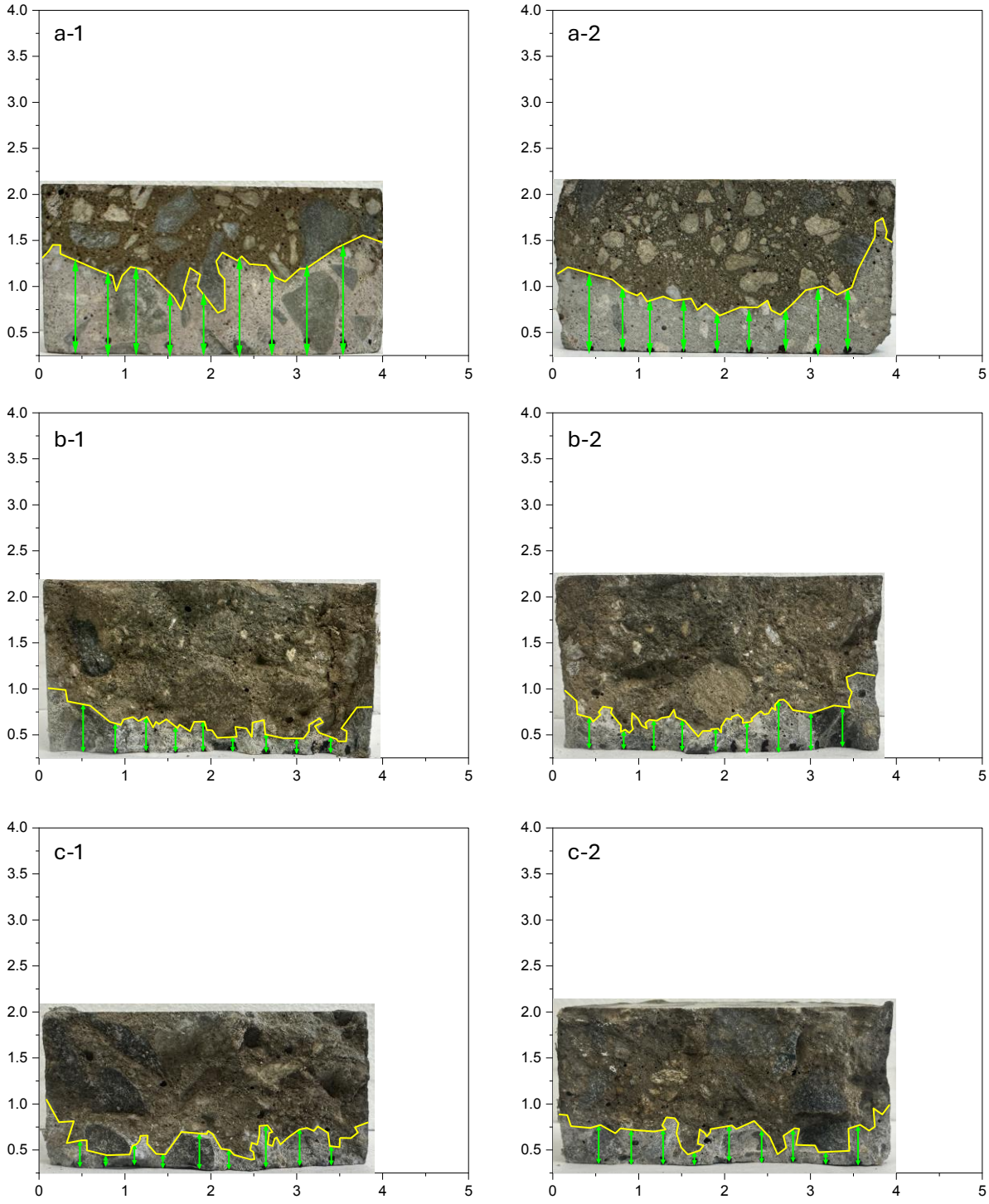
a-1
a-2
b-1
b-2
c-1
c-2

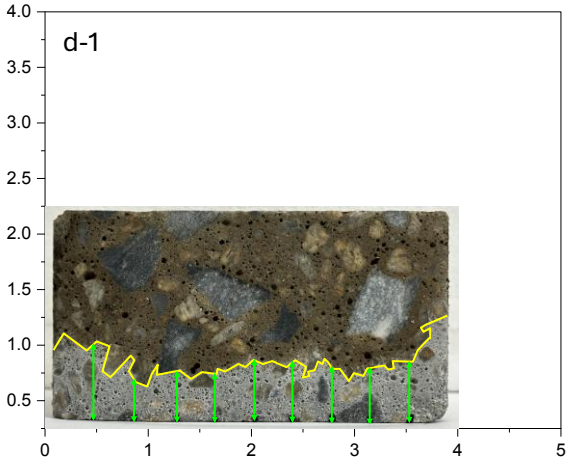
d-1

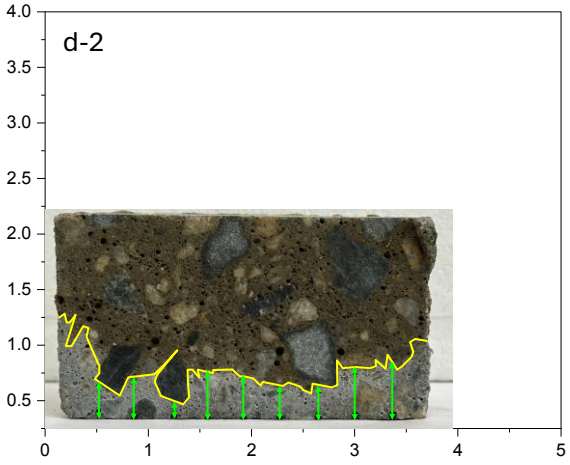
d-2

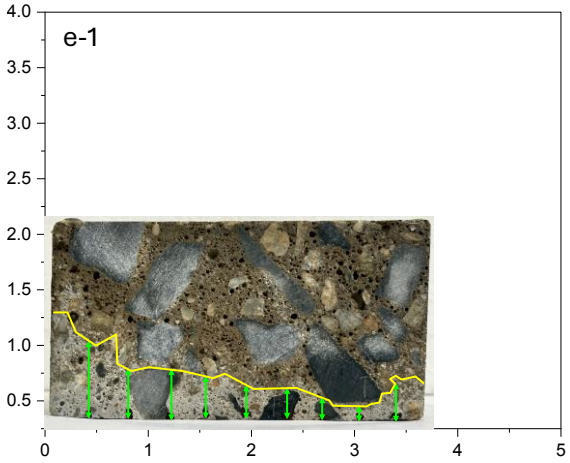
e-1

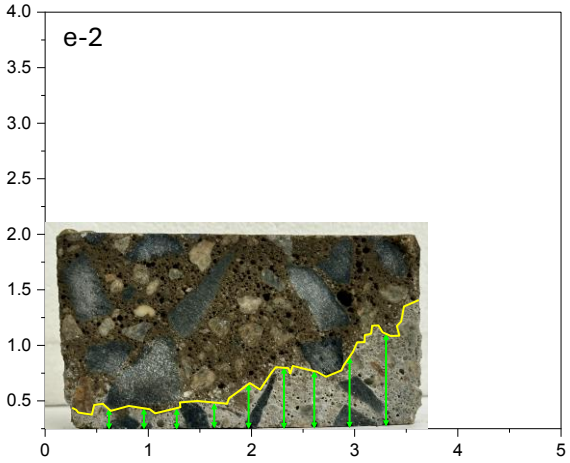
e-2

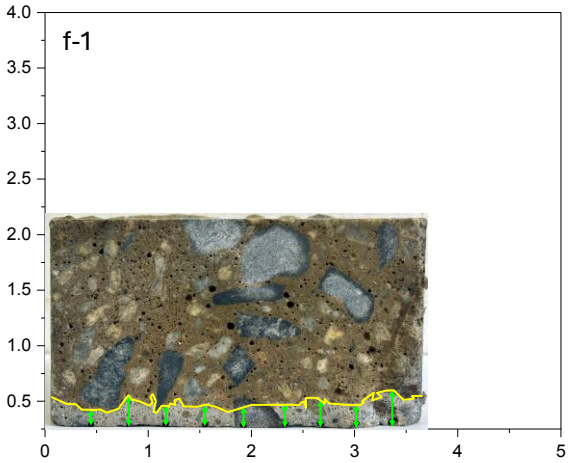
f-1

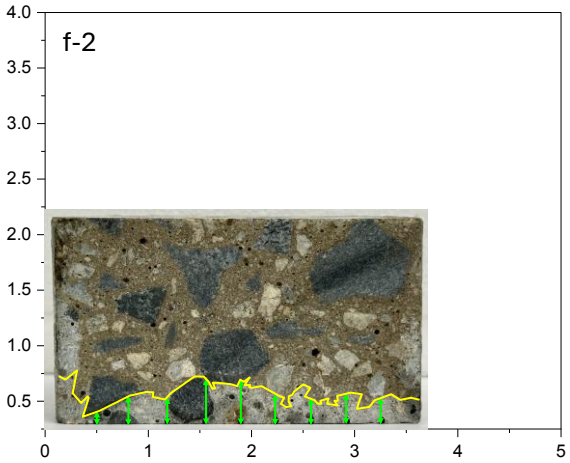
f-2

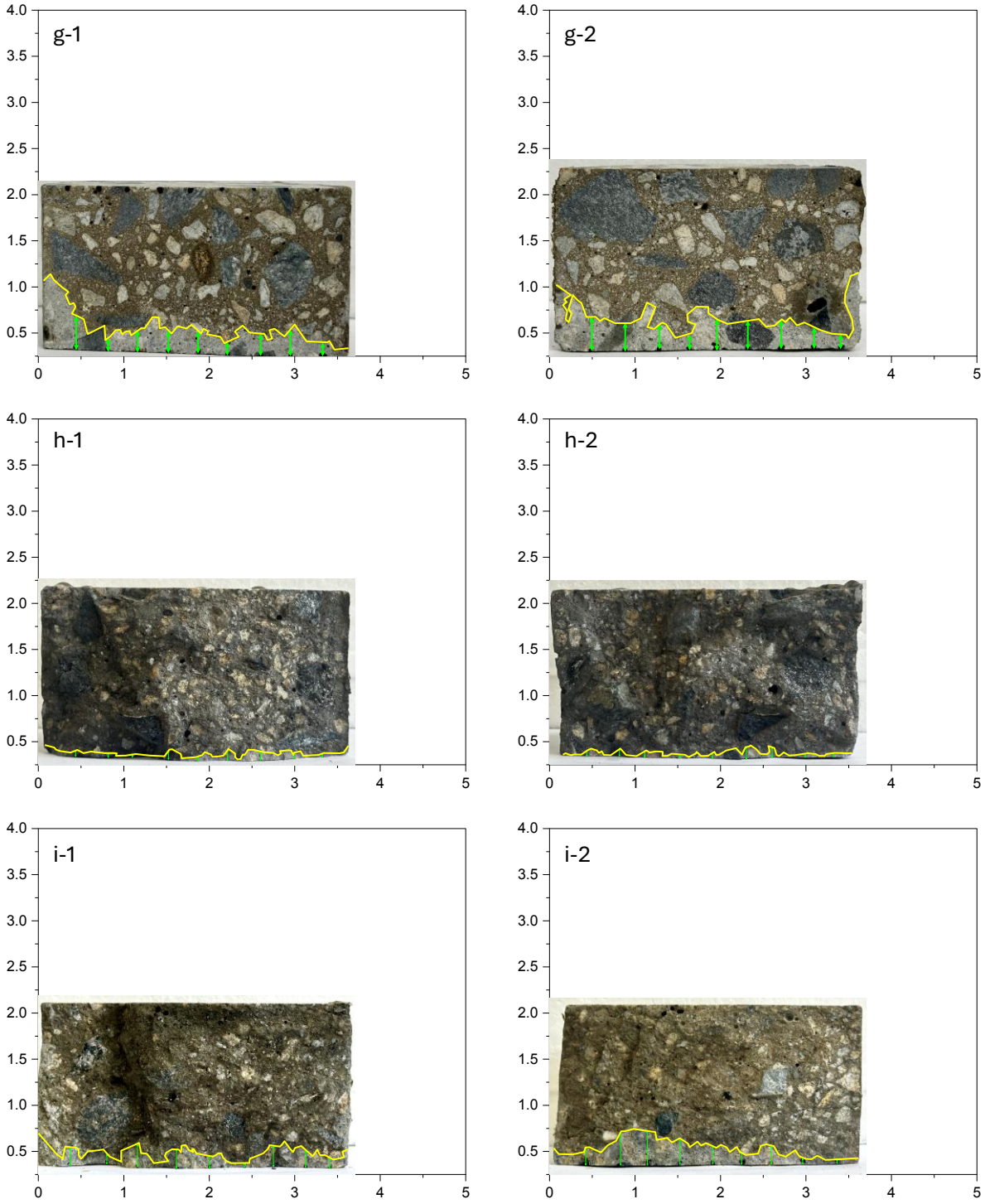

Figure 4.29: Chloride penetration depth of (a) Control, (b) Slag 40, (c) GGP-GS 30, (d) Nano silica, (e) Slag/Nano silica, (f) NP-MET 15, (g) Slag/NP-MET, (h) NP-DE 30, (i) Slag/NP-DE.

From Figure 4.30, it is evident that all the SCM-modified mixtures displayed significantly lower chloride penetration rates compared to the control group, which exhibited an average

penetration rate of 0.034 mm/V-h. The chart of recommendations for chloride penetration rate corresponding to FHWA HPC performance grade per AASHTO T 357 can be found in Appendix C. In line with the bulk resistivity results, the control group shows a high risk of chloride penetration. Compared to the control group, both the GGP-GS 30 and NP-MET 15 groups showed 65% better chloride resistance and fell under the low chloride penetration region, which shows a good agreement with the 56-day bulk resistivity testing results. An interesting finding lies in the penetration rate of the nano-silica group. The bulk resistivity results after 7 to 56 days showed a high chloride penetration rate, while a 33% improvement over the control group was observed from the rapid chloride migration testing results, which puts it in the moderate penetration rate range. This mismatch between the bulk resistivity and rapid chloride migration results might be due to the conductive nature of the nano-silica admixture. More information should be acquired from the manufacturer of admixtures.

The chloride penetration rate results show good agreement with previous observations from ASR expansion and bulk resistivity tests, particularly for GGP-GS 30, NP-MET 15, both of which showed reduced expansion and improved microstructure with time. Although the nano silica group showed the lowest resistivity due to their conductive nature, the reduction in chloride ingress compared to the control groups indicates their efficacy in improving the microstructure to a certain degree. However, the combined use of slag and liquid fly ash in the slag/nano silica group might have benefited from the pozzolanic reaction of slag and helped improve the chloride resistivity further by 13% compared to the nano silica group. The DE-30 and Slag/DE groups exhibited similar trends, like their bulk resistivity, and demonstrated a 92% and 85% reduction in chloride ingress compared to the control group, respectively. Similar findings regarding the role of SCM in improving the chloride resistance have been reported by Su et al. [247] and Papadakis [248], who mentioned that SCM can reduce the concentration of chloride ions and diffusion rate in the concrete.

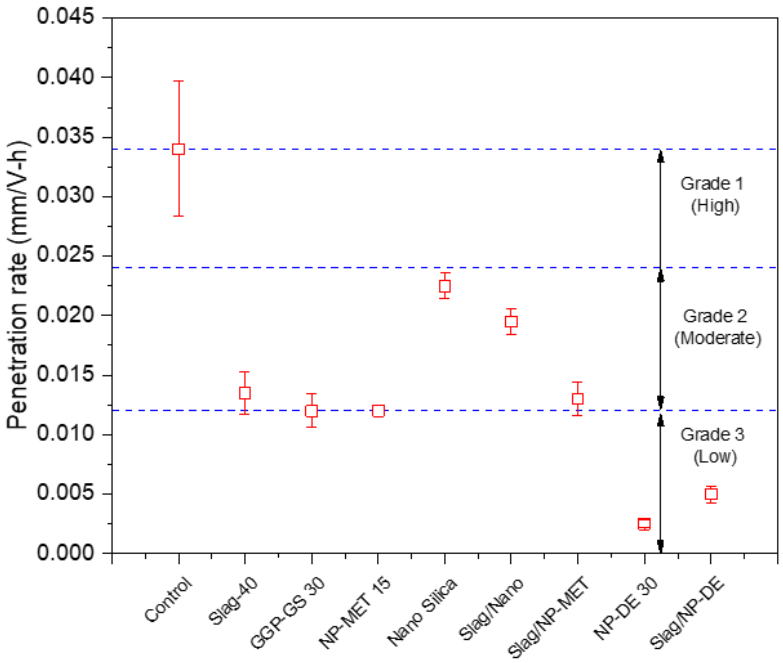

Figure 4.30: Recommended and experimental chloride penetration rate according to AASHTO T 357 (grade 3 has the lowest risk of chloride penetration, while grade 1 has the highest risk).

4.7.3. Influence of RGGP and alternative materials on ASR resistance of concrete

Aroused by the interaction between the poorly crystallized (or amorphous) silica minerals in aggregates and the alkali species in cement, the alkali-silica reaction (ASR), is one of the most severe and complicated deteriorations of concrete, commonly known as a "concrete virus" [168]. The formation and swelling of ASR products can induce deleterious pressure inside the concrete matrix, leading to volume expansion and cracks, which serve as channels for external salts and moisture to trigger multiple deteriorations and result in irreversible damage to concrete structures. Since its identification in the 1940s [249], extensive efforts have been invested to mitigate this complex physicochemical reaction including the use of high-quality materials including low-alkali cement and non-reactive aggregates, incorporation of supplementary cementitious materials (SCMs), such as fly [250], silica fume [251], slag [252], waste glasses [253], natural pozzolan, and calcined clay [254, 255], and the addition of lithium-based admixtures [256, 257]. Despite promising results, the inherent limitations of these conventional approaches impeded their wide applications. The use of low-alkali cement is insufficient to avoid ASR when highly reactive aggregates are used. The lack of high-quality SCMs may impact the ASR mitigation efficiency [258, 259], and compromised concrete performance can be caused when a high volume of SCMs that is enough to mitigate ASR is incorporated. The low abundance, increasing demand in the field of batteries, as well as the negative impact on cement hydration and shrinkage, have been identified as drawbacks and limitations of using lithium admixtures in concrete [202]. Furthermore, the current ASR mitigating approaches are centered on the applications in new concrete as they focus on using the modifications of the raw materials, and effective approaches for existing concrete structures are scarce. These existing challenges motivate the exploration of novel methods to suppress ASR in a more practical, cost-effective, and sustainable way. In this project, the roles of RGGP and alternative materials in improving the concrete resistance against ASR were studied by conducting two different tests: the mortar bar test per ASTM C1260 [128] that provides an aggressive alkaline condition for rapid measurements and the ACCT per AASHTO TP 142 [165] that comes with a relatively mild condition while needs a longer testing period. It is anticipated that the findings from these two tests will enable us to obtain a comprehensive understanding of the change in ASR resistance in the concrete containing RGGP and other alternative materials.

4.7.3.1 Mortar bar testing results

As shown in Figure 4.31, without cement modification, the control group expanded severely due to ASR and exhibited an expansion of >1% at 75 days. This indicates that the reactive silica from aggregate and alkali from cement reacted to form an expansive ASR gel, which led to a rapid and severe expansion due to the absence of mitigation mechanisms and resulted in higher expansion among all the mixtures. Slag-40 and GGP-GS 30 showed a 30.70% and 40.35% reduction in ASR expansion compared to the control group at 75 days, indicating a partial ASR mitigation. The limited mitigation potential of slag and RGGP might be due to

their lower early-age reactivity, and the high alkali content of RGGP may offset its mitigation role.

The incorporation of MK resulted in an effective decrease in ASR expansion, outperforming Slag and GGP by ~20% and ~8%, respectively, even at a lower cement replacement level (15% MK vs 40% slag and 30% RGGP). Replacing 30% cement with DE exhibited the lowest expansion of (0.22%) at 75 days, which is ~81% lower than that of the control group. This effective role of DE is likely due to its fine particle size and high pozzolanic reactivity, which enhances the consumption of free calcium hydroxide and the formation of additional C-S-H, refines the pore structure, reduces permeability, and improves the alkali binding capacity.

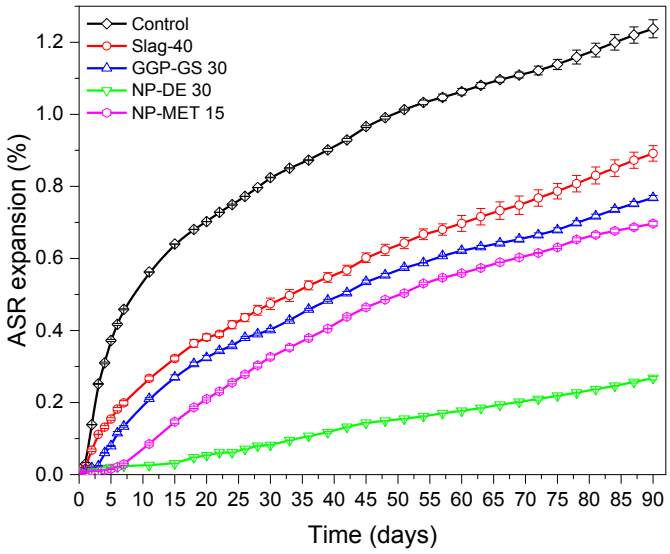

Figure 4.31: ASR expansion based on the mortar bar test.

4.7.3.2 ACCT results

Figure 4.32 illustrates the ASR-induced expansion of concrete cylinders in the ACCT tests over 45 days. The control mixture exhibited a sharp increase in expansion after around 25 days and reached over 1% expansion by 45 days. This aligns well with our previous findings from the accelerated mortar bar test, where the control group showed > 1% expansion after 75 days. In contrast, replacing 40% cement with slag was found to be effective in keeping the expansion below the 0.04% limit and can be considered as a non-reactive system based on the AASHTO TP 142-21 guidelines [260]. Replacing 30% cement with RGGP resulted in a lower reduction of ASR-induced expansion, which reached 0.12%, the boarder line between the slow and moderate reactivity levels. When changing RGGP to DE at the same cement substitution level (30%), the ASR expansion was further reduced, which agrees well with the permeability results and indicates the high pozzolanic reactivity of DE and the positive role of the amorphous silica of DE in mitigating ASR in concrete.

The nano-silica mix reached 0.19% expansion and falls under the moderate reactivity range. This indicates that the presence of liquid fly ash as an admixture in this mix helped to

suppress alkali-silica reaction (ASR) to a certain extent. Conversely, the slag and nano-silica blend showed only 0.09% expansion, similar to that of the DE group, which is 52% lower than that of the nano-silica group. This might be due to the extra calcium and alumina provided by slag, which work together with the liquid fly ash to reduce the alkalinity of the pore solution and improve the concrete's internal structure. Overall, the trend highlights that while nano-silica provides substantial ASR mitigation, pairing it with slag delivers a synergistic improvement that approaches the non-reactive threshold and offers a more robust defense against deleterious expansion. These results follow a similar trend observed in previous studies [165, 261, 262], where the use of SCMs such as fly ash has been shown to significantly reduce ASR-induced expansion.

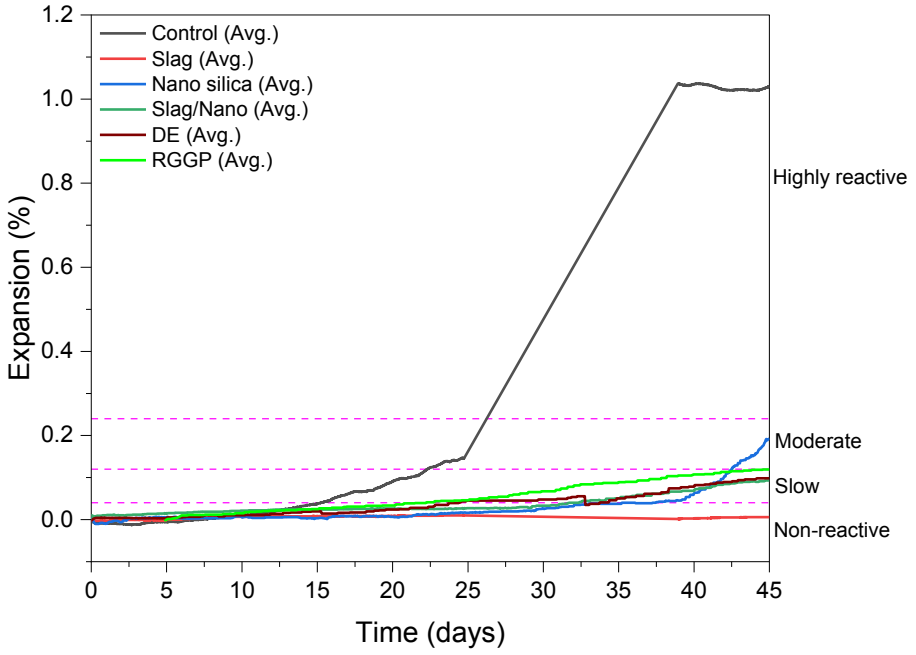

Figure 4.32: ACCT expansion of cylinders up to 45 days.

4.8 The role of carbonation in ASR mitigation

Recently, carbonation curing has been validated as an effective approach to mitigate ASR, which not only depresses the ASR-induced expansion but also permanently sequesters CO_2 in cementitious composites. In 1997, Kihara [263] attempted to mitigate ASR by carbonation curing and found that both the availability of calcium hydroxide (CH) and the porosity of concrete can be reduced after carbonation. Moreover, as the essential trigger for ASR, OH^- ions in the pore solution of concrete can be decreased by carbonation, resulting in suppressed ASR [264]. This was confirmed in a study by Shoji et al. [265] that the pH of the system can be lowered by carbonation and its integration with the addition of γ-C_2S, resulting in controlled ASR expansion. Chen and Yang [266] and Mohammad [267] reported that, with reduced alkalis in the specimens, the ASR-induced expansion was decreased with the

carbonation depth. In a recent work by Liu et al. [268], the ASR in concrete containing waste glass aggregates was suppressed by enforced carbonation curing at early ages.

Based on the previous works, the suppressed ASR under carbonation can be attributed to the decrease of CH content, reduction of pore solution pH, densified microstructure, and decreased porosity in the concrete matrix. Although extensive efforts have been conducted, the role of carbonation in ASR remain unclear and knowledge gaps still exist in this filed: (i) the roles of CO_2 concentration, carbonation time and duration in ASR are rarely elucidated in the simplex carbonation curing conditions, (ii) the interplay between carbonation curing and ASR, as well as its influence on concrete cracking, phase evolution, and carbon profile in new concrete mixes and ASR-impacted concrete are not fully understood, (iii) there exists a critical gap in understanding the changes in ASR products under carbonation curing, such as composition, mineralization, crystallization and moisture absorption, which determine the stress extent and the degree of deterioration in concrete with ASR, and (iv) different from early-age carbonation curing, weathering carbonation is considered a concrete deterioration process as it can result in shrinkage and rebar corrosion in mature concrete structures by converting CH and calcium silicate hydrate (C-S-H) into calcium carbonate (CC) with a smaller volume and reducing the pH of concrete pore solution [269].

This task aims to fill the aforementioned critical knowledge gaps and investigate the role of early-age enforced carbonation in ASR by answering three fundamental questions: (i) what is the interaction between carbonation and ASR in concrete containing reactive aggregates in terms of expansion, cracking, and evolution of ASR products? (ii) since ASR can change the microstructure and permeability of concrete, how do the starting point and duration of carbonation affect the efficacy? and (iii) what are the influences of carbonation on the components, structure, and hygroscopicity of ASR products that govern the destructivity to concrete? Towards this end, the ASR expansion and cracking behavior of mortar specimens containing highly reactive aggregates conditioned in enforced carbonation environments at 50ºC and 95% RH with CO_2 concentrations of 3%, 10%, and 20% were investigated via two carbonation protocols. In-situ characterizations of the changes in ASR products under carbonation were performed via Raman spectroscopy and energy-dispersive X-ray spectrometry (EDS). To further explain the underlying mechanisms at a lower scale, the evolutions of molecular structures, hygroscopicity, and water uptake behavior of ASR gels were analyzed through thermogravimetric analysis (TGA), X-ray diffraction (XRD), Rietveld refinement, attenuated total reflectance–Fourier transform infrared (ATR-FTIR) spectroscopy, and dynamic vapor sorption (DVS). It is expected that the findings from this study can advance the knowledge in alternative ASR suppression approaches and the understanding of mitigation mechanisms at a different scale.

4.8.1. The role of early age enforced carbonation in ASR

4.8.1.1 Volume expansion

The ASR-induced volume expansion quantified by linear length change of the mortar bars cured in the two enforced carbonation protocols is shown in Figure 4.33. It should be noted that the first expansion of the control group during the 7 days is an average value calculated

from C0 and the specimens in ECP-2, which were conditioned together without carbonation. It can be seen that, without carbonation (i.e., 0% CO_2), ASR resulted in a continuous volume expansion in C0, which reached 0.57% after 30 days, confirming the deterioration of ASR attacks on the mortar samples under the current conditions. Substantial decreases in ASR-induced expansion were observed under CO_2. C3 showed a negative expansion of around -0.003% during the first 4 days and a low expansion of 0.04% after 30 days, which is 93.0% lower than that of C0. By increasing the CO_2 concentration to 10%, C10 started expanding after 6 days, which was delayed for 2 days compared to C3. The 30-day expansion of 0.013% was obtained from C10, which is 67.5% and 97.9% lower than C3 and C0, respectively. C20 showed a further delayed and suppressed expansion, which started expanding at 10 days and yielded a negligible expansion of 0.006% after 21 days until the end of the test. The ASR-induced expansion of the specimens conditioned in ECP-2, i.e., pre-treated in the same condition as C0 for 8 days, followed by carbonation at different CO_2 concentrations, is shown in Figure 4.33b. In line with the results obtained from ECP-1, substantial suppressions in ASR expansion were again observed from these ASR-impacted mortar specimens right after being exposed to carbonation. C3-2 yielded an expansion of 0.23% after 30 days, which indicates a 0.03% increase during the 23 days of carbonation, resulting in a 60% lower expansion than C0. More interestingly, ceased expansion (0.01% and 0.02% lower than their volume at 7 days, which is mainly due to the testing error) was observed from C10-2 and C20-2. This effective volume suppression in ASR-attacked mortar specimens, even with an existing expansion of 0.2% confirmed the promising efficacy of early-age enforced carbonation in ASR mitigation.

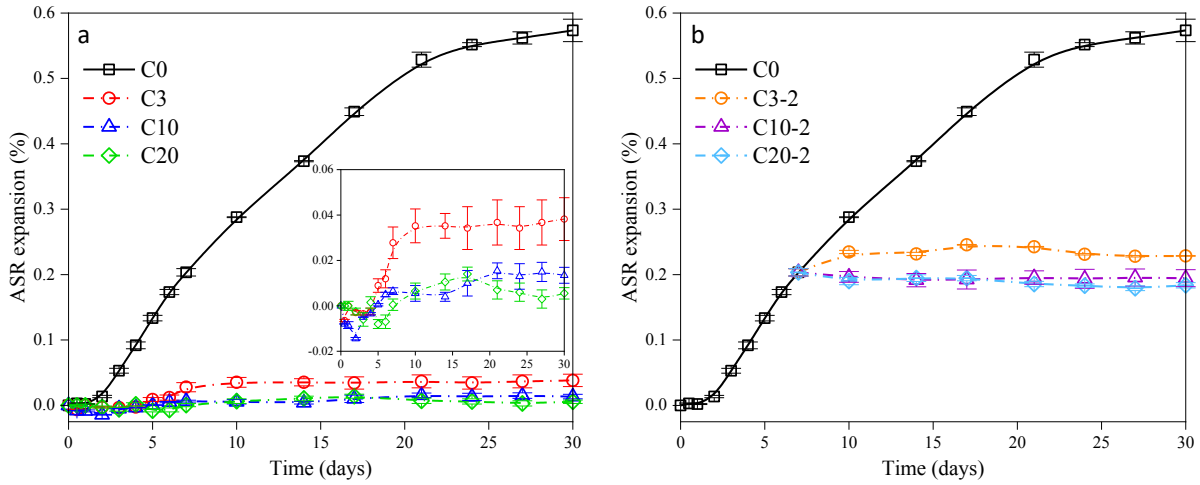

Figure 4.33: (a) ASR expansion of the mortar bars cured at various CO_2 curing conditions in carbonation (a) ECP-1, and (b) ECP-2.

As shown in Figure 4.34, the reductions in ASR expansion are positively correlated with the CO_2 uptakes by the mortars. A linear fitting shows R^2 values higher than 0.85 for all three groups. It is interesting to see that no significant ASR expansion reduction was observed when an initial CO_2 uptake was detected. As discussed above, a higher CO_2 uptake rate can be triggered in the presence of more concentrated CO_2. As a result, suppressed ASR expansion was not detected until the CO_2 uptake was beyond 0.5%, 0.8%, and 1.4% for C3,

C10, and C20, respectively. The final CO_2 uptake of C3 after 30 days of carbonation curing (1.58%) resulted in a 93.0% decrease in ASR expansion, while the same ASR expansion reduction was yielded at a CO_2 uptake of 2.65% and 4.00% in C10 and C20, respectively. A higher ASR expansion reduction was reached under a higher CO_2 concentration at the same period of curing.

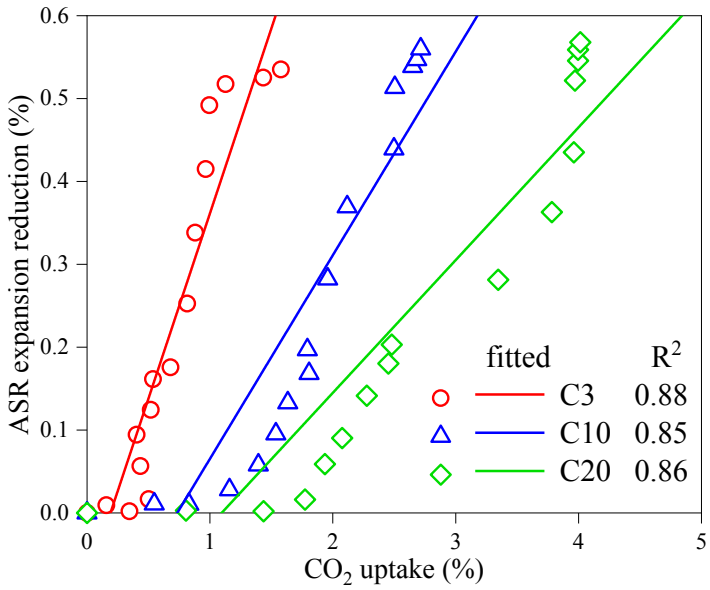

Figure 4.34: Correlations between the reduction of ASR expansion and CO_2 uptake.

4.8.1.2 Cracking behavior

The surface cracking behavior of representative cubic samples of C0, C3, and C10 at selected ages filtered with ImageJ is shown in Figure 4.35a to 4.35c. It should be noted that no detectable cracks can be observed on the surfaces of C20 even after 30 days, which is in line with the negligible length change and indicates the effective ASR suppression under 20% CO_2. From the investigated surfaces of C0, with the proceeded ASR, the number and size of cracks increased with time. When the mortar samples were cured in the CO_2 atmosphere, fewer and narrower surface cracks than those of the control group were observed. The number and size of the cracks were negatively correlated with the CO_2 concentration. Moreover, the time of initial observation of detectable cracks was delayed from 10 days for C0 to 12 days and 17 days for C3 and C10, respectively. To obtain a comprehensive understanding of the ASR-induced surface cracking of the mortar specimens and the role of CO_2 curing in suppressing ASR, the evolutions of crack density, average crack width, and maximum crack width over time were quantified via MATLAB based on the filtered images.

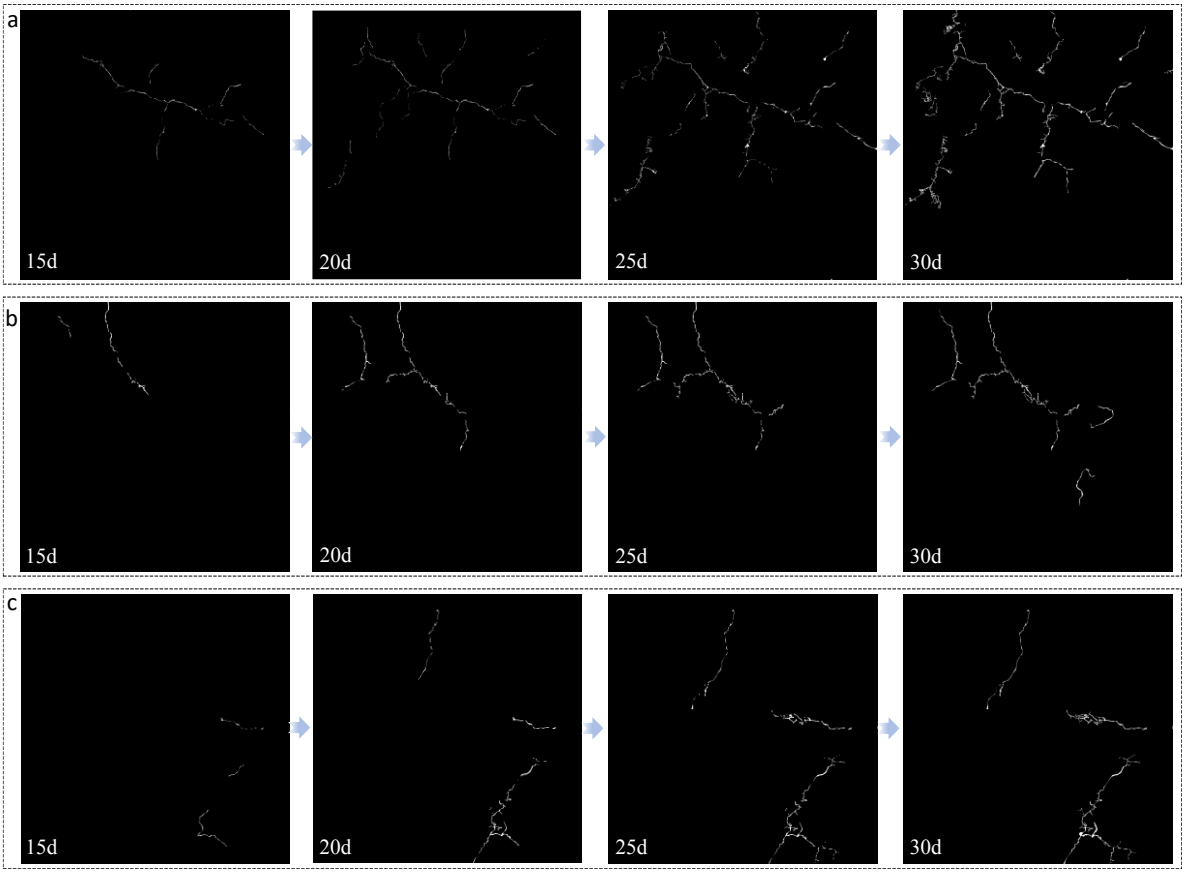

Figure 4.35: Representative filtered images showing the surface crack evolutions of (a) C0, (b) C3, and (c) C10 over time.

As shown in Figure 4.36a, C0 showed a crack density of 0.03% at 10 days of curing (12 days of casting), which increased to 0.78% and 1.37% after 20 and 30 days, respectively. Under 3% CO_2 concentration, C3 exhibited a crack density of 0.03% after 12 days (the initial observation of cracks). Then, the crack density of C3 increased to 0.13% and 0.45% after 20 and 30 days, respectively, which were 83.3% and 67.2% lower than that of C0 at the same ages. When the CO_2 concentration was increased to 10%, an initial crack density of 0.03% was observed from the surface of C10 at 17 days, which is 7 and 5 days later than C0 and C3, respectively. The 30-day crack density of 0.25% was yielded by C10, which is 81.8% and 44.4% lower than that of C0 and C3, respectively.

As shown in Figure 4.36b and Figure 4.36c, in line with the evolution of crack density, both the average and maximum crack width of the mortars increased over time but exhibited reverse correlations with the CO_2 concentration. After 10, 20, and 30 days of curing, the maximum crack width of C0 reached 43.64 μm, 237.14 μm, and 337.78 μm, respectively, with a corresponding average crack width of 21.26 μm, 63.27 μm, and 96.11 μm. When the mortar samples were carbonated under 3% and 10% CO_2 concentrations, although the initial crack density was comparable, the initial average crack widths of C3 (12 days) and C10 (17 days) were 7.56 μm and 5.36 μm, respectively, which were 64.4% and 74.8% lower than that of C0 (10 days). After 30 days of carbonation, C3 and C10 exhibited 54.6% and 31.2% lower

maximum crack widths than C0. Given the brittle nature of cement-based materials, the direct result of volume expansion in ASR-attacked concrete is cracking. The formation of cracks not only compromises the mechanical properties but also increases the permeability of concrete by providing pathways for external moisture and aggressive salts, resulting in secondary deteriorations and substantially shortened service life. The reduced crack density and crack width on the surface of mortar samples under CO_2 are in good agreement with the substantial decreases in ASR-induced expansion as shown in Figure 4.33, which again indicates the effective role of the enforced carbonation in suppressing ASR. It should be noted that, although the cracks detected on the specimen surface provide a solid indication of ASR under carbonation, the technique has its own limitations in identifying microcracks. The physical size of each pixel is 0.009 mm, rendering unfeasible the detection and measurement of cracks with a size smaller than 0.009 mm, which might underestimate the crack density results of the mortar specimens.

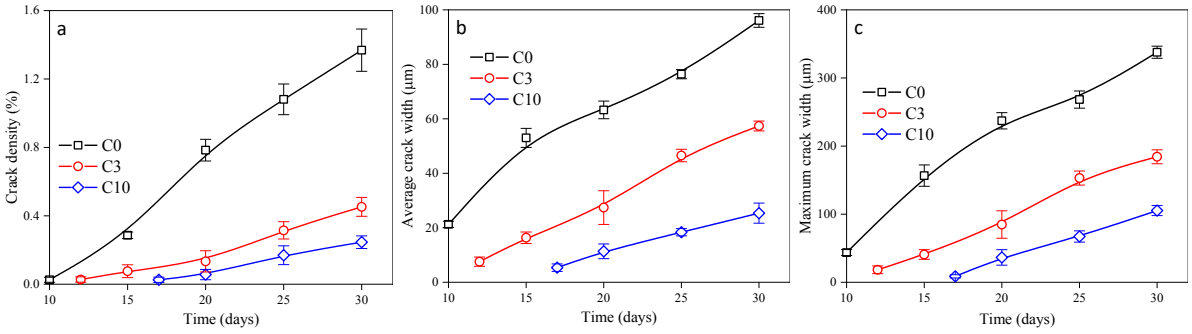

Figure 4.36: Evolutions of (a) crack density, (b) average crack width, and (c) maximum crack width.

4.8.2. In-situ characterizations of ASR products

4.8.2.1 Raman spectroscopy

The Raman spectra focusing on the ASR products located in aggregate cracks and cement pastes in the mortar samples after 30 days of carbonation curing are shown in Figure 4.37a and 4.36b, respectively. The peak at around ~1578 cm^{-1} is related to the stretching vibration of -OH from CH, which decreased in both ASR products inside aggregate cracks and cement pastes under carbonation curing and disappeared under 10% CO_2. Similarly, the peak attributed to the vibration of Q^2 Si-O-Si bonds in C-S-H (280 cm^{-1}) was found to decrease with increasing CO_2 concentration. Decreases were also observed from the peaks correlated with Q^3 sites of Si-O bonds in ASR-related products located at 615 cm^{-1}. It should be noted that the peak at 1185 cm^{-1} is shared by both Q^3 Si-O sites and CC. Given the decreased Q^3 sites under carbonation curing, it is believed that the high peak at 1185 cm^{-1} obtained from the surface layer of the carbonated mortar is mainly due to the formation of CC, which was evidenced by the increased CC-related peaks at around 204 cm^{-1}, 692 cm^{-1}, and 1175 cm^{-1}. The peak at 464 cm^{-1} detected from the aggregate cracks is likely caused by the Q^1 Si of quartz. From Figure 4.37b, an increased C-S-H peak was found in all layers of C10-1 and the surface of C20-1 in the area of cement pastes. This might be due to the enhanced cement hydration, as the production of CC can act as a filler, providing more nucleation sites for C-

S-H phases [270]. The evolutions of the related chemical bonds indicate the conversion of hydration and ASR products into carbonates under the enforced early-age carbonation.

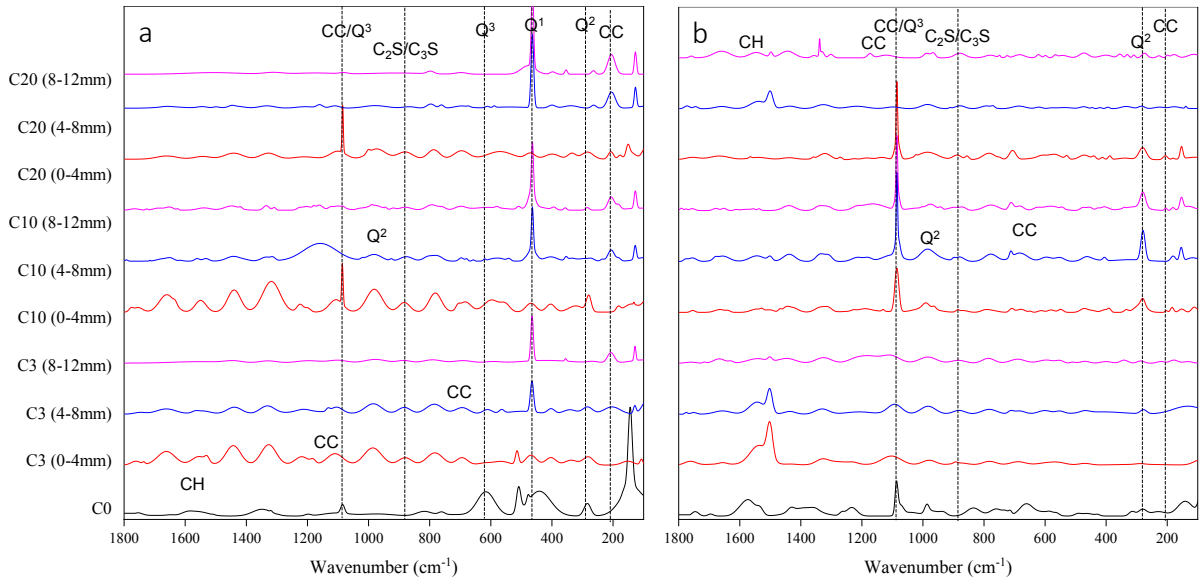

Figure 4.37: Raman spectra of (a) ASR products formed inside aggregate cracks and (b) cement pastes.

4.8.2.2 Energy dispersive X-ray spectroscopy

Figure 4.38a and 4.38b show the normalized molar percentages of the ASR gels obtained from EDS analysis in ternary phase diagrams of C-Ca-Si and [Na+K]-Ca-Si, respectively. One limitation of the EDS analysis lies in the focused elemental ratios from separate testing sites, which might be able to represent the overall composition of ASR products. To mitigate the impact of this limitation, testing results were collected from at least 30 points for each specimen. The ASR gels formed in C0 exhibited an averaged C/Si ratio of 0.64 and a Ca/Si molar ratio of 0.13, which falls in the typical Ca/Si range of 0.05-0.5 observed from ASR gels in concrete [149]. As expected, the C/Si ratio of ASR products was found to increase in the carbonated mortar, which reached 1.5 and 2.1 in C3 and C10, respectively. Under the highest CO_2 concentration of 20%, however, the microstructure of C20 may be densified due to the rapid carbonation of the mortar surface in the presence of highly concentrated CO_2, which might mitigate the diffusion of CO_2 to the center of the mortar samples and result in a C/Si ratio of 0.65. At the same time, the Ca/Si ratio of ASR products increased to 0.22, 0.30, and 0.45 in C3, C10, and C20, and the [Na+K]/Si ratio decreased from 0.44 in C0 to 0.08, 0.07, and 0.05 in C3, C10, and C20, respectively. The increases in the Ca/Si ratio and decreases in [Na+K]/Si ratio are favorable to obtaining ASR products with reduced water absorption and decreased swelling potential [271, 272], which possibly contributed to the suppressed ASR expansion and cracking under carbonation.

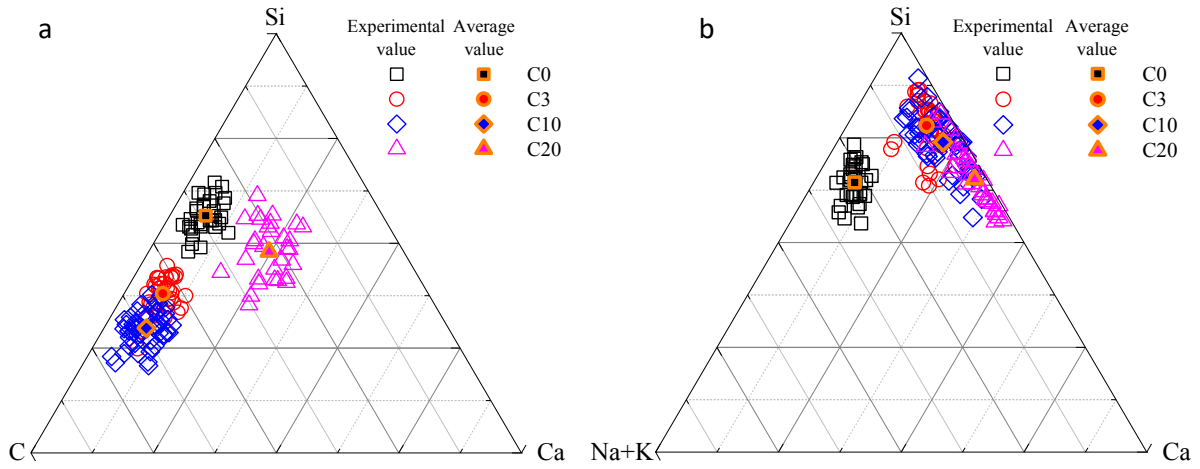

Figure 4.38: (a) C-Ca-Si and (b) [Na+K]-Ca-Si ternary phase diagrams of ASR gels formed in mortars with and without carbonation.

4.8.3. ASR gels' carbonation

4.8.3.1 Phase evolution in carbonated ASR gels

Figure 4.39 shows the XRD patterns of synthetic ASR gel with a calcium-silica (Ca/Si) ratio of 0.3 and an alkali-silica (Na+K/Si) ratio of 1.0 after being cured in a sealed condition for 420 days, followed by up to 7 days of enforced carbonation. Without carbonation, the control ASR gel (G0) showed semi-crystalline peaks at 29.4°, 31.9°, and 49.9° 2θ, which are characteristic of tobermorite-type C-S-H with a layered silicate structure [149, 273]. The amorphous part of the peak centered at 29.4° 2θ signifies the presence of the alkali silicate hydrates (ASH) comparable to kanemite, makatite, magadiite, kenyaite, and octosilicate [149, 274-276]. After 3 hours of carbonation under 3% CO_2, 75% RH, and 50°C, the reduction of full width at half measurement (FWHM) from the characteristic peaks suggested the enhanced crystallization of the ASR phases along with the appearance of crystalline peaks at 29.9° 2θ and 24.8° due to calcite and at 24.5°, 49.9° and 55.41° due to vaterite (Figure 4.39a). A metastable calcium-silicate carbonate phase known as galuskinite ($Ca_7(SiO_4)_3(CO_3)$) was also detected at 9.1° and 16.3° 2θ. Due to the high Na/Si ratio (0.8) of the synthetic ASR gel, one of the major products formed after 3 hours of carbonation was sodium bicarbonate or nahcolite ($NaHCO_3$) indicated by the peaks at 18.3 °, 28 °, 35.8 °, 36.9 °, 40.8 °, 44 °, and 52.8 ° 2θ and metastable sodium-calcium carbonate or nyerereite ($Na_2Ca(CO_3)_2$) signified by the peaks at 16.3° and 29.3° 2θ. After 24 hours of carbonation, the absence of tobermorite-type C-S-H and ASH suggested complete conversion of the ASR phases into carbonates. Although no new phases were formed, the vaterite (34.1° 2θ) was reduced and galuskinite was completely converted into more stable calcite or nahcolite after 24 hours. After 7 days of carbonation, further enhancement of nahcolite and reduced vaterite was observed without the formation of any new phases. As shown in Figure 4.39b, increasing the CO_2 concentration from 3% to 10% resulted in accelerated conversion of ASR phases in just 3 hours as indicated by the disappearance of the tobermorite-type C-S-H and ASH peaks. After 24 hours, the galuskinite was further converted to alkali-based carbonation products as

well as vaterite and calcite with no new phase formed after 3 days and 7 days. However, after 7 days of carbonation, G10 showed lower nahcolite intensity than G3, which indicates the preferential formation of CC over nahcolite under high CO_2 concentration.

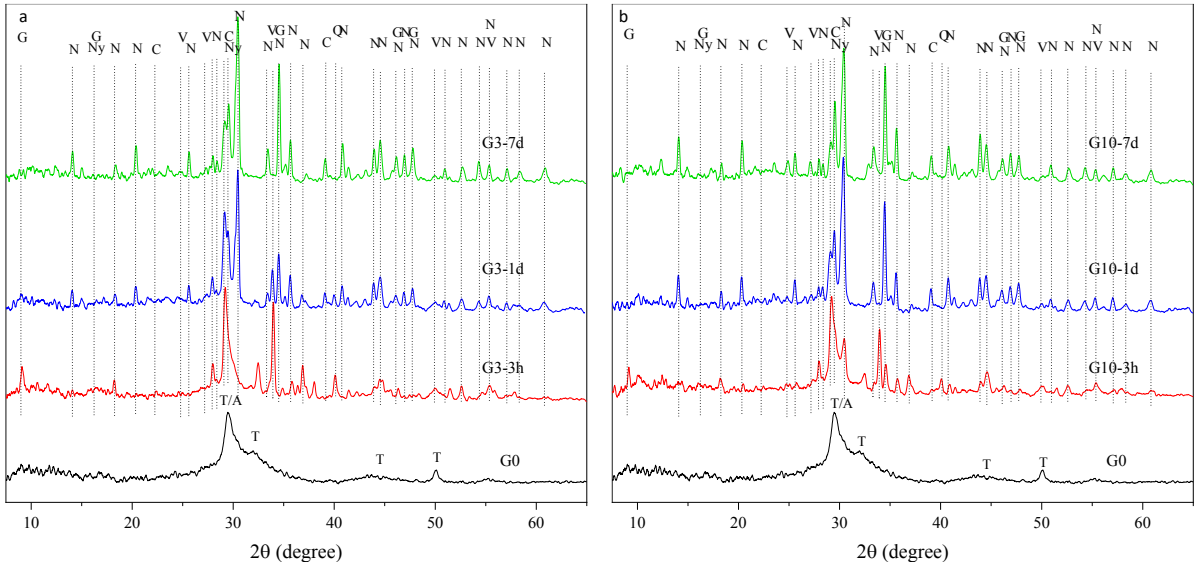

Figure 4.39: XRD patterns of ASR gels carbonated under (a) 3% and (b)10% CO_2, from 0 hours to 7 days. Note: A-ASH, C-Calcite, G-Galuskinite, N-Nahcolite, Ny-Nyerereite, Q-Quartz, T-Tobermorite-type C-S-H, V-Vaterite.

Figure 4.40 shows the weight percentages of the crystalline phases and the amorphous portion in the ASR gels carbonated after 0, 3, 24 and 167 hours. Without carbonation, the control ASR gel showed a 89.6% amorphous content. The crystalline tobermorite-type C-S-H and ASH showed contents of 4.4% and 6.1%, respectively. As shown in Figure 4.40a, under 3% CO_2 for 3 hours, the amorphousness was found to decrease by 20.7%, which is supported by the reduced FWHM of the peaks. It is worth noting that the main ASR products, tobermorite-type C-S-H and ASH, contain a large portion of amorphous phases, and the amorphous ASR products are typically considered more swellable than crystalline phases. The decrease in amorphousness indicates the conversion of ASR products into crystalline components, like carbonates. This change was accompanied by steady decreases in the crystalline ASR products as the carbonation progressed. After 7 days of carbonation under 3% CO_2, the contents of crystalline tobermorite-type C-S-H and ASH decreased by 70.5% and 65.6%, respectively. As a result, nahcolite was formed and dominated the products with a content of 24.9%. It is interesting to see that the content of calcium carbonates (calcite and vaterite) increased during the first 3 days followed by a reduction with further carbonation. As shown in Figure 4.40b, increasing the CO_2 concentration from 3% to 10% resulted in an enhanced reduction of amorphousness by 24.1% after 3 hours. Due to the rapid carbonation under this high CO_2 concentration, no significant further decrease in amorphousness was obtained over time. The enhanced carbonation in G10 was also evident from the more remarkable reductions of crystalline tobermorite-type C-S-H and ASH. After 7 days, the contents of tobermorite-type C-S-H and ASH were found to decrease by 86.3% and 93.4%, respectively. Similar to the finding under 3% CO2, the content of calcium

carbonates was found to increase during the first 3 hours, which became less with further carbonation accompanied by a slight increase in the nahcolite content. Although a 15.2% increase in the 7-day calcium carbonate content was obtained when increasing the CO_2 concentration from 3% to 10%, the relative contents of carbonate polymorphs were modified with a higher content of vaterite and less calcite.

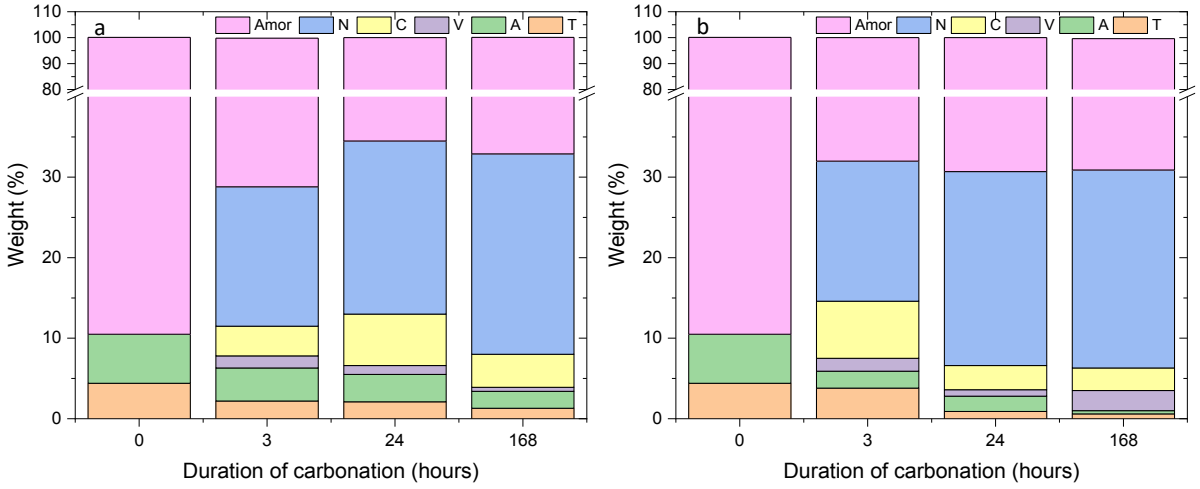

Figure 4.40: Rietveld refinement of ASR gels cured at (a) 3% and (b)10% CO2, 50ºC, and 75% RH from 0 hours to 7 days. Note: Amor- Amorphous content, A-ASH, C-Calcite, N-Nahcolite, T-Tobermorite-type C-S-H, V-Vaterite.

Figure 4.41 shows the TGA and DTG curves of the ASR gel before carbonation and conditioned under the 3% CO_2 concentration after 3 hours, 1 day and 7 days. The weight loss between 30°C and 105°C is attributed to the evaporation of free or the loss of loosely bound water, while the additional weight losses between 105°C and 250°C are due to the loss of chemically bound water in the ASR products such as tobermorite-type C-S-H [277] and ASH (might include kanemite, magadiite and kenyaite) [274, 276]. The control gel also shows a distinct compound weight loss between 250°C and 360°C where the first weight loss between 250°C and 288°C is attributed to the dehydration of Na-kanemite and the second weight loss between 288°C and 360°C is most likely due to the dehydration of Na-magadiite [276]. After carbonation under 3% CO_2 for 3 hours, the ASR gel showed a reduction in weight drop of free and loosely bound water by 11.3% due to drying and carbonation of the ASR gel. The amount of ASR phases was reduced by 82.7%. A distinct weight loss and DTG peak due to the decomposition of nahcolite was observed from the carbonated ASR gels between 100°C and 225°C [278]. The formation of CC, including aragonite, vaterite, and calcite was evidenced by the newly formed DTG peaks in the range between 450°C and 900°C. Aragonite and vaterite, the metastable polymorphs of CC, decompose in a range of 500-650°C, while the more thermally stable calcite decomposes between 680°C and 900°C [279]. After 24 hours of carbonation, the ASR-related components were completely converted. The weight drop due to free and loosely bound water was found to decrease by 69.1% and 87.7% after 24 hours and 7 days, respectively, which is in line with the FTIR results (see Figure 4.43 below) and suggests the mitigation of the moisture uptake capacity of

the ASR gel. Although nahcolite and vaterite were found to increase by up to 14.9% and 19.6% from 24 hours to 7 days, respectively, the amount of calcite reduced by 28.5%, which supports the XRD results.

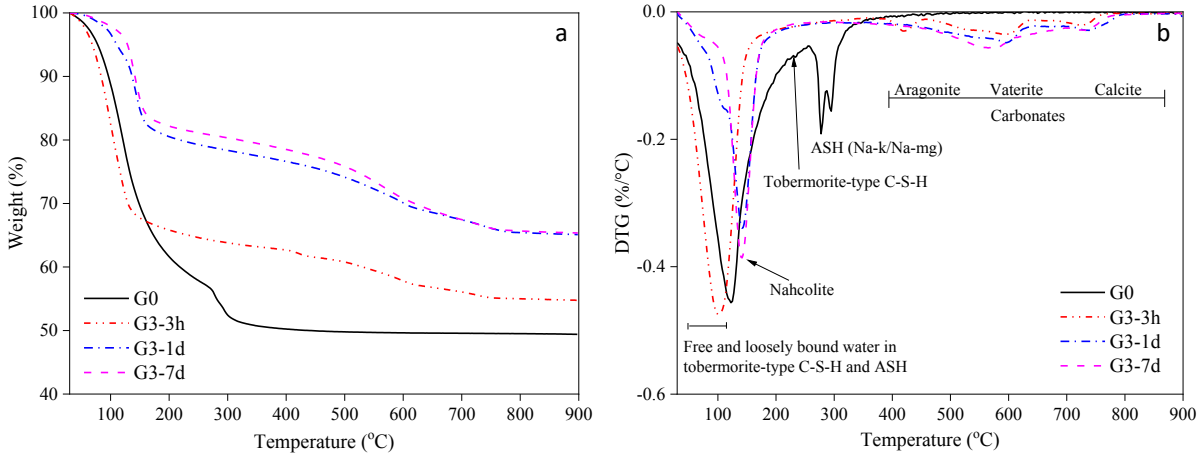

Figure 4.41: (a) TGA and (b) DTG curves of ASR gels carbonated under 3% CO_2 for up to 7 days.

As shown in Figure 4.42, under 10% CO_2, complete conversion of the ASR phases was reached after just 3 hours, along with a 14.3% lower weight drop due to free and loosely bound water. While the overall carbonation products (CC and nahcolite) were greater under 10% CO_2, 22.8% less nahcolite was formed when compared to G3 at 3 hours, which indicates that calcium-based carbonation products can be formed more rapidly under a higher CO_2 concentration. However, the content of nahcolite was found to increase by 102.2% from 3 to 24 hours, along with 21% and 14.2% reductions in vaterite and calcite, respectively. After 7 days of carbonation, G10 yielded 6.5% more overall carbonates than G3, indicating a higher degree of carbonation in the system.

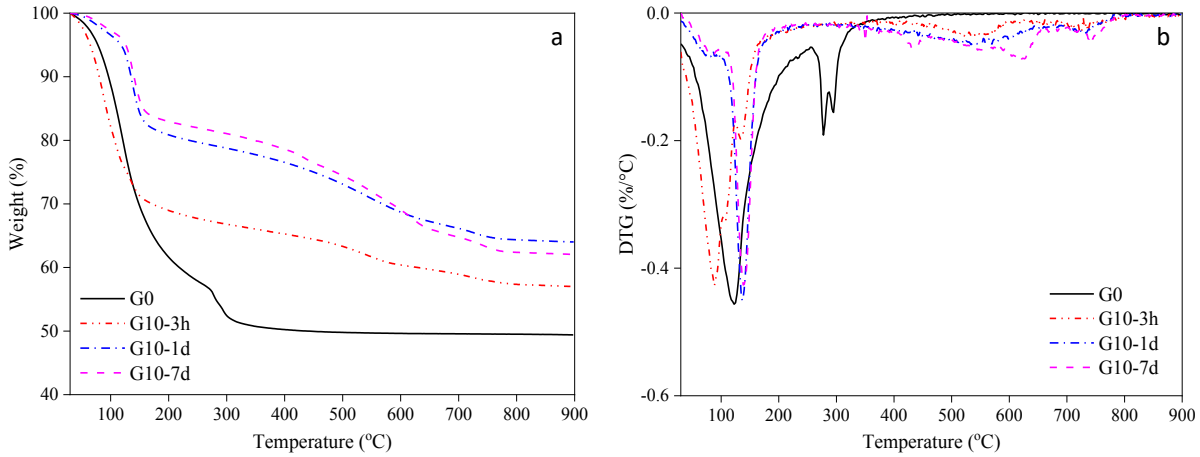

Figure 4.42: (a) TGA and (b) DTG curves of ASR gels carbonated under 10% CO_2 for up to 7 days.

From the FTIR spectra in Figure 4.43, characteristic peaks of Si-O-Si bending between 600 and 800 cm^{-1} and Si-O stretching between 900 and 1100 cm^{-1} were observed from the control ASR gel, indicating the presence of Q^2 and Q^3 silicate polymerization sites in the ASR gel [280]Fig. The peak at ~966 cm^{-1} is characteristic of the Q^2 structures in tobermorite-type C-S-H [281], whereas the peaks at 900 cm^{-1} and the shoulder at 1065 cm^{-1} suggest the co-existence of Q^2 and Q^3 sites in ASH (Na-kanemite) [209, 282]. The presence of the layered Q^3 sites is a unique feature of ASR gels and is considered to be the main reason for moisture uptake and swelling [283]. Under 3% CO_2 concentration, the Si-O and Si-O-Si peaks still existed but with lower intensities, indicating the partial carbonation of the ASR phases (Figure 4.43a). After 24 hours, the Si-O-Si and Si-O peaks are absent indicating the complete conversion of ASR gel to carbonates, which can be evidenced by the new peaks at 850 cm^{-1} and 1395-1450 cm^{-1} due to the out-of-plane bending (v_2) and symmetrical stretching (v_3) of carbonate (CO_3^{2-}) group and C=O bond, respectively, in CC (calcite, vaterite, and aragonite) [284]. The appearance of peaks at 680 cm^{-1}, 1029 cm^{-1}, and 1055 cm^{-1} indicates the formation of nahcolite [285, 286]. The appearance of the Q^4 peak of free silica at ~1175 cm^{-1} indicates the decalcification of the ASR phases under carbonation [287, 288]. The broad band between 2500 and 3750 cm^{-1} due to the vibration of the -OH in free or loosely bound water was found to decrease after 3 hours and disappear after 24 hours and 7 days of carbonation, which indicates the decreased hygroscopicity of the system. Similar carbonation products were observed under 10% CO_2, while the rapid carbonation resulted in the complete disappearance of ASR phases after only 3 hours. In line with the XRD and TGA data, less nahcolite, greater Q^4 sites due to decalcification, and further decreased vibration of -OH were observed under the higher CO_2 concentration after 24 hours and 7 days, indicating a more comprehensive carbonation and conversion of the ASR phases into non-expansive carbonates.

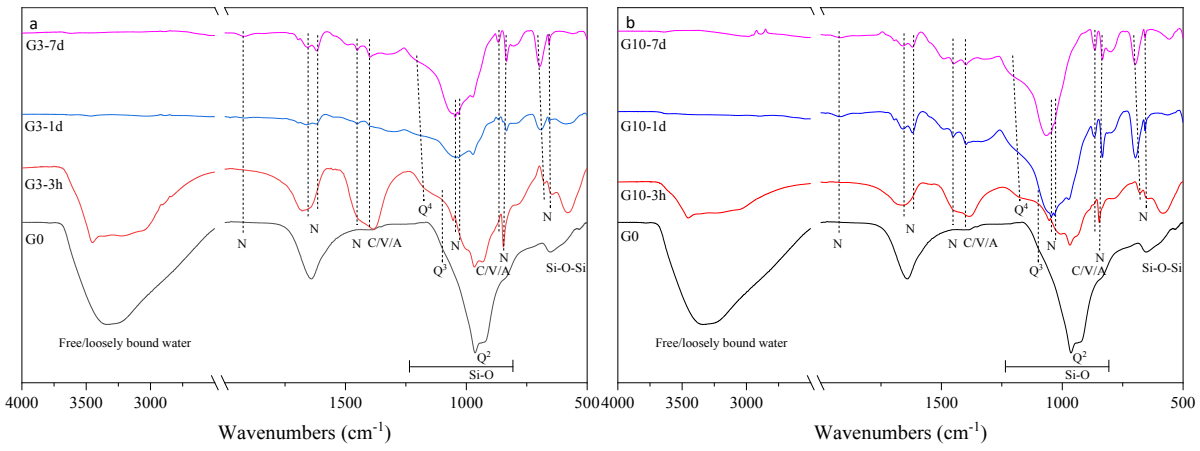

Figure 4.43: ATR-FTIR spectra of ASR gels carbonated under (a) 3% and (b) 10% CO_2 from 0 hours to 7 days. Note: A-Aragonite, C-Calcite, N-Nahcolite, and V-Vaterite.

4.8.3.2 Hygroscopicity and water uptake

The moisture sorption and desorption behavior, one of the most important characteristics of ASR gel governing its volumetric swelling, was studied via dynamic vapor sorption (DVS) after carbonating the gel under 3% and 10% CO_2 for 7 days. The control ASR gel shows overall moisture desorption and absorption of 125.7% and 124.5%, respectively, about 83% of which occurs in the high RH range of 70-95% (Figure 4.44a). Under 3%, the overall moisture absorption reduced by 10.65%, while no significant change was observed from the one carbonated under 10% CO_2. In addition, G3 and G10 showed 93% and 93.4% of their total absorption between 70% and 95% RH, respectively, which are higher than that of the control ASR gel. The reason for this may be the formation of the hygroscopic calcite, as well as silica gel from the decalcification of ASR products, which shows high moisture absorption at RH above 70% [289]. It should be noted that, although the formed calcite and silica gel can capture moisture, they do not exhibit significant volume expansion [290, 291] and hence no detrimental stress to the surrounding concrete matrix can be generated, which is contrary to the intrinsic swelling nature of ASR gels.

The DVS isotherms of the control and carbonated ASR gels are shown in Figure 4.44b, 4.43c, and 4.43d. According to Sing [292] and Thommes [293], the control ASR gel exhibited a Type III isotherm showing multilayer adsorption with weak adsorbate-adsorbent interactions. The negligible hysteresis between the desorption and absorption isotherms indicates the absence of ink-bottle shaped pores in the ASR gel. After carbonation in 3% CO_2 for 7 days, G3 yielded an isotherm shape similar to a Type II isotherm, indicating a monolayer or multilayer adsorption behavior in a non-porous or microporous structure. A distinct inflection point (B) was observed at 10% RH in both G3 and G10, indicating the monolayer and multilayer adsorption behavior of the ASR gels at different RH levels. Such a Point B can be signified by the sudden slope change, beyond which the dominant moisture uptake behavior converts from monolayer adsorption into multilayer adsorption. Different from Type II isotherms, a significant hysteresis was observed in the isotherms of G3 and G10. When the CO_2 concentration increased to 10% (G10), the isotherm changed to Type IV, indicating mesoporous adsorbents such as silica gel, where the adsorbate-adsorbent interaction initially follows the same monolayer-multilayer path as Type II isotherm, followed by pore condensation [293] (Figure 4.44d). The carbonated ASR gels exhibited an increase in hysteresis with RH, indicating the presence of ink-bottle-shaped pores with smaller pore necks that can entrap moisture and inhibit its drying by forming a meniscus in the pore neck [294]. G3 shows a maximum hysteresis width of 29.1% at 80% RH, while G10 shows a maximum hysteresis width of 31.4% at 70% RH, which is similar to the hysteresis behavior of silica gel [289]. The hysteresis in G3 and G10 is mainly due to the decreased moisture absorption capacity at RH below 80% indicating the decreased hygroscopicity of the ASR gel after carbonation.

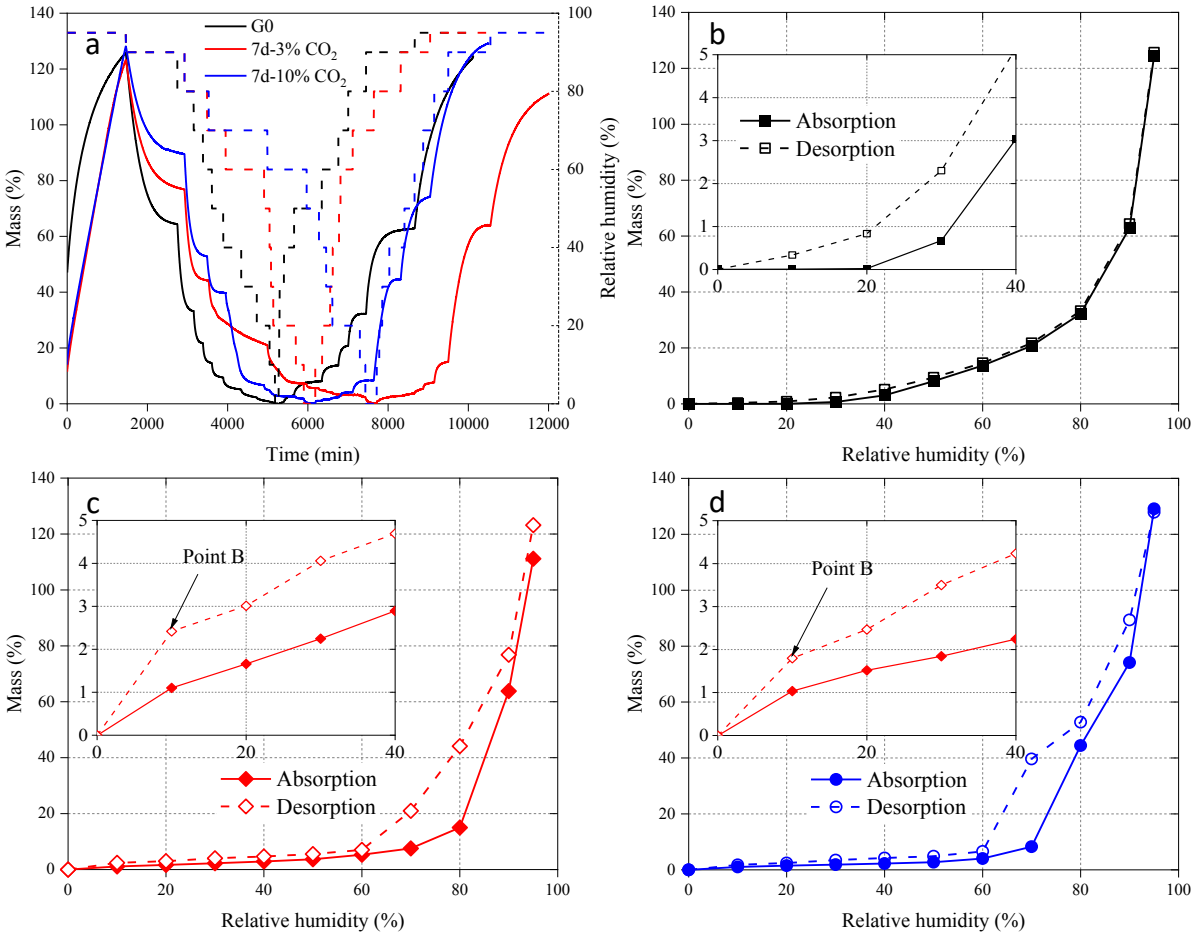

Figure 4.44: (a) Dynamic vapor sorption behavior of ASR gels and the isotherms (b) the control ASR gel and carbonated ASR gels under (c) 3% and (d) 10% CO_2.

The mass change curves, as well as the drying rate and drying acceleration curves obtained from wet ASR gels G0, G3, and G10 to equilibrium at 40 % RH and 40 °C, are shown in Figures 4.45a to 4.44c, respectively. Based on the mass development, WUC of the ASR gels before and after carbonation at CO_2 concentrations of 3% and 10% was determined and shown in Figure 4.45c. From the mass drops of the pre-saturated ASR gels shown in Fig. 4.45a, G3 and G10 showed 43% and 35% mass loss, respectively, which are 25.9% and 39.7% lower than that of the control ASR gel. The reductions in both moisture desorption and equilibrium time indicate lower WUC of the carbonated ASR gels. As shown in Figure 4.45c, the control ASR gel yielded a WUC of 41.4%, which decreased to 15.4% and 11.1% in G3 and G10, respectively. In line with the DVS results above, the substantial decrease in water absorption behavior in the carbonated ASR gels provided an additional mechanism for the suppressed ASR expansion and cracking and confirmed the promising efficacy of early-age enforced carbonation as a potential ASR mitigation approach at a lower length scale.

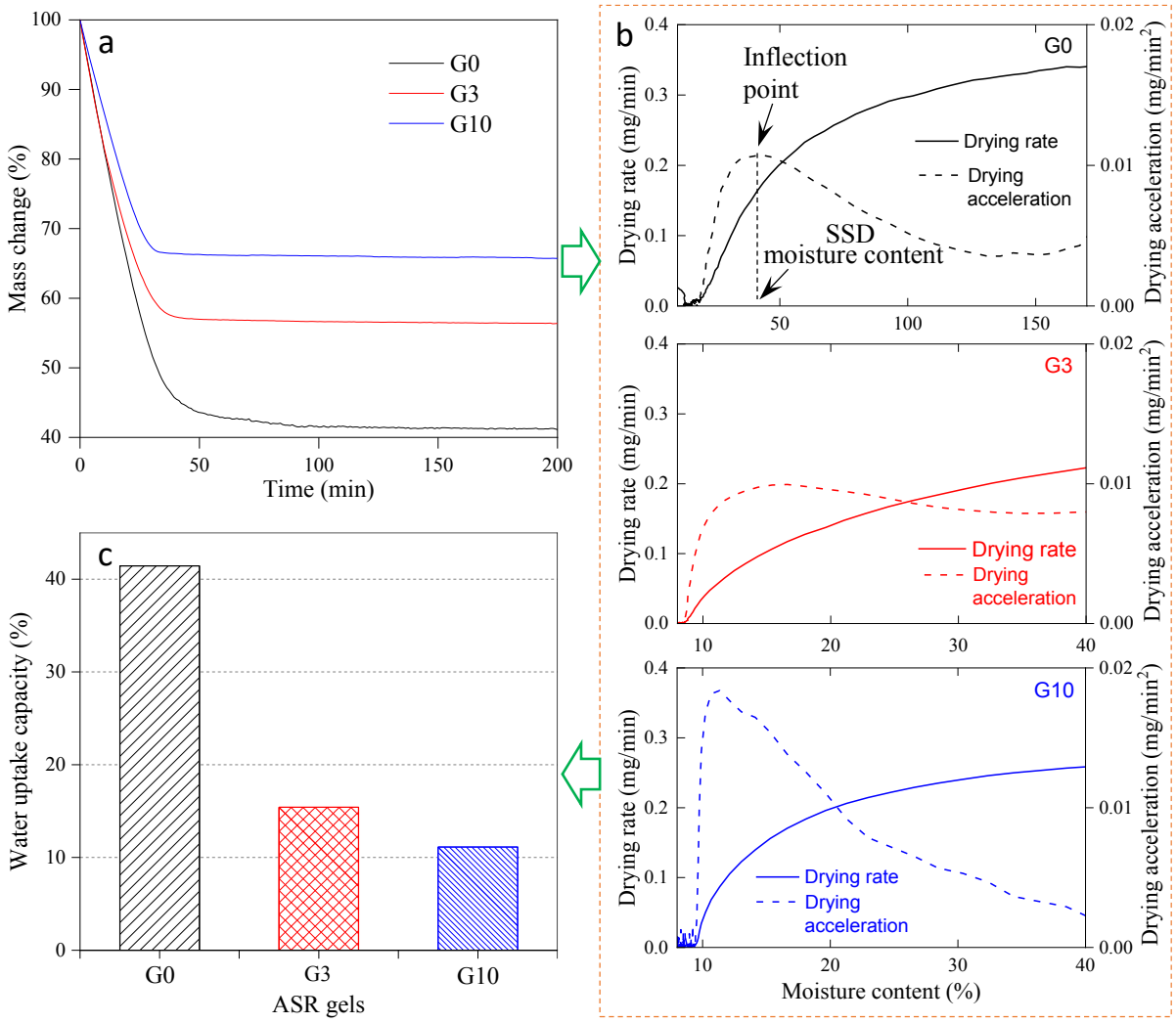

Figure 4.45: (a) Mass change curves, (b) drying rate (solid) and drying acceleration (dashed) curves, and (c) WUC of the control and 7-day carbonated ASR gels.

This page left blank This page left blank intentionally.

5.0 Field Tests

5.1 Field test outcomes and comparison between lab and field results

To evaluate field performance and to scale up the concrete mix, the same laboratory-tested mix with 25% RGGP was ordered from a MassDOT-approved ready-mix plant for casting sidewalk slabs. Detailed concrete mix design sheets can be found in the appendix. The delivered concrete had a slump of 7 inches and an air content of 7.5%.

5.1.1. Compression test results

To evaluate the compressive strength of concrete in a field setting, the mix with 25% RGGP was used to make a sidewalk slab. The slab was cured using wet burlap for 7 days. Strength was measured at 7 and 28 days. To study the effect of burlap curing, which is less ideal than curing in saturated lime water until the testing date, additional samples were prepared. For every test date, 3 samples were cured in lime water until testing, and three samples were cured with burlap for seven days outdoors in an environment similar to sidewalk slab. Figure 5.1 shows the average strength for each age. In the figure, bar heights represent the average of three samples, symbols in the bars show the results of each sample, and the different colors identifies the testing age.

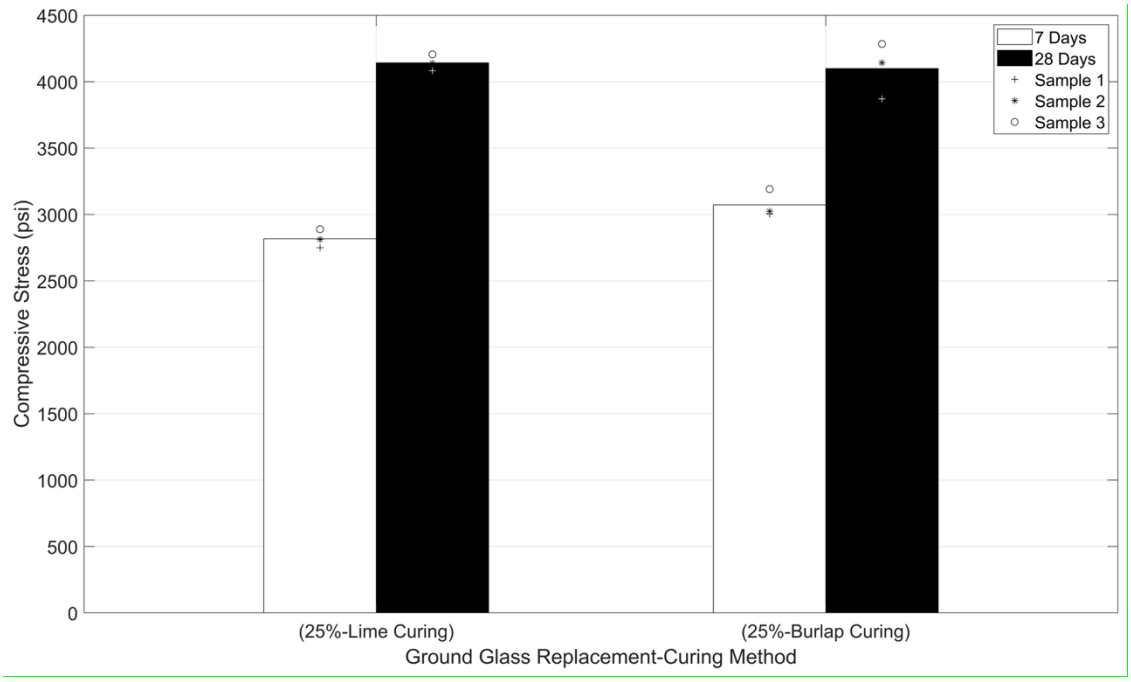

Figure 5.1: Average compressive strength of 25% RGGP concrete under burlap and lime curing at 7 and 28 days

As shown in Figure 5.1, the burlap-cured samples showed slightly higher strength at 7 days, and the 28-day strength was nearly equivalent between both curing methods. This outcome is likely due to the higher ambient temperature during summer outdoor curing, which accelerated the hydration and early strength gain in the burlap-cured specimens. Similarity of the strength at 28 days also suggests that the absence of curing beyond 7 days did not significantly impact the long-term strength development of the concrete with 25% RGGP.

In addition, a comparison was made between the compressive strength of the 25% RGGP concrete specimens, prepared in the lab and cured in lime water and the concrete samples made using the ready-mix concrete. As shown in Figure 5.2, the results indicate that the laboratory-prepared concrete samples exhibited higher compressive strength than their ready-mix counterpart.

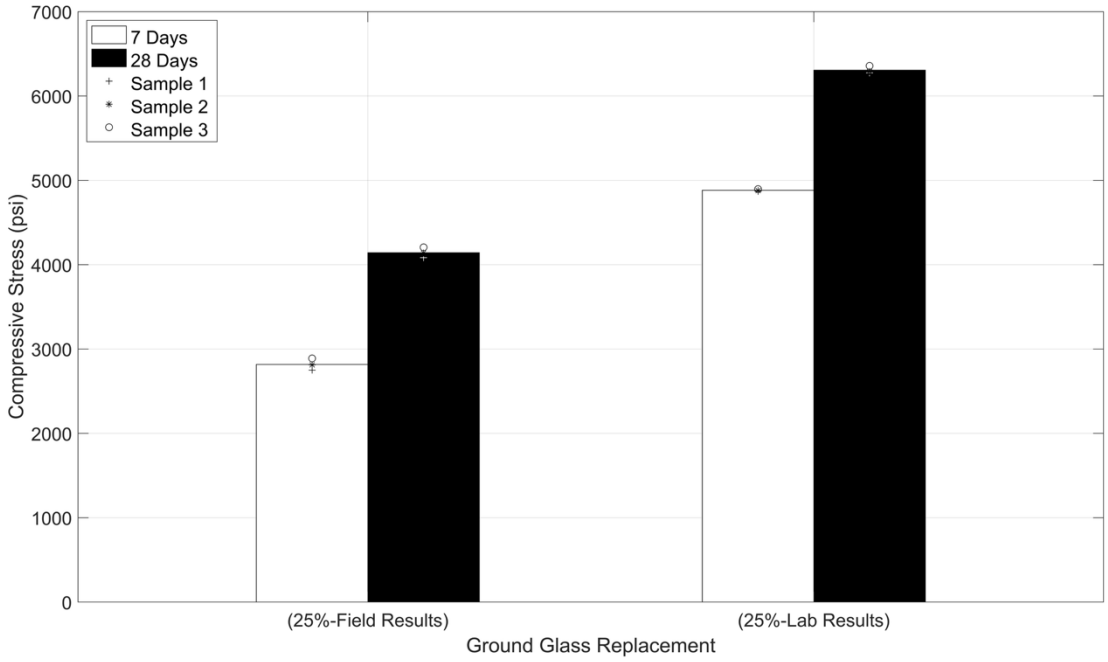

Figure 5.2:Compressive strength – lab vs. field samples

5.1.2. Splitting tensile test results

For each testing age of 7 and 28 days, three cylinders with 25% RGGP were prepared. The average splitting tensile strength results are presented in Figure 5.3. At both ages, the lab-prepared concrete showed slightly higher tensile strength compared to the field samples. However, the difference was less noticeable than the variation observed in compressive strength.

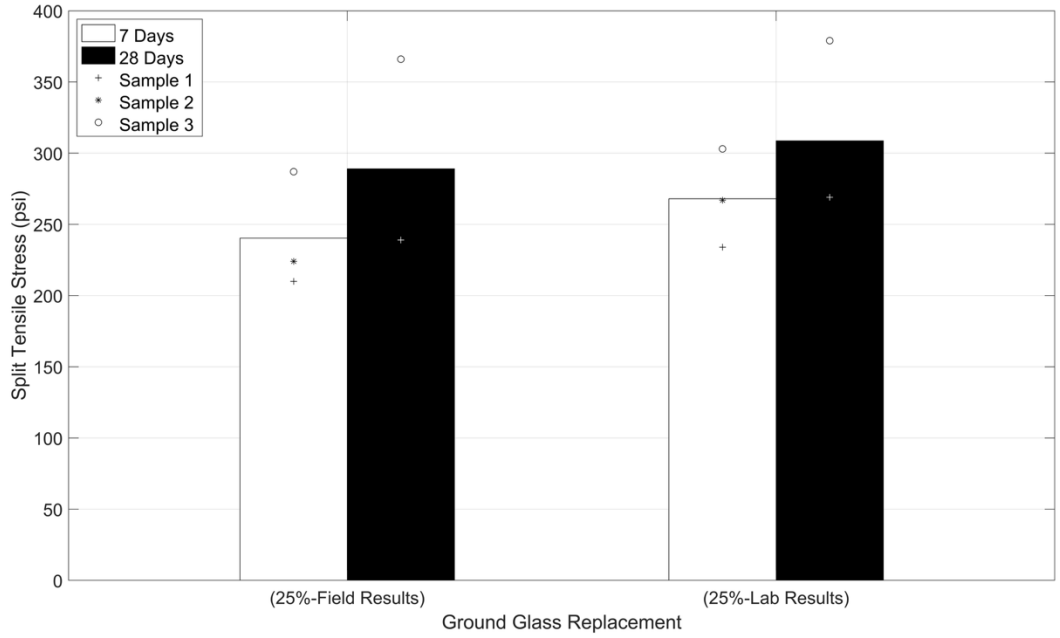

Figure 5.3: Splitting tensile strength – lab vs. field samples

5.1.3 Rupture strength test results

For further evaluation of the rupture strength of the concrete with 25% RGGP, four-point bending tests were performed. Two samples were tested at each curing age (7 and 28 days). As shown in Figure 5.4, the plant-sourced concrete outperformed the laboratory mix at both time intervals.

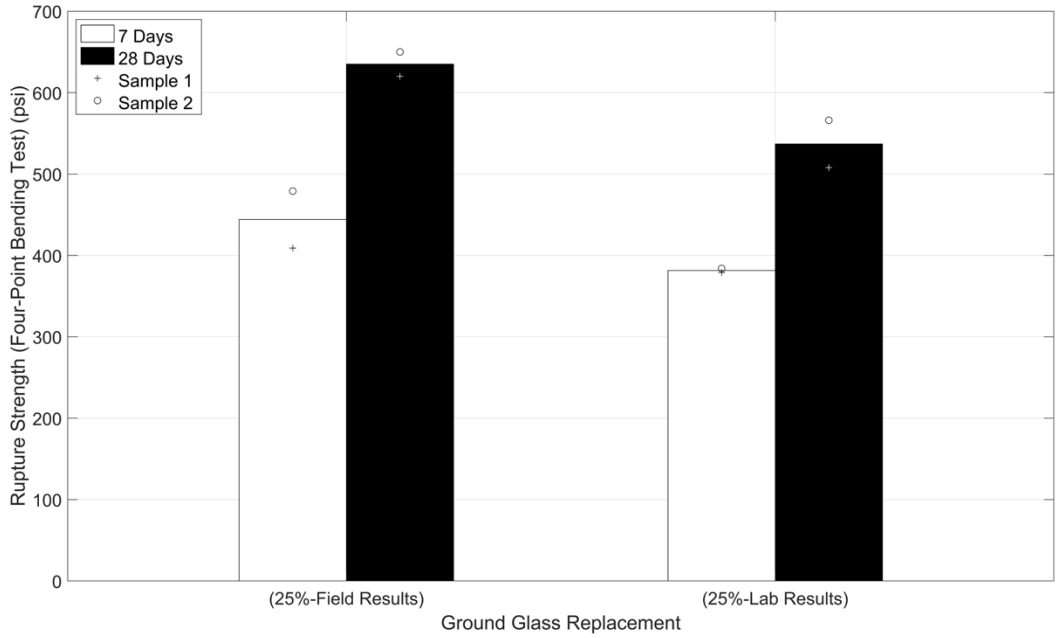

Figure 5.4: Rupture strength – lab vs. field samples

5.2 ASR Test

As shown in Figure 5.5 and Tables 5.1 and 5.2, the ASR reactivity test was conducted according to ASTM C1567. After 14 days of exposure, the average mortar expansion for the specimens containing 25% RGGP was 0.043%. This value is slightly lower than the expansion observed in the control specimens without RGGP, which was 0.056%. The results demonstrate that the replacement of 25% of RGGP sourced from Urban Mining not only does not increase the risk of ASR expansion for the used concrete mix, but also contributes to a slight improvement in performance compared to the control specimens. Furthermore, both expansion values remain below the 0.1% threshold.

Table 5.1: Expansion rate for control mix according to ASTM C1567

Reading Time	Control (0% RGGP Replacement)						
	Sample 1		Sample 2		Sample 3		Average Expansion (%)
	Length (in)	Expansion (%)	Length (in)	Expansion (%)	Length (in)	Expansion (%)	
Initial Reading	11.6076	0	11.5242	0	11.5674	0	0
Zero Reading	11.6102	0.02	11.5282	0.03	11.5718	0.03	0.026
3-day	11.6104	0.02	11.5295	0.04	11.5721	0.04	0.033
6-day	11.6110	0.03	11.5298	0.04	11.5732	0.05	0.04
9-day	11.6114	0.03	11.5302	0.05	11.5743	0.06	0.046
14-day	11.6142	0.05	11.5310	0.06	11.5752	0.06	0.056

Table 5.2: Expansion rate for the mix with 25% RGGP according to ASTM C1567

Reading Time	25% RGGP Replacement						
	Sample 1		Sample 2		Sample 3		Average Expansion (%)
	Length (in)	Expansion (%)	Length (in)	Expansion (%)	Length (in)	Expansion (%)	
Initial Reading	11.5898	0	11.5346	0	11.5605	0	0
Zero Reading	11.5921	0.01	11.5366	0.01	11.5625	0.01	0.01
3-day	11.5937	0.03	11.537	0.02	11.5632	0.02	0.023
6-day	11.5950	0.04	11.5377	0.02	11.5644	0.03	0.03
9-day	11.5954	0.04	11.5387	0.03	11.566	0.04	0.036
14-day	11.5966	0.05	11.5402	0.04	11.5662	0.04	0.043

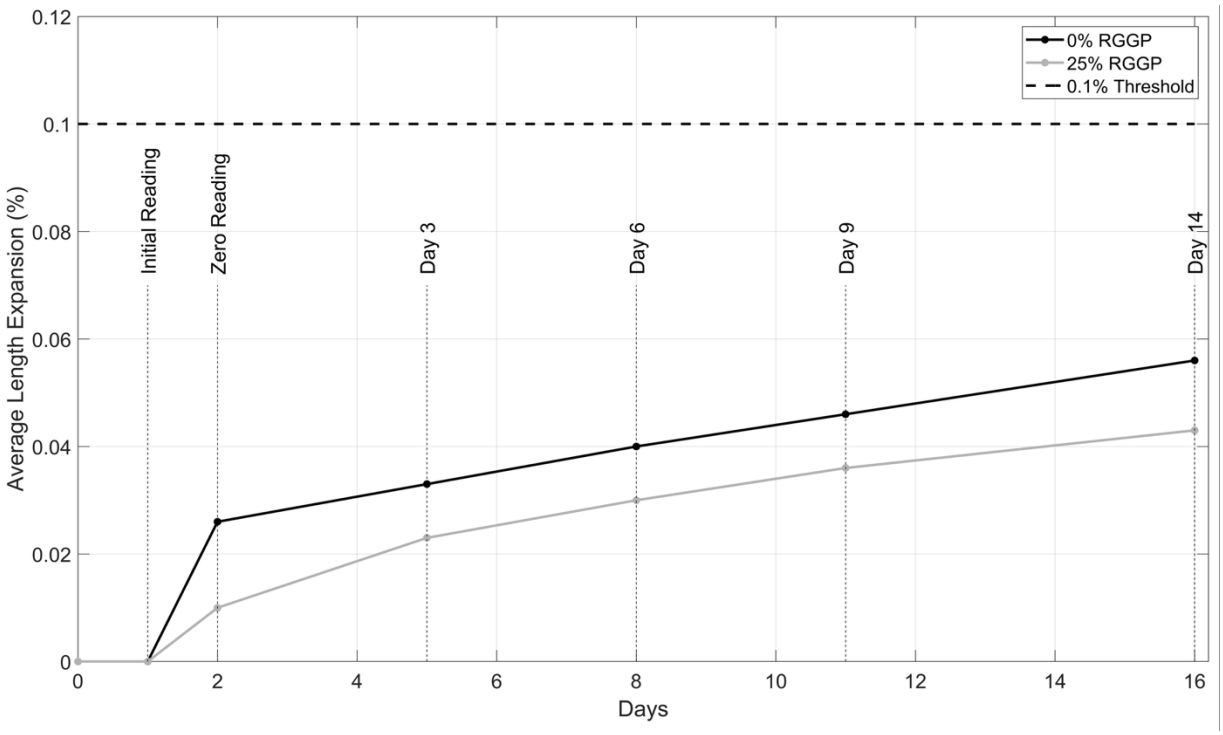

Figure 5.5: Average expansion of mortar samples over time due to ASR, based on ASTM C1567

This page left blank This page left blank intentionally.

6.0 Conclusions

This study involved a series of laboratory and field tests to examine how RGGP and other alternative materials affect concrete performance at different replacement levels. The investigations over the current state and challenges in applying RGGP into concrete, experimental characterizations of RGGP, evaluations of cement hydration in the presence of RGGP, assessment of fresh and hardened properties of mortar and concrete, and field tests. The following key conclusions can be drawn from this project:

(i) Although the unique amorphous nature and the high silicate contents in glass highlight the promising potential of RGGP in modifying cement and concrete as a sustainable supplementary cementitious material, particularly at replacement levels below 50%. Based on the literature review, while RGGP can contribute to long-term strength development and mitigate some durability concerns when properly formulated, challenges such as variations in chemical compositions, types of glass, high alkali content, reduced early-age strength, workability loss, increased shrinkage, and vulnerability to acid and sulfate attacks must be carefully managed. The performance of RGGP-modified concrete is highly dependent on the glass composition, fineness, and interaction with other mix components like cement, aggregates, and SCMs. Though low-alkali glasses offer better ASR resistance, their limited availability and high processing costs hinder widespread use. Ultimately, optimizing particle characteristics and blend proportions—especially in combination with materials like fly ash or slag—can help unlock the full potential of RGGP in low-carbon, durable concrete, paving the way for more sustainable construction practices.

(ii) This study confirms the high pozzolanic reactivity of RGGP, with its performance strongly influenced by particle size, chemical composition, and curing temperature. RGGP2, characterized by finer particles and higher amorphous content, consistently outperformed RGGP1, consuming up to 150.5 g CH/100 g RGGP at 40°C and showing a 93.6% increase in bound water between days 1 and 7. Elevated curing temperatures accelerated pozzolanic reactions, particularly in RGGP2, which maintained higher CH consumption and hydration product formation at both 23°C and 40°C. These results underscore the importance of material optimization to achieve effective high-volume cement replacement.

(iii) This study provides a comprehensive evaluation of how recycled ground glass powder (RGGP) influences cement hydration kinetics, phase evolution, and pozzolanic reactivity. Both RGGP1 and RGGP2 modified cement pastes followed the expected five-stage hydration behavior, but RGGP2 demonstrated superior performance due to its finer particle size and higher amorphous content. RGGP2 consistently exhibited higher early cumulative heat release, up to 7% greater than RGGP1, and more effective CH consumption, with up to 41% reduction in CH from 28 to 90 days at 50% replacement. TGA and DTG results confirmed that pozzolanic reactivity was more pronounced in RGGP2, especially at higher dosages. Although higher RGGP contents reduced the degree of reaction (DOR), RGGP2-30 maintained up to 86.6% greater

DOR than RGGP2-50 at 90 days. Thermodynamic modeling showed that hydration product development—particularly C-S-H formation—plateaus once CH is depleted, with natrolite and M-S-H emerging at higher reaction levels. Overall, the findings highlight the potential of finely ground RGGP for enhancing pozzolanic activity, supporting its use in higher-volume cement replacement strategies when particle characteristics and curing conditions are optimized.

(iv) The impacts of RGGP on mortar workability across different replacement levels were quantified. As RGGP1 content increased, flowability steadily dropped by 22% at 10% replacement and reached a 36.1% reduction at 50%. RGGP2 caused more decreases, with flow reductions of 41.2% and 52.2% at the same replacement levels. This greater loss in workability is attributed to RGGP2's finer particles and larger surface area, which increase water demand. To maintain adequate workability, flow values were controlled within ±5% of the control mix by adjusting the high-range water reducer dosage and up to 0.15% of superplasticizer based on the weight of cementitious binder is needed to obtain enough flowability from the fresh mortar containing 50% RGGP.

(v) The compressive strength results demonstrate the promising potential of RGGP, particularly RGGP2, as a supplementary cementitious material. Under lime water curing, RGGP1 exhibited delayed strength development, with RGGP1-30% achieving 90-day strength only 2.8% lower than the control mix and showing a 166% increase from 7 to 90 days. In contrast, RGGP2 enhanced both early and long-term strength due to its finer particle size and higher reactivity. RGGP2-5% exceeded the control by 3.8% at 7 days, while RGGP2-10% and RGGP2-30% surpassed it by 13.3% and 13.2%, respectively, at 90 days. Both types of RGGP satisfied the ASTM C618 pozzolanic strength activity index requirement by 90 days, even at high replacement levels. Steam curing at 70°C further improved early-age strength. RGGP1-50% and RGGP2-50% gained 81.4% and 55.7% more strength, respectively, compared to their lime-cured counterparts at 7 days, and it helped mitigate the long-term strength loss typically observed in steam-cured control mixes. These findings confirm that RGGP, particularly RGGP2, can effectively replace a significant portion of cement while maintaining or enhancing strength development, making it a viable candidate for sustainable high-volume cement substitution in mortar systems.

(vi) The role of Class N (MK) in modifying cement and the effects of MIC were investigated. The incorporation of dry MK resulted in a 17.8% decrease in the 90-day CH contents of the cement matrix, indicating the high pozzolanic reactivity of this calcined clay mineral. In the presence of MIC, enhancement of cement hydration played a dominant role in the early age (before 28 days), which is positively correlated to the DOS of MK. Different from dry MK, a decreasing trend of CH content was triggered by MIC after 28 days, indicating the increasingly dominant role of pozzolanic reaction over cement hydration at later ages, the benefit of the gradually released water from MIC in sustaining the reactivity of MK particles in the matrix of cement. Accelerated and enhanced cement hydration, confirmed by the higher heat release and earlier heat flow peaks, was triggered by MIC with increasing DOS of MK.

(vii) The effects of MK and MIC on the chemical, autogenous, and drying shrinkage behavior of cement and concrete were studied by focusing on its comparison with lithium nitrate, dry MK, as well as the coupled MIC and lithium, on the early-age shrinkage behavior of cement mixtures were investigated. Increases in the chemical shrinkage of cement pastes positively correlated with the DOS of MK were observed in the presence of MIC. FMIC exhibited the highest shrinkage of 0.09% at 28 days, which is 50%, 12.5%, and 28.6% higher than those of PC, LLi, and DMKEW, respectively, indicating the enhanced structural densification of cement during hydration. This is further confirmed by the linear correlation between chemical shrinkage and normalized cumulative heat, where increased chemical shrinkage with the DOS of MK was observed at the same hydration heat. Compared with dry MK, further decreases in early-age autogenous shrinkage of cement were triggered by MIC, the efficacy of which was found to decrease with the MK's degree of saturation. A synergistic effect between MIC and lithium in mitigating the self-desiccation of cement and offsetting the negative effect of lithium was obtained from FMIC-Li, which yielded the lowest autogenous shrinkage. A 17.6% increase in drying shrinkage of cement was induced by the incorporation of dry MK. A further increased drying shrinkage was observed in DMKEW. With the same total amount of water, FMIC showed a 28.0% lower drying shrinkage than DMKEW. 0.5MIC yielded a 32-day drying shrinkage of 0.167%, which is 11.0% and 31.3% lower than that of DMKEW and DMK, respectively. The superior water retention benefits of MIC and its coupling with lithium were further confirmed by the linearly positive correlations between drying shrinkage and water loss, from which decreased drying shrinkage sensitivity (lower drying shrinkage at the same water loss) was obtained.

(viii) Various cement replacement levels with RGGP were tested in a controlled lab setting, where both fresh and hardened concrete properties were evaluated at 7, 28, and 91-day intervals. To validate these findings on a larger scale, the most viable replacement mix was used to construct full-sized sidewalk slabs, with the concrete prepared by an approved MassDOT contractor. This allowed for a direct comparison between lab results and real-world performance. Additionally, a series of tests were conducted to assess the ASR reactivity of the concrete with the recommended RGGP replacement level. Higher RGGP replacement levels increase concrete workability, with slump values increasing from 7 in the control mix to 9 at 30% replacement.

- Compression strength testing at different time intervals revealed that:
    - At 7 days, strength increased up to 10% RGGP replacement but declined beyond this replacement level. All mixes with up to 20% RGGP replacement exceeded the strength of 5000 psi.
    - At 28 days, the trend remained similar to the 7-day results, with strength increasing up to 10% RGGP replacement and declining beyond this level. All mixes exceeded the compressive strength of 5000 psi. The 30% replacement mix remained above 5000 psi but showed a lower SAI than 75%, which is not acceptable.
    - At 91 days, strength continued to increase, with mixes up to 25% RGGP replacement performing on par with or better than the control.

- Splitting tensile strength testing at different time intervals revealed that:
  - At 7 days, tensile strength remained relatively consistent for mixes with up to 15% RGGP replacement but showed a decline beyond 20%.
  - At 28 days, the trend was similar to the 7-day results, with tensile strength remaining steady up to 15% RGGP replacement and declining beyond 20%.
  - At 91 days, tensile strength significantly increased across higher RGGP replacement levels, and all mixes exceeded the control tensile strength.
- Rupture strength testing at different time intervals revealed that:
  - At 7 days, rupture strength increased up to 10% RGGP replacement, then gradually declined as replacement levels extended to 30%.
  - At 28 days, all mixes, except the one with 30% RGGP replacement, showed higher rupture strength than the control.
  - At 91 days, all replacement levels from 5% to 30% performed on par with or better than the control concrete.

(ix) The early-age autogenous shrinkage results reveal that different supplementary cementitious materials (SCMs) significantly influence shrinkage behavior within the first 48 hours. Slag exhibited the highest shrinkage (~865 μm), 53.7% greater than the control, due to intensified self-desiccation. However, combining slag with metakaolin (MK) reduced shrinkage by 44% compared to slag alone, likely due to MK's effect on pore pressure and gel formation. NP-MET15 and NP-DE30 mixes reduced shrinkage by 32% and 14%, respectively, relative to the control, attributed to MK's densifying effect and DE's internal humidity regulation. In contrast, nano-silica and GGP-GS30 slightly increased shrinkage by 1% and 19%, respectively. Notably, RGGP unexpectedly increased shrinkage, potentially due to elevated chemical shrinkage from alkali-induced hydration acceleration. These findings highlight the critical role of SCM type and interactions in governing early-age autogenous shrinkage behavior.

(x) The permeability results, assessed via bulk electrical resistivity, show that all SCMs improved concrete durability to varying degrees. The control mix had low resistivity (28.8 Ω-m at 7 days, 60.22 Ω-m at 56 days), indicating high permeability. In contrast, NP-MET15 and GGP-GS30 showed significant improvements, with resistivity increases of ~193% and 442% over the control, respectively. The NP-DE30 mix achieved the highest resistivity, reaching 630 Ω-m at 56 days, which is ten times higher than the control, indicating very low chloride penetrability. Notably, while nano silica alone showed minimal improvement, its combination with slag enhanced resistivity by up to 72%. RGGP also contributed to long-term permeability reduction, with a 174% higher resistivity than slag at 56 days. These findings underscore that SCM effectiveness depends on reactivity, particle characteristics, and synergy, with diatomaceous earth and glass powder showing particularly strong long-term benefits.

(xi) The results show that all SCMs significantly reduced chloride penetration compared to the control mix, which had an average rate of 0.034 mm/V-h. The mixture with 30% cement replacement with DE achieved the greatest improvement, with a 92% reduction in chloride ingress, attributed to its ability to densify the matrix through additional C-S-H formation. Replacing cement with 20% RGGP or 15% MK also

performed well, each reducing chloride penetration by 65%, placing them in the low permeability category. These findings confirm that DE, RGGP, and MK are effective in enhancing concrete durability against chloride-induced deterioration.

(xii) The results from both the mortar bar test and the ACCT test demonstrate the effectiveness of various SCMs in mitigating ASR expansion. In the accelerated mortar bar test, the control mix showed severe expansion (>1% at 75 days), indicating high ASR susceptibility. Among the SCMs, the group replacing 30% cement with DE performed best, reducing expansion by ~81% to just 0.22%, followed by 15% MK, which outperformed 40% slag and 30% RGGP. Replacing 40% cement with slag and 30% cement with RGGP reduced expansion by 30.7% and 40.35%, respectively, though their lower early reactivity and high alkali content may have limited their effectiveness. In the ACCT test, which provides longer-term insight under milder conditions, the control again showed >1% expansion by 45 days, while the incorporation of 40% slag effectively kept expansion below the 0.04% threshold for non-reactivity. Nano-silica reached 0.19%, indicating moderate reactivity, but when combined with slag, expansion dropped to 0.09%, which is a 52% reduction, suggesting a synergistic effect. Together, these tests confirm that DE, MK, and slag-based blends are particularly effective in enhancing concrete's resistance to ASR, offering both short- and long-term mitigation benefits.

(xiii) Under enforced carbonation, substantial decreases in ASR-induced volume expansion (based on linear length change of mortar bars) from 0.57% to 0.006% were obtained. Under 10% and 20% CO_2 concentrations, decreased expansion was observed from ASR-attacked mortar specimens, even with an existing expansion of 0.2% indicating the promising role of carbonation curing in suppressing ASR. Under 3% and 10% CO_2 concentrations, the 30-day surface crack density of the ASR-attacked mortars decreased by 67.2% and 81.8%, respectively, along with substantial decreases in the maximum and average crack widths. In line with the negligible volume expansion, no detectable surface cracks can be observed in the mortar under 20% CO_2. Significant reductions in Q^3 polymerization sites, increases in C/Si and Ca/Si ratios, and decreases in alkali/Si ratios were obtained from the in-situ characterizations of ASR products in carbonated mortars, which reveal the decreased formation of ASR gels and explain the suppressed expansion and cracking behavior. The evolution of phases and chemical bonds of synthetic ASR gels under carbonation confirmed the promising efficacy of early-age enforced carbonation in suppressing ASR at a lower length scale. The ASR gels exhibited quick and complete conversions of the characteristic tobermorite and ASH phases into calcium carbonate and nahcolite in the presence of 3% and 10% CO_2. The disappearance of the -OH vibration indicates the decreased hygroscopicity of the carbonated ASR gels. The decreased dynamic vapor absorption at RH below 80%, the changes in hysteresis between isotherms, and the lower water uptake capacity of the ASR gels after carbonation evidence the reduced hygroscopicity of the ASR products, which is typically considered as one of the triggers for swelling. These results indicate that carbonation is an effective approach to mitigate ASR in addition to the incorporation of RGGP or other alternative materials.

(xiv) This research confirms MassDOT's current adoption of recycled ground-glass pozzolan and other alternative constituent materials in standard specifications is acceptable.

(xv) Implementation Recommendations
Based on the outcomes of this research project, the following recommendations are provided to support implementation:

- Promote RGGP as a sustainable material and partner with local suppliers and recycling facilities to establish reliable supply chains for high-quality, finely ground glass powders suitable for concrete production.
- Develop guidance for mix proportioning and admixture use by refining superplasticizer dosage adjustments and curing protocols to maintain workability and early-age strength in field mixes containing RGGP.
- Encourage blending RGGP with other SCMs, such as slag, fly ash, and MK, to balance workability, strength gain, shrinkage, permeability, and durability for different applications.
- Implement field trials on sidewalks, pavements, and bridge deck overlays with MassDOT contractors to confirm constructability and performance under local conditions.
- Develop performance-based acceptance criteria (e.g., compressive strength, resistivity, ASR expansion limits) for concrete containing RGGP.
- Engage with national standard-setting bodies, including ASTM and AASHTO, to align state-level specifications with evolving best practices.

7.0 References

1. Seifan, Mostafa, Samani, Ali Khajeh, and Berenjian, Aydin, *Bioconcrete: next generation of self-healing concrete.* Applied microbiology and biotechnology, 2016. **100**: p. 2591-2602.
2. Feldman, Rolf F. *Pore structure formation during hydration of fly ash and slag cement blends*. in *Proc. Symp. on Fly Ash Utilization in Cement and Concrete*. 1981.
3. Sellevold, EJ, Bager, DH, Klitgaard Jensen, E, and Knudsen, T, *Silica fume-cement pastes: hydration and pore structure.* Report BML, 1982. **82**: p. 19-50.
4. Ahsan, Mohammad Badrul and Hossain, Zahid, *Supplemental use of rice husk ash (RHA) as a cementitious material in concrete industry.* Construction and Building Materials, 2018. **178**: p. 1-9.
5. Manmohan, D and Mehta, PK, *Influence of pozzolanic, slag, and chemical admixtures on pore size distribution and permeability of hardened cement pastes.* Cement, Concrete, and Aggregates, 1981. **3**(1): p. 63-67.
6. Epa, U, *Advancing sustainable materials management: 2014 fact sheet.* United States Environmental Protection Agency, Office of Land and Emergency: Washington, DC, USA, 2015.
7. MassDOT, *COMMONWEALTH OF MASSACHUSETTS DEPARTMENT OF TRANSPORTATION STANDARD SPECIFICATIONS for Highways and Bridges 2024 Edition DIVISION III.*
8. Kaminsky, Amanda, Krstic, Marija, Rangaraju, Prasad, Tagnit-Hamou, Arezki, and Thomas, Michael DA, *Ground-glass pozzolan for use in concrete.* Concr. Int, 2020. **42**(11): p. 24-32.
9. Pattengil, M., & Shutt, T. C. *Use of ground glass as a pozzolan*. in *In Proc., Int. Symp. on Utilization of Waste Glass in Secondary Products, ASCE*. 1973. Albuquerque, New Mexico.
10. Chesner, Warren H, Collins, Robert J, MacKay, Michael H, and Emery, John, *User guidelines for waste and by-product materials in pavement construction*. 2002, Recycled Materials Resource Center.
11. Federico, LM and Chidiac, SE, *Waste glass as a supplementary cementitious material in concrete–critical review of treatment methods.* Cement and concrete composites, 2009. **31**(8): p. 606-610.
12. Meyer, Christian and Xi, Yunping, *Use of recycled glass and fly ash for precast concrete.* Journal of materials in civil engineering, 1999. **11**(2).
13. Carpenter, Andrea J and Cramer, Steven M, *Mitigation of alkali-silica reaction in pavement patch concrete that incorporates highly reactive fine aggregate.* Transportation research record, 1999. **1668**(1): p. 60-67.
14. Bažant, Zdeněk P, Zi, Goangseup, and Meyer, Christian, *Fracture mechanics of ASR in concretes with waste glass particles of different sizes.* Journal of engineering mechanics, 2000. **126**(3): p. 226-232.
15. Shao, Yixin, Lefort, Thibaut, Moras, Shylesh, and Rodriguez, Damian, *Studies on concrete containing ground waste glass.* Cement and concrete research, 2000. **30**(1): p. 91-100.

16. Shayan, Ahmad and Xu, Aimin, *Value-added utilisation of waste glass in concrete.* Cement and concrete research, 2004. **34**(1): p. 81-89.
17. Omran, Ahmed, Soliman, Nancy, Zidol, Ablam, and Tagnit-Hamou, Arezki, *Performance of ground-glass pozzolan as a cementitious material—A review.* Advances in Civil Engineering Materials, 2018. **7**(1): p. 237-270.
18. Aliabdo, Ali A, Abd Elmoaty, M, and Aboshama, Ahmed Y, *Utilization of waste glass powder in the production of cement and concrete.* Construction and Building Materials, 2016. **124**: p. 866-877.
19. Zidol, A, *Optimization of the fineness of glass powder in binary cementitious systems.* Master's Thesis, University of Sherbrooke, Sherbrooke, QC, 2009.
20. Niang, Arame, Roy, Nathalie, and Tagnit-Hamou, Arezki, *Structural behavior of concrete incorporating glass powder used in reinforced concrete columns.* Journal of Structural Engineering, 2015. **141**(3): p. B4014007.
21. Liang, Shuang, Zhou, Xiangming, Ruan, Shaoqin, Kastiukas, Gediminas, and Sun, Yuzhou, *Milled Waste Glass Powder in Magnesium-Silicate-Hydrate Cement: Technical and Environmental Assessment.* Journal of Materials in Civil Engineering, 2023. **35**(1).
22. Gebremichael, Negasi N., Jadidi, Kazem, and Karakouzian, Moses, *Waste glass recycling: The combined effect of particle size and proportion in concrete manufactured with waste recycled glass.* Construction and Building Materials, 2023. **392**.
23. Christiansen, Mary U. and Dymond, Benjamin Z., *Effect of composition on performance of ground glass pozzolan.* ACI Materials Journal, 2019. **116**(4): p. 89-98.
24. Kalakada, Z., Doh, J. H., and Zi, G., *Utilisation of coarse glass powder as pozzolanic cement—A mix design investigation.* Construction and Building Materials, 2020. **240**.
25. Kasaniya, Mahipal, Alaibani, Anfal, Thomas, Michael D. A., and Riding, Kyle A., *Exploring the efficacy of emerging reactivity tests in screening pozzolanic materials.* Construction and Building Materials, 2022. **325**.
26. Suraneni, Prannoy, Hajibabaee, Amir, Ramanathan, Sivakumar, Wang, Ying, and Weiss, Jason, *New insights from reactivity testing of supplementary cementitious materials.* Cement and Concrete Composites, 2019. **103**: p. 331-338.
27. Elaqra, Hossam A, Abou Haloub, Mohamed A, and Rustom, Rifat N, *Effect of new mixing method of glass powder as cement replacement on mechanical behavior of concrete.* Construction and Building Materials, 2019. **203**: p. 75-82.
28. Paul, Deepa, Bindhu, KR, Matos, Ana Mafalda, and Delgado, João, *Eco-friendly concrete with waste glass powder: A sustainable and circular solution.* Construction and building materials, 2022. **355**: p. 129217.
29. Ahmad, Jawad, Martinez-Garcia, Rebeca, Algarni, Salem, de-Prado-Gil, Jesús, Alqahtani, Talal, and Irshad, Kashif, *Characteristics of Sustainable Concrete with Partial Substitutions of Glass Waste as a Binder Material.* International Journal of Concrete Structures and Materials, 2022. **16**(1).
30. Patel, Dhirendra, Tiwari, RP, Shrivastava, R, and Yadav, RK, *Effective utilization of waste glass powder as the substitution of cement in making paste and mortar.* Construction and Building Materials, 2019. **199**: p. 406-415.

31. Khan, FASIH AHMED, Fahad, MUHAMMAD, Shahzada, KHAN, Alam, HARIS, and Ali, NAVEED, *Utilization of waste glass powder as a partial replacement of cement in concrete.* Magnesium, 2015. **2**(5).
32. Nassar, Roz-Ud-Din and Soroushian, Parviz, *FIELD INVESTIGATION OF CONCRETE INCORPORATING MILLED WASTE GLASS 307 FIELD INVESTIGATION OF CONCRETE INCORPORATING MILLED WASTE GLASS*.
33. Wang, Yingbin, Li, Yang, Su, Ying, He, Xingyang, and Strnadel, Bohumír, *Preparation of waste glass powder by different grinding methods and its utilization in cement-based materials.* Advanced Powder Technology, 2022. **33**(8): p. 103690.
34. Gao, X, Yu, Qingliang, Li, XS, and Yuan, Yuliang, *Assessing the modification efficiency of waste glass powder in hydraulic construction materials.* Construction and Building Materials, 2020. **263**: p. 120111.
35. Jiang, Xi, Xiao, Rui, Bai, Yun, Huang, Baoshan, and Ma, Yuetan, *Influence of waste glass powder as a supplementary cementitious material (SCM) on physical and mechanical properties of cement paste under high temperatures.* Journal of Cleaner Production, 2022. **340**: p. 130778.
36. Kalakada, Zameer, Doh, Jeung-Hwan, and Chowdhury, Sanaul, *Glass powder as replacement of cement for concrete–an investigative study.* European Journal of Environmental and Civil Engineering, 2022. **26**(3): p. 1046-1063.
37. Abdulazeez, Agboola Shamsudeen, Idi, Mamman Adamu, Kolawole, Musa Abdulhakeem, and Hamza, Bappah, *Effect of waste glass powder as a pozzolanic material in concrete production.* Int. J. Eng. Res, 2020. **9**: p. 589-594.
38. Ibrahim, KIM, *Recycled waste glass powder as a partial replacement of cement in concrete containing silica fume and fly ash.* Case Studies in Construction Materials, 2021. **15**: p. e00630.
39. Aliabdo, Ali A, Abd Elmoaty, M, Aboshama, Ahmed Y %J Construction, and Materials, Building, *Utilization of waste glass powder in the production of cement and concrete.* 2016. **124**: p. 866-877.
40. Güllü, Hamza, Canakci, Hanifi, Al Zangana, Imad Fareeq %J Construction, and Materials, Building, *Use of cement based grout with glass powder for deep mixing.* 2017. **137**: p. 12-20.
41. Lu, Jian-xin, Duan, Zhen-hua, Poon, Chi Sun %J Construction, and Materials, Building, *Fresh properties of cement pastes or mortars incorporating waste glass powder and cullet.* 2017. **131**: p. 793-799.
42. Ibrahim, Saber and Meawad, Amr %J Journal of Building Engineering, *Towards green concrete: Study the role of waste glass powder on cement/superplasticizer compatibility.* 2022. **47**: p. 103751.
43. Nahi, Samir, Leklou, Nordine, Khelidj, Abdelhafid, Oudjit, Mohamed N, and Zenati, Abdelfatah, *Properties of cement pastes and mortars containing recycled green glass powder.* Construction and Building Materials, 2020. **262**: p. 120875.
44. Yodsudjai, Wanchai and Wang, Kejin, *Chemical shrinkage behavior of pastes made with different types of cements.* Construction and Building Materials, 2013. **40**: p. 854-862.
45. Lu, Jian-Xin, Zhan, Bao-Jian, Duan, Zhen-Hua, and Poon, Chi Sun, *Using glass powder to improve the durability of architectural mortar prepared with glass aggregates.* Materials & Design, 2017. **135**: p. 102-111.

46. Wattanapornprom, Rungrawee and Stitmannaithum, Boonchai, *Comparison of properties of fresh and hardened concrete containing finely ground glass powder, fly ash, or silica fume.* Engineering Journal, 2015. **19**(3): p. 35-48.
47. Shariq, M, Prasad, J, and Abbas, H, *Creep and drying shrinkage of concrete containing GGBFS.* Cement and Concrete Composites, 2016. **68**: p. 35-45.
48. Brooks, JJ and Johari, MA Megat, *Effect of metakaolin on creep and shrinkage of concrete.* Cement and concrete composites, 2001. **23**(6): p. 495-502.
49. He, Zhi-hai, Li, Long-yuan, and Du, Shi-gui, *Creep analysis of concrete containing rice husk ash.* Cement and Concrete Composites, 2017. **80**: p. 190-199.
50. He, Zhi-hai, Zhan, Pei-min, Du, Shi-gui, Liu, Bao-ju, and Yuan, Wei-bin, *Creep behavior of concrete containing glass powder.* Composites Part B: Engineering, 2019. **166**: p. 13-20.
51. Sprince, Andina, Korjakins, Aleksandrs, and Pakrastinsh, Leonids. *Creep behaviour of concrete with glass waste microfiller*. in *ENVIRONMENT. TECHNOLOGIES. RESOURCES. Proceedings of the International Scientific and Practical Conference*. 2011.
52. Concrete, ASTM Committee C-09 on and Aggregates, Concrete, *Standard specification for coal fly ash and raw or calcined natural pozzolan for use in concrete*. 2013: ASTM international.
53. Jang, Jae Kyeong, Kalina, Ryan D, Al-Shmaisani, Saif, Ferron, Raissa D, and Juenger, Maria CG, *Assessing Pozzolanicity of supplementary cementitious materials using ASTM standard test methods.* Advances in Civil Engineering Materials, 2022. **11**(2): p. 485-499.
54. Schwarz, Nathan, Cam, Hieu, and Neithalath, Narayanan, *Influence of a fine glass powder on the durability characteristics of concrete and its comparison to fly ash.* Cement and Concrete composites, 2008. **30**(6): p. 486-496.
55. Balasubramanian, B, Krishna, GVT Gopala, Saraswathy, V, and Srinivasan, K, *Experimental investigation on concrete partially replaced with waste glass powder and waste E-plastic.* Construction and Building Materials, 2021. **278**: p. 122400.
56. Subramani, T. and Ram, S. B. Sankar, *Experimental Study on Concrete Using Cement With Glass Powder*, in *IOSR Journal of Engineering (IOSRJEN) www.iosrjen.org ISSN*. 2015. p. 3-43.
57. Islam, GM Sadiqul, Rahman, MdH, and Kazi, Nayem, *Waste glass powder as partial replacement of cement for sustainable concrete practice.* International Journal of Sustainable Built Environment, 2017. **6**(1): p. 37-44.
58. Idir, Rachida, Cyr, Martin, and Tagnit-Hamou, Arezki, *Pozzolanic properties of fine and coarse color-mixed glass cullet.* Cement and Concrete Composites, 2011. **33**(1): p. 19-29.
59. Kasaniya, Mahipal, Thomas, Michael D. A., and Moffatt, Edward G., *Efficiency of natural pozzolans, ground glasses and coal bottom ashes in mitigating sulfate attack and alkali-silica reaction.* Cement and Concrete Research, 2021. **149**.
60. Kasaniya, Mahipal, Thomas, Michael D. A., and Moffatt, Edward G., *Pozzolanic reactivity of natural pozzolans, ground glasses and coal bottom ashes and implication of their incorporation on the chloride permeability of concrete.* Cement and Concrete Research, 2021. **139**.

61. Orouji, Maedeh, Zahrai, Seyed Mehdi, and Najaf, Erfan. *Effect of glass powder & polypropylene fibers on compressive and flexural strengths, toughness and ductility of concrete: an environmental approach*. in *Structures*. 2021. Elsevier.
62. Najaf, Erfan, Orouji, Maedeh, and Zahrai, Seyed Mehdi, *Improving nonlinear behavior and tensile and compressive strengths of sustainable lightweight concrete using waste glass powder, nanosilica, and recycled polypropylene fiber.* Nonlinear Engineering, 2022. **11**(1): p. 58-70.
63. Li, Qiong, Qiao, Hongxia, Li, Aoyang, and Li, Guanjun, *Performance of waste glass powder as a pozzolanic material in blended cement mortar.* Construction and Building Materials, 2022. **324**: p. 126531.
64. Jain, Kishan Lal, Sancheti, Gaurav, and Gupta, Lalit Kumar, *Durability performance of waste granite and glass powder added concrete.* Construction and Building Materials, 2020. **252**: p. 119075.
65. Patel, Dhirendra, Shrivastava, R, Tiwari, RP, and Yadav, RK, *Properties of cement mortar in substitution with waste fine glass powder and environmental impact study.* Journal of Building Engineering, 2020. **27**: p. 100940.
66. Chand, Gaurav, Happy, Sugandh Kumar, and Ram, Shobha, *Assessment of the properties of sustainable concrete produced from quaternary blend of portland cement, glass powder, metakaolin and silica fume.* Cleaner Engineering and Technology, 2021. **4**: p. 100179.
67. Chu, SH, Li, L, Shen, PL, Lu, JX, and Poon, Chi Sun, *Recycling of waste glass powder as paste replacement in green UHPFRC.* Construction and Building Materials, 2022. **316**: p. 125719.
68. Boukhelf, Fouad, Cherif, Rachid, Trabelsi, Abdelkrim, Belarbi, Rafik, and Bouiadjra, Mohamed Bachir, *On the hygrothermal behavior of concrete containing glass powder and silica fume.* Journal of Cleaner Production, 2021. **318**: p. 128647.
69. Mohammadyan-Yasouj, Seyed Esmaeil and Ghaderi, Alireza, *Experimental investigation of waste glass powder, basalt fibre, and carbon nanotube on the mechanical properties of concrete.* Construction and Building Materials, 2020. **252**: p. 119115.
70. Ibrahim, K. I. M., *Recycled waste glass powder as a partial replacement of cement in concrete containing silica fume and fly ash.* Case Studies in Construction Materials, 2021. **15**.
71. Rahma, Afif, El Naber, Nabil, and Issa Ismail, Sherzad, *Effect of glass powder on the compression strength and the workability of concrete.* Cogent Engineering, 2017. **4**(1): p. 1373415.
72. Du, Hongjian and Tan, Kiang Hwee, *Properties of high volume glass powder concrete.* Cement and concrete composites, 2017. **75**: p. 22-29.
73. Soliman, NA and Tagnit-Hamou, A, *Development of ultra-high-performance concrete using glass powder–Towards ecofriendly concrete.* Construction and building materials, 2016. **125**: p. 600-612.
74. Anwar, Abdullah, *The influence of waste glass powder as a pozzolanic material in concrete.* Int. J. Civ. Eng. Technol, 2016. **7**(6): p. 131-148.
75. Patel, Dhirendra, Shrivastava, Ravikant, Tiwari, RP, and Yadav, RK, *The role of glass powder in concrete with respect to its engineering performances using two closely different particle sizes.* Structural Concrete, 2021. **22**: p. E228-E244.

76. Arivalagan, S and Sethuraman, VS, *Experimental study on the mechanical properties of concrete by partial replacement of glass powder as fine aggregate: An environmental friendly approach.* Materials Today: Proceedings, 2021. **45**: p. 6035-6041.
77. Wu, Jian-Dong, Guo, Li-Ping, Cao, Yuan-Zhang, and Lyu, Bang-Cheng, *Mechanical and fiber/matrix interfacial behavior of ultra-high-strength and high-ductility cementitious composites incorporating waste glass powder.* Cement and Concrete Composites, 2022. **126**: p. 104371.
78. Kim, Seong Kyum, Kang, Su Tae, Kim, Jin Kwang, and Jang, Il Young, *Effects of particle size and cement replacement of LCD glass powder in concrete.* Advances in Materials Science and Engineering, 2017. **2017**.
79. Li, AoYang, Qiao, Hongxia, Li, Qiong, Hakuzweyezu, Theogene, and Chen, Bin, *Study on the performance of pervious concrete mixed with waste glass powder.* Construction and Building Materials, 2021. **300**: p. 123997.
80. Asokan, Pappu, Osmani, Mohamed, and Price, Andrew DF, *Improvement of the mechanical properties of glass fibre reinforced plastic waste powder filled concrete.* Construction and Building Materials, 2010. **24**(4): p. 448-460.
81. Baikerikar, Abhijeet, Mudalgi, Shadab, and Ram, V Vinayaka, *Utilization of waste glass powder and waste glass sand in the production of Eco-Friendly concrete.* Construction and Building Materials, 2023. **377**: p. 131078.
82. Ramdani, Samiha, Guettala, Abdelhamid, Benmalek, ML, and Aguiar, José B, *Physical and mechanical performance of concrete made with waste rubber aggregate, glass powder and silica sand powder.* Journal of Building Engineering, 2019. **21**: p. 302-311.
83. Elaqra, Hossam and Rustom, Rifat, *Effect of using glass powder as cement replacement on rheological and mechanical properties of cement paste.* Construction and Building Materials, 2018. **179**: p. 326-335.
84. Raju, Akhil S, Anand, KB, and Rakesh, P, *Partial replacement of Ordinary Portland cement by LCD glass powder in concrete.* Materials Today: Proceedings, 2021. **46**: p. 5131-5137.
85. Asgarian, Atena, Roshan, Naeim, and Ghalehnovi, Mansour, *The Strength, Microstructure, and ecological assessment of concrete mix incorporating waste glass powder and polypropylene fiber.* Construction and Building Materials, 2023. **371**: p. 130726.
86. Omer, Brwa and Saeed, Jalal, *Characterizations and modeling the influence of Particle Size Distributions (PSD) of glass powder on the mechanical behavior of normal strength concrete.* Civil Engineering and Architecture, 2020. **8**(5): p. 993-1005.
87. Yuan, Xiaosa, Dai, Mingjiang, Gao, Yingjie, Zhou, Yanbo, and Liu, Fang, *Effect on mechanical properties and microstructure of high-strength eco-friendly concrete with waste glass powder-eggshell particles.* Journal of Building Engineering, 2023. **79**: p. 107871.
88. Sekhar, Malla Chandra, Kumar, Mavoori Hitesh, Raju, Surla Lova, and Saikrishnamacharyulu, Ippilli, *Influence of Metakaolin and glass powder on mechanical behaviour of concrete.* Materials Today: Proceedings, 2023.

89. Selvakumar, M, Geetha, S, Rangan, Sneha Kasturi, Sithrubi, T, and Sathyashriya, K, *Effect of glass powder as partial fine aggregate replacement on properties of basalt fibre reinforced concrete.* Materials Today: Proceedings, 2021. **43**: p. 1460-1464.
90. Kamali, Mahsa and Ghahremaninezhad, Ali, *Effect of glass powders on the mechanical and durability properties of cementitious materials.* Construction and building materials, 2015. **98**: p. 407-416.
91. Parghi, Anant and Alam, M Shahria, *Physical and mechanical properties of cementitious composites containing recycled glass powder (RGP) and styrene butadiene rubber (SBR).* Construction and Building Materials, 2016. **104**: p. 34-43.
92. Jiang, Yi, Ling, Tung-Chai, Mo, Kim Hung, and Shi, Caijun, *A critical review of waste glass powder–Multiple roles of utilization in cement-based materials and construction products.* Journal of environmental management, 2019. **242**: p. 440-449.
93. Amin, Muhammad Nasir, Alkadhim, Hassan Ali, Ahmad, Waqas, Khan, Kaffayatullah, Alabduljabbar, Hisham, and Mohamed, Abdullah, *Experimental and machine learning approaches to investigate the effect of waste glass powder on the flexural strength of cement mortar.* PloS one, 2023. **18**(1): p. e0280761.
94. Lu, Jian-xin, Duan, Zhen-hua, and Poon, Chi Sun, *Combined use of waste glass powder and cullet in architectural mortar.* Cement and Concrete Composites, 2017. **82**: p. 34-44.
95. Shoaei, Parham, Ameri, Farshad, Musaeei, Hamid Reza, Ghasemi, Tara, and Cheah, Chee Ban, *Glass powder as a partial precursor in Portland cement and alkali-activated slag mortar: A comprehensive comparative study.* Construction and Building Materials, 2020. **251**: p. 118991.
96. Du, Hongjian and Tan, Kiang Hwee, *Transport Properties of Concrete with Glass Powder as Supplementary Cementitious Material.* ACI Materials Journal, 2015. **112**(3): p. 429-437.
97. Carsana, Maddalena, Frassoni, Massimiliano, and Bertolini, Luca, *Comparison of ground waste glass with other supplementary cementitious materials.* Cement and Concrete Composites, 2014. **45**: p. 39-45.
98. Tagnit-Hamou, Arezki and Bengougam, Abdelkrim, *The Use of Glass Powder as Supplementary Cementitious Material.* Concrete International, 2012: p. 56-61.
99. Jain, Jitendra A and Neithalath, Narayanan, *Chloride transport in fly ash and glass powder modified concretes–influence of test methods on microstructure.* Cement and Concrete Composites, 2010. **32**(2): p. 148-156.
100. Omran, Ahmed and Tagnit-Hamou, Arezki, *Performance of glass-powder concrete in field applications.* Construction and Building Materials, 2016. **109**: p. 84-95.
101. Zidol, Ablam, Tognonvi, Monique Tohoue, and Tagnit-Hamou, Arezki, *Effect of glass powder on concrete sustainability.* New Journal of Glass and Ceramics, 2017. **7**(02): p. 34.
102. Wang, Zhi, Shi, Caijun, and Song, Jianming, *Effect of glass powder on chloride ion transport and alkali-aggregate reaction expansion of lightweight aggregate concrete.* Journal of Wuhan University of Technology-Mater. Sci. Ed., 2009. **24**: p. 312-317.
103. Bisht, Kunal, Kabeer, KI Syed Ahmed, and Ramana, PV, *Gainful utilization of waste glass for production of sulphuric acid resistance concrete.* Construction and Building Materials, 2020. **235**: p. 117486.

104. Daczko, JA, Johnson, DA, and Amey, SL, *Decreasing concrete sewer pipe degradation using admixtures.* Materials performance, 1997. **36**(1): p. 51-56.
105. Hendi, Ali, Behravan, Amir, Mostofinejad, Davood, Sedaghatdoost, Arash, and Amini, Morteza, *A step towards green concrete: Effect of waste silica powder usage under HCl attack.* Journal of Cleaner Production, 2018. **188**: p. 278-289.
106. Bassuoni, MT and Nehdi, ML, *Durability of self-consolidating concrete to sulfate attack under combined cyclic environments and flexural loading.* Cement and Concrete Research, 2009. **39**(3): p. 206-226.
107. Monteny, J, De Belie, Nele, Vincke, E, Verstraete, Willy, and Taerwe, Luc, *Chemical and microbiological tests to simulate sulfuric acid corrosion of polymer-modified concrete.* Cement and Concrete Research, 2001. **31**(9): p. 1359-1365.
108. Rendell, Frank and Jauberthie, Raoul, *The deterioration of mortar in sulphate environments.* Construction and building materials, 1999. **13**(6): p. 321-327.
109. Bassuoni, MT and Nehdi, ML, *Resistance of self-consolidating concrete to sulfuric acid attack with consecutive pH reduction.* Cement and Concrete Research, 2007. **37**(7): p. 1070-1084.
110. Concretes, P, *Standard test methods for chemical resistance of mortars, grouts, and monolithic.* Current, 1998. **4**(February): p. 1-6.
111. Ling, Tung-Chai and Poon, Chi-Sun, *Properties of architectural mortar prepared with recycled glass with different particle sizes.* Materials & Design, 2011. **32**(5): p. 2675-2684.
112. Mansour, Mohammed A, Ismail, Mohd Hanif Bin, Imran Latif, Qadir Bux alias, Alshalif, Abdullah Faisal, Milad, Abdalrhman, and Bargi, Walid Abdullah Al, *A systematic review of the concrete durability incorporating recycled glass.* Sustainability, 2023. **15**(4): p. 3568.
113. Ahmad, Jawad, Aslam, Fahid, Martinez-Garcia, Rebeca, de-Prado-Gil, Jesús, Qaidi, Shaker, and Brahmia, Ameni, *Effects of waste glass and waste marble on mechanical and durability performance of concrete.* Scientific reports, 2021. **11**(1).
114. Liu, Tiejun, Qin, Shanshan, Zou, Dujian, and Song, Wen, *Experimental investigation on the durability performances of concrete using cathode ray tube glass as fine aggregate under chloride ion penetration or sulfate attack.* Construction and Building Materials, 2018. **163**: p. 634-642.
115. Rahman, MM and Bassuoni, MT, *Thaumasite sulfate attack on concrete: Mechanisms, influential factors and mitigation.* Construction and Building Materials, 2014. **73**: p. 652-662.
116. Rashidian-Dezfouli, Hassan and Rao Rangaraju, Prasada, *Evaluation of selected durability properties of portland cement concretes containing ground glass fiber as a pozzolan.* Transportation Research Record, 2018. **2672**(27): p. 88-98.
117. Durgun, Muhammed Yasin and Sevinç, Ahmet Hayrullah, *Determination of the effectiveness of various mineral additives against sodium and magnesium sulfate attack in concrete by Taguchi method.* Journal of Building Engineering, 2022. **57**: p. 104849.
118. Esselami, Redha, Wilson, William, and Tagnit-Hamou, Arezki, *An accelerated physical sulfate attack test using an induction period and heat drying: First applications to concrete with different binders including ground glass pozzolan and limestone filler.* Construction and Building Materials, 2022. **345**.

119. Meyer, C, Egosi, N, and Andela, C, *Concrete with waste glass as aggregate*, in *Recycling and reuse of glass cullet*. 2001, Thomas Telford Publishing. p. 179-188.
120. Park, Seung Bum, Lee, Bong Chun, and Kim, Jeong Hwan, *Studies on mechanical properties of concrete containing waste glass aggregate.* Cement and concrete research, 2004. **34**(12): p. 2181-2189.
121. Ahmad, Jawad, Martinez-Garcia, Rebeca, Algarni, Salem, de-Prado-Gil, Jesús, Alqahtani, Talal, and Irshad, Kashif, *Characteristics of sustainable concrete with partial substitutions of glass waste as a binder material.* International Journal of Concrete Structures and Materials, 2022. **16**(1): p. 21.
122. Swamy, R Narayan, *The alkali-silica reaction in concrete*. 1991: CRC Press.
123. Jin, Weihua, Meyer, Christian, and Baxter, Stephen, *" Glascrete"-concrete with glass aggregate.* ACI Materials Journal, 2000. **97**(2): p. 208-213.
124. Polley, Craig, Cramer, Steven M, and Cruz, Rodolfo V de la, *Potential for using waste glass in Portland cement concrete.* Journal of materials in Civil Engineering, 1998. **10**(4): p. 210-219.
125. Ke, Guojun, Li, Wengui, Li, Ruyi, Li, Yuelin, and Wang, George, *Mitigation effect of waste glass powders on alkali–silica reaction (ASR) expansion in cementitious composite.* International Journal of Concrete Structures and Materials, 2018. **12**(1): p. 1-14.
126. Rajabipour, Farshad, Maraghechi, Hamed, and Fischer, Gregor, *Investigating the alkali-silica reaction of recycled glass aggregates in concrete materials.* Journal of Materials in Civil Engineering, 2010. **22**(12): p. 1201-1208.
127. Corinaldesi, V, Gnappi, G, Moriconi, G, and Montenero, AJWM, *Reuse of ground waste glass as aggregate for mortars.* waste management, 2005. **25**(2): p. 197-201.
128. Fanijo, Ebenezer O, Kassem, Emad, and Ibrahim, Ahmed, *ASR mitigation using binary and ternary blends with waste glass powder.* Construction and Building Materials, 2021. **280**: p. 122425.
129. Afshinnia, Kaveh and Rangaraju, Prasada Rao, *Influence of fineness of ground recycled glass on mitigation of alkali–silica reaction in mortars.* Construction and Building Materials, 2015. **81**: p. 257-267.
130. Gökşen, Yusuf, Durak, Uğur, İlkentapar, Serhan, Atabey, İsmail İsa, Kaya, Mehmet, Karahan, Okan, and Duran Atiş, Cengiz, *Synergistic effect of waste glass powder and fly ash on some properties of mortar and notably suppressing alkali-silica reaction.* Revista de la construcción, 2023. **22**(2): p. 419-430.
131. Guo, Shuaicheng, Dai, Qingli, Sun, Xiao, Xiao, Xianghui, Si, Ruizhe, and Wang, Jiaqing, *Reduced alkali-silica reaction damage in recycled glass mortar samples with supplementary cementitious materials.* Journal of Cleaner Production, 2018. **172**: p. 3621-3633.
132. Tamanna, Nafisa, Tuladhar, Rabin, and Sivakugan, Nagaratnam, *Performance of recycled waste glass sand as partial replacement of sand in concrete.* Construction and Building Materials, 2020. **239**: p. 117804.
133. Jaroszyńska-Wolińska, J., *Chemistry of Construction Materials*. 2016, Lublin: Polish Academy of Sciences, Lublin Branch,.
134. Dhir, Ravindra K, Dyer, TD, and Tang, MC, *Alkali-silica reaction in concrete containing glass.* Materials and Structures, 2009. **42**: p. 1451-1462.

135. Thomas, Michael, *The effect of supplementary cementing materials on alkali-silica reaction: A review.* Cement and concrete research, 2011. **41**(12): p. 1224-1231.
136. Rashidian-Dezfouli, Hassan, Afshinnia, Kaveh, and Rangaraju, Prasada Rao, *Efficiency of Ground Glass Fiber as a cementitious material, in mitigation of alkali-silica reaction of glass aggregates in mortars and concrete.* Journal of Building Engineering, 2018. **15**: p. 171-180.
137. Mejdi, M., Wilson, William, Saillio, Mickael, Chaussadent, Thierry, Divet, Loic, and Tagnit-Hamou, Arezki, *Investigating the pozzolanic reaction of post-consumption glass powder and the role of portlandite in the formation of sodium-rich C-S-H.* Cement and Concrete Research, 2019. **123**.
138. Kasaniya, Mahipal and Thomas, Michael D. A., *Role of the alkalis of supplementary cementing materials in controlling pore solution chemistry and alkali-silica reaction.* Cement and Concrete Research, 2022. **162**.
139. Yin, Weisong, Li, Xinping, Sun, Tao, Chen, Youzhi, Xu, Fang, Yan, Ge, Xu, Mingnan, Tian, Kun %J Construction, and Materials, Building, *Utilization of waste glass powder as partial replacement of cement for the cementitious grouts with superplasticizer and viscosity modifying agent binary mixtures: Rheological and mechanical performances.* 2021. **286**: p. 122953.
140. International, ASTM C940-16 %J ASTM, *Standard test method for expansion and bleeding of freshly mixed grouts for preplaced-aggregate concrete in the laboratory.* 2016.
141. Mohammadi, Mohammad Mahdi, Azadgoleh, Mehrdad Asadi, Ghodrati, Ali, Zalnezhad, Mahdi, Ayar, Pooyan, Fini, Elham %J Construction, and Materials, Building, *Introducing waste glass powder as a sustainable constituent in microsurfacing.* 2023. **395**: p. 132271.
142. Taha, Bashar, Nounu, Ghassan %J Construction, and Materials, Building, *Properties of concrete contains mixed colour waste recycled glass as sand and cement replacement.* 2008. **22**(5): p. 713-720.
143. Lu, Jian-xin, Zheng, Haibing, Yang, Shuqing, He, Pingping, Poon, Chi Sun %J Construction, and Materials, Building, *Co-utilization of waste glass cullet and glass powder in precast concrete products.* 2019. **223**: p. 210-220.
144. ASTM, ASTM, *C150/C150M-17, standard specification for Portland cement.* Am. Soc. Test. Mater. West Conshohocken, PA, USA, 2017.
145. ASTM, ASTM, *C1866/C1866M-20, Standard Specification for Ground-Glass Pozzolan for Use in Concrete.* Am. Soc. Test. Mater. West Conshohocken, PA, USA, 2020.
146. ASTM, ASTM, *C1897/C1897M-20, Measuring the Reactivity of Supplementary Cementitious Materials by Isothermal Calorimetry and Bound Water Measurements.* Am. Soc. Test. Mater. West Conshohocken, PA, USA, 2020.
147. ASTM, ASTM, *C109/C109M-20, Standard Test Method for Compressive Strength of Hydraulic Cement Mortars (Using 2-in. or [50-mm] Cube Specimens).* Am. Soc. Test. Mater. West Conshohocken, PA, USA, 2020.
148. ASTMC1260, *Standard Test Method for Potential Alkali Reactivity of Aggregates (Mortar-Bar Method)*. 2021.

149. Hou, Xiaoqiang, Kirkpatrick, R James, Struble, Leslie J, and Monteiro, Paulo JM, *Structural investigations of alkali silicate gels.* Journal of the American Ceramic Society, 2005. **88**(4): p. 943-949.
150. Kim, Taehwan and Olek, Jan, *Effects of sample preparation and interpretation of thermogravimetric curves on calcium hydroxide in hydrated pastes and mortars.* Transportation research record, 2012. **2290**(1): p. 10-18.
151. Luo, Dayou and Wei, Jianqiang, *Hydration kinetics and phase evolution of Portland cement composites containing sodium-montmorillonite functionalized with a Non-Ionic surfactant.* Construction and Building Materials, 2022. **333**: p. 127386.
152. Luo, Dayou and Wei, Jianqiang, *Hydration and phase evolution of blended cement composites containing lithium and saturated metakaolin.* Cement and Concrete Composites, 2023. **144**: p. 105268.
153. Wang, Xiao-Yong and Lee, Han-Seung, *Modeling the hydration of concrete incorporating fly ash or slag.* Cement and concrete Research, 2010. **40**(7): p. 984-996.
154. Young, J Francis and Hansen, Will, *Volume relationships for CSH formation based on hydration stoichiometries.* MRS Online Proceedings Library, 1986. **85**: p. 313-322.
155. Kulik, Dmitrii A, Wagner, Thomas, Dmytrieva, Svitlana V, Kosakowski, Georg, Hingerl, Ferdinand F, Chudnenko, Konstantin V, and Berner, Urs R, *GEM-Selektor geochemical modeling package: revised algorithm and GEMS3K numerical kernel for coupled simulation codes.* Computational Geosciences, 2013. **17**(1): p. 1-24.
156. Wagner, Thomas, Kulik, Dmitrii A, Hingerl, Ferdinand F, and Dmytrieva, Svitlana V, *GEM-Selektor geochemical modeling package: TSolMod library and data interface for multicomponent phase models.* The Canadian Mineralogist, 2012. **50**(5): p. 1173-1195.
157. Thoenen, Tres, Hummel, Wolfgang, Berner, Urs, and Curti, Enzo, *The PSI/Nagra Chemical Thermodynamic Database 12/07.* 2014.
158. Lothenbach, Barbara, Kulik, Dmitrii A, Matschei, Thomas, Balonis, Magdalena, Baquerizo, Luis, Dilnesa, Belay, Miron, George D, and Myers, Rupert J, *Cemdata18: A chemical thermodynamic database for hydrated Portland cements and alkali-activated materials.* Cement and Concrete Research, 2019. **115**: p. 472-506.
159. Astm, C, *1437.* Standard Test Method for Flow of Hydraulic Cement Mortar, 2001.
160. ASTM, ASTM, *C109/C109M: Standard Test Method for Compressive Strength of Hydraulic Cement Mortars (Using 2-in. or [50-mm] Cube Specimens).* Annual book of ASTM Standards, 2016. **4**.
161. Mishra, RK, Tripathi, RK, and Dubey, Vikas, *Early age shrinkage pattern of concrete on replacement of fine aggregate with industrial by-product.* Journal of radiation research and applied sciences, 2016. **9**(4): p. 386-391.
162. ASTMC1608, *Standard Test Method for Chemical Shrinkage of Hydraulic Cement Paste*. 2017.
163. ASTMC596, *Standard Test Method for Drying Shrinkage of Mortar Containing Hydraulic Cement*. 2018.
164. ASTM, C, *Standard test method for bulk electrical resistivity or bulk conductivity of concrete.* ASTM International, 2019.

165. Liu, Kai-Wei and Mukhopadhyay, Anol K., *Accelerated Concrete-Cylinder Test for Alkali–Silica Reaction.* Journal of Testing and Evaluation, 2016. **44**(3): p. 1229-1238.
166. AASHTO, TP, *64-03. Standard method of test for prediction of chloride penetration in hydraulic cement concrete by the rapid migration procedure.* Washington: American Association of State Highway and Transportation Officials, 2003.
167. Luo, Yan, Li, SH, Klima, KM, Brouwers, HJH, and Yu, Qingliang, *Degradation mechanism of hybrid fly ash/slag based geopolymers exposed to elevated temperatures.* Cement and Concrete Research, 2022. **151**: p. 106649.
168. Luo, Dayou, Sinha, Arkabrata, Adhikari, Madhab, and Wei, Jianqiang, *Mitigating alkali-silica reaction through metakaolin-based internal conditioning: New insights into property evolution and mitigation mechanism.* Cement and Concrete Research, 2022. **159**: p. 106888.
169. Kawamura, Masashi and Kasai, Yoshio, *Methods to determine the saturated surface-dry condition of soils*, in *Geotechnics of High Water Content Materials*. 2000, ASTM International.
170. Luo, Dayou and Wei, Jianqiang, *Upgrading sodium montmorillonite into a reactive internal curing agent for sustainable cement composites through non-ionic functionalization.* Composites Part B: Engineering, 2022. **242**: p. 110076.
171. Noumowe, Albert, *Effet de hautes températures (20-600 C) sur le béton: cas particulier du béton a hautes performances*. 1995, Lyon, INSA.
172. Shekhawat, Bhupendra Singh and Aggarwal, Dr Vanita, *Utilisation of waste glass powder in concrete–A Literature Review.* International Journal of Innovative Research in Science, Engineering and Technology, 2014. **3**(7).
173. Lu, Jian-xin, Duan, Zhen-hua, and Poon, Chi Sun, *Fresh properties of cement pastes or mortars incorporating waste glass powder and cullet.* Construction and Building Materials, 2017. **131**: p. 793-799.
174. ASTM, ASTM, *C618/C618-22, Standard Specification for Coal Fly Ash and Raw or Calcined Natural Pozzolan for Use in Concrete.* Am. Soc. Test. Mater. West Conshohocken, PA, USA, 2022.
175. Tran, Van Mien and Nguyen, Thi Hai Yen, *Enhancing the effectiveness of steam curing for cement paste incorporating fly ash based on long-term compressive strength and reaction degree of fly ash.* Case Studies in Construction Materials, 2022. **16**: p. e01146.
176. Zeyad, Abdullah M, Tayeh, Bassam A, Adesina, Adeyemi, de Azevedo, Afonso RG, Amin, Mohamed, Hadzima-Nyarko, Marijana, and Agwa, Ibrahim Saad, *Review on effect of steam curing on behavior of concrete.* Cleaner Materials, 2022. **3**: p. 100042.
177. ASTMC150/C150M, *Standard Specification for Portland Cement*. 2022, ASTM International: West Conshohocken, PA.
178. ASTMD281-12, *Standard Test Method for Oil Absorption of Pigments by Spatula Rub-out*. 2021.
179. ASTMC1761, *Standard Specification for Lightweight Aggregate for Internal Curing of Concrete*, in *Annual Book of ASTM Standards*. 2023.
180. Luo, Dayou and Wei, Jianqiang, *Hydration and phase evolution of blended cement composites containing lithium and saturated metakaolin.* Cement and Concrete Composites, 2023: p. 105268.

181. Reinosa, JJ, García-Baños, Beatriz, Catalá-Civera, José Manuel, and Fernández, JF, *A step ahead on efficient microwave heating for kaolinite.* Applied Clay Science, 2019. **168**: p. 237-243.
182. Frost, Ray L, Horváth, Erzsébet, Makó, Éva, Kristóf, János, and Rédey, Ákos, *Slow transformation of mechanically dehydroxylated kaolinite to kaolinite—an aged mechanochemically activated formamide-intercalated kaolinite study.* Thermochimica Acta, 2003. **408**(1-2): p. 103-113.
183. Rocha, João, Adams, John M, and Klinowski, Jacek, *The rehydration of metakaolinite to kaolinite: evidence from solid-state NMR and cognate techniques.* Journal of Solid State Chemistry, 1990. **89**(2): p. 260-274.
184. Yusiharni, Emielda and Gilkes, Robert, *Rehydration of heated gibbsite, kaolinite and goethite: An assessment of properties and environmental significance.* Applied clay science, 2012. **64**: p. 61-74.
185. Tatang, Hervé Barye, Mbey, Jean Aimé, Sabouang, Cyrill Joël Ngally, Mache, Jacques Richard, Gley, Renaud, and Kong, Sakeo, *Kaolinites structural defects related to urea and dimethyl sulfoxide intercalation.* Applied Clay Science, 2024. **255**: p. 107415.
186. Santos, Andreia, Andrejkovičová, Slavka, Perná, Ivana, Almeida, Fernando, and Rocha, Fernando, *Mechanical and thermal properties of geopolymers derived from metakaolin with iron mine waste.* Applied Clay Science, 2024. **258**: p. 107452.
187. Nwosu, Friday Onyekwere, Ajala, Oluwaseun Jacob, Owoyemi, Rukayat Motunrayo, and Raheem, Bukola Ganiyat, *Preparation and characterization of adsorbents derived from bentonite and kaolin clays.* Applied Water Science, 2018. **8**: p. 1-10.
188. Dewi, R, Agusnar, H, Alfian, Z, and Tamrin. *Characterization of technical kaolin using XRF, SEM, XRD, FTIR and its potentials as industrial raw materials*. in *Journal of Physics: Conference Series*. 2018. IOP Publishing.
189. Han, Weiwei, Sun, Tao, Li, Xinping, Shui, Zhonghe, Chen, Youzhi, and Sun, Mian, *Influence of Lithium Carbonate on C3A Hydration.* Advances in Materials Science Engineering, 2018. **2018**: p. 1-8.
190. Coumes, Céline Cau Dit, Dhoury, Mélanie, Champenois, Jean-Baptiste, Mercier, Cyrille, and Damidot, Denis *Physico-chemical mechanisms involved in the acceleration of the hydration of calcium sulfoaluminate cement by lithium ions.* Cement and Concrete Research, 2017. **96**: p. 42-51.
191. Lee, Yongju and Jung, Duk-Young, *Lithium intercalation and deintercalation of thermally decomposed LiAl2-layered double hydroxides.* Applied Clay Science, 2022. **228**: p. 106631.
192. He, Hang, Wang, Yuli, He, Fengxia, Luo, Shuqiong, and Liu, Songhui, *Effect of Li 2 CO 3 on the properties of Portland cement paste.* Materials and Structures, 2021. **54**: p. 1-10.
193. Viallis-Terrisse, Hélène, Nonat, André, and Petit, Jean-Claude, *Zeta-potential study of calcium silicate hydrates interacting with alkaline cations.* Journal of Colloid Interface Science, 2001. **244**(1): p. 58-65.
194. Markandeya, A, Mapa, DG, Fincan, M, Shanahan, N, Stetsko, YP, Riding, KA, and Zayed, A, *Chemical Shrinkage and Cracking Resilience of Metakaolin Concrete.* ACI Materials Journal, 2019. **116**(4).

195. Fu, Tengfei, *Autogenous deformation and chemical shrinkage of high performance cementitious systems.* 2011.
196. Mounanga, Pierre, Khelidj, Abdelhafid, Loukili, Ahmed, and Baroghel-Bouny, Véronique, *Predicting Ca(OH)2 content and chemical shrinkage of hydrating cement pastes using analytical approach.* Cement and Concrete Research, 2004. **34**(2): p. 255-265.
197. Hu, Xiang, Shi, Caijun, Shi, Zhenguo, Tong, Baihui, and Wang, Dehui, *Early age shrinkage and heat of hydration of cement-fly ash-slag ternary blends.* Construction and Building Materials, 2017. **153**: p. 857-865.
198. Saje, Drago, *Reduction of the early autogenous shrinkage of high strength concrete.* Advances in Materials Science and Engineering, 2015. **2015**.
199. Kumar, Aditya, Bishnoi, Shashank, and Scrivener, Karen L, *Modelling early age hydration kinetics of alite.* Cement and Concrete Research, 2012. **42**(7): p. 903-918.
200. Sant, Gaurav, Lothenbach, Barbara, Juilland, Patrick, Le Saout, Gwenn, Weiss, Jason, and Scrivener, Karen, *The origin of early age expansions induced in cementitious materials containing shrinkage reducing admixtures.* Cement and concrete research, 2011. **41**(3): p. 218-229.
201. Neto, Antonio A Melo, Cincotto, Maria Alba, and Repette, Wellington, *Drying and autogenous shrinkage of pastes and mortars with activated slag cement.* Cement and Concrete Research, 2008. **38**(4): p. 565-574.
202. Millard, MJ and Kurtis, KE, *Effects of lithium nitrate admixture on early-age cement hydration.* Cement and Concrete Research, 2008. **38**(4): p. 500-510.
203. Akcay, Burcu and Tasdemir, Mehmet Ali, *Autogenous Shrinkage, Pozzolanic Activity and Mechanical Properties of Metakaolin Blended Cementitious Materials.* KSCE Journal of Civil Engineering, 2019. **23**(11): p. 4727-4734.
204. Geiker, Metter Rica, Bentz, Dale P, and Jensen, Ole Mejlhede, *Mitigating autogenous shrinkage by internal curing.* ACI Special Publications, 2004: p. 143-154.
205. Shen, Dejian, Wang, Xudong, Cheng, Dabao, Zhang, Jinyang, and Jiang, Guoqing, *Effect of internal curing with super absorbent polymers on autogenous shrinkage of concrete at early age.* Construction and Building Materials, 2016. **106**: p. 512-522.
206. Henkensiefken, Ryan, Bentz, Dale, Nantung, Tommy, and Weiss, Jason, *Volume change and cracking in internally cured mixtures made with saturated lightweight aggregate under sealed and unsealed conditions.* Cement and Concrete Composites, 2009. **31**(7): p. 427-437.
207. Shen, Yan, Zhang, Wei, Wang, Peifang, Chen, Xi, and Zhu, Hangyu, *Influence of lithium salt on the performance of calcium sulfoaluminate cement.* Journal of Thermal Analysis and Calorimetry, 2022: p. 1-9.
208. Araiza, Daniel G, Plascencia-Hernández, Fernando, and Pfeiffer, Heriberto, *Enhanced CO2 capture over Li-containing β-NaFeO2 materials: effect of lithium nitrate addition.* Fuel, 2022. **324**: p. 124605.
209. Sinha, Arkabrata and Wei, Jianqiang, *Phase evolution and mechanical-hydroscopic properties of alkali-silica reaction gels modified by magnesium nitrate.* Cement and Concrete Composites, 2023. **144**: p. 105283.
210. Qin, Changpei, Zhao, Junxian, Wang, Yixuan, Zou, Yongqi, Al Sairafia, Fares Ali, and Jiang, Chaohua, *A Comparative Study of Metakaolin and Silica Fume on the*

Properties and Microstructure of Ultrafine Dredged Sand Mortars. Advances in Materials Science and Engineering, 2023. **2023**.
211. Fu, Dabao, Xia, Chang, Xu, Song, Zhang, Chao, and Jia, Xiaojuan, *Effect of concrete composition on drying shrinkage behavior of ultra-high performance concrete.* Journal of Building Engineering, 2022. **62**: p. 105333.
212. Lai, Junying, Zhang, Lifeng, Qian, Xiaoqian, Shen, Chong, and Zhang, Jinjian, *Influence of superplasticizers on early age drying shrinkage of cement paste with the same consistency.* Journal of Wuhan University of Technology-Mater. Sci. Ed., 2014. **29**: p. 1201-1207.
213. Wianglor, Kornnika, Sinthupinyo, Sakprayut, Piyaworapaiboon, Manow, and Chaipanich, Arnon, *Effect of alkali-activated metakaolin cement on compressive strength of mortars.* Applied Clay Science, 2017. **141**: p. 272-279.
214. Poon, Chi Sun, Kou, SC, and Lam, L, *Pore size distribution of high performance metakaolin concrete.* Journal of Wuhan University of Technology-Mater. Sci. Ed., 2002. **17**(1): p. 42-46.
215. Zhang, Wenyan, Zakaria, Mohamed, and Hama, Yukio, *Influence of aggregate materials characteristics on the drying shrinkage properties of mortar and concrete.* Construction and building materials, 2013. **49**: p. 500-510.
216. Ferraris, CF and Wittmann, Folker H, *Shrinkage mechanisms of hardened cement paste.* Cement and Concrete Research, 1987. **17**(3): p. 453-464.
217. Saje, Drago, *Reduction of the early autogenous shrinkage of high strength concrete.* Advances in Materials Science and Engineering, 2015. **2015**(1): p. 310641.
218. Luo, Dayou and Wei, Jianqiang, *Early-age shrinkage behavior of cement mixtures regulated with metakaolin-based internal conditioning.* Applied Clay Science, 2024. **261**: p. 107583.
219. Cartwright, Christopher, Rajabipour, Farshad, and Radlińska, Aleksandra, *Shrinkage characteristics of alkali-activated slag cements.* Journal of materials in civil engineering, 2015. **27**(7): p. B4014007.
220. Zhang, Yingda, Liu, Xinyue, Xu, Ziyi, Yuan, Weiguang, Xu, Yong, Yao, Zuobang, Liu, Zihao, and Si, Ruizhe, *Early-Age Cracking of Fly Ash and GGBFS Concrete Due to Shrinkage, Creep, and Thermal Effects: A Review.* Materials, 2024. **17**(10): p. 2288.
221. Li, Zhenming, Chen, Yun, Provis, John L, Cizer, Özlem, and Ye, Guang, *Autogenous shrinkage of alkali-activated slag: A critical review.* Cement and Concrete Research, 2023. **172**: p. 107244.
222. Li, Zhenming, Nedeljković, Marija, Chen, Boyu, and Ye, Guang, *Mitigating the autogenous shrinkage of alkali-activated slag by metakaolin.* Cement and Concrete Research, 2019. **122**: p. 30-41.
223. Akcay, Burcu and Tasdemir, Mehmet Ali, *Autogenous shrinkage, pozzolanic activity and mechanical properties of metakaolin blended cementitious materials.* KSCE Journal of Civil Engineering, 2019. **23**: p. 4727-4734.
224. Li, Shuangxi, Liu, Shunyi, and Jiang, Chunmeng, *Analysis of the Influence and Mechanism of Diatomaceous Earth Internal Curing on the Autogenous Shrinkage and Early Crack Resistance of Cement-Based Materials with Low Water–Binder Ratio.* Applied Sciences, 2024. **14**(13): p. 5397.

225. Niu, Yanfei, Cheng, Congmi, Luo, Chuanglian, Yang, Pengfei, Guo, Wei, and Liu, Qi, *Study on rheological property, volumetric deformation, mechanical strength and microstructure of mortar incorporated with waste glass powder (WGP).* Construction and Building Materials, 2023. **408**: p. 133420.
226. Scrivener, KL, John, VM, and Gartner, EM, *Eco-efficient cements: Potential economically viable solutions for a low-CO2 cement-based materials industry.* Cem. Concr. Res., 2018. **114**(Dec): p. 2-26.
227. Ghoddousi, P and Saadabadi, L Adelzade, *Study on hydration products by electrical resistivity for self-compacting concrete with silica fume and metakaolin.* Construction and Building Materials, 2017. **154**: p. 219-228.
228. Parande, Anand Kuber, Babu, B Ramesh, Karthik, M Aswin, Kumaar, KK Deepak, and Palaniswamy, N, *Study on strength and corrosion performance for steel embedded in metakaolin blended concrete/mortar.* Construction and Building Materials, 2008. **22**(3): p. 127-134.
229. Ramezanianpour, Ali Akhbar and Jovein, H Bahrami, *Influence of metakaolin as supplementary cementing material on strength and durability of concretes.* Construction and Building materials, 2012. **30**: p. 470-479.
230. Li, Yingjie, Zeng, Xiaohui, He, Xiangyu, Long, Guangcheng, Wang, Jilin, and Zeng, Luomin, *Effects of paraffin, metakaolin, and steam curing regimes on the electrical resistivity of steam-cured cement-based materials.* Construction and Building Materials, 2025. **458**: p. 139615.
231. Siad, Hocine, Lachemi, Mohamed, Sahmaran, Mustafa, Mesbah, Habib A, and Hossain, Khandaker M Anwar, *Use of recycled glass powder to improve the performance properties of high volume fly ash-engineered cementitious composites.* Construction and Building Materials, 2018. **163**: p. 53-62.
232. Tariq, Samia, Scott, Allan N, Mackechnie, James R, and Shah, Vineet, *Durability of high volume glass powder self-compacting concrete.* Applied Sciences, 2020. **10**(22): p. 8058.
233. Azarsa, Pejman and Gupta, Rishi, *Electrical resistivity of concrete for durability evaluation: a review.* Advances in Materials Science and Engineering, 2017. **2017**(1): p. 8453095.
234. Canadian Standards Association, Mississauga, ON, Canada., *CSA A23.2-26C (2019) Bulk electrical resistivity of concrete.* 2019.
235. Yılmaz, Bülent and Ediz, Nezahat, *The use of raw and calcined diatomite in cement production.* Cement and Concrete Composites, 2008. **30**(3): p. 202-211.
236. Ferreira, Ruan LS, Pinto, Licarion, Nóbrega, Aline F, and Carneiro, Arnaldo MP, *Diatomaceous earth: A review of its characteristics and effects on the properties of mortars.* Construction and Building Materials, 2024. **421**: p. 135711.
237. Lemesre, Louise, Idir, Rachida, and Cyr, Martin, *Strength Development and Environmental Impact of Waste-Glass-Based Cements Activated with Portland Cement, NaOH, Na-Silicate or Na-Carbonates at Ambient Temperature.* Materials, 2024. **17**(20): p. 5097.
238. Moreira, Othon, Camões, Aires, Malheiro, Raphaele, and Ribeiro, Manuel, *High-Volume Glass Powder Concrete as an Alternative to High-Volume Fly Ash Concrete.* Sustainability, 2025. **17**(9): p. 4142.

239. Cheng, Xinyuan, Zhang, Hongru, Li, Wei, and Zhang, Liquan, *Utilizing diatomaceous earth (DE) as a sustainable substitute in alkali-activated cementitious materials: Performance and life cycle assessment.* Construction and Building Materials, 2024. **452**: p. 138889.
240. Tagnit-Hamou, Arezki, Petrov, Nikola, and Luke, Karen, *Properties of concrete containing diatomaceous earth.* ACI Materials Journal, 2003. **100**(1): p. 73-78.
241. Alex, Alexander Gladwin, Jose, Prakash Arul, Antony, Maria Rajesh, and Dhanalakshmi, Krishnan, *The effect of partial replacement of cement with Diatomaceous Earth (DE) and polypropylene fibers (PPF) on fresh, hardened, and durability properties of concrete.* International Journal of Concrete Structures and Materials, 2024. **18**(1): p. 24.
242. Homayoonmehr, Reza, Ramezanianpour, Ali Akbar, Moodi, Faramarz, Ramezanianpour, Amir Mohammad, and Gevaudan, Juan Pablo, *A review on the effect of metakaolin on the chloride binding of concrete, mortar, and paste specimens.* Sustainability, 2022. **14**(22): p. 15022.
243. Garcia, R, De La Rubia, MA, Enriquez, E, Del Campo, A, Fernandez, J, and Moragues, A, *Chloride binding capacity of metakaolin and nanosilica supplementary pozzolanic cementitious materials in aqueous phase.* Construction and Building Materials, 2021. **298**: p. 123903.
244. Chang, Honglei, Wang, Xiaolong, Wang, Yunfei, Li, Chencong, Guo, Zhengkun, Fan, Shuyuan, Zhang, Hongzhi, and Feng, Pan, *Chloride binding behavior of cement paste influenced by metakaolin dosage and chloride concentration.* Cement and Concrete Composites, 2023. **135**: p. 104821.
245. Du, Hongjian and Tan, Kiang Hwee, *Transport properties of concrete with glass powder as supplementary cementitious material.* ACI Materials Journal, 2015. **112**(3): p. 429.
246. Guignone, Guilherme Cunha, Vieira, Geilma Lima, Zulcão, Robson, Degen, Maxwell Klein, de Moraes Mittri, Sérgio Hémerson, and Baptista, Gercyr, *Incorporation of glass powder and metakaolin as cement partial replacement to improve concrete mechanical properties and increase service life.* Journal of Composite Materials, 2020. **54**(21): p. 2965-2983.
247. Su, Peifeng, Dai, Qingli, and Kane, Evan S, *Predicting chloride ingression in concrete containing different SCMs based on chloride binding and electrical resistivity.* Construction and Building Materials, 2024. **414**: p. 134928.
248. Papadakis, Vagelis G, *Effect of supplementary cementing materials on concrete resistance against carbonation and chloride ingress.* Cement and concrete research, 2000. **30**(2): p. 291-299.
249. Stanton, Thomas E, *Influence of cement and aggregate on concrete expansion.* Engineering News-Record, 1940.
250. Shehata, Medhat H and Thomas, Michael DA, *The effect of fly ash composition on the expansion of concrete due to alkali–silica reaction.* Cement and Concrete Research, 2000. **30**(7): p. 1063-1072.
251. Boddy, AM, Hooton, RD, and Thomas, MDA, *The effect of the silica content of silica fume on its ability to control alkali–silica reaction.* Cement and Concrete research, 2003. **33**(8): p. 1263-1268.

252. Nguyen, Quang Dieu, Castel, Arnaud, Kim, Taehwan, and Khan, Mohammad SH, *Performance of fly ash concrete with ferronickel slag fine aggregate against alkali-silica reaction and chloride diffusion.* Cement and Concrete Research, 2021. **139**: p. 106265.
253. Bueno, Eduard Tora, Paris, Jerry M, Clavier, Kyle A, Spreadbury, Chad, Ferraro, Christopher C, and Townsend, Timothy G, *A review of ground waste glass as a supplementary cementitious material: A focus on alkali-silica reaction.* Journal of Cleaner Production, 2020. **257**: p. 120180.
254. Wei, Jianqiang, Gencturk, Bora, Jain, Amit, and Hanifehzadeh, Mohammad, *Mitigating alkali-silica reaction induced concrete degradation through cement substitution by metakaolin and bentonite.* Applied Clay Science, 2019. **182**: p. 105257.
255. Luo, Dayou and Wei, Jianqiang, *Efficacy of functionalized sodium-montmorillonite in mitigating alkali-silica reaction.* Applied Clay Science, 2023. **245**: p. 107139.
256. Feng, X, Thomas, MDA, Bremner, TW, Folliard, Kevin J, and Fournier, B, *Summary of research on the effect of LiNO3 on alkali–silica reaction in new concrete.* Cement and Concrete Research, 2010. **40**(4): p. 636-642.
257. Collins, CL, Ideker, Jason H, Willis, GS, and Kurtis, KE, *Examination of the effects of LiOH, LiCl, and LiNO3 on alkali–silica reaction.* Cement and Concrete Research, 2004. **34**(8): p. 1403-1415.
258. Venkatanarayanan, Harish Kizhakkumodom and Rangaraju, Prasada Rao, *Decoupling the effects of chemical composition and fineness of fly ash in mitigating alkali-silica reaction.* Cement and Concrete Composites, 2013. **43**: p. 54-68.
259. Tapas, Marie Joshua, Vessalas, Kirk, Thomas, Paul, and Sirivivatnanon, Vute, *Influence of limestone mineral addition in cements on the efficacy of SCMs in mitigating alkali-silica reaction assessed by accelerated mortar bar test.* Journal of Materials in Civil Engineering, 2021.
260. AASHTO, TP 142-21(2023), *Standard Specification For Accelerated Determination of Potentially Deleterious Expansion of Concrete Cylinder due to Alkali-Silica Reaction (Accelerated Concrete Cylinder Test, ACCT)*. 2024: Washington, DC 20004.
261. Saraswatula, Pravin, Mukhopadhyay, Anol, and Liu, Kai-Wei, *Development of a screening tool for rapid fly ash evaluation for mitigating alkali silica reaction in concrete.* Transportation Research Record, 2022. **2676**(11): p. 583-595.
262. Mukhopadhyay, Anol K, Liu, Kai-Wei, and Jalal, Mostafa, *An innovative approach to fly ash characterization and evaluation to prevent alkali-silica reaction.* ACI Materials Journal, 2019. **116**(4): p. 173-181.
263. Kihara, Yushiro. *The influence of carbonation on the alkali-aggregate reaction mechanism*. in *Proceedings of the 10th International Congress on the Chemistry of Cement*. 1997.
264. Wang, Yingting, Mo, Kim Hung, Du, Hongjian, and Ling, Tung-Chai, *Effects of CO2 curing treatment on alkali-silica reaction of mortars containing glass aggregate.* Construction and Building Materials, 2022. **323**: p. 126637.
265. Shoji, Makoto, Higuchi, Takayuki, Morioka, Minoru, and Yokozeki, Kosuke, *Inhibitory effect of alkali-silica reaction by the carbonation reaction.* Cem. Sci. Concr. Technol, 2015. **69**(1): p. 504-510.

266. Chen, C and Yang, W. *Mitigation of Alkali-Silica reaction in mortar with limestone addition and carbonation*. in *Proceedings of the 3rd Inter-national Conference on Sustainable Construction Materials and Technologies, Kyoto, Japan*. 2013.
267. Mohammad, Naweed, *Effect of early carbonation curing on alkali-silica reaction in concrete*. 2018: McGill University (Canada).
268. Liu, Zhuo, Shi, Caijun, Shi, Qiantao, Tan, Xiao, and Meng, Weina, *Recycling waste glass aggregate in concrete: Mitigation of alkali-silica reaction (ASR) by carbonation curing.* Journal of Cleaner Production, 2022. **370**: p. 133545.
269. Zhang, Shipeng, Ghouleh, Zaid, and Shao, Yixin, *Effect of carbonation curing on efflorescence formation in concrete paver blocks.* Journal of Materials in Civil Engineering, 2020. **32**(6): p. 04020127.
270. Zajac, Maciej, Skocek, Jan, Durdzinski, Pawel, Bullerjahn, Frank, Skibsted, Jørgen, and Haha, Mohsen Ben, *Effect of carbonated cement paste on composite cement hydration and performance.* Cement and concrete research, 2020. **134**: p. 106090.
271. Saha, Ashish K and Sarker, Prabir K, *Potential alkali silica reaction expansion mitigation of ferronickel slag aggregate by fly ash.* Structural Concrete, 2018. **19**(5): p. 1376-1386.
272. Leemann, Andreas, Lörtscher, Luzia, Bernard, Laetitia, Le Saout, Gwenn, Lothenbach, Barbara, and Espinosa-Marzal, Rosa M, *Mitigation of ASR by the use of LiNO3—characterization of the reaction products.* Cement and concrete research, 2014. **59**: p. 73-86.
273. Hou, Xiaoqiang, Struble, Leslie J, and Kirkpatrick, R James, *Formation of ASR gel and the roles of CSH and portlandite.* Cement and Concrete research, 2004. **34**(9): p. 1683-1696.
274. Kirkpatrick, RJ, Kalinichev, AG, Hou, X, and Struble, L, *Experimental and molecular dynamics modeling studies of interlayer swelling: water incorporation in kanemite and ASR gel.* Materials and Structures, 2005. **38**(4): p. 449-458.
275. Guthrie, George D and Carey, J William, *A thermodynamic and kinetic model for paste–aggregate interactions and the alkali–silica reaction.* Cement and Concrete Research, 2015. **76**: p. 107-120.
276. Almond, Graham G, *a nuclear magnetic resonance study of hydrous layer silicates*. 1995, Durham University.
277. Földvári, Mária, *Handbook of thermogravimetric system of minerals and its use in geological practice*. Vol. 213. 2011: Geological Institute of Hungary Budapest.
278. Palayangoda, Sujeewa S and Nguyen, Quoc P, *Thermal behavior of raw oil shale and its components.* Oil shale, 2015. **32**(2): p. 160.
279. Siva, T, Muralidharan, S, Sathiyanarayanan, S, Manikandan, E, and Jayachandran, M, *Enhanced polymer induced precipitation of polymorphous in calcium carbonate: calcite aragonite vaterite phases.* Journal of Inorganic and Organometallic Polymers and Materials, 2017. **27**: p. 770-778.
280. Shi, Zhenguo, Geng, Guoqing, Leemann, Andreas, and Lothenbach, Barbara, *Synthesis, characterization, and water uptake property of alkali-silica reaction products.* Cement and Concrete Research, 2019. **121**: p. 58-71.
281. Mostafa, NY, Shaltout, AA, Omar, H, and Abo-El-Enein, SA, *Hydrothermal synthesis and characterization of aluminium and sulfate substituted 1.1 nm tobermorites.* Journal of Alloys and Compounds, 2009. **467**(1-2): p. 332-337.

282. Huang, Yining, Jiang, Zhimei, and Schwieger, Wilhelm, *A vibrational spectroscopic study of kanemite.* Microporous and mesoporous materials, 1998. **26**(1-3): p. 215-219.
283. Ekolu, Stephen, Rakgosi, Gift, and Hooton, Doug, *Long-term mitigating effect of lithium nitrate on delayed ettringite formation and ASR in concrete–Microscopic analysis.* Materials Characterization, 2017. **133**: p. 165-175.
284. Chakrabarty, Debojit and Mahapatra, Samiran, *Aragonite crystals with unconventional morphologies.* Journal of materials chemistry, 1999. **9**(11): p. 2953-2957.
285. Herron, Michael M, Machlus, Malka, and Herron, Susan L, *Log Interpretation Parameters Determined by Analysis of Green River Oil Shale Samples: Initial Steps.* parameters (Herron and Herron, 1997), 2008. **13**: p. 15.
286. Luo, Dan, Pei, Xianglin, Fu, Hai, Yang, Xin, Long, Siyu, Zhang, Linyu, and Gong, Wei, *Modification of sodium bicarbonate and its effect on foaming behavior of polypropylene.* e-Polymers, 2021. **21**(1): p. 366-376.
287. Liu, Xin, Feng, Pan, Cai, Yuxi, Yu, Xiaohan, Yu, Cheng, and Ran, Qianping, *Carbonation behavior of calcium silicate hydrate (CSH): Its potential for CO2 capture.* Chemical Engineering Journal, 2022. **431**: p. 134243.
288. Wu, Bei and Ye, Guang, *Study of carbonation rate of synthetic CSH by XRD, NMR and FTIR.* Heron, 2019. **64**(1/2): p. 21-38.
289. White, John, *Computational fluid dynamics modelling and experimental study on a single silica gel type B.* Modelling and Simulation in Engineering, 2012. **2012**.
290. Bonnell, D. G. R., *Studies in gels IV.—The swelling of silica gel.* Transactions of the Faraday Society, 1933. **29**(140): p. 1217-1220.
291. Murphy, Jennifer N., Schneider, Céline M., Hawboldt, Kelly, and Kerton, Francesca M., *Hard to Soft: Biogenic Absorbent Sponge-like Material from Waste Mussel Shells.* Matter, 2020. **3**(6): p. 2029-2041.
292. Sing, Kenneth SW, *Reporting physisorption data for gas/solid systems with special reference to the determination of surface area and porosity (Recommendations 1984).* Pure and applied chemistry, 1985. **57**(4): p. 603-619.
293. Thommes, Matthias, Kaneko, Katsumi, Neimark, Alexander V, Olivier, James P, Rodriguez-Reinoso, Francisco, Rouquerol, Jean, and Sing, Kenneth SW, *Physisorption of gases, with special reference to the evaluation of surface area and pore size distribution (IUPAC Technical Report).* Pure and applied chemistry, 2015. **87**(9-10): p. 1051-1069.
294. Ravikovitch, Peter I and Neimark, Alexander V, *Experimental confirmation of different mechanisms of evaporation from ink-bottle type pores: equilibrium, pore blocking, and cavitation.* Langmuir, 2002. **18**(25): p. 9830-9837.

8.0 Appendices

8.1 Appendix A: Failure modes

HP-1L-GG-00-07-CT-01

HP-1L-GG-00-07-CT-02

HP-1L-GG-00-07-CT-03

HP-1L-GG-05-07-CT-01

HP-1L-GG-05-07-CT-02

HP-1L-GG-05-07-CT-03

HP-1L-GG-10-07-CT-01

HP-1L-GG-10-07-CT-02

HP-1L-GG-10-07-CT-03

HP-1L-GG-15-07-CT-01

HP-1L-GG-15-07-CT-02

HP-1L-GG-15-07-CT-03

HP-1L-GG-20-07-CT-01

HP-1L-GG-20-07-CT-02

HP-1L-GG-20-07-CT-03

HP-1L-GG-25-07-CT-01

HP-1L-GG-25-07-CT-02

HP-1L-GG-25-07-CT-03

HP-1L-GG-30-07-CT-01

HP-1L-GG-30-07-CT-02

HP-1L-GG-30-07-CT-02

HP-1L-GG-00-28-CT-01

HP-1L-GG-00-28-CT-02

HP-1L-GG-00-28-CT-03

HP-1L-GG-05-28-CT-01

HP-1L-GG-05-28-CT-02

HP-1L-GG-05-28-CT-03

HP-1L-GG-10-28-CT-01

HP-1L-GG-10-28-CT-02

HP-1L-GG-10-28-CT-03

HP-1L-GG-15-28-CT-01

HP-1L-GG-15-28-CT-02

HP-1L-GG-15-28-CT-03

HP-1L-GG-20-28-CT-01

HP-1L-GG-20-28-CT-02

HP-1L-GG-20-28-CT-03

HP-1L-GG-25-28-CT-01

HP-1L-GG-25-28-CT-02

HP-1L-GG-25-28-CT-03

HP-1L-GG-30-28-CT-01

HP-1L-GG-30-28-CT-02

HP-1L-GG-30-28-CT-03

8.2 Appendix B: Test results per batch

Batch 01		
Slump (in.)	**Air Content (%)**	**Density (lb./ft3)**
7.5	8.0	146.8

Sample ID #	Weight (lb.)	Stress (psi)
HP-1L-GG-00-07-CT-01	8.9	5,457.0
HP-1L-GG-00-07-CT-02	8.9	5,691.0
HP-1L-GG-00-07-CT-03	8.9	5,720.0
HP-1L-GG-00-07-ST-01	8.9	425.0
HP-1L-GG-00-07-ST-02	8.9	316.0

HP-1L-GG-00-07-ST-03	8.9	336.0
HP-1L-GG-00-07-BT-01	65.0	398.0
HP-1L-GG-00-07-BT-02	65.0	485.0
HP-1L-GG-00-28-CT-01	8.8	6,706.0
HP-1L-GG-00-28-CT-02	8.8	6,638.0
HP-1L-GG-00-28-ST-01	8.8	442.0
HP-1L-GG-00-28-BT-01	65.0	428.0

Batch 02		
Slump (in.)	**Air Content (%)**	**Density (lb./ft3)**
6.5	5.0	155.2

Sample ID #	**Weight (lb.)**	**Stress (psi)**
HP-1L-GG-00-28-CT-03	9.0	7,796.0
HP-1L-GG-00-28-ST-02	9.0	378.0
HP-1L-GG-00-28-ST-03	9.0	516.0
HP-1L-GG-00-28-BT-02	70.4	542.0
HP-1L-GG-00-91-CT-01	9.1	8,404.0
HP-1L-GG-00-91-CT-02	9.1	8,742.0
HP-1L-GG-00-91-CT-03	9.1	8,471.0
HP-1L-GG-00-91-ST-01	9.1	498.0
HP-1L-GG-00-91-ST-02	9.1	435.0
HP-1L-GG-00-91-ST-03	9.1	439.0
HP-1L-GG-00-91-BT-01	71.2	844.0
HP-1L-GG-00-91-BT-02	69.8	781.0

Batch 03		
Slump (in.)	**Air Content (%)**	**Density (lb./ft3)**
8.0	6.2	147.2

Sample ID #	**Weight (lb.)**	**Stress (psi)**
HP-1L-GG-05-07-CT-01	8.9	6,037.0
HP-1L-GG-05-07-CT-02	8.9	5,824.0
HP-1L-GG-05-07-CT-03	8.9	6,271.0
HP-1L-GG-05-07-ST-01	8.9	325.0
HP-1L-GG-05-07-ST-02	8.9	434.0
HP-1L-GG-05-07-ST-03	8.9	321.0
HP-1L-GG-05-07-BT-01	65.0	484.0
HP-1L-GG-05-07-BT-02	65.0	455.0
HP-1L-GG-05-28-CT-01	8.9	7,188.0
HP-1L-GG-05-28-CT-02	8.9	7,033.0

HP-1L-GG-05-28-ST-01	8.9	508.0
HP-1L-GG-05-28-BT-01	67.6	493.0

Batch 04		
Slump (in.)	**Air Content (%)**	**Density (lb./ft3)**
7.5	7.5	150.4

Sample ID #	**Weight (lb.)**	**Stress (psi)**
HP-1L-GG-05-28-CT-03	8.9	7,526.0
HP-1L-GG-05-28-ST-02	8.9	386.0
HP-1L-GG-05-28-ST-03	8.9	434.0
HP-1L-GG-05-28-BT-02	67.4	616.0
HP-1L-GG-05-91-CT-01	9.0	8,362.0
HP-1L-GG-05-91-CT-02	9.0	8,428.0
HP-1L-GG-05-91-CT-03	9.0	8,337.0
HP-1L-GG-05-91-ST-01	9.0	439.0
HP-1L-GG-05-91-ST-02	9.0	523.0
HP-1L-GG-05-91-ST-03	9.0	635.0
HP-1L-GG-05-91-BT-01	68.8	834.0
HP-1L-GG-05-91-BT-02	69	852.0

Batch 05		
Slump (in.)	**Air Content (%)**	**Density (lb./ft3)**
7.0	7.0	152.8

Sample ID #	**Weight (lb.)**	**Stress (psi)**
HP-1L-GG-10-07-CT-01	8.9	7,044.0
HP-1L-GG-10-07-CT-02	8.9	6,747.0
HP-1L-GG-10-07-CT-03	8.9	6,861.0
HP-1L-GG-10-07-ST-01	8.9	448.0
HP-1L-GG-10-07-ST-02	8.9	330.0
HP-1L-GG-10-07-ST-03	8.9	404.0
HP-1L-GG-10-07-BT-01	68.0	470.0
HP-1L-GG-10-07-BT-02	68.0	476.0
HP-1L-GG-10-28-CT-01	9.0	8,506.0
HP-1L-GG-10-28-CT-02	9.0	8,278.0
HP-1L-GG-10-28-ST-01	9.0	428.0
HP-1L-GG-10-28-BT-01	69.6	570.0

Batch 06		
Slump (in.)	**Air Content (%)**	**Density (lb./ft3)**

7.5	8.0	145.6

Sample ID #	Weight (lb.)	Stress (psi)
HP-1L-GG-10-28-CT-03	8.7	6,211.0
HP-1L-GG-10-28-ST-02	8.7	449.0
HP-1L-GG-10-28-ST-03	8.7	410.0
HP-1L-GG-10-28-BT-02	65.4	500.0
HP-1L-GG-10-91-CT-01	8.7	7,482.0
HP-1L-GG-10-91-CT-02	8.7	7,194.0
HP-1L-GG-10-91-CT-03	8.7	7,040.0
HP-1L-GG-10-91-ST-01	8.7	411.0
HP-1L-GG-10-91-ST-02	8.7	574.0
HP-1L-GG-10-91-ST-03	8.7	478.0
HP-1L-GG-10-91-BT-01	66.2	757.0
HP-1L-GG-10-91-BT-02	66.4	699.9

Batch 07		
Slump (in.)	**Air Content (%)**	**Density (lb./ft3)**
8.0	8.0	148.8

Sample ID #	Weight (lb.)	Stress (psi)
HP-1L-GG-15-07-CT-01	8.8	5,546.0
HP-1L-GG-15-07-CT-02	8.8	5,639.0
HP-1L-GG-15-07-CT-03	8.8	5,616.0
HP-1L-GG-15-07-ST-01	8.8	383.0
HP-1L-GG-15-07-ST-02	8.8	316.0
HP-1L-GG-15-07-ST-03	8.8	313.0
HP-1L-GG-15-07-BT-01	66.2	410.0
HP-1L-GG-15-07-BT-02	66.2	412.0
HP-1L-GG-15-28-CT-01	8.8	7,068.0
HP-1L-GG-15-28-CT-02	8.8	6,933.0
HP-1L-GG-15-28-ST-01	8.8	489.0
HP-1L-GG-15-28-BT-01	66.6	596.0

Batch 08		
Slump (in.)	**Air Content (%)**	**Density (lb./ft3)**
8.0	8.0	147.2

Sample ID #	Weight (lb.)	Stress (psi)
HP-1L-GG-15-28-CT-03	8.7	6,472.0
HP-1L-GG-15-28-ST-02	8.7	310.0

HP-1L-GG-15-28-ST-03	8.7	559.0
HP-1L-GG-15-28-BT-02	66.8	518.0
HP-1L-GG-15-91-CT-01	8.8	8,430.0
HP-1L-GG-15-91-CT-02	8.8	8,218.0
HP-1L-GG-15-91-CT-03	8.8	8,317.0
HP-1L-GG-15-91-ST-01	8.8	502.0
HP-1L-GG-15-91-ST-02	8.8	433.0
HP-1L-GG-15-91-ST-03	8.8	530.0
HP-1L-GG-15-91-BT-01	65.6	865.0
HP-1L-GG-15-91-BT-02	66.4	783.0

Batch 09		
Slump (in.)	**Air Content (%)**	**Density (lb./ft3)**
8.0	6.2	148.0

Sample ID #	**Weight (lb.)**	**Stress (psi)**
HP-1L-GG-20-07-CT-01	8.8	5,142.0
HP-1L-GG-20-07-CT-02	8.8	5,478.0
HP-1L-GG-20-07-CT-03	8.8	5,272.0
HP-1L-GG-20-07-ST-01	8.8	432.0
HP-1L-GG-20-07-ST-02	8.8	321.0
HP-1L-GG-20-07-ST-03	8.8	320.0
HP-1L-GG-20-07-BT-01	67.0	434.0
HP-1L-GG-20-07-BT-02	67.0	448.0
HP-1L-GG-20-28-CT-01	8.9	6,715.0
HP-1L-GG-20-28-CT-02	8.9	6,730.0
HP-1L-GG-20-28-ST-01	8.9	470.0
HP-1L-GG-20-28-BT-01	65.2	545.0

Batch 10		
Slump (in.)	**Air Content (%)**	**Density (lb./ft3)**
8.5	8.5	147.2

Sample ID #	**Weight (lb.)**	**Stress (psi)**
HP-1L-GG-20-28-CT-03	8.8	6,685.0
HP-1L-GG-20-28-ST-02	8.8	273.0
HP-1L-GG-20-28-ST-03	8.8	390.0
HP-1L-GG-20-28-BT-02	65.8	550.0
HP-1L-GG-20-91-CT-01	8.8	8,329.0
HP-1L-GG-20-91-CT-02	8.8	8,294.0
HP-1L-GG-20-91-CT-03	8.8	8,456.0

HP-1L-GG-20-91-ST-01	8.8	750.0
HP-1L-GG-20-91-ST-02	8.8	325.0
HP-1L-GG-20-91-ST-03	8.8	424.0
HP-1L-GG-20-91-BT-01	66.2	917.0
HP-1L-GG-20-91-BT-02	65.0	912.0

Batch 11		
Slump (in.)	**Air Content (%)**	**Density (lb./ft3)**
8.7	7.0	147.2

Sample ID #	**Weight (lb.)**	**Stress (psi)**
HP-1L-GG-25-07-CT-01	8.7	4,896.0
HP-1L-GG-25-07-CT-02	8.7	4,869.0
HP-1L-GG-25-07-CT-03	8.7	4,879.0
HP-1L-GG-25-07-ST-01	8.7	267.0
HP-1L-GG-25-07-ST-02	8.7	303.0
HP-1L-GG-25-07-ST-03	8.7	234.0
HP-1L-GG-25-07-BT-01	66.4	384.0
HP-1L-GG-25-07-BT-02	66.4	379.0
HP-1L-GG-25-28-CT-01	8.8	6,274.0
HP-1L-GG-25-28-CT-02	8.8	6,357.0
HP-1L-GG-25-28-ST-01	8.8	278.0
HP-1L-GG-25-28-BT-01	66.8	566.0

Batch 12		
Slump (in.)	**Air Content (%)**	**Density (lb./ft3)**
8.7	7.0	147.2

Sample ID #	**Weight (lb.)**	**Stress (psi)**
HP-1L-GG-25-28-CT-03	8.7	6,291.0
HP-1L-GG-25-28-ST-02	8.7	379.0
HP-1L-GG-25-28-ST-03	8.7	269.0
HP-1L-GG-25-28-BT-02	65.8	508.0
HP-1L-GG-25-91-CT-01	8.8	8,346.0
HP-1L-GG-25-91-CT-02	8.8	8,054.0
HP-1L-GG-25-91-CT-03	8.8	8,516.0
HP-1L-GG-25-91-ST-01	8.8	574.0
HP-1L-GG-25-91-ST-02	8.8	539.0
HP-1L-GG-25-91-ST-03	8.8	416.0
HP-1L-GG-25-91-BT-01	65.2	889.0
HP-1L-GG-25-91-BT-02	65.8	867.0

Batch 13		
Slump (in.)	**Air Content (%)**	**Density (lb./ft3)**
9.0	7.5	145.6

Sample ID #	Weight (lb.)	Stress (psi)
HP-1L-GG-30-07-CT-01	8.6	3,917.0
HP-1L-GG-30-07-CT-02	8.6	3,962.0
HP-1L-GG-30-07-CT-03	8.6	3,773.0
HP-1L-GG-30-07-ST-01	8.6	247.0
HP-1L-GG-30-07-ST-02	8.6	287.0
HP-1L-GG-30-07-ST-03	8.6	298.0
HP-1L-GG-30-07-BT-01	65.2	339.0
HP-1L-GG-30-07-BT-02	65.2	304.0
HP-1L-GG-30-28-CT-01	8.6	5,197.0
HP-1L-GG-30-28-CT-02	8.6	5,640.0
HP-1L-GG-30-28-ST-01	8.6	463.0
HP-1L-GG-30-28-BT-01	65.0	506.0

Batch 14		
Slump (in.)	**Air Content (%)**	**Density (lb./ft3)**
9.0	8.0	144.0

Sample ID #	Weight (lb.)	Stress (psi)
HP-1L-GG-30-28-CT-03	8.4	4,364.0
HP-1L-GG-30-28-ST-02	8.4	245.0
HP-1L-GG-30-28-ST-03	8.4	308.0
HP-1L-GG-30-28-BT-02	62.6	421.0
HP-1L-GG-30-91-CT-01	8.4	6,328.0
HP-1L-GG-30-91-CT-02	8.4	6,373.0
HP-1L-GG-30-91-CT-03	8.4	6,596.0
HP-1L-GG-30-91-ST-01	8.4	472.0
HP-1L-GG-30-91-ST-02	8.4	588.0
HP-1L-GG-30-91-ST-03	8.4	540.0
HP-1L-GG-30-91-BT-01	64.2	947.0
HP-1L-GG-30-91-BT-02	64.2	886.0

8.3 Appendix C: Key threshold of chloride penetration results

Recommendations for chloride penetration rate corresponding to FHWA HPC performance grade per AASHTO T 357

	FHWA HPC Performance Grade		
Rate of penetration (mm/V-h)	1	2	3
	$0.034 \geq x \geq 0.024$	$0.024 \geq x \geq 0.012$	$0.012 \geq x$

8.4 Appendix D: Concrete mix design sheets used at Construction Service

massDOT Massachusetts Department of Transportation Highway Division

Rev. 08/22/2025

2025 CEMENT CONCRETE MIX DESIGN SHEET

RMS 043

PLANT INFORMATION		MAILING ADDRESS			MIX DESIGN SHEET IDENTIFICATION	
PLANT NAME	LOCATION	STREET NO. & ADDRESS	CITY/TOWN	EMAIL ADDRESS	CONTRACT	SHEET IDENTIFICATION NO.
CONSTRUCTION SERVICE	SPRINGFIELD, MA	2420 Boston Road	Wilbraham, MA 01095	rolds@cs-ma.us	ALT MAT-D	25-09-15-08-25-48

CONSTITUENT MATERIALS

	AGGREGATE								PERCENT PASSING BY MASS (%)											
ID	SOURCE	LOCATION	NMAS	DESCRIPTION	SPEC.	SG	UW_{DR} (PCF)	VC (%)	2 IN.	1 1/2 IN.	1 IN.	3/4 IN.	1/2 IN.	3/8 IN.	#4	#8	#16	#30	#50	#100	#200	FM
FINE	DELTA SAND AND GRAVEL	SUNDERLAND, MA	FINE	NORMAL WEIGHT	M 6	2.64	106.8	35.1	100.0	100.0	100.0	100.0	100.0	100.0	96.7	89.4	73.2	42.1	14.3	2.1	1.3	2.82
CA1	J S LANE	AMHERST, MA	3/4 IN.	NORMAL WEIGHT - 67	M 80	2.92	110.4	39.3	100.0	100.0	100.0	98.1	64.3	32.4	5.2	2.6	2.2	1.9	1.5	1.2	0.9	6.55
CA2																						
CA3																						

CEMENT; SUPPLEMENTARY CEMENTITIOUS MATERIALS; PACKAGED; FIBERS							CHEMICAL ADMIXTURES					
ID	SOURCE	LOCATION / PRODUCT	TYPE	DESCRIPTION	SPEC.	SG	ID	SOURCE	PRODUCT	TYPE	DESCRIPTION	SPEC.	V_S (%)
CEM	AMRIZE (HOLCIM)	ST CONSTANT, QC (IL(11)MS)	IL(11)MS	11% LIMESTONE BLEND (MS)	M 240	3.10	AD1	GCP APPLIED TECHNOLOGIES	AIRALON 7000	AEA	AIR ENTTRAINING	M 154	6.62
SCM1	URBAN MINING	POZZOTIVE	GGP-GS	SODA-LIME-SILICA GLASS (GS)	C1866	2.90	AD2	CHRYSO INC	CHRYSO QUAD 842	F	HIGH RANGE WATER REDUCING	M 194	17.05
SCM2							AD3	GCP APPLIED TECHNOLOGIES	RECOVER	D	ATER REDUCING AND RETARDI	M 194	15.53
SCM3							AD4	GCP APPLIED TECHNOLOGIES	DCI	C/CIA	TYPE C / CORROSION INHIBITIN	194/C15	20.69
PKG							AD5	MASTER BUILDERS SOLUTIONS	MASTERSURE 1390	S-ADA	AIR DETRAINING	M 194	5.51
FIBER							AD6						

MIX DESIGN FORMULATION

MIX DESIGN			C	NMAS	S	AC	W/CM	PC	AGGREGATE (LBS.)				CEMENTITIOUS; PACKAGED; FIBER (LBS.)						WATER (GAL.)		ADMIXTURES (FL. OZ.)						YIELD	UW
ID	PRODUCER ID	MIX DESIGN TYPE	(PSI)	(IN.)	(IN.)	(%)	RATIO	(%)	FINE	CA1	CA2	CA3	CEM	SCM1	SCM2	SCM3	PKG	FIBER	W_T	W_{ADMIX}	AD1	AD2	AD3	AD4	AD5	AD6	(CF)	(PCF)
01	GGP-GS (25%)	HPC	5000	3/4	6.00	6.0	0.40	28.5	1185.0	1890.0			495.0	165.0					31.5	2.9	5.0	56.1	23.1	384.0			27.00	148.5
01	ACTUAL BATCH	HPC	5000	3/4	6.00	7.5	0.39	27.8	1257.1	1805.7			495.0	165.0					30.8	3.1	4.6	45.1	22.3	402.3	20.0		27.29	146.3

COMBINED AGGREGATE AND PASTE SYSTEM

MIX DESIGN		PERCENT BY MASS PASSING (%)													GRADATION OPTIMIZATION		VOID CONTENT (%)				PC_A / VC_0	PC_A / VC_{CM}	SCM (%)			TCM	ECC	THICK
ID	PRODUCER ID	2 IN.	1 1/2 IN.	1 IN.	3/4 IN.	1/2 IN.	3/8 IN.	#4	#8	#16	#30	#50	#100	#200	TARANTULA	SHILSTONE	VC_0	VC_{0M}	VC_C	VC_{CM}			SCM1	SCM2	SCM3	(LBS.)	(LBS.)	(FT.)
01	GGP-GS (25%)	100.0	100.0	100.0	98.8	78.1	58.5	40.5	36.0	29.6	17.4	6.4	1.5	1.1	OUTSIDE	II: 3/4 - 2 IN.	37.6	24.5			1.41		25.0	0.0	0.0	660.0	577.5	1.5
01	ACTUAL BATCH	100.0	100.0	100.0	98.9	79.0	60.1	42.8	38.2	31.3	18.4	6.8	1.6	1.1	WITHIN	IV: TOO FINE	37.5	24.1			1.46		25.0	0.0	0.0	660.0	577.5	1.5

We agree to produce cement concrete mix designs per the precise proportions, quantities, types, and sources of constituent materials identified on the approved RMS 043 Cement Concrete Mix Design Sheet for MassDOT construction contracts.

Mr. Ralph Olds	Quality Control Coordinator		9/15/2025
NAME	*TITLE*	*AUTHORIZED SIGNATURE*	*DATE*

8.5 Appendix E: Concrete mix design sheets used at Boston Concrete

massDOT Massachusetts Department of Transportation Highway Division

Rev. 04/18/2025

2025 CEMENT CONCRETE MIX DESIGN SHEET

RMS 043

PLANT INFORMATION		MAILING ADDRESS			MIX DESIGN SHEET IDENTIFICATION	
PLANT NAME	LOCATION	STREET NO. & ADDRESS	CITY/TOWN	EMAIL ADDRESS	CONTRACT	SHEET IDENTIFICATION NO.
BOSTON CONCRETE CORPORATION	LOWELL, MA	706 Broadway Street	Lowell, MA 01854	kstjean@bostonconcrete.com	ALT MAT-A	25-07-14-11-14-34

CONSTITUENT MATERIALS

	AGGREGATE								PERCENT PASSING BY MASS (%)											
ID	SOURCE	LOCATION	NMAS	DESCRIPTION	SPEC.	SG	UW_{DR} (PCF)	VC (%)	2 IN.	1 1/2 IN	1 IN.	3/4 IN.	1/2 IN.	3/8 IN.	#4	#8	#16	#30	#50	#100	#200	FM
FINE	GMI BOSCAWEN GRAVEL	BOSCAWEN, NH	FINE	NORMAL WEIGHT	M 6	2.66	102.1	38.4	100.0	100.0	100.0	100.0	100.0	100.0	98.0	80.0	65.0	53.0	30.0	9.0	2.1	2.65
CA1	BROX INDUSTRIES	HUDSON, NH	3/4 IN.	NORMAL WEIGHT - 6	M 80	2.61	91.1	44.0	100.0	100.0	100.0	90.0	30.0	7.0	1.0	1.0	1.0	0.0	0.0	0.0	0.0	7.00
CA2	BROX INDUSTRIES	HUDSON, NH	3/8 IN.	NORMAL WEIGHT - 8	M 80	2.55	90.5	43.0	100.0	100.0	100.0	100.0	100.0	99.0	29.0	7.0	4.0	0.0	0.0	0.0	0.0	5.61
CA3																						

	CEMENT; SUPPLEMENTARY CEMENTITIOUS MATERIALS; PACKAGED; FIBERS						CHEMICAL ADMIXTURES					
ID	SOURCE	LOCATION / PRODUCT	TYPE	DESCRIPTION	SPEC.	SG	ID	SOURCE	PRODUCT	TYPE	DESCRIPTION	SPEC.	V_S (%)
CEM	DRAGON PRODUCTS	MONJOS, SPAIN (I / II)	I / II	GENERAL / MOD. SULFATE	M 85	3.15	AD1	SIKA	SIKA VISCOCRETE-1000	F	HIGH RANGE WATER REDUCING	M 194	20.61
SCM1	URBAN MINING	POZZOTIVE	GGP-GS	SODA-LIME-SILICA GLASS (GS)	C1866	2.50	AD2	SIKA	SIKA AIR 360	AEA	AIR ENTRAINING	M 154	6.19
SCM2	DICALITE	BASALT, NV	NP-DE	DIATOMACEOUS EARTH (NP)	C1945	2.25	AD3	SIKA	SIKA PLASTIMENT	D	ATER REDUCING AND RETARDI	M 194	23.72
SCM3	SIKA	SIKACRETE M-100	NP-MET	METAKAOLIN (N)	M 295	2.60	AD4	SIKA	SIKA-CNI	C/CIA	ACCELERATING	194/C1	21.38
PKG							AD5	E5	LIQUID FLY ASH	S-NSA	NANO SILICA	M 194	21.60
FIBER							AD6	E5	INTERNAL CURE	S-NSA	NANO SILICA	M 194	47.99

MIX DESIGN FORMULATION

MIX DESIGN			C	NMAS	S	AC	W/CM	PC	AGGREGATE (LBS.)				CEMENTITIOUS; PACKAGED; FIBER (LBS.)						WATER (GAL.)		ADMIXTURES (FL. OZ.)						YIELD	UW
ID	PRODUCER ID	MIX DESIGN TYPE	(PSI)	(IN.)	(IN.)	(%)	RATIO	(%)	FINE	CA1	CA2	CA3	CEM	SCM1	SCM2	SCM3	PKG	FIBER	W_T	W_{ADMIX}	AD1	AD2	AD3	AD4	AD5	AD6	(CF)	(PCF)
01	GGP-GS (30%)	HPC	5000	3/4	6.00	6.0	0.40	30.2	1142.0	1180.0	475.0		480.0	205.0					32.8	2.6	24.0	3.5	13.7	384.0			27.00	139.5
01	ACTUAL BATCH	HPC	5000	3/4	9.50	7.7	0.40	29.7	1142.0	1180.0	475.0		480.0	205.0					32.8	2.6	24.0	3.5	13.7	384.0			27.46	137.2
02	NP-DE (10%)	HPC	5000	3/4	6.00	6.0	0.40	29.7	1154.0	1190.0	475.0		617.0		68.0				32.8	2.6	24.0	3.5	13.7	384.0			27.00	140.3
02	ACTUAL BATCH	HPC	5000	3/4	1.75	2.8	0.40	30.6	1154.0	1190.0	475.0		617.0		68.0				32.8	3.0	88.4	7.0	13.7	384.0			26.15	144.9
03	NP-MET (15%)	HPC	5000	3/4	6.00	6.0	0.40	29.6	1154.0	1190.0	480.0		582.0			103.0			32.8	2.6	24.0	3.5	13.7	384.0			27.00	140.5
03	ACTUAL BATCH	HPC	5000	3/4	3.50	3.6	0.40	30.3	1154.0	1190.0	475.0		582.0			103.0			32.8	2.7	33.6	3.5	13.7	384.0			26.33	143.9
04	NANO SILICA	HPC	5000	3/4	6.00	6.0	0.44	27.7	1258.0	1190.0	455.0		615.0						32.6	3.0	21.5	3.1	12.3	384.0	49.2	24.6	27.00	140.8
04	ACTUAL BATCH	HPC	5000	3/4	6.50	7.6	0.44	27.7	1154.0	1200.0	480.0		615.0						32.6	3.0	21.5	3.5	12.3	384.0	49.2	24.6	27.03	138.2
05	I / II (100%)	HPC	5000	3/4	6.00	6.0	0.40	29.2	1161.0	1200.0	480.0		685.0						32.8	2.6	24.0	3.5	13.7	384.0			27.00	141.1
05	ACTUAL BATCH	HPC	5000	3/4	7.00	6.2	0.40	29.1	1161.0	1205.0	480.0		685.0						32.8	2.6	24.0	3.5	13.7	384.0			27.08	140.9

COMBINED AGGREGATE AND PASTE SYSTEM

MIX DESIGN		PERCENT BY MASS PASSING (%)													GRADATION OPTIMIZATION		VOID CONTENT (%)				PC_A / VC_0	PC_A / VC_{CM}	SCM (%)			TCM	ECC	THICK
ID	PRODUCER ID	2 IN.	1 1/2 IN.	1 IN.	3/4 IN.	1/2 IN.	3/8 IN.	#4	#8	#16	#30	#50	#100	#200	TARANTULA	SHILSTONE	VC_0	VC_{0M}	VC_C	VC_{CM}			SCM1	SCM2	SCM3	(LBS.)	(LBS.)	(FT.)
01	GGP-GS (30%)	100.0	100.0	100.0	95.8	70.5	60.6	45.4	34.3	27.6	21.6	12.2	3.7	0.9	OUTSIDE	II: 3/4 - 2 IN.	41.6	26.4			1.37		29.9	0.0	0.0	685.0	582.5	1.5
01	ACTUAL BATCH	100.0	100.0	100.0	95.8	70.5	60.6	45.4	34.3	27.6	21.6	12.2	3.7	0.9	OUTSIDE	II: 3/4 - 2 IN.	41.6	26.0			1.44		29.9	0.0	0.0	685.0	582.5	1.5
02	NP-DE (10%)	100.0	100.0	100.0	95.8	70.5	60.6	45.4	34.4	27.7	21.7	12.3	3.7	0.9	OUTSIDE	II: 3/4 - 2 IN.	41.6	26.6			1.34		0.0	9.9	0.0	685.0	698.6	1.0
02	ACTUAL BATCH	100.0	100.0	100.0	95.8	70.5	60.6	45.4	34.4	27.7	21.7	12.3	3.7	0.9	OUTSIDE	II: 3/4 - 2 IN.	41.6	27.5			1.21		0.0	9.9	0.0	685.0	698.6	1.0
03	NP-MET (15%)	100.0	100.0	100.0	95.8	70.5	60.6	45.4	34.3	27.7	21.7	12.3	3.7	0.9	OUTSIDE	II: 3/4 - 2 IN.	41.6	26.7			1.33		0.0	0.0	15.0	685.0	705.6	0.5
03	ACTUAL BATCH	100.0	100.0	100.0	95.8	70.5	60.6	45.4	34.4	27.7	21.7	12.3	3.7	0.9	OUTSIDE	II: 3/4 - 2 IN.	41.6	27.3			1.24		0.0	0.0	15.0	685.0	705.6	0.5
04	NANO SILICA	100.0	100.0	100.0	95.9	71.3	61.7	47.4	36.2	29.2	23.0	13.0	3.9	0.9	OUTSIDE	II: 3/4 - 2 IN.	41.4	27.3			1.23		0.0	0.0	0.0	615.0	615.0	1.5
04	ACTUAL BATCH	100.0	100.0	100.0	95.8	70.4	60.5	45.2	34.2	27.6	21.6	12.2	3.7	0.9	OUTSIDE	II: 3/4 - 2 IN.	41.6	26.7			1.32		0.0	0.0	0.0	615.0	615.0	1.5
05	I / II (100%)	100.0	100.0	100.0	95.8	70.4	60.5	45.4	34.3	27.7	21.7	12.3	3.7	0.9	OUTSIDE	II: 3/4 - 2 IN.	41.6	26.8			1.31		0.0	0.0	0.0	685.0	685.0	1.0
05	ACTUAL BATCH	100.0	100.0	100.0	95.8	70.4	60.5	45.3	34.2	27.6	21.6	12.2	3.7	0.9	OUTSIDE	II: 3/4 - 2 IN.	41.6	26.8			1.32		0.0	0.0	0.0	685.0	685.0	1.0

We agree to produce cement concrete mix designs per the precise proportions, quantities, types, and sources of constituent materials identified on the approved RMS 043 Cement Concrete Mix Design Sheet for MassDOT construction contracts.

Mr. Keith St. Jean	Quality Control Manager		9/15/2025
NAME	*TITLE*	*AUTHORIZED SIGNATURE*	*DATE*

massDOT Massachusetts Department of Transportation Highway Division

Rev. 05/14/2025

2025 CEMENT CONCRETE MIX DESIGN SHEET

RMS 043

PLANT INFORMATION		MAILING ADDRESS			MIX DESIGN SHEET IDENTIFICATION	
PLANT NAME	LOCATION	STREET NO. & ADDRESS	CITY/TOWN	EMAIL ADDRESS	CONTRACT	SHEET IDENTIFICATION NO.
BOSTON CONCRETE CORPORATION	LOWELL, MA	706 Broadway Street	Lowell, MA 01854	kstjean@bostonconcrete.com	ALT MAT-B	25-07-14-10-50-41

CONSTITUENT MATERIALS

	AGGREGATE								PERCENT PASSING BY MASS (%)											
ID	SOURCE	LOCATION	NMAS	DESCRIPTION	SPEC.	SG	UW_{DR} (PCF)	VC (%)	2 IN.	1 1/2 IN	1 IN.	3/4 IN.	1/2 IN.	3/8 IN.	#4	#8	#16	#30	#50	#100	#200	FM
FINE	GMI BOSCAWEN GRAVEL	BOSCAWEN, NH	FINE	NORMAL WEIGHT	M 6	2.66	102.1	38.4	100.0	100.0	100.0	100.0	100.0	100.0	98.0	80.0	65.0	53.0	30.0	9.0	2.1	2.65
CA1	BROX INDUSTRIES	HUDSON, NH	3/4 IN.	NORMAL WEIGHT - 6	M 80	2.61	91.1	44.0	100.0	100.0	100.0	90.0	30.0	7.0	1.0	1.0	1.0	0.0	0.0	0.0	0.0	7.00
CA2	BROX INDUSTRIES	HUDSON, NH	3/8 IN.	NORMAL WEIGHT - 8	M 80	2.55	90.5	43.0	100.0	100.0	100.0	100.0	100.0	99.0	29.0	7.0	4.0	0.0	0.0	0.0	0.0	5.61
CA3																						

	CEMENT; SUPPLEMENTARY CEMENTITIOUS MATERIALS; PACKAGED; FIBERS						CHEMICAL ADMIXTURES					
ID	SOURCE	LOCATION / PRODUCT	TYPE	DESCRIPTION	SPEC.	SG	ID	SOURCE	PRODUCT	TYPE	DESCRIPTION	SPEC.	V_S (%)
CEM	DRAGON PRODUCTS	MONJOS, SPAIN (I / II)	I / II	GENERAL / MOD. SULFATE	M 85	3.15	AD1	SIKA	SIKA VISCOCRETE-1000	F	HIGH RANGE WATER REDUCING	M 194	20.61
SCM1	HEIDELBERG MATERIALS	FLEETWOOD, PA	S-120	HIGH ACTIVITY (120)	M 302	2.88	AD2	SIKA	SIKA AIR 360	AEA	AIR ENTRAINING	M 154	6.19
SCM2	DICALITE	BASALT, NV	NP-DE	DIATOMACEOUS EARTH (NP)	C1945	2.25	AD3	SIKA	SIKA PLASTIMENT	D	ATER REDUCING AND RETARDI	M 194	23.72
SCM3	SIKA	SIKACRETE M-100	NP-MET	METAKAOLIN (N)	M 295	2.60	AD4	SIKA	SIKA-CNI	C/CIA	ACCELERATING	194/C1	21.38
PKG							AD5	E5	LIQUID FLY ASH	S-NSA	NANO SILICA	M 194	21.60
FIBER							AD6	E5	INTERNAL CURE	S-NSA	NANO SILICA	M 194	47.99

MIX DESIGN FORMULATION

MIX DESIGN			C	NMAS	S	AC	W/CM	PC	AGGREGATE (LBS.)				CEMENTITIOUS; PACKAGED; FIBER (LBS.)						WATER (GAL.)		ADMIXTURES (FL. OZ.)						YIELD	UW
ID	PRODUCER ID	MIX DESIGN TYPE	(PSI)	(IN.)	(IN.)	(%)	RATIO	(%)	FINE	CA1	CA2	CA3	CEM	SCM1	SCM2	SCM3	PKG	FIBER	W_T	W_{ADMIX}	AD1	AD2	AD3	AD4	AD5	AD6	(CF)	(PCF)
01	S-120 (40%)	HPC	5000	3/4	6.00	6.0	0.40	29.7	1150.0	1190.0	480.0		411.0	274.0					32.8	2.6	24.0	3.5	13.7	384.0			27.00	140.3
01	ACTUAL BATCH	HPC	5000	3/4	8.75	6.5	0.40	29.5	1150.0	1190.0	480.0		411.0	274.0					32.8	2.6	24.0	3.5	13.7	384.0			27.14	139.7
02	S-120 / NANO	HPC	5000	3/4	6.00	6.0	0.44	28.2	1249.0	1185.0	450.0		369.0	246.0					32.6	3.0	21.5	3.1	12.3	384.0	49.2	24.6	27.00	140.1
02	ACTUAL BATCH	HPC	5000	3/4	8.75	8.0	0.44	27.6	1249.0	1185.0	450.0		369.0	246.0					32.6	3.0	21.5	3.5	12.3	384.0	49.2	24.6	27.54	137.4
03	S-120 / NP-DE	HPC	5000	3/4	6.00	6.0	0.40	29.7	1154.0	1190.0	475.0		514.0	137.0	34.0				32.8	2.6	24.0	3.5	13.7	384.0			27.00	140.3
03	ACTUAL BATCH	HPC	5000	3/4	5.00	4.4	0.40	30.1	1154.0	1190.0	475.0		514.0	137.0	34.0				32.8	2.8	47.3	5.5	13.7	384.0			26.57	142.6
04	S-120 / NP-MET	HPC	5000	3/4	6.00	6.0	0.40	29.6	1157.0	1190.0	475.0		498.0	137.0		50.0			32.8	2.6	24.0	3.5	13.7	384.0			27.00	140.4
04	ACTUAL BATCH	HPC	5000	3/4	4.25	4.6	0.40	30.0	1157.0	1190.0	475.0		498.0	137.0		50.0			32.8	2.6	24.0	6.0	13.7	384.0			26.62	142.4

COMBINED AGGREGATE AND PASTE SYSTEM

MIX DESIGN		PERCENT BY MASS PASSING (%)													GRADATION OPTIMIZATION		VOID CONTENT (%)				PC_A /	PC_A /	SCM (%)			TCM	ECC	THICK
ID	PRODUCER ID	2 IN.	1 1/2 IN.	1 IN.	3/4 IN.	1/2 IN.	3/8 IN.	#4	#8	#16	#30	#50	#100	#200	TARANTULA	SHILSTONE	VC_0	VC_{0M}	VC_C	VC_{CM}	VC_{0M}	VC_{CM}	SCM1	SCM2	SCM3	(LBS.)	(LBS.)	(FT.)
01	S-120 (40%)	100.0	100.0	100.0	95.8	70.5	60.6	45.3	34.2	27.6	21.6	12.2	3.7	0.9	OUTSIDE	II: 3/4 - 2 IN.	41.6	26.6			1.34		40.0	0.0	0.0	685.0	685.0	1.0
01	ACTUAL BATCH	100.0	100.0	100.0	95.8	70.5	60.6	45.3	34.2	27.6	21.6	12.2	3.7	0.9	OUTSIDE	II: 3/4 - 2 IN.	41.6	26.5			1.36		40.0	0.0	0.0	685.0	685.0	1.0
02	S-120 / NANO	100.0	100.0	100.0	95.9	71.2	61.6	47.4	36.1	29.2	23.0	13.0	3.9	0.9	OUTSIDE	II: 3/4 - 2 IN.	41.4	27.1			1.26		40.0	0.0	0.0	615.0	615.0	1.5
02	ACTUAL BATCH	100.0	100.0	100.0	95.9	71.2	61.6	47.4	36.1	29.2	23.0	13.0	3.9	0.9	OUTSIDE	II: 3/4 - 2 IN.	41.4	26.5			1.34		40.0	0.0	0.0	615.0	615.0	1.5
03	S-120 / NP-DE	100.0	100.0	100.0	95.8	70.5	60.6	45.4	34.4	27.7	21.7	12.3	3.7	0.9	OUTSIDE	II: 3/4 - 2 IN.	41.6	26.6			1.34		20.0	5.0	0.0	685.0	691.8	1.0
03	ACTUAL BATCH	100.0	100.0	100.0	95.8	70.5	60.6	45.4	34.4	27.7	21.7	12.3	3.7	0.9	OUTSIDE	II: 3/4 - 2 IN.	41.6	27.0			1.28		20.0	5.0	0.0	685.0	691.8	1.0
04	S-120 / NP-MET	100.0	100.0	100.0	95.8	70.5	60.6	45.5	34.4	27.7	21.7	12.3	3.7	0.9	OUTSIDE	II: 3/4 - 2 IN.	41.6	26.6			1.34		20.0	0.0	7.3	685.0	695.0	1.0
04	ACTUAL BATCH	100.0	100.0	100.0	95.8	70.5	60.6	45.5	34.4	27.7	21.7	12.3	3.7	0.9	OUTSIDE	II: 3/4 - 2 IN.	41.6	27.0			1.28		20.0	0.0	7.3	685.0	695.0	1.0

We agree to produce cement concrete mix designs per the precise proportions, quantities, types, and sources of constituent materials identified on the approved RMS 043 Cement Concrete Mix Design Sheet for MassDOT construction contracts.

Mr. Keith St. Jean	Quality Control Manager		9/15/2025
NAME	*TITLE*	*AUTHORIZED SIGNATURE*	*DATE*

massDOT Massachusetts Department of Transportation Highway Division

Rev. 04/18/2025

2025 CEMENT CONCRETE MIX DESIGN SHEET

RMS 043

PLANT INFORMATION		MAILING ADDRESS			MIX DESIGN SHEET IDENTIFICATION	
PLANT NAME	LOCATION	STREET NO. & ADDRESS	CITY/TOWN	EMAIL ADDRESS	CONTRACT	SHEET IDENTIFICATION NO.
BOSTON CONCRETE CORPORATION	LOWELL, MA	706 Broadway Street	Lowell, MA 01854	kstjean@bostonconcrete.com	ALT MAT-C	25-08-08-08-19-04

CONSTITUENT MATERIALS

	AGGREGATE						UW_{DR}	VC	PERCENT PASSING BY MASS (%)												
ID	SOURCE	LOCATION	NMAS	DESCRIPTION	SPEC.	SG	(PCF)	(%)	2 IN.	1 1/2 IN	1 IN.	3/4 IN.	1/2 IN.	3/8 IN.	#4	#8	#16	#30	#50	#100	#200	FM
FINE	GMI BOSCAWEN GRAVEL	BOSCAWEN, NH	FINE	NORMAL WEIGHT	M 6	2.66	102.1	38.4	100.0	100.0	100.0	100.0	100.0	100.0	98.0	80.0	65.0	53.0	30.0	9.0	2.1	2.65
CA1	BROX INDUSTRIES	HUDSON, NH	3/4 IN.	NORMAL WEIGHT - 6	M 80	2.61	91.1	44.0	100.0	100.0	100.0	90.0	30.0	7.0	1.0	1.0	1.0	0.0	0.0	0.0	0.0	7.00
CA2	BROX INDUSTRIES	HUDSON, NH	3/8 IN.	NORMAL WEIGHT - 8	M 80	2.55	90.5	43.0	100.0	100.0	100.0	100.0	100.0	99.0	29.0	7.0	4.0	0.0	0.0	0.0	0.0	5.61
CA3																						

	CEMENT; SUPPLEMENTARY CEMENTITIOUS MATERIALS; PACKAGED; FIBERS						CHEMICAL ADMIXTURES					
ID	SOURCE	LOCATION / PRODUCT	TYPE	DESCRIPTION	SPEC.	SG	ID	SOURCE	PRODUCT	TYPE	DESCRIPTION	SPEC.	V_S (%)
CEM	DRAGON PRODUCTS	MONJOS, SPAIN (I / II)	I / II	GENERAL / MOD. SULFATE	M 85	3.15	AD1	SIKA	SIKA VISCOCRETE-1000	F	HIGH RANGE WATER REDUCING	M 194	20.61
SCM1	HEIDELBERG MATERIALS	FLEETWOOD, PA	S-120	HIGH ACTIVITY (120)	M 302	2.88	AD2	SIKA	SIKA AIR 360	AEA	AIR ENTRAINING	M 154	6.19
SCM2	URBAN MINING	POZZOTIVE	GGP-GS	SODA-LIME-SILICA GLASS (GS)	C1866	2.50	AD3	SIKA	SIKA PLASTIMENT	D	ATER REDUCING AND RETARDI	M 194	23.72
SCM3							AD4	SIKA	SIKA-CNI	C/CIA	ACCELERATING	194/C19	21.38
PKG							AD5						
FIBER							AD6						

MIX DESIGN FORMULATION

MIX DESIGN			C	NMAS	S	AC	W/CM	PC	AGGREGATE (LBS.)				CEMENTITIOUS; PACKAGED; FIBER (LBS.)						WATER (GAL.)		ADMIXTURES (FL. OZ.)						YIELD	UW
ID	PRODUCER ID	MIX DESIGN TYPE	(PSI)	(IN.)	(IN.)	(%)	RATIO	(%)	FINE	CA1	CA2	CA3	CEM	SCM1	SCM2	SCM3	PKG	FIBER	W_T	W_{ADMIX}	AD1	AD2	AD3	AD4	AD5	AD6	(CF)	(PCF)
01	S-120 / GGP-GS	HPC	5000	3/4	6.00	6.0	0.40	30.0	1147.0	1185.0	475.0		479.0	69.0	137.0				32.8	2.6	24.0	3.5	13.7	384.0			27.00	139.9
01	ACTUAL BATCH	HPC	5000	3/4	8.75	6.0	0.40	30.0	1147.0	1185.0	475.0		479.0	69.0	137.0				32.8	2.6	24.0	3.0	13.7	384.0			27.00	139.9

COMBINED AGGREGATE AND PASTE SYSTEM

MIX DESIGN		PERCENT BY MASS PASSING (%)													GRADATION OPTIMIZATION		VOID CONTENT (%)				PC_A /	PC_A /	SCM (%)			TCM	ECC	THICK
ID	PRODUCER ID	2 IN.	1 1/2 IN.	1 IN.	3/4 IN.	1/2 IN.	3/8 IN.	#4	#8	#16	#30	#50	#100	#200	TARANTULA	SHILSTONE	VC_0	VC_{0M}	VC_C	VC_{CM}	VC_{0M}	VC_{CM}	SCM1	SCM2	SCM3	(LBS.)	(LBS.)	(FT.)
01	S-120 / GGP-GS	100.0	100.0	100.0	95.8	70.4	60.6	45.4	34.3	27.7	21.7	12.3	3.7	0.9	OUTSIDE	II: 3/4 - 2 IN.	41.6	26.5			1.36		10.1	20.0	0.0	685.0	616.5	1.5
01	ACTUAL BATCH	100.0	100.0	100.0	95.8	70.4	60.6	45.4	34.3	27.7	21.7	12.3	3.7	0.9	OUTSIDE	II: 3/4 - 2 IN.	41.6	26.5			1.36		10.1	20.0	0.0	685.0	616.5	1.5

We agree to produce cement concrete mix designs per the precise proportions, quantities, types, and sources of constituent materials identified on the approved RMS 043 Cement Concrete Mix Design Sheet for MassDOT construction contracts.

Mr. Keith St. Jean	Quality Control Manager		9/15/2025
NAME	*TITLE*	*AUTHORIZED SIGNATURE*	*DATE*

8.6 Appendix F: 28-day testing results of concrete specimens cast at Boston Concrete

Rev. 04/08/2025	SAMPLE TYPE: VER	775A-T SAMPLE OF CEMENT CONCRETE	DATE RECEIVED: 8/8/25	SAMPLE NUMBER: 2025-016278

PROJECT INFORMATION

Town/City:	STATEWIDE	*Contract No.:*	VER-CON
Contractor:	#N/A	*Federal Aid No.:*	#N/A
Report to District:	RMS	*Cost Account No.:*	#N/A
Resident Engineer:	#N/A	*District Mat. Engr.*	#N/A

MATERIAL INFORMATION

Bid Item:	VER.M4	*Specification No.:*	M4
Bid Item Description:	VERIFICATION OF CEMENT CONCRETE AND RELATED MATERIALS		
Sub-Item Description:	VER.M4 - TRIAL BATCH HIGH PERFORMANCE CONCRETE		
Bid Item Quantity:	#N/A	*Date to be Used:*	2025
MassDOT Mix ID No.:	25-07-14-11-14-34-05	*Producer Mix ID No.:*	Control
Produced by:	BOSTON CONCRETE CORPORATION	*Town/City, State:*	LOWELL, MA
Design Strength (psi):	5000	*Nom. Agg. Size (in.):*	3/4
Tot. Cementitious (lbs.)	685	*Mix Design Type:*	HPC
Proposed Use:	VERIFICATION OF CEMENT CONCRE	*Additional Information:*	

SAMPLING INFORMATION (R 60 / C172)

Date Sampled:	8/7/25	*Sampled By:*	George Gilbert
Sampling Location:	BOSTON CONCRETE Yard	*Town/City, State:*	LOWELL, MA
Truck No.:	N/A	*Ticket No.:*	N/A
Sample Time:	8:40am		
Job Water Added:	N/A	*Admixtures Added:*	N/A
Random Sample:	Y	*Lot & Sub Lot No.:*	1-1
Quantity Represented:	N/A	*Weather & Temp. (°F):*	63-sunny

PREPARATION OF SPECIMENS IN THE FIELD (R 100 / C31)

Specimen Size:	☑ 4 x 8" ☐ 6 x 12"	*Field Curing Method:*	☑ Curing Box ☐ Field Cured
Specimens Covered:	☑ Yes ☐ No	*Curing Temp. (°F):*	Low: 50 High: 90

SAMPLE PROPERTIES BY FIELD TESTS

Test Method	Quality Characteristic	Result	Spec. Min.	Spec. Max.	Pass/Fail	Remarks
T 119 (C143)	Slump (in.)	7.00	3.00	6.00	FIO	
T 152 (C231)	Air Content (%)	6.2	4.5	7.5	FIO	
T 309 (C1064)	Concrete Temp. (°F)	75	50	90	FIO	
T 121 (C231)	Unit Weight (pcf)	141.4	138.1	144.1	FIO	

REMARKS

Need to perform T 358 testing at 7, 28, and 56-days

FIELD TESTING OFFICE, TECHNICIAN(S), AND REVIEW

Office:	RMS	*Office Location:*	HOPKINTON, MA
Tested By:	Keith St.Jean	*Test Date:*	8/7/25
Witnessed By:	George Gilbert	*Witness Date:*	8/7/25
Reviewed By:		*Review Date:*	

SPECIFICATION LIMITS & APPROVAL

Results are within specification limits:		*Results are outside specification limits:*	

By typing my name below, I understand and agree that this form of electronic signature has the same legal force and effect as a manual signature.

Approved By:		*Approve Date:*	

Rev. 04/08/2025	SAMPLE TYPE: VER	775A-T SAMPLE OF CEMENT CONCRETE	DATE RECEIVED: 8/8/25	SAMPLE NUMBER: 2025-016278

PROJECT INFORMATION

Town/City:	STATEWIDE	*Contract No.:*	VER-CON
Contractor:	#N/A	*Federal Aid No.:*	#N/A
Report to District:	RMS	*Cost Account No.:*	#N/A
Resident Engineer:	#N/A	*District Mat. Engr.*	#N/A

CHLORIDE ION PENETRATION RESISTANCE TESTING (T 358)

Specimen Size: 4 x 8" *Curing Method:* Moist Cured

	Cylinder 1		Cylinder 2		Cylinder 3	
Specimen	00090990		00090991		00090992	
Temp. (°F)	72.4		72.3		72.0	
Angle	**Cylinder 1 (kΩ-cm)**		**Cylinder 2 (kΩ-cm)**		**Cylinder 3 (kΩ-cm)**	
	1st Test	**Repeat**	**1st Test**	**Repeat**	**1st Test**	**Repeat**
0°	7.95		8.17		7.95	
90°	7.9		7.59		7.5	
180°	7.78		7.28		7.31	
270°	7.64		7.62		7.07	
0°	7.86		8.07		7.86	
90°	8.19		7.74		7.54	
180°	7.54		7.4		7.28	
270°	7.78		7.76		7.02	
Average	7.8	Not Req'd	7.7	Not Req'd	7.4	Not Req'd
%CV	2.5%	Not Req'd	3.9%	Not Req'd	4.6%	Not Req'd
Average 16	Not Req'd		Not Req'd		Not Req'd	

Set Average Resistivity Determination (kΩ-cm)

Age (Days):	7
Curing Factor:	1.0
Cyl. 1 Average:	7.8
Cyl. 2 Average:	7.7
Cyl. 3 Average:	7.4
Set Average:	8
Penetrability:	High
Spec. Min.:	-
Pass/Fail:	FIO

	Cylinder 1		Cylinder 2		Cylinder 3	
Specimen	00090993		00090994		00090995	
Temp. (°F)	70.6		70.4		70.5	
Angle	**Cylinder 1 (kΩ-cm)**		**Cylinder 2 (kΩ-cm)**		**Cylinder 3 (kΩ-cm)**	
	1st Test	**Repeat**	**1st Test**	**Repeat**	**1st Test**	**Repeat**
0°	10.4		11.3		10.3	
90°	10.6		11.9		10.4	
180°	11.6		10.1		10.5	
270°	10.6		11.4		11.6	
0°	10.4		11.5		10.3	
90°	10.6		11.9		10.6	
180°	11.6		10		10.4	
270°	10.6		11.2		11.5	
Average	10.8	Not Req'd	11.2	Not Req'd	10.7	Not Req'd
%CV	4.6%	Not Req'd	6.6%	Not Req'd	5.0%	Not Req'd
Average 16	Not Req'd		Not Req'd		Not Req'd	

Set Average Resistivity Determination (kΩ-cm)

Age (Days):	28
Curing Factor:	1.0
Cyl. 1 Average:	10.8
Cyl. 2 Average:	11.2
Cyl. 3 Average:	10.7
Set Average:	11
Penetrability:	High
Spec. Min.:	-
Pass/Fail:	FIO

Calculate the average and the %CV for each sample in the set. If the %CV is > 7.5%, immerse sample in water bath (68 to 77 °F) for 2 h, and record results in the "Repeat" Column. If the %CV on the "Repeat" Set is < 7.5%, use the average of the "Repeat" Set. If the %CV is > 7.5%, average all 16 readings.

Rev. 04/08/2025	SAMPLE TYPE: VER	775A-T SAMPLE OF CEMENT CONCRETE	DATE RECEIVED: 8/8/25	SAMPLE NUMBER: 2025-016278

PROJECT INFORMATION

Town/City:	STATEWIDE	*Contract No.:*	VER-CON
Contractor:	#N/A	*Federal Aid No.:*	#N/A
Report to District:	RMS	*Cost Account No.:*	#N/A
Resident Engineer:	#N/A	*District Mat. Engr.*	#N/A
Specimen Size:	4 x 8"	*Curing Method:*	Moist Cured

	Cylinder 1		Cylinder 2		Cylinder 3	
Specimen						
Temp. (°F)						

Angle	Cylinder 1 (kΩ-cm)		Cylinder 2 (kΩ-cm)		Cylinder 3 (kΩ-cm)	
	1st Test	Repeat	1st Test	Repeat	1st Test	Repeat
0°						
90°						
180°						
270°						
0°						
90°						
180°						
270°						
Average						
%CV						
Average 16						

Set Average Resistivity Determination (kΩ-cm)

Age (Days):	
Curing Factor:	1.0
Cyl. 1 Average:	
Cyl. 2 Average:	
Cyl. 3 Average:	
Set Average:	
Penetrability:	High
Spec. Min.:	
Pass/Fail:	

	Cylinder 1		Cylinder 2		Cylinder 3	
Specimen						
Temp. (°F)						

Angle	Cylinder 1 (kΩ-cm)		Cylinder 2 (kΩ-cm)		Cylinder 3 (kΩ-cm)	
	1st Test	Repeat	1st Test	Repeat	1st Test	Repeat
0°						
90°						
180°						
270°						
0°						
90°						
180°						
270°						
Average		Not Req'd		Not Req'd		Not Req'd
%CV		Not Req'd		Not Req'd		Not Req'd
Average 16	Not Req'd		Not Req'd		Not Req'd	

Set Average Resistivity Determination (kΩ-cm)

Age (Days):	
Curing Factor:	1.0
Cyl. 1 Average:	
Cyl. 2 Average:	
Cyl. 3 Average:	
Set Average:	
Penetrability:	High
Spec. Min.:	
Pass/Fail:	

Calculate the average and the %CV for each sample in the set. If the %CV is > 7.5%, immerse sample in water bath (68 to 77 °F) for 2 h, and record results in the "Repeat" Column. If the %CV on the "Repeat" Set is < 7.5%, use the average of the "Repeat" Set. If the %CV is > 7.5%, average all 16 readings.

massDOT Highway	SAMPLE TYPE:	775A-T	DATE RECEIVED:	SAMPLE NUMBER:
Rev. 04/08/2025	VER	SAMPLE OF CEMENT CONCRETE	8/8/25	2025-016278

PROJECT INFORMATION

Town/City:	STATEWIDE	*Contract No.:*	VER-CON
Contractor:	#N/A	*Federal Aid No.:*	#N/A
Report to District:	RMS	*Cost Account No.:*	#N/A
Resident Engineer:	#N/A	*District Mat. Engr.*	#N/A

LABORATORY PREPARATION, COMPRESSIVE STRENGTH TESTING (T 22 / C39)

Sample Condition: [✓] Acceptable [ ] Unacceptable (See Remarks) *Lab Curing Method:* Moist Cured

Lab Preparation: [ ] Sulfur (T 231) [✓] Neoprene (C1231) [ ] Cutting (T 22) [ ] Grinding (T 22)

Specimen ID	Age	Unit	Break Date	Weight (lbs)	Diameter (in)	Area (in^2)	Load (lbf)	Strength (psi)	Average (psi)	Break Type	Omit
00090990	7	DAY	8/14/25	8.42	4.01	12.63	83080	6578		3	
00090991	7	DAY	8/14/25	8.42	4.01	12.63	85386	6761	6630	3	
00090992	7	DAY	8/14/25	8.42	4.01	12.63	82779	6555		2	
00090993	28	DAY	9/4/25	8.42	4.01	12.63	97898	7752		2	
00090994	28	DAY	9/4/25	8.42	4.01	12.63	97907	7752	7780	2	
00090995	28	DAY	9/4/25	8.42	4.01	12.63	98885	7830		2	
00090996	56	DAY	10/2/25								
00090997	56	DAY	10/2/25								
00090998	56	DAY	10/2/25								

Break Type T 22: 1 Cone  2 Cone & Split  3 Columnar  4 Shear  5 Side Fracture  6 Pointed 

56-day cylinders discarded: [ ] Yes

REMARKS

Need to perform T 358 testing at 7, 28, and 56-days

TESTING LABORATORY, TECHNICIAN(S), AND REVIEW

Laboratory:	RMS	*Location:*	HOPKINTON, MA
T 358 (Set 1):	Timothy Berard	*Test Date:*	8/14/25
T 358 (Set 2):	Timothy Berard	*Test Date:*	9/4/25
T 358 (Set 3):		*Test Date:*	
T 358 (Set 4):		*Test Date:*	
T 22 (Set 1):	Chris Dinoia (RF)	*Test Date:*	8/14/25
T 22 (Set 2):	Frehiywot Tale	*Test Date:*	9/4/25
T 22 (Set 3):		*Test Date:*	
T 22 (Set 4):		*Test Date:*	
Reviewed By:		*Review Date:*	

SPECIFICATION LIMITS AND APPROVAL

Results are within specification limits: [ ] *Results are outside specification limits:* [ ]

Approved By:

Signature:

Date:

***Results relate only to the items inspected or tested.**

****This report shall not be reproduced, except in full, without the prior written approval of the agency.**

Rev. 04/08/2025	SAMPLE TYPE: VER	775A-T SAMPLE OF CEMENT CONCRETE	DATE RECEIVED: 8/15/25	SAMPLE NUMBER: 2025-016445

PROJECT INFORMATION

Town/City:	STATEWIDE	*Contract No.:*	VER-CON
Contractor:	#N/A	*Federal Aid No.:*	#N/A
Report to District:	RMS	*Cost Account No.:*	#N/A
Resident Engineer:	#N/A	*District Mat. Engr.*	#N/A

MATERIAL INFORMATION

Bid Item:	VER.M4	*Specification No.:*	M4
Bid Item Description:	VERIFICATION OF CEMENT CONCRETE AND RELATED MATERIALS		
Sub-Item Description:	VER.M4 - TRIAL BATCH HIGH PERFORMANCE CONCRETE		
Bid Item Quantity:	#N/A	*Date to be Used:*	2025
MassDOT Mix ID No.:	25-07-14-10-50-41-01	*Producer Mix ID No.:*	S-120 (40%)
Produced by:	BOSTON CONCRETE CORPORATION	*Town/City, State:*	LOWELL, MA
Design Strength (psi):	5000	*Nom. Agg. Size (in.):*	3/4
Tot. Cementitious (lbs.)	685	*Mix Design Type:*	HPC
Proposed Use:	VERIFICATION OF CEMENT CONCRE	*Additional Information:*	

SAMPLING INFORMATION (R 60 / C172)

Date Sampled:	8/13/25	*Sampled By:*	George Gilbert
Sampling Location:	BOSTON CONCRETE CORPORATION	*Town/City, State:*	LOWELL, MA
Truck No.:	N/A	*Ticket No.:*	N/A
Sample Time:	8:39am		
Job Water Added:	N/A	*Admixtures Added:*	N/A
Random Sample:	Y	*Lot & Sub Lot No.:*	B
Quantity Represented:	1cy	*Weather & Temp. (°F):*	75-Sunny

PREPARATION OF SPECIMENS IN THE FIELD (R 100 / C31)

Specimen Size:	☑ 4 x 8" ☐ 6 x 12"	*Field Curing Method:*	☑ Curing Box ☐ Field Cured
Specimens Covered:	☑ Yes ☐ No	*Curing Temp. (°F):*	Low: 50 High: 90

SAMPLE PROPERTIES BY FIELD TESTS

Test Method	Quality Characteristic	Result	Spec. Min.	Spec. Max.	Pass/Fail	Remarks
T 119 (C143)	Slump (in.)	8.75	4.50	7.50	FIO	
T 152 (C231)	Air Content (%)	6.5	4.5	7.5	FIO	
T 309 (C1064)	Concrete Temp. (°F)	78	50	90	FIO	
T 121 (C231)	Unit Weight (pcf)	140.4	137.3	143.3	FIO	

REMARKS

T358 testing at 7,28,and 56-days

FIELD TESTING OFFICE, TECHNICIAN(S), AND REVIEW

Office:	RMS	*Office Location:*	HOPKINTON, MA
Tested By:	Keith St. Jean	*Test Date:*	8/13/25
Witnessed By:	George Gilbert	*Witness Date:*	8/13/25
Reviewed By:		*Review Date:*	

SPECIFICATION LIMITS & APPROVAL

Results are within specification limits:		*Results are outside specification limits:*	

By typing my name below, I understand and agree that this form of electronic signature has the same legal force and effect as a manual signature.

Approved By:		*Approve Date:*	

Rev. 04/08/2025	SAMPLE TYPE: VER	775A-T SAMPLE OF CEMENT CONCRETE	DATE RECEIVED: 8/15/25	SAMPLE NUMBER: 2025-016445

PROJECT INFORMATION

Town/City:	STATEWIDE	*Contract No.:*	VER-CON
Contractor:	#N/A	*Federal Aid No.:*	#N/A
Report to District:	RMS	*Cost Account No.:*	#N/A
Resident Engineer:	#N/A	*District Mat. Engr.*	#N/A

CHLORIDE ION PENETRATION RESISTANCE TESTING (T 358)

Specimen Size: 4 x 8" *Curing Method:* Moist Cured

	Cylinder 1		Cylinder 2		Cylinder 3	
Specimen	00091077		00091078		00091079	
Temp. (°F)	77.0		76.4		75.9	
Angle	**Cylinder 1 (kΩ-cm)**		**Cylinder 2 (kΩ-cm)**		**Cylinder 3 (kΩ-cm)**	
	1st Test	**Repeat**	**1st Test**	**Repeat**	**1st Test**	**Repeat**
0°	14.1		13		13.6	
90°	13.4		13.8		13.6	
180°	13.5		13.7		14.2	
270°	13.5		14.9		13.3	
0°	14		13		13.7	
90°	13.3		13.8		13.3	
180°	13.3		13.6		14	
270°	13.6		14.7		13	
Average	13.6	Not Req'd	13.8	Not Req'd	13.6	Not Req'd
%CV	2.2%	Not Req'd	5.0%	Not Req'd	2.9%	Not Req'd
Average 16	Not Req'd		Not Req'd		Not Req'd	

Set Average Resistivity Determination (kΩ-cm)

Age (Days):	7
Curing Factor:	1.0
Cyl. 1 Average:	13.6
Cyl. 2 Average:	13.8
Cyl. 3 Average:	13.6
Set Average:	14
Penetrability:	Moderate
Spec. Min.:	-
Pass/Fail:	FIO

	Cylinder 1		Cylinder 2		Cylinder 3	
Specimen	00091080		00091081		00091082	
Temp. (°F)	71.1		71.0		70.9	
Angle	**Cylinder 1 (kΩ-cm)**		**Cylinder 2 (kΩ-cm)**		**Cylinder 3 (kΩ-cm)**	
	1st Test	**Repeat**	**1st Test**	**Repeat**	**1st Test**	**Repeat**
0°	24.2		23.6		25.3	
90°	24.7		24		22.2	
180°	26.9		23.8		22.8	
270°	24.4		24		26.1	
0°	24.3		23.5		25.5	
90°	24.6		24.1		22.4	
180°	26.6		23.8		22.7	
270°	24.3		23.9		26	
Average	25.0	Not Req'd	23.8	Not Req'd	24.1	Not Req'd
%CV	4.4%	Not Req'd	0.9%	Not Req'd	7.2%	Not Req'd
Average 16	Not Req'd		Not Req'd		Not Req'd	

Set Average Resistivity Determination (kΩ-cm)

Age (Days):	28
Curing Factor:	1.0
Cyl. 1 Average:	25.0
Cyl. 2 Average:	23.8
Cyl. 3 Average:	24.1
Set Average:	24
Penetrability:	Low
Spec. Min.:	21
Pass/Fail:	

Calculate the average and the %CV for each sample in the set. If the %CV is > 7.5%, immerse sample in water bath (68 to 77 °F) for 2 h, and record results in the "Repeat" Column. If the %CV on the "Repeat" Set is < 7.5%, use the average of the "Repeat" Set. If the %CV is > 7.5%, average all 16 readings.

massDOT Highway	SAMPLE TYPE:	775A-T	DATE RECEIVED:	SAMPLE NUMBER:
Rev. 04/08/2025	VER	SAMPLE OF CEMENT CONCRETE	8/15/25	2025-016445

PROJECT INFORMATION

Town/City:	STATEWIDE	*Contract No.:*	VER-CON
Contractor:	#N/A	*Federal Aid No.:*	#N/A
Report to District:	RMS	*Cost Account No.:*	#N/A
Resident Engineer:	#N/A	*District Mat. Engr.*	#N/A

	Cylinder 1		Cylinder 2		Cylinder 3	
Specimen	00091083		00091083		00091084	
Temp. (°F)						

Angle	Cylinder 1 (kΩ-cm)		Cylinder 2 (kΩ-cm)		Cylinder 3 (kΩ-cm)	
	1st Test	**Repeat**	**1st Test**	**Repeat**	**1st Test**	**Repeat**
0°						
90°						
180°						
270°						
0°						
90°						
180°						
270°						
Average						
%CV						
Average 16						

Set Average Resistivity Determination (kΩ-cm)

Age (Days):	56
Curing Factor:	1.0
Cyl. 1 Average:	
Cyl. 2 Average:	
Cyl. 3 Average:	
Set Average:	
Penetrability:	Low
Spec. Min.:	
Pass/Fail:	

Calculate the average and the %CV for each sample in the set. If the %CV is > 7.5%, immerse sample in water bath (68 to 77 °F) for 2 h, and record results in the "Repeat" Column. If the %CV on the "Repeat" Set is < 7.5%, use the average of the "Repeat" Set. If the %CV is > 7.5%, average all 16 readings.

Rev. 04/08/2025	SAMPLE TYPE: VER	775A-T SAMPLE OF CEMENT CONCRETE	DATE RECEIVED: 8/15/25	SAMPLE NUMBER: 2025-016445

PROJECT INFORMATION

Town/City:	STATEWIDE	*Contract No.:*	VER-CON
Contractor:	#N/A	*Federal Aid No.:*	#N/A
Report to District:	RMS	*Cost Account No.:*	#N/A
Resident Engineer:	#N/A	*District Mat. Engr.*	#N/A

LABORATORY PREPARATION, COMPRESSIVE STRENGTH TESTING (T 22 / C39)

Sample Condition: [✓] Acceptable [ ] Unacceptable (See Remarks) *Lab Curing Method:* Moist Cured

Lab Preparation: [ ] Sulfur (T 231) [✓] Neoprene (C1231) [ ] Cutting (T 22) [ ] Grinding (T 22)

Specimen ID	Age	Unit	Break Date	Weight (lbs)	Diameter (in)	Area (in^2)	Load (lbf)	Strength (psi)	Average (psi)	Break Type	Omit
00091077	7	DAY	8/20/25	8.47	4.01	12.63	76037	6021	6020	5	
00091078	7	DAY	8/20/25	8.47	4.01	12.63	77028	6099		5	
00091079	7	DAY	8/20/25	8.47	4.01	12.63	74968	5936		2	
00091080	28	DAY	9/10/25	8.47	4.00	12.57	86823	6909	7170	2	
00091081	28	DAY	9/10/25	8.47	4.00	12.57	93447	7436		3	
00091082	28	DAY	9/10/25	8.47	4.00	12.57	90215	7179		2	
00091083	56	DAY	10/8/25								
00091084	56	DAY	10/8/25								
00091085	56	DAY	10/8/25								

Break Type T 22: 1 Cone 2 Cone & Split 3 Columnar 4 Shear 5 Side Fracture 6 Pointed

56-day cylinders discarded: [ ] Yes

REMARKS

T358 testing at 7,28,and 56-days

TESTING LABORATORY, TECHNICIAN(S), AND REVIEW

Laboratory:	RMS	*Location:*	HOPKINTON, MA
T 358 (Set 1):	Casey Flynn	*Test Date:*	8/20/25
T 358 (Set 2):	Timothy Berard	*Test Date:*	9/10/25
T 358 (Set 3):	Casey Flynn	*Test Date:*	8/20/25
T 22 (Set 1):	Timothy Berard	*Test Date:*	9/10/25
T 22 (Set 2):		*Test Date:*	
T 22 (Set 3):		*Test Date:*	
T 22 (Set 4):		*Test Date:*	
Reviewed By:		*Review Date:*	

SPECIFICATION LIMITS AND APPROVAL

Results are within specification limits: [ ] *Results are outside specification limits:* [ ]

Approved By:

Signature:

Date:

***Results relate only to the items inspected or tested.**

****This report shall not be reproduced, except in full, without the prior written approval of the agency.**

Rev. 04/08/2025	SAMPLE TYPE: VER	775A-T SAMPLE OF CEMENT CONCRETE	DATE RECEIVED: 8/8/25	SAMPLE NUMBER: 2025-016279

PROJECT INFORMATION

Town/City:	STATEWIDE	*Contract No.:*	VER-CON
Contractor:	#N/A	*Federal Aid No.:*	#N/A
Report to District:	RMS	*Cost Account No.:*	#N/A
Resident Engineer:	#N/A	*District Mat. Engr.*	#N/A

MATERIAL INFORMATION

Bid Item:	VER.M4	*Specification No.:*	M4
Bid Item Description:	VERIFICATION OF CEMENT CONCRETE AND RELATED MATERIALS		
Sub-Item Description:	VER.M4 - TRIAL BATCH HIGH PERFORMANCE CONCRETE		
Bid Item Quantity:	#N/A	*Date to be Used:*	2025
MassDOT Mix ID No.:	25-07-14-11-14-34-01	*Producer Mix ID No.:*	GGP-GS(30%)
Produced by:	BOSTON CONCRETE CORPORATION	*Town/City, State:*	LOWELL, MA
Design Strength (psi):	5000	*Nom. Agg. Size (in.):*	3/4
Tot. Cementitious (lbs.)	685	*Mix Design Type:*	HPC
Proposed Use:	VERIFICATION OF CEMENT CONCRE	*Additional Information:*	

SAMPLING INFORMATION (R 60 / C172)

Date Sampled:	8/7/25	*Sampled By:*	GEORGE GILBERT
Sampling Location:	BOSTON CONCRETE YARD	*Town/City, State:*	LOWELL, MA
Truck No.:	N/A	*Ticket No.:*	N/A
Sample Time:	9:00AM		
Job Water Added:	N/A	*Admixtures Added:*	N/A
Random Sample:	Y	*Lot & Sub Lot No.:*	1-1
Quantity Represented:	N/A	*Weather & Temp. (°F):*	63-SUNNY

PREPARATION OF SPECIMENS IN THE FIELD (R 100 / C31)

Specimen Size:	☑ 4 x 8" ☐ 6 x 12"	*Field Curing Method:*	☑ Curing Box ☐ Field Cured
Specimens Covered:	☑ Yes ☐ No	*Curing Temp. (°F):*	Low: 50 High: 90

SAMPLE PROPERTIES BY FIELD TESTS

Test Method	Quality Characteristic	Result	Spec. Min.	Spec. Max.	Pass/Fail	Remarks
T 119 (C143)	Slump (in.)	9.50	3.00	6.00	FIO	
T 152 (C231)	Air Content (%)	7.7	4.5	7.5	FIO	
T 309 (C1064)	Concrete Temp. (°F)	76	50	90	FIO	
T 121 (C231)	Unit Weight (pcf)	136.4	136.5	142.5	FIO	

REMARKS

FIELD TESTING OFFICE, TECHNICIAN(S), AND REVIEW

Office:	RMS	*Office Location:*	HOPKINTON, MA
Tested By:	Keith St.Jean	*Test Date:*	8/7/25
Witnessed By:	George Gilbert	*Witness Date:*	8/7/25
Reviewed By:		*Review Date:*	

SPECIFICATION LIMITS & APPROVAL

Results are within specification limits:		*Results are outside specification limits:*	

By typing my name below, I understand and agree that this form of electronic signature has the same legal force and effect as a manual signature.

Approved By:		*Approve Date:*	

Rev. 04/08/2025	SAMPLE TYPE: VER	775A-T SAMPLE OF CEMENT CONCRETE	DATE RECEIVED: 8/8/25	SAMPLE NUMBER: 2025-016279

PROJECT INFORMATION

Town/City:	STATEWIDE	*Contract No.:*	VER-CON
Contractor:	#N/A	*Federal Aid No.:*	#N/A
Report to District:	RMS	*Cost Account No.:*	#N/A
Resident Engineer:	#N/A	*District Mat. Engr.*	#N/A

CHLORIDE ION PENETRATION RESISTANCE TESTING (T 358)

Specimen Size: 4 x 8" *Curing Method:* Moist Cured

	Cylinder 1		Cylinder 2		Cylinder 3	
Specimen	00091026		00091027		00091028	
Temp. (°F)	72.0		72.0		71.9	
Angle	**Cylinder 1 (kΩ-cm)**		**Cylinder 2 (kΩ-cm)**		**Cylinder 3 (kΩ-cm)**	
	1st Test	**Repeat**	**1st Test**	**Repeat**	**1st Test**	**Repeat**
0°	5.06		4.78		4.58	
90°	4.78		4.66		4.7	
180°	5.11		4.61		4.44	
270°	5.04		4.37		4.68	
0°	5.2		4.73		4.51	
90°	4.92		4.54		4.7	
180°	4.99		4.66		4.42	
270°	5.16		4.42		4.75	
Average	5.0	Not Req'd	4.6	Not Req'd	4.6	Not Req'd
%CV	2.7%	Not Req'd	3.1%	Not Req'd	2.8%	Not Req'd
Average 16	Not Req'd		Not Req'd		Not Req'd	

Set Average Resistivity Determination (kΩ-cm)

Age (Days):	7
Curing Factor:	1.0
Cyl. 1 Average:	5.0
Cyl. 2 Average:	4.6
Cyl. 3 Average:	4.6
Set Average:	5
Penetrability:	High
Spec. Min.:	-
Pass/Fail:	FIO

	Cylinder 1		Cylinder 2		Cylinder 3	
Specimen	00091029		00091030		00091031	
Temp. (°F)	70.3		69.7		70.0	
Angle	**Cylinder 1 (kΩ-cm)**		**Cylinder 2 (kΩ-cm)**		**Cylinder 3 (kΩ-cm)**	
	1st Test	**Repeat**	**1st Test**	**Repeat**	**1st Test**	**Repeat**
0°	14.5		15.4		13.5	
90°	14.7		14.5		14	
180°	14.6		14.9		14.6	
270°	15.7		14.6		13.8	
0°	14.7		15.4		13.5	
90°	14.7		14.7		14.1	
180°	14.5		14.8		14.6	
270°	15.7		14.6		13.8	
Average	14.9	Not Req'd	14.9	Not Req'd	14.0	Not Req'd
%CV	3.4%	Not Req'd	2.4%	Not Req'd	3.1%	Not Req'd
Average 16	Not Req'd		Not Req'd		Not Req'd	

Set Average Resistivity Determination (kΩ-cm)

Age (Days):	28
Curing Factor:	1.0
Cyl. 1 Average:	14.9
Cyl. 2 Average:	14.9
Cyl. 3 Average:	14.0
Set Average:	15
Penetrability:	Moderate
Spec. Min.:	-
Pass/Fail:	FIO

Calculate the average and the %CV for each sample in the set. If the %CV is > 7.5%, immerse sample in water bath (68 to 77 °F) for 2 h, and record results in the "Repeat" Column. If the %CV on the "Repeat" Set is < 7.5%, use the average of the "Repeat" Set. If the %CV is > 7.5%, average all 16 readings.

massDOT Highway	SAMPLE TYPE:	775A-T	DATE RECEIVED:	SAMPLE NUMBER:
Rev. 04/08/2025	VER	SAMPLE OF CEMENT CONCRETE	8/8/25	2025-016279

PROJECT INFORMATION

Town/City:	STATEWIDE	*Contract No.:*	VER-CON
Contractor:	#N/A	*Federal Aid No.:*	#N/A
Report to District:	RMS	*Cost Account No.:*	#N/A
Resident Engineer:	#N/A	*District Mat. Engr.*	#N/A
Specimen Size:	4 x 8"	*Curing Method:*	Moist Cured

	Cylinder 1		Cylinder 2		Cylinder 3	
Specimen						
Temp. (°F)						

Angle	Cylinder 1 (kΩ-cm)		Cylinder 2 (kΩ-cm)		Cylinder 3 (kΩ-cm)	
	1st Test	Repeat	1st Test	Repeat	1st Test	Repeat
0°						
90°						
180°						
270°						
0°						
90°						
180°						
270°						
Average						
%CV						
Average 16						

Set Average Resistivity Determination (kΩ-cm)

Age (Days):	
Curing Factor:	1.0
Cyl. 1 Average:	
Cyl. 2 Average:	
Cyl. 3 Average:	
Set Average:	
Penetrability:	High
Spec. Min.:	
Pass/Fail:	

	Cylinder 1		Cylinder 2		Cylinder 3	
Specimen						
Temp. (°F)						

Angle	Cylinder 1 (kΩ-cm)		Cylinder 2 (kΩ-cm)		Cylinder 3 (kΩ-cm)	
	1st Test	Repeat	1st Test	Repeat	1st Test	Repeat
0°						
90°						
180°						
270°						
0°						
90°						
180°						
270°						
Average		Not Req'd		Not Req'd		Not Req'd
%CV		Not Req'd		Not Req'd		Not Req'd
Average 16	Not Req'd		Not Req'd		Not Req'd	

Set Average Resistivity Determination (kΩ-cm)

Age (Days):	
Curing Factor:	1.0
Cyl. 1 Average:	
Cyl. 2 Average:	
Cyl. 3 Average:	
Set Average:	
Penetrability:	Moderate
Spec. Min.:	
Pass/Fail:	

Calculate the average and the %CV for each sample in the set. If the %CV is > 7.5%, immerse sample in water bath (68 to 77 °F) for 2 h, and record results in the "Repeat" Column. If the %CV on the "Repeat" Set is < 7.5%, use the average of the "Repeat" Set. If the %CV is > 7.5%, average all 16 readings.

Rev. 04/08/2025	SAMPLE TYPE: VER	775A-T SAMPLE OF CEMENT CONCRETE	DATE RECEIVED: 8/8/25	SAMPLE NUMBER: 2025-016279

PROJECT INFORMATION

Town/City:	STATEWIDE	*Contract No.:*	VER-CON
Contractor:	#N/A	*Federal Aid No.:*	#N/A
Report to District:	RMS	*Cost Account No.:*	#N/A
Resident Engineer:	#N/A	*District Mat. Engr.*	#N/A

LABORATORY PREPARATION, COMPRESSIVE STRENGTH TESTING (T 22 / C39)

Sample Condition: [✓] Acceptable [ ] Unacceptable (See Remarks) *Lab Curing Method:* Moist Cured

Lab Preparation: [ ] Sulfur (T 231) [✓] Neoprene (C1231) [ ] Cutting (T 22) [ ] Grinding (T 22)

Specimen ID	Age	Unit	Break Date	Weight (lbs)	Diameter (in)	Area (in^2)	Load (lbf)	Strength (psi)	Average (psi)	Break Type	Omit
00091026	7	DAY	8/14/25	8.18	4.01	12.63	47327	3747		2	
00091027	7	DAY	8/14/25	8.18	4.01	12.63	49386	3910	3820	3	
00091028	7	DAY	8/14/25	8.18	4.01	12.63	47941	3796		3	
00091029	28	DAY	9/4/25	8.18	4.01	12.63	69450	5499		2	
00091030	28	DAY	9/4/25	8.18	4.01	12.63	70160	5555	5460	2	
00091031	28	DAY	9/4/25	8.18	4.01	12.63	67287	5328		5	
00091032	56	DAY	10/2/25								
00091033	56	DAY	10/2/25								
00091034	56	DAY	10/2/25								

Break Type T 22: 1 Cone 2 Cone & Split 3 Columnar 4 Shear 5 Side Fracture 6 Pointed

56-day cylinders discarded: [ ] Yes

REMARKS

TESTING LABORATORY, TECHNICIAN(S), AND REVIEW

Laboratory:	RMS	*Location:*	HOPKINTON, MA
T 358 (Set 1):	Timothy Berard	*Test Date:*	8/14/25
T 358 (Set 2):	Timothy Berard	*Test Date:*	9/4/25
T 358 (Set 3):		*Test Date:*	
T 358 (Set 4):		*Test Date:*	
T 22 (Set 1):	Chris Dinoia (RF)	*Test Date:*	8/14/25
T 22 (Set 2):	Frehiywot Tale	*Test Date:*	9/4/25
T 22 (Set 3):		*Test Date:*	
T 22 (Set 4):		*Test Date:*	
Reviewed By:		*Review Date:*	

SPECIFICATION LIMITS AND APPROVAL

Results are within specification limits: [ ] *Results are outside specification limits:* [ ]

Approved By:

Signature:

Date:

***Results relate only to the items inspected or tested.**

****This report shall not be reproduced, except in full, without the prior written approval of the agency.**

Rev. 04/08/2025	SAMPLE TYPE: VER	775A-T SAMPLE OF CEMENT CONCRETE	DATE RECEIVED: 8/8/25	SAMPLE NUMBER: 2025-016280

PROJECT INFORMATION

Town/City:	STATEWIDE	*Contract No.:*	VER-CON
Contractor:	#N/A	*Federal Aid No.:*	#N/A
Report to District:	RMS	*Cost Account No.:*	#N/A
Resident Engineer:	#N/A	*District Mat. Engr.*	#N/A

MATERIAL INFORMATION

Bid Item:	VER.M4	*Specification No.:*	M4
Bid Item Description:	VERIFICATION OF CEMENT CONCRETE AND RELATED MATERIALS		
Sub-Item Description:	VER.M4 - TRIAL BATCH HIGH PERFORMANCE CONCRETE		
Bid Item Quantity:	#N/A	*Date to be Used:*	2025
MassDOT Mix ID No.:	25-07-14-11-14-34-03	*Producer Mix ID No.:*	NP-MET(15%)
Produced by:	BOSTON CONCRETE CORPORATION	*Town/City, State:*	LOWELL, MA
Design Strength (psi):	5000	*Nom. Agg. Size (in.):*	3/4
Tot. Cementitious (lbs.)	685	*Mix Design Type:*	HPC
Proposed Use:	VERIFICATION OF CEMENT CONCRE	*Additional Information:*	

SAMPLING INFORMATION (R 60 / C172)

Date Sampled:	8/7/25	*Sampled By:*	George Gilbert
Sampling Location:	BOSTON CONCRETE CORPORATION	*Town/City, State:*	LOWELL, MA
Truck No.:	N/A	*Ticket No.:*	N/A
Sample Time:	10:30am		
Job Water Added:	N/A	*Admixtures Added:*	N/A
Random Sample:	Y	*Lot & Sub Lot No.:*	1-1
Quantity Represented:	N/A	*Weather & Temp. (°F):*	63-sunny

PREPARATION OF SPECIMENS IN THE FIELD (R 100 / C31)

Specimen Size:	☑ 4 x 8"	☐ 6 x 12"	*Field Curing Method:*	☑ Curing Box	☐ Field Cured
Specimens Covered:	☑ Yes	☐ No	*Curing Temp. (°F):*	Low: 50	High: 90

SAMPLE PROPERTIES BY FIELD TESTS

Test Method	Quality Characteristic	Result	Spec. Min.	Spec. Max.	Pass/Fail	Remarks
T 119 (C143)	Slump (in.)	3.50	3.00	6.00	FIO	
T 152 (C231)	Air Content (%)	3.6	4.5	7.5	FIO	
T 309 (C1064)	Concrete Temp. (°F)	76	50	90	FIO	
T 121 (C231)	Unit Weight (pcf)	145.4	137.5	143.5	FIO	

REMARKS

Need to perform T 358 testing at 7, 28, and 56-days

FIELD TESTING OFFICE, TECHNICIAN(S), AND REVIEW

Office:	RMS	*Office Location:*	HOPKINTON, MA
Tested By:	Keith St. Jean	*Test Date:*	8/7/25
Witnessed By:	George Gilbert	*Witness Date:*	8/7/25
Reviewed By:		*Review Date:*	

SPECIFICATION LIMITS & APPROVAL

Results are within specification limits:		*Results are outside specification limits:*	

By typing my name below, I understand and agree that this form of electronic signature has the same legal force and effect as a manual signature.

Approved By:		*Approve Date:*	

Rev. 04/08/2025	SAMPLE TYPE: VER	775A-T SAMPLE OF CEMENT CONCRETE	DATE RECEIVED: 8/8/25	SAMPLE NUMBER: 2025-016280

PROJECT INFORMATION

Town/City:	STATEWIDE	*Contract No.:*	VER-CON
Contractor:	#N/A	*Federal Aid No.:*	#N/A
Report to District:	RMS	*Cost Account No.:*	#N/A
Resident Engineer:	#N/A	*District Mat. Engr.*	#N/A

CHLORIDE ION PENETRATION RESISTANCE TESTING (T 358)

Specimen Size: 4 x 8" *Curing Method:* Moist Cured

	Cylinder 1		Cylinder 2		Cylinder 3	
Specimen	00091017		00091018		00091019	
Temp. (°F)	71.6		71.8		71.5	
Angle	**Cylinder 1 (kΩ-cm)**		**Cylinder 2 (kΩ-cm)**		**Cylinder 3 (kΩ-cm)**	
	1st Test	**Repeat**	**1st Test**	**Repeat**	**1st Test**	**Repeat**
0°	6.28		6.73		6.14	
90°	6.37		6.69		5.97	
180°	6.14		6.42		6.21	
270°	6.71		6.47		6.28	
0°	6.35		6.92		6.16	
90°	6.45		6.9		6.16	
180°	6.26		6.3		6.16	
270°	6.76		6.45		6.16	
Average	6.4	Not Req'd	6.6	Not Req'd	6.2	Not Req'd
%CV	3.4%	Not Req'd	3.5%	Not Req'd	1.4%	Not Req'd
Average 16	Not Req'd		Not Req'd		Not Req'd	

Set Average Resistivity Determination (kΩ-cm)

Age (Days):	7
Curing Factor:	1.0
Cyl. 1 Average:	6.4
Cyl. 2 Average:	6.6
Cyl. 3 Average:	6.2
Set Average:	6
Penetrability:	High
Spec. Min.:	-
Pass/Fail:	FIO

	Cylinder 1		Cylinder 2		Cylinder 3	
Specimen	00091020		00091021		00091022	
Temp. (°F)	71.6		70.1			
Angle	**Cylinder 1 (kΩ-cm)**		**Cylinder 2 (kΩ-cm)**		**Cylinder 3 (kΩ-cm)**	
	1st Test	**Repeat**	**1st Test**	**Repeat**	**1st Test**	**Repeat**
0°	13.9		15.6		14.3	
90°	14.7		14.5		14.8	
180°	14.1		13.5		14.3	
270°	14.1		14.4		13.9	
0°	14		15.4		14.5	
90°	14.7		14.3		14.7	
180°	14		13.4		14.2	
270°	14.2		14.1		14	
Average	14.2	Not Req'd	14.4	Not Req'd	14.3	Not Req'd
%CV	2.2%	Not Req'd	5.5%	Not Req'd	2.2%	Not Req'd
Average 16	Not Req'd		Not Req'd		Not Req'd	

Set Average Resistivity Determination (kΩ-cm)

Age (Days):	28
Curing Factor:	1.0
Cyl. 1 Average:	14.2
Cyl. 2 Average:	14.4
Cyl. 3 Average:	14.3
Set Average:	14
Penetrability:	Moderate
Spec. Min.:	-
Pass/Fail:	FIO

Calculate the average and the %CV for each sample in the set. If the %CV is > 7.5%, immerse sample in water bath (68 to 77 °F) for 2 h, and record results in the "Repeat" Column. If the %CV on the "Repeat" Set is < 7.5%, use the average of the "Repeat" Set. If the %CV is > 7.5%, average all 16 readings.

Rev. 04/08/2025	SAMPLE TYPE: VER	775A-T SAMPLE OF CEMENT CONCRETE	DATE RECEIVED: 8/8/25	SAMPLE NUMBER: 2025-016280

PROJECT INFORMATION

Town/City:	STATEWIDE	*Contract No.:*	VER-CON
Contractor:	#N/A	*Federal Aid No.:*	#N/A
Report to District:	RMS	*Cost Account No.:*	#N/A
Resident Engineer:	#N/A	*District Mat. Engr.*	#N/A
Specimen Size:	4 x 8"	*Curing Method:*	Moist Cured

	Cylinder 1		Cylinder 2		Cylinder 3	
Specimen						
Temp. (°F)						

Angle	Cylinder 1 (kΩ-cm)		Cylinder 2 (kΩ-cm)		Cylinder 3 (kΩ-cm)	
	1st Test	Repeat	1st Test	Repeat	1st Test	Repeat
0°						
90°						
180°						
270°						
0°						
90°						
180°						
270°						
Average						
%CV						
Average 16						

Set Average Resistivity Determination (kΩ-cm)

Age (Days):	
Curing Factor:	1.0
Cyl. 1 Average:	
Cyl. 2 Average:	
Cyl. 3 Average:	
Set Average:	
Penetrability:	High
Spec. Min.:	
Pass/Fail:	

	Cylinder 1		Cylinder 2		Cylinder 3	
Specimen						
Temp. (°F)						

Angle	Cylinder 1 (kΩ-cm)		Cylinder 2 (kΩ-cm)		Cylinder 3 (kΩ-cm)	
	1st Test	Repeat	1st Test	Repeat	1st Test	Repeat
0°						
90°						
180°						
270°						
0°						
90°						
180°						
270°						
Average		Not Req'd		Not Req'd		Not Req'd
%CV		Not Req'd		Not Req'd		Not Req'd
Average 16	Not Req'd		Not Req'd		Not Req'd	

Set Average Resistivity Determination (kΩ-cm)

Age (Days):	
Curing Factor:	1.0
Cyl. 1 Average:	
Cyl. 2 Average:	
Cyl. 3 Average:	
Set Average:	
Penetrability:	Moderate
Spec. Min.:	
Pass/Fail:	

Calculate the average and the %CV for each sample in the set. If the %CV is > 7.5%, immerse sample in water bath (68 to 77 °F) for 2 h, and record results in the "Repeat" Column. If the %CV on the "Repeat" Set is < 7.5%, use the average of the "Repeat" Set. If the %CV is > 7.5%, average all 16 readings.

Rev. 04/08/2025	SAMPLE TYPE: VER	775A-T SAMPLE OF CEMENT CONCRETE	DATE RECEIVED: 8/8/25	SAMPLE NUMBER: 2025-016280

PROJECT INFORMATION

Town/City:	STATEWIDE	*Contract No.:*	VER-CON
Contractor:	#N/A	*Federal Aid No.:*	#N/A
Report to District:	RMS	*Cost Account No.:*	#N/A
Resident Engineer:	#N/A	*District Mat. Engr.*	#N/A

LABORATORY PREPARATION, COMPRESSIVE STRENGTH TESTING (T 22 / C39)

Sample Condition: [✓] Acceptable [ ] Unacceptable (See Remarks) *Lab Curing Method:* Moist Cured

Lab Preparation: [ ] Sulfur (T 231) [✓] Neoprene (C1231) [ ] Cutting (T 22) [ ] Grinding (T 22)

Specimen ID	Age	Unit	Break Date	Weight (lbs)	Diameter (in)	Area (in^2)	Load (lbf)	Strength (psi)	Average (psi)	Break Type	Omit
00091017	7	DAY	8/14/25	8.59	4.00	12.57	86926	6917		3	
00091018	7	DAY	8/14/25	8.59	4.00	12.57	86120	6853	6970	2	
00091019	7	DAY	8/14/25	8.59	4.00	12.57	89719	7140		2	
00091020	28	DAY	9/4/25	8.59	4.00	12.57	105051	8360		3	
00091021	28	DAY	9/4/25	8.59	4.00	12.57	111116	8842	8710	2	
00091022	28	DAY	9/4/25	8.59	4.00	12.57	112061	8918		2	
00091023	56	DAY	10/2/25								
00091024	56	DAY	10/2/25								
00091025	56	DAY	10/2/25								

Break Type T 22: 1 Cone  2 Cone & Split  3 Columnar  4 Shear  5 Side Fracture  6 Pointed 

56-day cylinders discarded: [ ] Yes

REMARKS

Need to perform T 358 testing at 7, 28, and 56-days

TESTING LABORATORY, TECHNICIAN(S), AND REVIEW

Laboratory:	RMS	*Location:*	HOPKINTON, MA
T 358 (Set 1):	Timothy Berard	*Test Date:*	8/14/25
T 358 (Set 2):	Timothy Berard	*Test Date:*	9/4/25
T 358 (Set 3):		*Test Date:*	
T 358 (Set 4):		*Test Date:*	
T 22 (Set 1):	Chris Dinoia (RF)	*Test Date:*	8/14/25
T 22 (Set 2):	Chris Dinoia (RF)	*Test Date:*	9/4/25
T 22 (Set 3):		*Test Date:*	
T 22 (Set 4):		*Test Date:*	
Reviewed By:		*Review Date:*	

SPECIFICATION LIMITS AND APPROVAL

Results are within specification limits: [ ] *Results are outside specification limits:* [ ]

Approved By:

Signature:

Date:

***Results relate only to the items inspected or tested.**

****This report shall not be reproduced, except in full, without the prior written approval of the agency.**

Rev. 04/08/2025	SAMPLE TYPE: VER	775A-T SAMPLE OF CEMENT CONCRETE	DATE RECEIVED: 8/15/25	SAMPLE NUMBER: 2025-016449

PROJECT INFORMATION

Town/City:	STATEWIDE	*Contract No.:*	VER-CON
Contractor:	#N/A	*Federal Aid No.:*	#N/A
Report to District:	RMS	*Cost Account No.:*	#N/A
Resident Engineer:	#N/A	*District Mat. Engr.*	#N/A

MATERIAL INFORMATION

Bid Item:	VER.M4	*Specification No.:*	M4
Bid Item Description:	VERIFICATION OF CEMENT CONCRETE AND RELATED MATERIALS		
Sub-Item Description:	VER.M4 - TRIAL BATCH HIGH PERFORMANCE CONCRETE		
Bid Item Quantity:	#N/A	*Date to be Used:*	2025
MassDOT Mix ID No.:	25-07-14-11-14-34-02	*Producer Mix ID No.:*	NP/DE
Produced by:	BOSTON CONCRETE CORPORATION	*Town/City, State:*	LOWELL, MA
Design Strength (psi):	5000	*Nom. Agg. Size (in.):*	3/4
Tot. Cementitious (lbs.)	685	*Mix Design Type:*	HPC
Proposed Use:	VERIFICATION OF CEMENT CONCRE	*Additional Information:*	Batch A-2 Redo

SAMPLING INFORMATION (R 60 / C172)

Date Sampled:	8/13/25	*Sampled By:*	George Gilbert
Sampling Location:	BOSTON CONCRETE CORPORATION	*Town/City, State:*	LOWELL, MA
Truck No.:	N/A	*Ticket No.:*	N/A
Sample Time:	10:26am		
Job Water Added:	N/A	*Admixtures Added:*	N/A
Random Sample:	Y	*Lot & Sub Lot No.:*	B
Quantity Represented:	1cy	*Weather & Temp. (°F):*	75-Sunny

PREPARATION OF SPECIMENS IN THE FIELD (R 100 / C31)

Specimen Size:	☑ 4 x 8" ☐ 6 x 12"	*Field Curing Method:*	☑ Curing Box ☐ Field Cured
Specimens Covered:	☑ Yes ☐ No	*Curing Temp. (°F):*	Low: 50 High: 90

SAMPLE PROPERTIES BY FIELD TESTS

Test Method	Quality Characteristic	Result	Spec. Min.	Spec. Max.	Pass/Fail	Remarks
T 119 (C143)	Slump (in.)	1.75	4.50	7.50	FIO	
T 152 (C231)	Air Content (%)	2.8	4.5	7.5	FIO	
T 309 (C1064)	Concrete Temp. (°F)	78	50	90	FIO	
T 121 (C231)	Unit Weight (pcf)	145.2	135.6	141.6	FIO	this is the Redo*

REMARKS

This is the Redo of Mix A-2, so Targets may be off, no new 043 for numbers. T358 testing at 7,28,and 56-days

FIELD TESTING OFFICE, TECHNICIAN(S), AND REVIEW

Office:	RMS	*Office Location:*	HOPKINTON, MA
Tested By:	Keith St. Jean	*Test Date:*	8/13/25
Witnessed By:	George Gilbert	*Witness Date:*	8/13/25
Reviewed By:		*Review Date:*	

SPECIFICATION LIMITS & APPROVAL

Results are within specification limits:		*Results are outside specification limits:*	

By typing my name below, I understand and agree that this form of electronic signature has the same legal force and effect as a manual signature.

Approved By:		*Approve Date:*	

Rev. 04/08/2025	SAMPLE TYPE: VER	775A-T SAMPLE OF CEMENT CONCRETE	DATE RECEIVED: 8/15/25	SAMPLE NUMBER: 2025-016449

PROJECT INFORMATION

Town/City:	STATEWIDE	*Contract No.:*	VER-CON
Contractor:	#N/A	*Federal Aid No.:*	#N/A
Report to District:	RMS	*Cost Account No.:*	#N/A
Resident Engineer:	#N/A	*District Mat. Engr.*	#N/A

CHLORIDE ION PENETRATION RESISTANCE TESTING (T 358)

Specimen Size: 4 x 8" *Curing Method:* Moist Cured

	Cylinder 1		Cylinder 2		Cylinder 3	
Specimen	00091008		00091009		00091010	
Temp. (°F)	75.9		75.9		75.5	
Angle	**Cylinder 1 (kΩ-cm)**		**Cylinder 2 (kΩ-cm)**		**Cylinder 3 (kΩ-cm)**	
	1st Test	**Repeat**	**1st Test**	**Repeat**	**1st Test**	**Repeat**
0°	7.9		7.97		7.74	
90°	7.4		8.19		8.26	
180°	7.35		7.23		7.9	
270°	6.95		7.78		7.81	
0°	8.07		8.05		7.69	
90°	7.38		8.19		8.17	
180°	7.43		7.31		7.78	
270°	7.16		7.74		7.69	
Average	7.5	Not Req'd	7.8	Not Req'd	7.9	Not Req'd
%CV	4.9%	Not Req'd	4.8%	Not Req'd	2.8%	Not Req'd
Average 16	Not Req'd		Not Req'd		Not Req'd	

Set Average Resistivity Determination (kΩ-cm)

Age (Days):	7
Curing Factor:	1.0
Cyl. 1 Average:	7.5
Cyl. 2 Average:	7.8
Cyl. 3 Average:	7.9
Set Average:	8
Penetrability:	High
Spec. Min.:	-
Pass/Fail:	FIO

	Cylinder 1		Cylinder 2		Cylinder 3	
Specimen	00091011		00091012		00091013	
Temp. (°F)	70.2		70.3		70.3	
Angle	**Cylinder 1 (kΩ-cm)**		**Cylinder 2 (kΩ-cm)**		**Cylinder 3 (kΩ-cm)**	
	1st Test	**Repeat**	**1st Test**	**Repeat**	**1st Test**	**Repeat**
0°	37.3		35.7		33.6	
90°	33.3		35.2		34.8	
180°	33.1		32.9		34.4	
270°	34.1		35.1		35.4	
0°	37.2		36.1		33.6	
90°	33.1		35.5		34.7	
180°	33.2		33		34.5	
270°	34.2		35.3		35.6	
Average	34.4	Not Req'd	34.9	Not Req'd	34.6	Not Req'd
%CV	5.2%	Not Req'd	3.5%	Not Req'd	2.1%	Not Req'd
Average 16	Not Req'd		Not Req'd		Not Req'd	

Set Average Resistivity Determination (kΩ-cm)

Age (Days):	28
Curing Factor:	1.0
Cyl. 1 Average:	34.4
Cyl. 2 Average:	34.9
Cyl. 3 Average:	34.6
Set Average:	35
Penetrability:	Low
Spec. Min.:	21
Pass/Fail:	

Calculate the average and the %CV for each sample in the set. If the %CV is > 7.5%, immerse sample in water bath (68 to 77 °F) for 2 h, and record results in the "Repeat" Column. If the %CV on the "Repeat" Set is < 7.5%, use the average of the "Repeat" Set. If the %CV is > 7.5%, average all 16 readings.

Rev. 04/08/2025	SAMPLE TYPE: VER	775A-T SAMPLE OF CEMENT CONCRETE	DATE RECEIVED: 8/15/25	SAMPLE NUMBER: 2025-016449

PROJECT INFORMATION

Town/City:	STATEWIDE	*Contract No.:*	VER-CON
Contractor:	#N/A	*Federal Aid No.:*	#N/A
Report to District:	RMS	*Cost Account No.:*	#N/A
Resident Engineer:	#N/A	*District Mat. Engr.*	#N/A

	Cylinder 1		Cylinder 2		Cylinder 3	
Specimen	00091014		00091015		00091016	
Temp. (°F)						

Angle	Cylinder 1 (kΩ-cm)		Cylinder 2 (kΩ-cm)		Cylinder 3 (kΩ-cm)	
	1st Test	Repeat	1st Test	Repeat	1st Test	Repeat
0°						
90°						
180°						
270°						
0°						
90°						
180°						
270°						
Average						
%CV						
Average 16						

Set Average Resistivity Determination (kΩ-cm)

Age (Days):	56
Curing Factor:	1.0
Cyl. 1 Average:	
Cyl. 2 Average:	
Cyl. 3 Average:	
Set Average:	
Penetrability:	Low
Spec. Min.:	
Pass/Fail:	

Calculate the average and the %CV for each sample in the set. If the %CV is > 7.5%, immerse sample in water bath (68 to 77 °F) for 2 h, and record results in the "Repeat" Column. If the %CV on the "Repeat" Set is < 7.5%, use the average of the "Repeat" Set. If the %CV is > 7.5%, average all 16 readings.

Rev. 04/08/2025	SAMPLE TYPE: VER	775A-T SAMPLE OF CEMENT CONCRETE	DATE RECEIVED: 8/15/25	SAMPLE NUMBER: 2025-016449

PROJECT INFORMATION

Town/City:	STATEWIDE	*Contract No.:*	VER-CON
Contractor:	#N/A	*Federal Aid No.:*	#N/A
Report to District:	RMS	*Cost Account No.:*	#N/A
Resident Engineer:	#N/A	*District Mat. Engr.*	#N/A

LABORATORY PREPARATION, COMPRESSIVE STRENGTH TESTING (T 22 / C39)

Sample Condition: [✓] Acceptable [ ] Unacceptable (See Remarks) *Lab Curing Method:* Moist Cured

Lab Preparation: [ ] Sulfur (T 231) [✓] Neoprene (C1231) [ ] Cutting (T 22) [✓] Grinding (T 22)

Specimen ID	Age	Unit	Break Date	Weight (lbs)	Diameter (in)	Area (in^2)	Load (lbf)	Strength (psi)	Average (psi)	Break Type	Omit
00091008	7	DAY	8/20/25	8.61	4.01	12.63	90524	7168	7100	5	
00091009	7	DAY	8/20/25	8.61	4.01	12.63	90558	7170		5	
00091010	7	DAY	8/20/25	8.61	4.01	12.63	88095	6975		5	
00091011	28	DAY	9/10/25	8.61	4.01	12.63	108561	8596	8670	3	
00091012	28	DAY	9/10/25	8.61	4.01	12.63	106095	8401		2	
00091013	28	DAY	9/10/25	8.61	4.01	12.63	113971	9024		2	
00091014	56	DAY	10/8/25								
00091015	56	DAY	10/8/25								
00091016	56	DAY	10/8/25								

Break Type T 22: 1 Cone 2 Cone & Split 3 Columnar 4 Shear 5 Side Fracture 6 Pointed

56-day cylinders discarded: [ ] Yes

REMARKS

T358 testing at 7,28,and 56-days

TESTING LABORATORY, TECHNICIAN(S), AND REVIEW

Laboratory:	RMS	*Location:*	HOPKINTON, MA
T 358 (Set 1):	Casey Flynn	*Test Date:*	8/20/25
T 358 (Set 2):	Timothy Berard	*Test Date:*	9/10/25
T 358 (Set 3):	Casey Flynn	*Test Date:*	8/20/25
T 22 (Set 1):	Timothy Berard	*Test Date:*	9/10/25
T 22 (Set 2):		*Test Date:*	
T 22 (Set 3):		*Test Date:*	
T 22 (Set 4):		*Test Date:*	
Reviewed By:		*Review Date:*	

SPECIFICATION LIMITS AND APPROVAL

Results are within specification limits: [ ] *Results are outside specification limits:* [ ]

Approved By:

Signature:

Date:

Rev. 04/08/2025	SAMPLE TYPE: VER	775A-T SAMPLE OF CEMENT CONCRETE	DATE RECEIVED: 8/8/25	SAMPLE NUMBER: 2025-016281

PROJECT INFORMATION

Town/City:	STATEWIDE	*Contract No.:*	VER-CON
Contractor:	#N/A	*Federal Aid No.:*	#N/A
Report to District:	RMS	*Cost Account No.:*	#N/A
Resident Engineer:	#N/A	*District Mat. Engr.*	#N/A

MATERIAL INFORMATION

Bid Item:	VER.M4	*Specification No.:*	M4
Bid Item Description:	VERIFICATION OF CEMENT CONCRETE AND RELATED MATERIALS		
Sub-Item Description:	VER.M4 - TRIAL BATCH HIGH PERFORMANCE CONCRETE		
Bid Item Quantity:	#N/A	*Date to be Used:*	2025
MassDOT Mix ID No.:	25-07-14-11-14-34-04	*Producer Mix ID No.:*	NANO SILICA
Produced by:	BOSTON CONCRETE CORPORATION	*Town/City, State:*	LOWELL, MA
Design Strength (psi):	5000	*Nom. Agg. Size (in.):*	3/4
Tot. Cementitious (lbs.)	615	*Mix Design Type:*	HPC
Proposed Use:	VERIFICATION OF CEMENT CONCRE	*Additional Information:*	

SAMPLING INFORMATION (R 60 / C172)

Date Sampled:	8/7/25	*Sampled By:*	George Gilbert
Sampling Location:	BOSTON CONCRETE CORPORATION	*Town/City, State:*	LOWELL, MA
Truck No.:	N/A	*Ticket No.:*	N/A
Sample Time:	11:20am		
Job Water Added:	N/A	*Admixtures Added:*	N/A
Random Sample:	Y	*Lot & Sub Lot No.:*	1-1
Quantity Represented:	N/A	*Weather & Temp. (°F):*	63-sunny

PREPARATION OF SPECIMENS IN THE FIELD (R 100 / C31)

Specimen Size:	☑ 4 x 8" ☐ 6 x 12"	*Field Curing Method:*	☑ Curing Box ☐ Field Cured
Specimens Covered:	☑ Yes ☐ No	*Curing Temp. (°F):*	Low: 50 High: 90

SAMPLE PROPERTIES BY FIELD TESTS

Test Method	Quality Characteristic	Result	Spec. Min.	Spec. Max.	Pass/Fail	Remarks
T 119 (C143)	Slump (in.)	6.50	3.00	6.00	FIO	
T 152 (C231)	Air Content (%)	7.6	4.5	7.5	FIO	
T 309 (C1064)	Concrete Temp. (°F)	76	50	90	FIO	
T 121 (C231)	Unit Weight (pcf)	137.8	137.8	143.8	FIO	

REMARKS

Need to perform T-358 testing at 7,28, and 56 days.

FIELD TESTING OFFICE, TECHNICIAN(S), AND REVIEW

Office:	RMS	*Office Location:*	HOPKINTON, MA
Tested By:	Kieth St. Jean	*Test Date:*	8/7/25
Witnessed By:	George Gilbert	*Witness Date:*	8/7/25
Reviewed By:		*Review Date:*	

SPECIFICATION LIMITS & APPROVAL

Results are within specification limits:		*Results are outside specification limits:*	

By typing my name below, I understand and agree that this form of electronic signature has the same legal force and effect as a manual signature.

Approved By:		*Approve Date:*	

massDOT Highway	SAMPLE TYPE:	775A-T	DATE RECEIVED:	SAMPLE NUMBER:
Rev. 04/08/2025	VER	SAMPLE OF CEMENT CONCRETE	8/8/25	2025-016281

PROJECT INFORMATION

Town/City:	STATEWIDE	*Contract No.:*	VER-CON
Contractor:	#N/A	*Federal Aid No.:*	#N/A
Report to District:	RMS	*Cost Account No.:*	#N/A
Resident Engineer:	#N/A	*District Mat. Engr.*	#N/A

CHLORIDE ION PENETRATION RESISTANCE TESTING (T 358)

Specimen Size: 4 x 8" *Curing Method:* Moist Cured

	Cylinder 1		Cylinder 2		Cylinder 3	
Specimen	00090999		00091000		9091001	
Temp. (°F)	71.5		71.4		71.4	
Angle	**Cylinder 1 (kΩ-cm)**		**Cylinder 2 (kΩ-cm)**		**Cylinder 3 (kΩ-cm)**	
	1st Test	**Repeat**	**1st Test**	**Repeat**	**1st Test**	**Repeat**
0°	6.66		6.61		6.42	
90°	6.3		6.26		6.14	
180°	6.02		6.26		5.85	
270°	6.54		6.57		5.92	
0°	6.66		6.57		6.28	
90°	6.18		6.18		6.09	
180°	5.97		6.16		5.87	
270°	6.4		6.59		5.92	
Average	6.3	Not Req'd	6.4	Not Req'd	6.1	Not Req'd
%CV	4.3%	Not Req'd	3.1%	Not Req'd	3.4%	Not Req'd
Average 16	Not Req'd		Not Req'd		Not Req'd	

Set Average Resistivity Determination (kΩ-cm)

Age (Days):	7
Curing Factor:	1.0
Cyl. 1 Average:	6.3
Cyl. 2 Average:	6.4
Cyl. 3 Average:	6.1
Set Average:	6
Penetrability:	High
Spec. Min.:	-
Pass/Fail:	FIO

	Cylinder 1		Cylinder 2		Cylinder 3	
Specimen	00091002		00091003		00091004	
Temp. (°F)	71.4		71.7		70.9	
Angle	**Cylinder 1 (kΩ-cm)**		**Cylinder 2 (kΩ-cm)**		**Cylinder 3 (kΩ-cm)**	
	1st Test	**Repeat**	**1st Test**	**Repeat**	**1st Test**	**Repeat**
0°	9.12		8.95		9.22	
90°	8.76		9.36		9	
180°	9.48		9.6		9.03	
270°	9.17		9.34		9.19	
0°	9.03		8.93		9.14	
90°	8.86		9.43		9.12	
180°	9.36		9.1		9.03	
270°	9.14		9.26		9.22	
Average	9.1	Not Req'd	9.2	Not Req'd	9.1	Not Req'd
%CV	2.6%	Not Req'd	2.6%	Not Req'd	1.0%	Not Req'd
Average 16	Not Req'd		Not Req'd		Not Req'd	

Set Average Resistivity Determination (kΩ-cm)

Age (Days):	28
Curing Factor:	1.0
Cyl. 1 Average:	9.1
Cyl. 2 Average:	9.2
Cyl. 3 Average:	9.1
Set Average:	9
Penetrability:	High
Spec. Min.:	-
Pass/Fail:	FIO

Calculate the average and the %CV for each sample in the set. If the %CV is > 7.5%, immerse sample in water bath (68 to 77 °F) for 2 h, and record results in the "Repeat" Column. If the %CV on the "Repeat" Set is < 7.5%, use the average of the

Rev. 04/08/2025	SAMPLE TYPE: VER	775A-T SAMPLE OF CEMENT CONCRETE	DATE RECEIVED: 8/8/25	SAMPLE NUMBER: 2025-016281

PROJECT INFORMATION

Town/City:	STATEWIDE	*Contract No.:*	VER-CON
Contractor:	#N/A	*Federal Aid No.:*	#N/A
Report to District:	RMS	*Cost Account No.:*	#N/A
Resident Engineer:	#N/A	*District Mat. Engr.*	#N/A

"Repeat" Set. If the %CV is > 7.5%, average all 16 readings.

Specimen Size:	4 x 8"	*Curing Method:*	Moist Cured

	Cylinder 1		Cylinder 2		Cylinder 3	
Specimen						
Temp. (°F)						

Angle	**Cylinder 1 (kΩ-cm)**		**Cylinder 2 (kΩ-cm)**		**Cylinder 3 (kΩ-cm)**	
	1st Test	**Repeat**	**1st Test**	**Repeat**	**1st Test**	**Repeat**
0°						
90°						
180°						
270°						
0°						
90°						
180°						
270°						
Average						
%CV						
Average 16						

Set Average Resistivity Determination (kΩ-cm)

Age (Days):	
Curing Factor:	1.0
Cyl. 1 Average:	
Cyl. 2 Average:	
Cyl. 3 Average:	
Set Average:	
Penetrability:	High
Spec. Min.:	
Pass/Fail:	

	Cylinder 1		Cylinder 2		Cylinder 3	
Specimen						
Temp. (°F)						

Angle	**Cylinder 1 (kΩ-cm)**		**Cylinder 2 (kΩ-cm)**		**Cylinder 3 (kΩ-cm)**	
	1st Test	**Repeat**	**1st Test**	**Repeat**	**1st Test**	**Repeat**
0°						
90°						
180°						
270°						
0°						
90°						
180°						
270°						
Average		Not Req'd		Not Req'd		Not Req'd
%CV		Not Req'd		Not Req'd		Not Req'd
Average 16	Not Req'd		Not Req'd		Not Req'd	

Set Average Resistivity Determination (kΩ-cm)

Age (Days):	
Curing Factor:	1.0
Cyl. 1 Average:	
Cyl. 2 Average:	
Cyl. 3 Average:	
Set Average:	
Penetrability:	High
Spec. Min.:	
Pass/Fail:	

Calculate the average and the %CV for each sample in the set. If the %CV is > 7.5%, immerse sample in water bath (68 to 77 °F) for 2 h, and record results in the "Repeat" Column. If the %CV on the "Repeat" Set is < 7.5%, use the average of the "Repeat" Set. If the %CV is > 7.5%, average all 16 readings.

Rev. 04/08/2025	SAMPLE TYPE: VER	775A-T SAMPLE OF CEMENT CONCRETE	DATE RECEIVED: 8/8/25	SAMPLE NUMBER: 2025-016281

PROJECT INFORMATION

Town/City:	STATEWIDE	*Contract No.:*	VER-CON
Contractor:	#N/A	*Federal Aid No.:*	#N/A
Report to District:	RMS	*Cost Account No.:*	#N/A
Resident Engineer:	#N/A	*District Mat. Engr.*	#N/A

LABORATORY PREPARATION, COMPRESSIVE STRENGTH TESTING (T 22 / C39)

Sample Condition: [✓] Acceptable [ ] Unacceptable (See Remarks) *Lab Curing Method:* Moist Cured

Lab Preparation: [ ] Sulfur (T 231) [✓] Neoprene (C1231) [ ] Cutting (T 22) [ ] Grinding (T 22)

Specimen ID	Age	Unit	Break Date	Weight (lbs)	Diameter (in)	Area (in^2)	Load (lbf)	Strength (psi)	Average (psi)	Break Type	Omit
00090999	7	DAY	8/14/25	8.37	4.00	12.57	64571	5138		3	
00091000	7	DAY	8/14/25	8.37	4.00	12.57	64816	5158	5200	3	
00091001	7	DAY	8/14/25	8.37	4.00	12.57	66508	5293		3	
00091002	28	DAY	9/4/25	8.37	4.00	12.57	76564	6093		2	
00091003	28	DAY	9/4/25	8.37	4.00	12.57	76425	6082	6130	3	
00091004	28	DAY	9/4/25	8.37	4.00	12.57	78017	6208		3	
00091005	56	DAY	10/2/25								
00091006	56	DAY	10/2/25								
00091007	56	DAY	10/2/25								

Break Type T 22: 1 Cone  2 Cone & Split  3 Columnar  4 Shear  5 Side Fracture  6 Pointed 

56-day cylinders discarded: [ ] Yes

REMARKS

Need to perform T-358 testing at 7,28, and 56 days.

TESTING LABORATORY, TECHNICIAN(S), AND REVIEW

Laboratory:	RMS	*Location:*	HOPKINTON, MA
T 358 (Set 1):	Timothy Berard	*Test Date:*	8/14/25
T 358 (Set 2):	Timothy Berard	*Test Date:*	9/4/25
T 358 (Set 3):		*Test Date:*	
T 358 (Set 4):		*Test Date:*	
T 22 (Set 1):	Chris Dinoia (RF)	*Test Date:*	8/14/25
T 22 (Set 2):	Chris Dinoia (RF)	*Test Date:*	9/4/25
T 22 (Set 3):		*Test Date:*	
T 22 (Set 4):		*Test Date:*	
Reviewed By:		*Review Date:*	

SPECIFICATION LIMITS AND APPROVAL

Results are within specification limits: [ ] *Results are outside specification limits:* [ ]

Approved By:

Signature:

Date:

***Results relate only to the items inspected or tested.**

****This report shall not be reproduced, except in full, without the prior written approval of the agency.**

Rev. 04/08/2025	SAMPLE TYPE: VER	775A-T SAMPLE OF CEMENT CONCRETE	DATE RECEIVED: 8/15/25	SAMPLE NUMBER: 2025-016450

PROJECT INFORMATION

Town/City:	STATEWIDE	*Contract No.:*	VER-CON
Contractor:	#N/A	*Federal Aid No.:*	#N/A
Report to District:	RMS	*Cost Account No.:*	#N/A
Resident Engineer:	#N/A	*District Mat. Engr.*	#N/A

MATERIAL INFORMATION

Bid Item:	VER.M4	*Specification No.:*	M4
Bid Item Description:	VERIFICATION OF CEMENT CONCRETE AND RELATED MATERIALS		
Sub-Item Description:	VER.M4 - TRIAL BATCH HIGH PERFORMANCE CONCRETE		
Bid Item Quantity:	#N/A	*Date to be Used:*	2025
MassDOT Mix ID No.:	25-08-08-08-19-04-01	*Producer Mix ID No.:*	S-120/GGP-GS
Produced by:	BOSTON CONCRETE CORPORATION	*Town/City, State:*	LOWELL, MA
Design Strength (psi):	5000	*Nom. Agg. Size (in.):*	3/4
Tot. Cementitious (lbs.)	685	*Mix Design Type:*	HPC
Proposed Use:	VERIFICATION OF CEMENT CONCRE	*Additional Information:*	

SAMPLING INFORMATION (R 60 / C172)

Date Sampled:	8/13/25	*Sampled By:*	George Gilbert
Sampling Location:	BOSTON CONCRETE CORPORATION	*Town/City, State:*	LOWELL, MA
Truck No.:	N/A	*Ticket No.:*	N/A
Sample Time:	10:44am		
Job Water Added:	N/A	*Admixtures Added:*	N/A
Random Sample:	Y	*Lot & Sub Lot No.:*	B
Quantity Represented:	1cy	*Weather & Temp. (°F):*	75-Sunny

PREPARATION OF SPECIMENS IN THE FIELD (R 100 / C31)

Specimen Size:	☑ 4 x 8" ☐ 6 x 12"	*Field Curing Method:*	☑ Curing Box ☐ Field Cured
Specimens Covered:	☑ Yes ☐ No	*Curing Temp. (°F):*	Low: 50 High: 90

SAMPLE PROPERTIES BY FIELD TESTS

Test Method	Quality Characteristic	Result	Spec. Min.	Spec. Max.	Pass/Fail	Remarks
T 119 (C143)	Slump (in.)	8.75	4.50	7.50	FIO	
T 152 (C231)	Air Content (%)	6.0	4.5	7.5	FIO	
T 309 (C1064)	Concrete Temp. (°F)	78	50	90	FIO	
T 121 (C231)	Unit Weight (pcf)	139.8	136.9	142.9	FIO	

REMARKS

T358 testing at 7,28,and 56-days

FIELD TESTING OFFICE, TECHNICIAN(S), AND REVIEW

Office:	RMS	*Office Location:*	HOPKINTON, MA
Tested By:	Keith St. Jean	*Test Date:*	8/13/25
Witnessed By:	George Gilbert	*Witness Date:*	8/13/25
Reviewed By:		*Review Date:*	

SPECIFICATION LIMITS & APPROVAL

Results are within specification limits:		*Results are outside specification limits:*	

By typing my name below, I understand and agree that this form of electronic signature has the same legal force and effect as a manual signature.

Approved By:		*Approve Date:*	

Rev. 04/08/2025	SAMPLE TYPE: VER	775A-T SAMPLE OF CEMENT CONCRETE	DATE RECEIVED: 8/15/25	SAMPLE NUMBER: 2025-016450

PROJECT INFORMATION

Town/City:	STATEWIDE	*Contract No.:*	VER-CON
Contractor:	#N/A	*Federal Aid No.:*	#N/A
Report to District:	RMS	*Cost Account No.:*	#N/A
Resident Engineer:	#N/A	*District Mat. Engr.*	#N/A

CHLORIDE ION PENETRATION RESISTANCE TESTING (T 358)

Specimen Size: 4 x 8" *Curing Method:* Moist Cured

	Cylinder 1		Cylinder 2		Cylinder 3	
Specimen	00091086		00091087		00091088	
Temp. (°F)	74.3		73.6		73.4	
Angle	**Cylinder 1 (kΩ-cm)**		**Cylinder 2 (kΩ-cm)**		**Cylinder 3 (kΩ-cm)**	
	1st Test	**Repeat**	**1st Test**	**Repeat**	**1st Test**	**Repeat**
0°	6.47		6.69		6.8	
90°	6.85		6.88		7.26	
180°	6.52		6.33		6.83	
270°	6.78		6.59		6.66	
0°	6.47		6.57		6.71	
90°	6.8		6.76		7.28	
180°	6.59		6.3		6.85	
270°	6.61		6.45		6.73	
Average	6.6	Not Req'd	6.6	Not Req'd	6.9	Not Req'd
%CV	2.3%	Not Req'd	3.1%	Not Req'd	3.5%	Not Req'd
Average 16	Not Req'd		Not Req'd		Not Req'd	

Set Average Resistivity Determination (kΩ-cm)

Age (Days):	7
Curing Factor:	1.0
Cyl. 1 Average:	6.6
Cyl. 2 Average:	6.6
Cyl. 3 Average:	6.9
Set Average:	7
Penetrability:	High
Spec. Min.:	-
Pass/Fail:	FIO

	Cylinder 1		Cylinder 2		Cylinder 3	
Specimen	00091089		00091090		00091091	
Temp. (°F)	70.1		70.1		70.3	
Angle	**Cylinder 1 (kΩ-cm)**		**Cylinder 2 (kΩ-cm)**		**Cylinder 3 (kΩ-cm)**	
	1st Test	**Repeat**	**1st Test**	**Repeat**	**1st Test**	**Repeat**
0°	21.3		22.5		20.3	
90°	20.7		20.6		21.5	
180°	19.1		19.7		21.8	
270°	19.3		20.2		20.1	
0°	21.3		22.6		20.1	
90°	20.5		20.4		21.6	
180°	19.2		19.5		21.5	
270°	19.6		20.2		20	
Average	20.1	Not Req'd	20.7	Not Req'd	20.9	Not Req'd
%CV	4.6%	Not Req'd	5.7%	Not Req'd	3.8%	Not Req'd
Average 16	Not Req'd		Not Req'd		Not Req'd	

Set Average Resistivity Determination (kΩ-cm)

Age (Days):	28
Curing Factor:	1.0
Cyl. 1 Average:	20.1
Cyl. 2 Average:	20.7
Cyl. 3 Average:	20.9
Set Average:	21
Penetrability:	Moderate
Spec. Min.:	21
Pass/Fail:	

Calculate the average and the %CV for each sample in the set. If the %CV is > 7.5%, immerse sample in water bath (68 to 77 °F) for 2 h, and record results in the "Repeat" Column. If the %CV on the "Repeat" Set is < 7.5%, use the average of the "Repeat" Set. If the %CV is > 7.5%, average all 16 readings.

Rev. 04/08/2025	SAMPLE TYPE: VER	775A-T SAMPLE OF CEMENT CONCRETE	DATE RECEIVED: 8/15/25	SAMPLE NUMBER: 2025-016450

PROJECT INFORMATION

Town/City:	STATEWIDE	*Contract No.:*	VER-CON
Contractor:	#N/A	*Federal Aid No.:*	#N/A
Report to District:	RMS	*Cost Account No.:*	#N/A
Resident Engineer:	#N/A	*District Mat. Engr.*	#N/A

	Cylinder 1		Cylinder 2		Cylinder 3	
Specimen	00091092		00091093		00091094	
Temp. (°F)						

Angle	Cylinder 1 (kΩ-cm)		Cylinder 2 (kΩ-cm)		Cylinder 3 (kΩ-cm)	
	1st Test	Repeat	1st Test	Repeat	1st Test	Repeat
0°						
90°						
180°						
270°						
0°						
90°						
180°						
270°						
Average		Not Req'd		Not Req'd		Not Req'd
%CV		Not Req'd		Not Req'd		Not Req'd
Average 16	Not Req'd		Not Req'd		Not Req'd	

Set Average Resistivity Determination (kΩ-cm)

Age (Days):	56
Curing Factor:	1.0
Cyl. 1 Average:	Not Req'd
Cyl. 2 Average:	Not Req'd
Cyl. 3 Average:	Not Req'd
Set Average:	
Penetrability:	Moderate
Spec. Min.:	
Pass/Fail:	

Calculate the average and the %CV for each sample in the set. If the %CV is > 7.5%, immerse sample in water bath (68 to 77 °F) for 2 h, and record results in the "Repeat" Column. If the %CV on the "Repeat" Set is < 7.5%, use the average of the "Repeat" Set. If the %CV is > 7.5%, average all 16 readings.

Rev. 04/08/2025	SAMPLE TYPE: VER	775A-T SAMPLE OF CEMENT CONCRETE	DATE RECEIVED: 8/15/25	SAMPLE NUMBER: 2025-016450

PROJECT INFORMATION

Town/City:	STATEWIDE	*Contract No.:*	VER-CON
Contractor:	#N/A	*Federal Aid No.:*	#N/A
Report to District:	RMS	*Cost Account No.:*	#N/A
Resident Engineer:	#N/A	*District Mat. Engr.*	#N/A

LABORATORY PREPARATION, COMPRESSIVE STRENGTH TESTING (T 22 / C39)

Sample Condition: [✓] Acceptable [ ] Unacceptable (See Remarks) *Lab Curing Method:* Moist Cured

Lab Preparation: [ ] Sulfur (T 231) [✓] Neoprene (C1231) [ ] Cutting (T 22) [ ] Grinding (T 22)

Specimen ID	Age	Unit	Break Date	Weight (lbs)	Diameter (in)	Area (in^2)	Load (lbf)	Strength (psi)	Average (psi)	Break Type	Omit
00091086	7	DAY	8/20/25	8.34	4.01	12.63	58742	4651		5	
00091087	7	DAY	8/20/25	8.34	4.01	12.63	60370	4780	4740	5	
00091088	7	DAY	8/20/25	8.34	4.01	12.63	60490	4790		5	
00091089	28	DAY	9/10/25	8.34	4.01	12.63	80934	6408		2	
00091090	28	DAY	9/10/25	8.34	4.01	12.63	82513	6533	6480	3	
00091091	28	DAY	9/10/25	8.34	4.01	12.63	82126	6503		3	
00091092	56	DAY	10/8/25								
00091093	56	DAY	10/8/25								
00091094	56	DAY	10/8/25								

Break Type T 22: 1 Cone  2 Cone & Split  3 Columnar  4 Shear  5 Side Fracture  6 Pointed 

56-day cylinders discarded: [ ] Yes

REMARKS

T358 testing at 7,28,and 56-days

TESTING LABORATORY, TECHNICIAN(S), AND REVIEW

Laboratory:	RMS	*Location:*	HOPKINTON, MA
T 358 (Set 1):	Casey Flynn	*Test Date:*	8/20/25
T 358 (Set 2):	Timothy Berard	*Test Date:*	9/10/25
T 358 (Set 3):	Casey Flynn	*Test Date:*	8/20/25
T 22 (Set 1):	Chris Dinoia (RF)	*Test Date:*	9/10/25
T 22 (Set 2):		*Test Date:*	
T 22 (Set 3):		*Test Date:*	
T 22 (Set 4):		*Test Date:*	
Reviewed By:		*Review Date:*	

SPECIFICATION LIMITS AND APPROVAL

Results are within specification limits: [ ] *Results are outside specification limits:* [ ]

Approved By:

Signature:

Date:

***Results relate only to the items inspected or tested.**

****This report shall not be reproduced, except in full, without the prior written approval of the agency.**

Rev. 04/08/2025	SAMPLE TYPE: VER	775A-T SAMPLE OF CEMENT CONCRETE	DATE RECEIVED: 8/15/25	SAMPLE NUMBER: 2025-016446

PROJECT INFORMATION

Town/City:	STATEWIDE	*Contract No.:*	VER-CON
Contractor:	#N/A	*Federal Aid No.:*	#N/A
Report to District:	RMS	*Cost Account No.:*	#N/A
Resident Engineer:	#N/A	*District Mat. Engr.*	#N/A

MATERIAL INFORMATION

Bid Item:	VER.M4	*Specification No.:*	M4
Bid Item Description:	VERIFICATION OF CEMENT CONCRETE AND RELATED MATERIALS		
Sub-Item Description:	VER.M4 - TRIAL BATCH HIGH PERFORMANCE CONCRETE		
Bid Item Quantity:	#N/A	*Date to be Used:*	2025
MassDOT Mix ID No.:	25-07-14-10-50-41-02	*Producer Mix ID No.:*	S-120 (40%)
Produced by:	BOSTON CONCRETE CORPORATION	*Town/City, State:*	LOWELL, MA
Design Strength (psi):	5000	*Nom. Agg. Size (in.):*	3/4
Tot. Cementitious (lbs.)	615	*Mix Design Type:*	HPC
Proposed Use:	VERIFICATION OF CEMENT CONCRE	*Additional Information:*	

SAMPLING INFORMATION (R 60 / C172)

Date Sampled:	8/13/25	*Sampled By:*	George Gilbert
Sampling Location:	BOSTON CONCRETE CORPORATION	*Town/City, State:*	LOWELL, MA
Truck No.:	N/A	*Ticket No.:*	N/A
Sample Time:	9:00am		
Job Water Added:	N/A	*Admixtures Added:*	N/A
Random Sample:	Y	*Lot & Sub Lot No.:*	B
Quantity Represented:	1cy	*Weather & Temp. (°F):*	75-Sunny

PREPARATION OF SPECIMENS IN THE FIELD (R 100 / C31)

Specimen Size:	☑ 4 x 8" ☐ 6 x 12"	*Field Curing Method:*	☑ Curing Box ☐ Field Cured
Specimens Covered:	☑ Yes ☐ No	*Curing Temp. (°F):*	Low: 50 High: 90

SAMPLE PROPERTIES BY FIELD TESTS

Test Method	Quality Characteristic	Result	Spec. Min.	Spec. Max.	Pass/Fail	Remarks
T 119 (C143)	Slump (in.)	8.75	4.50	7.50	FIO	
T 152 (C231)	Air Content (%)	8.0	4.5	7.5	FIO	
T 309 (C1064)	Concrete Temp. (°F)	78	50	90	FIO	
T 121 (C231)	Unit Weight (pcf)	136.4	137.1	143.1	FIO	

REMARKS

T358 testing at 7,28,and 56-days

FIELD TESTING OFFICE, TECHNICIAN(S), AND REVIEW

Office:	RMS	*Office Location:*	HOPKINTON, MA
Tested By:	Keith St. Jean	*Test Date:*	8/13/25
Witnessed By:	George Gilbert	*Witness Date:*	8/13/25
Reviewed By:		*Review Date:*	

SPECIFICATION LIMITS & APPROVAL

Results are within specification limits:		*Results are outside specification limits:*	

By typing my name below, I understand and agree that this form of electronic signature has the same legal force and effect as a manual signature.

Approved By:		*Approve Date:*	

Rev. 04/08/2025	SAMPLE TYPE: VER	775A-T SAMPLE OF CEMENT CONCRETE	DATE RECEIVED: 8/15/25	SAMPLE NUMBER: 2025-016446

PROJECT INFORMATION

Town/City:	STATEWIDE	*Contract No.:*	VER-CON
Contractor:	#N/A	*Federal Aid No.:*	#N/A
Report to District:	RMS	*Cost Account No.:*	#N/A
Resident Engineer:	#N/A	*District Mat. Engr.*	#N/A

CHLORIDE ION PENETRATION RESISTANCE TESTING (T 358)

Specimen Size: 4 x 8" *Curing Method:* Moist Cured

	Cylinder 1		Cylinder 2		Cylinder 3	
Specimen	00091062		00091063		00091064	
Temp. (°F)	76.4		76.1		75.9	
Angle	**Cylinder 1 (kΩ-cm)**		**Cylinder 2 (kΩ-cm)**		**Cylinder 3 (kΩ-cm)**	
	1st Test	**Repeat**	**1st Test**	**Repeat**	**1st Test**	**Repeat**
0°	12.2		12.1		13.2	
90°	12.2		12.4		12.9	
180°	12.8		12.9		12.2	
270°	12		12		12.1	
0°	12.1		12.2		12.9	
90°	12.4		12.2		12.9	
180°	12.9		13.1		11.9	
270°	12.2		11.9		12	
Average	12.4	Not Req'd	12.4	Not Req'd	12.5	Not Req'd
%CV	2.7%	Not Req'd	3.5%	Not Req'd	4.1%	Not Req'd
Average 16	Not Req'd		Not Req'd		Not Req'd	

Set Average Resistivity Determination (kΩ-cm)

Age (Days):	7
Curing Factor:	1.0
Cyl. 1 Average:	12.4
Cyl. 2 Average:	12.4
Cyl. 3 Average:	12.5
Set Average:	12
Penetrability:	Moderate
Spec. Min.:	-
Pass/Fail:	FIO

	Cylinder 1		Cylinder 2		Cylinder 3	
Specimen	00091065		00091066		00091067	
Temp. (°F)	70.6		70.6		70.9	
Angle	**Cylinder 1 (kΩ-cm)**		**Cylinder 2 (kΩ-cm)**		**Cylinder 3 (kΩ-cm)**	
	1st Test	**Repeat**	**1st Test**	**Repeat**	**1st Test**	**Repeat**
0°	21.5		23		23.6	
90°	21.1		21.8		25.3	
180°	21.6		20.8		21.6	
270°	20.6		22.8		22.4	
0°	21.6		23		23.4	
90°	21.5		22.1		25.7	
180°	21.5		20.7		21.4	
270°	20.8		22.6		22.4	
Average	21.3	Not Req'd	22.1	Not Req'd	23.2	Not Req'd
%CV	1.8%	Not Req'd	4.2%	Not Req'd	6.9%	Not Req'd
Average 16	Not Req'd		Not Req'd		Not Req'd	

Set Average Resistivity Determination (kΩ-cm)

Age (Days):	28
Curing Factor:	1.0
Cyl. 1 Average:	21.3
Cyl. 2 Average:	22.1
Cyl. 3 Average:	23.2
Set Average:	22
Penetrability:	Low
Spec. Min.:	21
Pass/Fail:	

Calculate the average and the %CV for each sample in the set. If the %CV is > 7.5%, immerse sample in water bath (68 to 77 °F) for 2 h, and record results in the "Repeat" Column. If the %CV on the "Repeat" Set is < 7.5%, use the average of the "Repeat" Set. If the %CV is > 7.5%, average all 16 readings.

Rev. 04/08/2025	SAMPLE TYPE: VER	775A-T SAMPLE OF CEMENT CONCRETE	DATE RECEIVED: 8/15/25	SAMPLE NUMBER: 2025-016446

PROJECT INFORMATION

Town/City:	STATEWIDE	*Contract No.:*	VER-CON
Contractor:	#N/A	*Federal Aid No.:*	#N/A
Report to District:	RMS	*Cost Account No.:*	#N/A
Resident Engineer:	#N/A	*District Mat. Engr.*	#N/A

	Cylinder 1		Cylinder 2		Cylinder 3	
Specimen	00091068		00091069		00091070	
Temp. (°F)						

Angle	Cylinder 1 (kΩ-cm)		Cylinder 2 (kΩ-cm)		Cylinder 3 (kΩ-cm)	
	1st Test	Repeat	1st Test	Repeat	1st Test	Repeat
0°						
90°						
180°						
270°						
0°						
90°						
180°						
270°						
Average						
%CV						
Average 16						

Set Average Resistivity Determination (kΩ-cm)

Age (Days):	56
Curing Factor:	1.0
Cyl. 1 Average:	
Cyl. 2 Average:	
Cyl. 3 Average:	
Set Average:	
Penetrability:	Low
Spec. Min.:	
Pass/Fail:	

Calculate the average and the %CV for each sample in the set. If the %CV is > 7.5%, immerse sample in water bath (68 to 77 °F) for 2 h, and record results in the "Repeat" Column. If the %CV on the "Repeat" Set is < 7.5%, use the average of the "Repeat" Set. If the %CV is > 7.5%, average all 16 readings.

massDOT Highway	SAMPLE TYPE:	775A-T	DATE RECEIVED:	SAMPLE NUMBER:
Rev. 04/08/2025	VER	SAMPLE OF CEMENT CONCRETE	8/15/25	2025-016446

PROJECT INFORMATION

Town/City:	STATEWIDE	*Contract No.:*	VER-CON
Contractor:	#N/A	*Federal Aid No.:*	#N/A
Report to District:	RMS	*Cost Account No.:*	#N/A
Resident Engineer:	#N/A	*District Mat. Engr.*	#N/A

LABORATORY PREPARATION, COMPRESSIVE STRENGTH TESTING (T 22 / C39)

Sample Condition: [✓] Acceptable [ ] Unacceptable (See Remarks) *Lab Curing Method:* Moist Cured

Lab Preparation: [ ] Sulfur (T 231) [✓] Neoprene (C1231) [ ] Cutting (T 22) [ ] Grinding (T 22)

Specimen ID	Age	Unit	Break Date	Weight (lbs)	Diameter (in)	Area (in^2)	Load (lbf)	Strength (psi)	Average (psi)	Break Type	Omit
00091062	7	DAY	8/20/25	8.08	4.01	12.63	54605	4324		5	
00091063	7	DAY	8/20/25	8.08	4.01	12.63	54143	4287	4230	5	
00091064	7	DAY	8/20/25	8.08	4.01	12.63	51406	4070		5	
00091065	28	DAY	9/10/25	8.08	4.01	12.63	64523	5109		5	
00091066	28	DAY	9/10/25	8.08	4.01	12.63	68818	5449	5440	3	
00091067	28	DAY	9/10/25	8.08	4.01	12.63	72675	5754		5	
00091068	56	DAY	10/8/25								
00091069	56	DAY	10/8/25								
00091070	56	DAY	10/8/25								

Break Type T 22: 1 Cone 2 Cone & Split 3 Columnar 4 Shear 5 Side Fracture 6 Pointed

56-day cylinders discarded: [ ] Yes

REMARKS

T358 testing at 7,28,and 56-days

TESTING LABORATORY, TECHNICIAN(S), AND REVIEW

Laboratory:	RMS	*Location:*	HOPKINTON, MA
T 358 (Set 1):	Casey Flynn	*Test Date:*	8/20/25
T 358 (Set 2):	Timothy Berard	*Test Date:*	9/10/25
T 358 (Set 3):		*Test Date:*	
T 22 (Set 1):	Casey Flynn	*Test Date:*	8/20/25
T 22 (Set 2):	Timothy Berard	*Test Date:*	9/10/25
T 22 (Set 3):		*Test Date:*	
T 22 (Set 4):		*Test Date:*	
Reviewed By:		*Review Date:*	

SPECIFICATION LIMITS AND APPROVAL

Results are within specification limits: [ ] *Results are outside specification limits:* [ ]

Approved By:

Signature:

Date:

***Results relate only to the items inspected or tested.**

****This report shall not be reproduced, except in full, without the prior written approval of the agency.**

Rev. 04/08/2025	SAMPLE TYPE: VER	775A-T SAMPLE OF CEMENT CONCRETE	DATE RECEIVED: 8/15/25	SAMPLE NUMBER: 2025-016448

PROJECT INFORMATION

Town/City:	STATEWIDE	*Contract No.:*	VER-CON
Contractor:	#N/A	*Federal Aid No.:*	#N/A
Report to District:	RMS	*Cost Account No.:*	#N/A
Resident Engineer:	#N/A	*District Mat. Engr.*	#N/A

MATERIAL INFORMATION

Bid Item:	VER.M4	*Specification No.:*	M4
Bid Item Description:	VERIFICATION OF CEMENT CONCRETE AND RELATED MATERIALS		
Sub-Item Description:	VER.M4 - TRIAL BATCH HIGH PERFORMANCE CONCRETE		
Bid Item Quantity:	#N/A	*Date to be Used:*	2025
MassDOT Mix ID No.:	25-07-14-10-50-41-04	*Producer Mix ID No.:*	S-120 /NP-MET
Produced by:	BOSTON CONCRETE CORPORATION	*Town/City, State:*	LOWELL, MA
Design Strength (psi):	5000	*Nom. Agg. Size (in.):*	3/4
Tot. Cementitious (lbs.)	685	*Mix Design Type:*	HPC
Proposed Use:	VERIFICATION OF CEMENT CONCRE	*Additional Information:*	

SAMPLING INFORMATION (R 60 / C172)

Date Sampled:	8/13/25	*Sampled By:*	George Gilbert
Sampling Location:	BOSTON CONCRETE CORPORATION	*Town/City, State:*	LOWELL, MA
Truck No.:	N/A	*Ticket No.:*	N/A
Sample Time:	9:48am		
Job Water Added:	N/A	*Admixtures Added:*	N/A
Random Sample:	Y	*Lot & Sub Lot No.:*	B
Quantity Represented:	1cy	*Weather & Temp. (°F):*	75-Sunny

PREPARATION OF SPECIMENS IN THE FIELD (R 100 / C31)

Specimen Size:	☑ 4 x 8" ☐ 6 x 12"	*Field Curing Method:*	☑ Curing Box ☐ Field Cured
Specimens Covered:	☑ Yes ☐ No	*Curing Temp. (°F):*	Low: 50 High: 90

SAMPLE PROPERTIES BY FIELD TESTS

Test Method	Quality Characteristic	Result	Spec. Min.	Spec. Max.	Pass/Fail	Remarks
T 119 (C143)	Slump (in.)	4.25	4.50	7.50	FIO	
T 152 (C231)	Air Content (%)	4.6	4.5	7.5	FIO	
T 309 (C1064)	Concrete Temp. (°F)	78	50	90	FIO	
T 121 (C231)	Unit Weight (pcf)	142.8	137.4	143.4	FIO	

REMARKS

T358 testing at 7,28,and 56-days

FIELD TESTING OFFICE, TECHNICIAN(S), AND REVIEW

Office:	RMS	*Office Location:*	HOPKINTON, MA
Tested By:	Keith St. Jean	*Test Date:*	8/13/25
Witnessed By:	George Gilbert	*Witness Date:*	8/13/25
Reviewed By:		*Review Date:*	

SPECIFICATION LIMITS & APPROVAL

Results are within specification limits:		*Results are outside specification limits:*	

By typing my name below, I understand and agree that this form of electronic signature has the same legal force and effect as a manual signature.

Approved By:		*Approve Date:*	

Rev. 04/08/2025	SAMPLE TYPE: VER	775A-T SAMPLE OF CEMENT CONCRETE	DATE RECEIVED: 8/15/25	SAMPLE NUMBER: 2025-016448

PROJECT INFORMATION

Town/City:	STATEWIDE	*Contract No.:*	VER-CON
Contractor:	#N/A	*Federal Aid No.:*	#N/A
Report to District:	RMS	*Cost Account No.:*	#N/A
Resident Engineer:	#N/A	*District Mat. Engr.*	#N/A

CHLORIDE ION PENETRATION RESISTANCE TESTING (T 358)

Specimen Size: 4 x 8" *Curing Method:* Moist Cured

	Cylinder 1		Cylinder 2		Cylinder 3	
Specimen	00091044		00091045		00091046	
Temp. (°F)	74.8		74.2		73.9	
Angle	**Cylinder 1 (kΩ-cm)**		**Cylinder 2 (kΩ-cm)**		**Cylinder 3 (kΩ-cm)**	
	1st Test	**Repeat**	**1st Test**	**Repeat**	**1st Test**	**Repeat**
0°	9.07		8.36		8.31	
90°	8.64		8.76		8.4	
180°	8.31		8.45		8.5	
270°	8.57		8.33		8.55	
0°	9.03		8.45		8.33	
90°	8.57		8.88		8.5	
180°	8.36		8.36		8.6	
270°	8.6		8.33		8.55	
Average	8.6	Not Req'd	8.5	Not Req'd	8.5	Not Req'd
%CV	3.2%	Not Req'd	2.5%	Not Req'd	1.3%	Not Req'd
Average 16	Not Req'd		Not Req'd		Not Req'd	

Set Average Resistivity Determination (kΩ-cm)

Age (Days):	7
Curing Factor:	1.0
Cyl. 1 Average:	8.6
Cyl. 2 Average:	8.5
Cyl. 3 Average:	8.5
Set Average:	9
Penetrability:	High
Spec. Min.:	-
Pass/Fail:	FIO

	Cylinder 1		Cylinder 2		Cylinder 3	
Specimen	00091047		00091048		00091049	
Temp. (°F)	70.6		70.4		70.5	
Angle	**Cylinder 1 (kΩ-cm)**		**Cylinder 2 (kΩ-cm)**		**Cylinder 3 (kΩ-cm)**	
	1st Test	**Repeat**	**1st Test**	**Repeat**	**1st Test**	**Repeat**
0°	20.3		19.9		21.1	
90°	21.4		22.4		21.8	
180°	19.1		19.4		20.4	
270°	18.6		19.9		21.7	
0°	20.7		20.2		21.3	
90°	21.4		22.3		21.6	
180°	19.4		19.4		20	
270°	18.8		19.9		21.6	
Average	20.0	Not Req'd	20.4	Not Req'd	21.2	Not Req'd
%CV	5.7%	Not Req'd	6.0%	Not Req'd	3.1%	Not Req'd
Average 16	Not Req'd		Not Req'd		Not Req'd	

Set Average Resistivity Determination (kΩ-cm)

Age (Days):	28
Curing Factor:	1.0
Cyl. 1 Average:	20.0
Cyl. 2 Average:	20.4
Cyl. 3 Average:	21.2
Set Average:	21
Penetrability:	Moderate
Spec. Min.:	21
Pass/Fail:	

Calculate the average and the %CV for each sample in the set. If the %CV is > 7.5%, immerse sample in water bath (68 to 77 °F) for 2 h, and record results in the "Repeat" Column. If the %CV on the "Repeat" Set is < 7.5%, use the average of the "Repeat" Set. If the %CV is > 7.5%, average all 16 readings.

Rev. 04/08/2025	SAMPLE TYPE: VER	775A-T SAMPLE OF CEMENT CONCRETE	DATE RECEIVED: 8/15/25	SAMPLE NUMBER: 2025-016448

PROJECT INFORMATION

Town/City:	STATEWIDE	*Contract No.:*	VER-CON
Contractor:	#N/A	*Federal Aid No.:*	#N/A
Report to District:	RMS	*Cost Account No.:*	#N/A
Resident Engineer:	#N/A	*District Mat. Engr.*	#N/A

	Cylinder 1		Cylinder 2		Cylinder 3	
Specimen	00091050		00091051		00091052	
Temp. (°F)						

Angle	Cylinder 1 (kΩ-cm)		Cylinder 2 (kΩ-cm)		Cylinder 3 (kΩ-cm)	
	1st Test	Repeat	1st Test	Repeat	1st Test	Repeat
0°						
90°						
180°						
270°						
0°						
90°						
180°						
270°						
Average						
%CV						
Average 16						

Set Average Resistivity Determination (kΩ-cm)

Age (Days):	56
Curing Factor:	1.0
Cyl. 1 Average:	
Cyl. 2 Average:	
Cyl. 3 Average:	
Set Average:	
Penetrability:	Moderate
Spec. Min.:	
Pass/Fail:	

Calculate the average and the %CV for each sample in the set. If the %CV is > 7.5%, immerse sample in water bath (68 to 77 °F) for 2 h, and record results in the "Repeat" Column. If the %CV on the "Repeat" Set is < 7.5%, use the average of the "Repeat" Set. If the %CV is > 7.5%, average all 16 readings.

Rev. 04/08/2025	SAMPLE TYPE: VER	775A-T SAMPLE OF CEMENT CONCRETE	DATE RECEIVED: 8/15/25	SAMPLE NUMBER: 2025-016448

PROJECT INFORMATION

Town/City:	STATEWIDE	*Contract No.:*	VER-CON
Contractor:	#N/A	*Federal Aid No.:*	#N/A
Report to District:	RMS	*Cost Account No.:*	#N/A
Resident Engineer:	#N/A	*District Mat. Engr.*	#N/A

LABORATORY PREPARATION, COMPRESSIVE STRENGTH TESTING (T 22 / C39)

Sample Condition: [✓] Acceptable [ ] Unacceptable (See Remarks) *Lab Curing Method:* Moist Cured

Lab Preparation: [ ] Sulfur (T 231) [✓] Neoprene (C1231) [ ] Cutting (T 22) [ ] Grinding (T 22)

Specimen ID	Age	Unit	Break Date	Weight (lbs)	Diameter (in)	Area (in^2)	Load (lbf)	Strength (psi)	Average (psi)	Break Type	Omit
00091044	7	DAY	8/20/25	8.55	4.01	12.63	75927	6012	5980	5	
00091045	7	DAY	8/20/25	8.55	4.01	12.63	74851	5927		5	
00091046	7	DAY	8/20/25	8.55	4.01	12.63	75948	6014		5	
00091047	28	DAY	9/10/25	8.55	4.01	12.63	93210	7380	7690	2	
00091048	28	DAY	9/10/25	8.55	4.01	12.63	98683	7814		2	
00091049	28	DAY	9/10/25	8.55	4.01	12.63	99566	7884		5	
00091050	56	DAY	10/8/25								
00091051	56	DAY	10/8/25								
00091052	56	DAY	10/8/25								

Break Type T 22: 1 Cone 2 Cone & Split 3 Columnar 4 Shear 5 Side Fracture 6 Pointed

56-day cylinders discarded: [ ] Yes

REMARKS

T358 testing at 7,28,and 56-days

TESTING LABORATORY, TECHNICIAN(S), AND REVIEW

Laboratory:	RMS	*Location:*	HOPKINTON, MA
T 358 (Set 1):	Casey Flynn	*Test Date:*	8/20/25
T 358 (Set 2):	Timothy Berard	*Test Date:*	9/10/25
T 358 (Set 3):	Casey Flynn	*Test Date:*	8/20/25
T 22 (Set 1):	Timothy Berard	*Test Date:*	9/10/25
T 22 (Set 2):		*Test Date:*	
T 22 (Set 3):		*Test Date:*	
T 22 (Set 4):		*Test Date:*	
Reviewed By:		*Review Date:*	

SPECIFICATION LIMITS AND APPROVAL

Results are within specification limits: [ ] *Results are outside specification limits:* [ ]

Approved By:

Signature:

Date:

***Results relate only to the items inspected or tested.**

****This report shall not be reproduced, except in full, without the prior written approval of the agency.**

Rev. 04/08/2025	SAMPLE TYPE: VER	775A-T SAMPLE OF CEMENT CONCRETE	DATE RECEIVED: 8/15/25	SAMPLE NUMBER: 2025-016447

PROJECT INFORMATION

Town/City:	STATEWIDE	*Contract No.:*	VER-CON
Contractor:	#N/A	*Federal Aid No.:*	#N/A
Report to District:	RMS	*Cost Account No.:*	#N/A
Resident Engineer:	#N/A	*District Mat. Engr.*	#N/A

MATERIAL INFORMATION

Bid Item:	VER.M4	*Specification No.:*	M4
Bid Item Description:	VERIFICATION OF CEMENT CONCRETE AND RELATED MATERIALS		
Sub-Item Description:	VER.M4 - TRIAL BATCH HIGH PERFORMANCE CONCRETE		
Bid Item Quantity:	#N/A	*Date to be Used:*	2025
MassDOT Mix ID No.:	25-07-14-10-50-41-03	*Producer Mix ID No.:*	S-120 /NP-DE
Produced by:	BOSTON CONCRETE CORPORATION	*Town/City, State:*	LOWELL, MA
Design Strength (psi):	5000	*Nom. Agg. Size (in.):*	3/4
Tot. Cementitious (lbs.)	685	*Mix Design Type:*	HPC
Proposed Use:	VERIFICATION OF CEMENT CONCRE	*Additional Information:*	

SAMPLING INFORMATION (R 60 / C172)

Date Sampled:	8/13/25	*Sampled By:*	George Gilbert
Sampling Location:	BOSTON CONCRETE CORPORATION	*Town/City, State:*	LOWELL, MA
Truck No.:	N/A	*Ticket No.:*	N/A
Sample Time:	9:30am		
Job Water Added:	N/A	*Admixtures Added:*	N/A
Random Sample:	Y	*Lot & Sub Lot No.:*	B
Quantity Represented:	1cy	*Weather & Temp. (°F):*	75-Sunny

PREPARATION OF SPECIMENS IN THE FIELD (R 100 / C31)

Specimen Size:	☑ 4 x 8"	☐ 6 x 12"	*Field Curing Method:*	☑ Curing Box	☐ Field Cured
Specimens Covered:	☑ Yes	☐ No	*Curing Temp. (°F):*	Low: 50	High: 90

SAMPLE PROPERTIES BY FIELD TESTS

Test Method	Quality Characteristic	Result	Spec. Min.	Spec. Max.	Pass/Fail	Remarks
T 119 (C143)	Slump (in.)	5.00	4.50	7.50	FIO	
T 152 (C231)	Air Content (%)	4.4	4.5	7.5	FIO	
T 309 (C1064)	Concrete Temp. (°F)	78	50	90	FIO	
T 121 (C231)	Unit Weight (pcf)	143.8	137.3	143.3	FIO	

REMARKS

T358 testing at 7,28,and 56-days

FIELD TESTING OFFICE, TECHNICIAN(S), AND REVIEW

Office:	RMS	*Office Location:*	HOPKINTON, MA
Tested By:	Keith St. Jean	*Test Date:*	8/13/25
Witnessed By:	George Gilbert	*Witness Date:*	8/13/25
Reviewed By:		*Review Date:*	

SPECIFICATION LIMITS & APPROVAL

Results are within specification limits:		*Results are outside specification limits:*	

By typing my name below, I understand and agree that this form of electronic signature has the same legal force and effect as a manual signature.

Approved By:		*Approve Date:*	

Rev. 04/08/2025	SAMPLE TYPE: VER	775A-T SAMPLE OF CEMENT CONCRETE	DATE RECEIVED: 8/15/25	SAMPLE NUMBER: 2025-016447

PROJECT INFORMATION

Town/City:	STATEWIDE	*Contract No.:*	VER-CON
Contractor:	#N/A	*Federal Aid No.:*	#N/A
Report to District:	RMS	*Cost Account No.:*	#N/A
Resident Engineer:	#N/A	*District Mat. Engr.*	#N/A

CHLORIDE ION PENETRATION RESISTANCE TESTING (T 358)

Specimen Size: 4 x 8" *Curing Method:* Moist Cured

	Cylinder 1		Cylinder 2		Cylinder 3	
Specimen	00091053		00091054		00091055	
Temp. (°F)	75.3		74.5		74.2	
Angle	**Cylinder 1 (kΩ-cm)**		**Cylinder 2 (kΩ-cm)**		**Cylinder 3 (kΩ-cm)**	
	1st Test	**Repeat**	**1st Test**	**Repeat**	**1st Test**	**Repeat**
0°	9.5		9.55		9.31	
90°	9.36		9.17		9.38	
180°	9.1		9.24		9	
270°	8.64		10.5		8.95	
0°	9.6		9.5		9.43	
90°	9.19		9.41		9.24	
180°	9.17		9.17		8.95	
270°	8.62		9.79		9.07	
Average	9.1	Not Req'd	9.5	Not Req'd	9.2	Not Req'd
%CV	4.0%	Not Req'd	4.6%	Not Req'd	2.1%	Not Req'd
Average 16	Not Req'd		Not Req'd		Not Req'd	

Set Average Resistivity Determination (kΩ-cm)

Age (Days):	7
Curing Factor:	1.0
Cyl. 1 Average:	9.1
Cyl. 2 Average:	9.5
Cyl. 3 Average:	9.2
Set Average:	9
Penetrability:	High
Spec. Min.:	-
Pass/Fail:	FIO

	Cylinder 1		Cylinder 2		Cylinder 3	
Specimen	00091056		00091057		00091058	
Temp. (°F)	70.6		70.8		70.9	
Angle	**Cylinder 1 (kΩ-cm)**		**Cylinder 2 (kΩ-cm)**		**Cylinder 3 (kΩ-cm)**	
	1st Test	**Repeat**	**1st Test**	**Repeat**	**1st Test**	**Repeat**
0°	27		26.1		28.3	
90°	24.9		26		26.2	
180°	25.2		25.5		24.1	
270°	26.5		26.2		28.6	
0°	26.8		26.4		28.3	
90°	25		26.2		26	
180°	25.5		25.7		24.2	
270°	26.8		26.3		28.8	
Average	26.0	Not Req'd	26.1	Not Req'd	26.8	Not Req'd
%CV	3.5%	Not Req'd	1.2%	Not Req'd	7.3%	Not Req'd
Average 16	Not Req'd		Not Req'd		Not Req'd	

Set Average Resistivity Determination (kΩ-cm)

Age (Days):	28
Curing Factor:	1.0
Cyl. 1 Average:	26.0
Cyl. 2 Average:	26.1
Cyl. 3 Average:	26.8
Set Average:	26
Penetrability:	Low
Spec. Min.:	21
Pass/Fail:	

Calculate the average and the %CV for each sample in the set. If the %CV is > 7.5%, immerse sample in water bath (68 to 77 °F) for 2 h, and record results in the "Repeat" Column. If the %CV on the "Repeat" Set is < 7.5%, use the average of the "Repeat" Set. If the %CV is > 7.5%, average all 16 readings.

Rev. 04/08/2025	SAMPLE TYPE: VER	775A-T SAMPLE OF CEMENT CONCRETE	DATE RECEIVED: 8/15/25	SAMPLE NUMBER: 2025-016447

PROJECT INFORMATION

Town/City:	STATEWIDE	*Contract No.:*	VER-CON
Contractor:	#N/A	*Federal Aid No.:*	#N/A
Report to District:	RMS	*Cost Account No.:*	#N/A
Resident Engineer:	#N/A	*District Mat. Engr.*	#N/A

	Cylinder 1		Cylinder 2		Cylinder 3	
Specimen	00091059		00091060		00091061	
Temp. (°F)						

Angle	Cylinder 1 (kΩ-cm)		Cylinder 2 (kΩ-cm)		Cylinder 3 (kΩ-cm)	
	1st Test	Repeat	1st Test	Repeat	1st Test	Repeat
0°						
90°						
180°						
270°						
0°						
90°						
180°						
270°						
Average						
%CV						
Average 16						

Set Average Resistivity Determination (kΩ-cm)

Age (Days):	56
Curing Factor:	1.0
Cyl. 1 Average:	
Cyl. 2 Average:	
Cyl. 3 Average:	
Set Average:	
Penetrability:	Low
Spec. Min.:	
Pass/Fail:	

Calculate the average and the %CV for each sample in the set. If the %CV is > 7.5%, immerse sample in water bath (68 to 77 °F) for 2 h, and record results in the "Repeat" Column. If the %CV on the "Repeat" Set is < 7.5%, use the average of the "Repeat" Set. If the %CV is > 7.5%, average all 16 readings.

Rev. 04/08/2025	SAMPLE TYPE: VER	775A-T SAMPLE OF CEMENT CONCRETE	DATE RECEIVED: 8/15/25	SAMPLE NUMBER: 2025-016447

PROJECT INFORMATION

Town/City:	STATEWIDE	*Contract No.:*	VER-CON
Contractor:	#N/A	*Federal Aid No.:*	#N/A
Report to District:	RMS	*Cost Account No.:*	#N/A
Resident Engineer:	#N/A	*District Mat. Engr.*	#N/A

LABORATORY PREPARATION, COMPRESSIVE STRENGTH TESTING (T 22 / C39)

Sample Condition: [✓] Acceptable [ ] Unacceptable (See Remarks) *Lab Curing Method:* Moist Cured

Lab Preparation: [ ] Sulfur (T 231) [✓] Neoprene (C1231) [ ] Cutting (T 22) [ ] Grinding (T 22)

Specimen ID	Age	Unit	Break Date	Weight (lbs)	Diameter (in)	Area (in^2)	Load (lbf)	Strength (psi)	Average (psi)	Break Type	Omit
00091053	7	DAY	8/20/25	8.43	4.01	12.63	79397	6287		5	
00091054	7	DAY	8/20/25	8.43	4.01	12.63	79605	6303	6290	5	
00091055	7	DAY	8/20/25	8.43	4.01	12.63	79337	6282		5	
00091056	28	DAY	9/10/25	8.43	4.02	12.69	100415	7911		5	
00091057	28	DAY	9/10/25	8.43	4.02	12.69	100416	7912	7890	3	
00091058	28	DAY	9/10/25	8.43	4.02	12.69	99645	7851		3	
00091059	56	DAY	10/8/25								
00091060	56	DAY	10/8/25								
00091061	56	DAY	10/8/25								

Break Type T 22: 1 Cone 2 Cone & Split 3 Columnar 4 Shear 5 Side Fracture 6 Pointed

56-day cylinders discarded: [ ] Yes

REMARKS

T358 testing at 7,28,and 56-days

TESTING LABORATORY, TECHNICIAN(S), AND REVIEW

Laboratory:	RMS	*Location:*	HOPKINTON, MA
T 358 (Set 1):	Casey Flynn	*Test Date:*	8/20/25
T 358 (Set 2):	Timothy Berard	*Test Date:*	9/10/25
T 358 (Set 3):	Casey Flynn	*Test Date:*	8/20/25
T 22 (Set 1):	Timothy Berard	*Test Date:*	9/10/25
T 22 (Set 2):		*Test Date:*	
T 22 (Set 3):		*Test Date:*	
T 22 (Set 4):		*Test Date:*	
Reviewed By:		*Review Date:*	

SPECIFICATION LIMITS AND APPROVAL

Results are within specification limits: [ ] *Results are outside specification limits:* [ ]

Approved By:

Signature:

Date:

***Results relate only to the items inspected or tested.**

****This report shall not be reproduced, except in full, without the prior written approval of the agency.**